# Combination Delivery of C-peptide and Lisofylline for the Treatment of Diabetic Nephropathy

**THESIS**

Submitted in partial fulfilment

of the requirements for the degree of

**DOCTOR OF PHILOSOPHY**

by

**Arihant Kumar Singh**

**2018PHXF0039P**

Under the Supervision of

**Prof. Anupama Mittal**

and Co-supervision of

**Prof. Deepak Chitkara**


**BIRLA INSTITUTE OF TECHNOLOGY & SCIENCE**

**PILANI-333031 (RAJASTHAN) INDIA**

**2024**

# CERTIFICATE

This is to certify that the thesis entitled **"Combination Delivery of C-peptide and Lisofylline for the Treatment of Diabetic Nephropathy"** was submitted by **Mr. Arihant Kumar Singh,** ID. No. **2018PHXF0039P** for award of Ph.D. Degree of the Institute, embodies original work done by him under our supervision.

| | |
|---|---|
| Supervisor | Co-supervisor |
| **Prof. Anupama Mittal** | **Prof. Deepak Chitkara** |
| Associate Professor | Associate Professor |
| Department of Pharmacy | Department of Pharmacy |
| BITS Pilani, Pilani Campus | BITS Pilani, Pilani Campus |
| Date: | Date: |
| Place: | Place: |

# Table of Content

# Acknowledgements

First and foremost, I would like to express my deep and sincere gratitude to my Ph.D. research supervisor **Prof. Anupama Mittal**, Associate Professor, Department of Pharmacy for giving me an opportunity to work under her expert guidance despite all my naivety and also for providing her untiring attention which bequeathed right from the inception to the completion of the present research work. I would also like to express my sincere feelings for my co-supervisor **Prof. Deepak Chitkara,** Associate Professor, Department of Pharmacy for constant support and motivation throughout my journey. His inspiration always kept me going throughout my tenure.

I would like to personally thank and appreciate **Prof. S. Murugesan** and **Prof. Aniruddha Roy**, who are members of the Doctoral Advisory Committee (DAC), for taking their priceless time to carefully review my thesis and enrich it with their invaluable comments and insights.

I am thankful to **Prof. V. Ramagopal Rao**, Hon. Vice-Chancellor, BITS-Pilani, **Prof. Sudhirkumar Barai**, Director, BITS Pilani, Pilani Campus, **Col. Soumyabrata Chakraborty** (Retd), Registrar, BITS Pilani, Pilani Campus, **Prof. Shamik Chakraborty**, Associate Dean, AGSRD, BITS Pilani, Pilani Campus, for providing excellent work facilities and an absorbing research environment. I wish to express sincere thanks to **Prof. Anil B. Gaikwad**, Head, Department of Pharmacy, for constant support in providing the guidance and resources required during my research work. I would like to convey my heartfelt thanks to **Prof. Anil Jindal** (DRC member) for his prodigious assistance throughout my Ph.D. and thesis submission.

I offer heartfelt thanks and gratitude to **Prof. Rajdeep Chowdhury** (Head, Department of Biological Sciences, BITS Pilani, Pilani campus) for his constant support and encouragement. My special thanks to the faculty members **Prof. R. Mahesh, Prof. Hemant R. Jadhav** & **Prof. Atish T. Paul, Prof. Rajiv Taliyan**, **Prof. Gautam Singhvi**, **Prof. M. M. Pandey**, **Prof. Sandeep Sundriyal, Dr. Richa Shrivastava**, **Dr. Pragyanshu Khare** and **Dr. Sushil K. Yadav**, (Sr. Vet. In-charge, Central Animal Facility).

This work would not have been possible without the wholehearted encouragement, guidance, support and cooperation of my beloved BITSian colleagues, friends and well-wishers. With profound appreciation, I acknowledge all the Research scholars in the Department of Pharmacy, Chemistry and Biological Sciences**,** especially my seniors **Dr. Saurabh Sharma, Dr. Kishan S. Italiya, Dr. K.V. Krishna, Dr. Pracheta Sengupta, Dr. Dhanashree Surve, Dr. Ginson George,**

**Dr. Samrat Mazumdar, Dr. Sudeep Pukale, Dr. Vamsi K. Rapalli, Dr. Vajir Malek, Dr. Nisha Sharma & Dr. Abhilasha Srivastava**. I feel fortunate to meet a bunch of bright minds as labmates-cum-juniors of ***Nanomedicine and Gene delivery Lab***, including **Dr. Deepak K. Sahel, Ms. Moumita Basak**, **Mr. Prabhjeet Singh, Mr. Imran Ansari, Mr. N. Saibhargav, Mr. Subham A. Salunkhe, Mr. K. Sai Pradyuth, Ms. Reena Jatyan, Mr. Abhay Tharmatt, Ms. Sonia Guha, Mr. G. Giriprasad** and **Mr. Pratik Shinde**. I would also like to thank **Mr. Jay Chadokiya and Mr. Sudarshan**, post-graduate students, whose presence gave me a tremendous opportunity to explore my leadership potential, which I believe would be useful for my future endeavors. Also, I would like to thank **Dr. Swati Sharma, Dr. Shweta Sharma, Dr. Kedar Prayag, Dr. Ajinath Kale, Dr. Paramita Saha, Dr. Amritansh Bhanot, Dr. Sharyu Kesharvani, Dr. Tejashree Waghule, Dr. Atharva Bhide, Ms. M. Kavya Shree, Dr. Rajesh Pradhan, Dr. Rupesh Jain, Dr. Mahipal Reddy, Ms. Shreya Das, Ms. Nikita Hinge, Mr. Viswadeep Shelke, Mr. Prashant Auti, Ms. Manisha Choudhari, Ms. Nisha Yadav, Ms. Sriravelli, Mr. Ala Chandu, Mr. Yash Patidar, Mr. Yash Katakia, Mr. Srikant Kirwale** and **Ms. Shobha Kumari** for being the valuable part of my BITS journey.

I am thankful to administrative staff, **Mr. Puran Singh Ji**, **Laxman Ji, Tarachand Ji, Abhishek Ji**, **Ram Suthar Ji, Surender Ji, Vikas Ji, Naveen Ji**, **Mahender Ji**, **Suman Ji**, **Omprakash Ji, Sandeep Ji, Kuldeep Ji**, **Virendra Ji**, **Mahipal Ji and Nitin Ji** for their continuous support.

Without loving friends, my world would never be complete, especially my roommates (**Dr. Karan Kumar Banoth and Dr. Himanshu Sankrityayan**), who encouraged and shared the joyful journey at TSF 23/3. A support system while walking toward the heights of a Ph.D. degree should also be acknowledged, and therefore, I want to thank **Dr. Moumita Basak** and **Dr. Geetika Wadhwa** for all the care and encouragment throughout the journey.

This acknowledgement would be partial without citing the names of my loving and caring **Mrs. Mamta Singh** (Mother), **Mr. Ajay Kumar Singh** (Father), **Mr. Vijayant Singh** (Brother) and **Mrs. Swati Singh** (Spouse). I would like to thank them for always motivating me and supporting me in my tough times. Their positive thoughts gave me the energy to carry out difficult things very simply with a smiling face. Their unconditional love and support are the pillars of my life.

**(Arihant Kumar Singh)**

# List of Abbreviations

| | |
|---|---|
| % | Percentage |
| % DL | Percentage drug loading |
| % EE | Percentage entrapment efficiency |
| % RSD | Percentage relative standard deviation |
| % v/v | Percentage volume by volume |
| % w/v | Percentage weight by volume |
| $\lambda_{max}$ | Wavelength of maximum absorbance |
| < | Less than |
| > | More than |
| ≤ | Less than or equal to |
| ≥ | More than or equal to |
| = | Equal to |
| ~ | Approximately equal to |
| ± | Plus or minus |
| º C | Degree centigrade |
| nm | Nanometer |
| mg | Milligram |
| mg/mL | Milligram per milliliter |
| µg/mL | Microgram per milliliter |
| ng/mL | Nanogram per milliliter |
| AGE | Advanced glycation end products |
| BGL | Blood glucose level |
| $C_{max}$ | Maximum concentration |
| CD | Circular dichroism |
| CMC | Critical micellar concentration |
| CPep | C-peptide |
| cAMP | Cyclic adenosine monophosphate |
| DMEM | Dulbecco's Modified Eagle Medium |
| DMSO | Dimethyl sulfoxide |
| DKD | Diabetic kidney disease |
| DLS | Dynamic light scattering |
| DN | Diabetic nephropathy |
| ECM | Extracellular matrix |
| EDTA | Ethylene diamine tetra acetic acid |
| EDC.HCl | N-(3-dimethylaminopropyl)-N-ethylcarbodiimide hydrochloride |
| EMT | Epithelial-to-mesenchymal transition |
| ELISA | Enzyme linked immunosorbent assay |
| ERK | Extracellular regulated protein kinases |
| FBS | Fetal bovine serum |
| FCP | FITC tagged C-peptide |
| FESEM | Field emission scanning electron microscopy |
| FA | Fatty acid |

| | |
|---|---|
| g | Gram |
| GBM | Glomerular basement membrane |
| GDM | gestational diabetes mellitus |
| GLP-1 | Glucagon like peptide-1 |
| h | Hour |
| HCl | Hydrochloric acid |
| HPLC | High performance liquid chromatography |
| HRP | Horseradish peroxidase |
| IL-6 | Interleukin-1 |
| i.v. | Intravenous |
| IAEC | Institutional animal ethical committee |
| IBMX | 3-isobutyl 1-methyl xanthine |
| ICH | International council for harmonization |
| IFN-γ | Interferon gamma |
| IPA | Isopropyl alcohol |
| IHC | Immunohistochemistry |
| IS | Internal standard |
| IU | International Unit |
| LOD | Limit of detection |
| LOQ | Limit of quantification |
| LPAT | Lysophosphatidate acyltransferase |
| NC | Normal control |
| DC | Diabetic control |
| NK | Natural killer cells |
| INS-1 | Insulinoma cells-1 |
| NOD | Non-obese diabetic |
| MRT | Mean residence time |
| MTT | 3-(4,5-dimethylthiazol-2-yl)-2,5 diphenyltetrazolium bromide |
| mV | Millivolt |
| MWCO | Molecular weight cut off |
| $N_{agg}$ | Aggregation number |
| NF-kB | Nuclear factor kappa B |
| NOX | Nicotinamide adenine dinucleotide phosphate oxidases |
| NPs | Nanoparticles |
| ω-6 | Omega-6 |
| OA | Oleic acid |
| OD | Optical density |
| QC | Quality control |
| PAGE | Polyacrylamine gel electrophoresis |
| PBS | Phosphate buffer saline |
| PDI | Polydispersity Index |
| PFA | Paraformaldehyde |
| PK | Pharmacokinetics |
| PI | Protease inhibitor |

| | |
|---|---|
| PTX | Paclitaxel |
| PUFA | Polyunsaturated fatty acids |
| $R^2$ | Regression coefficient |
| ROS | Reactive oxygen species |
| rpm | Rotations per minute |
| $R_t$ | Retention time |
| RP-HPLC | Reverse-phase high-pressure liquid chromatography |
| RT | Room temperature |
| SD | Standard deviation |
| SDS | Sodium dodecyl sulphate |
| sec | Second |
| SGLT2 | Sodium glucose cotransporter 2 |
| STZ | Streptozotocin |
| $t_{1/2}$ | Half-life |
| $T_{max}$ | Time to reach maximum concentration |
| TEMED | N,N,N′,N′ -Tetramethylethylenediamine |
| TNF-α | Tumour necrosis factor-α |
| TLC | Thin layer chromatography |
| UC | Ultracentrifuge |
| UV | Ultra-violet |
| $V_d$ | Apparent volume of distribution |
| WB | Western blot |
| WHO | World health organization |
| ZP | Zeta potential |

# List of Tables

# List of Figures

# Abstract

The thesis entitled "Combination Delivery of C-peptide and Lisofylline for the Treatment of Diabetic Nephropathy" focuses upon the formulation development strategies and *in-vitro* and *in-vivo* evaluation of the nanoformulation of Lisofylline (LSF) and C-peptide (CPep) individually as well in combination for the treatment of streptozotocin (STZ) induced diabetic nephropathy (DN). The rationale for considering LSF and CPep as the active molecules of choice for the treatment of DN treatment was based upon literature survey.

LSF is an anti-inflammatory and immunomodulatory agent with proven therapeutic benefits in Type 1 diabetes mellitus (T1DM). It was found to improve oral glucose tolerance, along with insulin level, which could be the result of enhanced pancreatic β-cell functioning in STZ-induced T1DM animals. It was observed that the glucose-induced insulin secretion was significantly elevated to ~1.5 fold and significantly reduced mean serum glucose level in LSF-treated animals than the level observed in the vehicle-treated animals within 60 min of the oral glucose dose (250 mg/100 gm). It has been shown to protect pancreatic islets from IL-1α-induced inhibitory effects on insulin release. However, its clinical utility is compromised due to its hydrophilicity and rapid metabolism to its metabolite Pentoxifylline (PTX), resulting in poor oral bioavailability and short half-life.

CPep is a 31 amino-acid peptide that is released from pancreatic β-cells into the blood circulation in equimolar concentration as insulin. The beneficial effects of CPep have been reported against various diabetic complications in T1DM including diabetic retinopathy, nephropathy, neuropathy, diabetic wound, and many more. CPep is reported to prevent hyperglycemia-induced endothelial apoptosis by suppressing oxidative stress and mitochondrial dysfunction. However, there are clinical limitations to CPep usage due to its short circulating half-life (30 min) and rapid liver enzymatic degradation and clearance. This demands repeated peptide administration to achieve therapeutic benefits; which increases the cost of the therapy as well as is patient-incompliant.

Our major challenges in this thesis work were to overcome the barriers to clinical translation of LSF and CPep individually and then develop a combination formulation to harness their expected additive/synergistic activity in the STZ-induced DN animals. The thesis work was broadly classified into three major objectives, a brief outlook of each is mentioned in the following paragraphs.

The **first objective** was to develop a fatty acid (FA) conjugate of LSF to overcome its hydrophilicity and form an amphiphilic compound that can self-assemble to form micelles. After screening the FAs belonging to different classes with different levels of saturation and chain length, LSF-oleic acid (OA with an 18-carbon chain and a single, double bond at ω-9) was chosen based on the release profile of LSF in plasma and protein binding affinity. Reportedly, LSF-OA showed only 9.74 ± 2.3 % cumulative release in 72 h and a higher binding constant ($6.32 \times 10^4$) along with a lower aggregation number ($N_{agg}$= 61), which confirmed its longer residence in the systemic circulation. Additionally, it showed higher cellular internalization in the mouse insulinoma cells, MIN-6, owing to the enhanced hydrophobicity and self-assembly into nano-sized micellar structures. The promising outcomes from the *in-vivo* studies could be further correlated to observed ~6 fold higher $t_{½}$ and ~11 fold enhanced mean residence time in *in-vivo* pharmacokinetic studies, as indicated by LSF-OA when compared to free LSF. Also, LSF-OA showed the best control of glucose level with decreased mortality compared to other prodrugs. Interestingly, LSF-OA reduced plasma ASAT and, ALAT level along with the uric acid level when compared to T1DM control animals, which demonstrated the oxidative stress reduction efficiency and renoprotectiveness of LSF-OA. The presence of pro-inflammatory cytokines induces the infiltration of CD4+ and CD8+ T lymphocytes in the pancreas, causing destruction of β-cells in the islets in the diabetic model. LSF released from the LSF-OA prodrug reduced T cells (CD4+ and CD8+) entry into the islets when compared to the diabetic control (DC) group. Hence, the therapeutic application of the LSF-OA in the DN was established.

In the **second objective**, we designed a cationic polymeric nano-formulation that could conjugate CPep and deliver it efficiently in a controlled manner to overcome its short half-life. A polyethylene carbonate-based polymer was synthesized with a cationic polycarbonate-grafted-DMDP chain and employed to prepare the cationic blank nanospheres (BNP), and final CPep nano-complexes (**NPX)** was formed by simple incubation of BNP with CPep. The novelty of this strategy was utilizing electrostatic interaction for complexing the peptide to the carrier system instead of a chemical-based reaction/ conjugation, which resulted in NPX with 87.50 % complexation efficiency of CPep. NPX maintained the CPep release in a controlled manner till 180 h, wherein only ~40 % release was observed within the initial seven days. The observed cytoprotection rendered by NPX in the oxidative and metabolic stress-induced rat kidney epithelial NRK-52E cells was correlated to the increased GSH level and reduced NO level and differential expression levels of anti-apoptotic

proteins and EMT-marker protein in the metabolic stress-induced cells. Additionally, NPX administration in Wistar rats (i.v.) revealed a steady plasma concentration of CPep, maintained till 72 h (above the normal CPep concentration) and demonstrated t½ of ~22 h. The anti-inflammatory activity of NPX reduced the predominantly elevated proinflammatory cytokine IL-6 level in plasma to 3 fold less than the DC group, along with 2.3 fold reduction in the expression of TGF-β. NPX treated kidney tissue samples showed protected pancreatic islets, glomerulus, tubular structures and mesangial cells in comparison to the DC animals in histology. This clearly proved the efficiency of NPX to treat DN.

In the **final objective**, we developed an LSF-OA loaded cationic polymeric nano-formulation that was further complexed with CPep to enable co-delivery of both for DN treatment. After proving the efficiency of NPX in DN and the possible application of LSF-OA, we were keen to investigate the overall impact of the nanoformulation having both LSF-OA and CPep in the treatment of DN. After encapsulating LSF-OA in the cationic nanoformulation, CPep was complexed with the LSF-OA nanoformulation to develop **mPLM-LSF-OA-CPep nanoparticles**. mPLM-LSF-OA-CPep with nano-size (238.6 ± 14.4 nm) and zeta-potential (+5.2 ± 2.37 mV) maintained its size till 30 days under physiological conditions, after which the particle size gradually increased in the benchtop stability study. mPLM-LSF-OA-Cep showed minimal hemolysis with 1.68 ± 0.52 %, almost 2 fold lesser than the mPLM-LSF-OA, which indicated the complexation of the CPep to the surface of the mPLM-LSF-OA. Herein, both MIN-6 and NRK-52E under metabolic stress were used to evaluate the *in-vitro* efficacy of the combination formulation. While mPLM-LSF-OA was able to increase the GSH level by 1.57 and 1.94 fold, mPLM-LSF-OA-CPep was able to elevate the level by 1.31 and 1.79 fold in metabolic stress-induced MIN-6 and NRK-52E cells respectively. This clearly indicated the efficiency of the combination formulation over the free CPep, NPX and, mPLM-LSF-OA. Additionally, an *in-vivo* PK study indicated that mPLM-LSF-OA and mPLM-LSF-OA-CPep increased the t½ of LSF-OA by ~2.6 and ~5.3 fold, whereas NPX already showed an increase in CPep t½ up to 22 h. Also, mPLM-LSF-OA-CPep treated animals demonstrated ~2.69 and ~2.05 fold reduction in pro-inflammatory cytokine (IL-6 and TNF-α) levels in comparison to DN control. Finally, the efficiency of the combination formulation was evident by ~6.8 fold improved insulin level, and significantly higher Ki-67 stained cells in the pancreatic islet of the mPLM-LSF-OA-CPep treated group. Along with, Haematoxylin and Eosin (H&E) and Periodic acid-Schiff (PAS) staining of kidney sections demonstrated reduced intracellular glycogen

accumulation, diminished infiltration of inflammatory cells, mild mesangial expansion, lesser deposition of the mesangial matrix, and near normal relative glomerular basement membrane thickness upon treatment with the combination formulation.

# CHAPTER 1

# Introduction

## 1.1 Background: Diabetes Mellitus (DM)

Diabetes has seen a steady rise in prevalence all around the world in recent years, from 463 million in 2019 to 700 million in 2045, the number of people with diabetes is predicted to rise by 51%. Furthermore, developing nations of Africa, the Middle East, South-East Asia, South America, and Central America are estimated to experience a sharp rise in diabetes and diabetes associated disorders **(Figure 1.1)**. The Western Pacific region is home to around 1 in 3 adult diabetic patients, and also accounts for 1 in 3 diabetes-related deaths. By 2045, it is anticipated that the annual global health expenditure on diabetes will increase from 760 billion USD in 2019 to 845 billion USD. The treatment of diabetic complications accounts for more than half of the direct costs incurred. Furthermore, the health and life expectancy of diabetes patients have recently come under threat from newly discovered diabetes-related health issues like cancer, dementia, bone disease, non-alcoholic fatty liver disease, and oral diseases, and many others. Therefore, the true cost of diabetes-related health care and lifespan loss are likely to have been greatly underestimated mainly attributed to the fact that diabetes-related epidemiological data, health care information, and emerging issues are still understudied in Asia and other developing nations around the world.

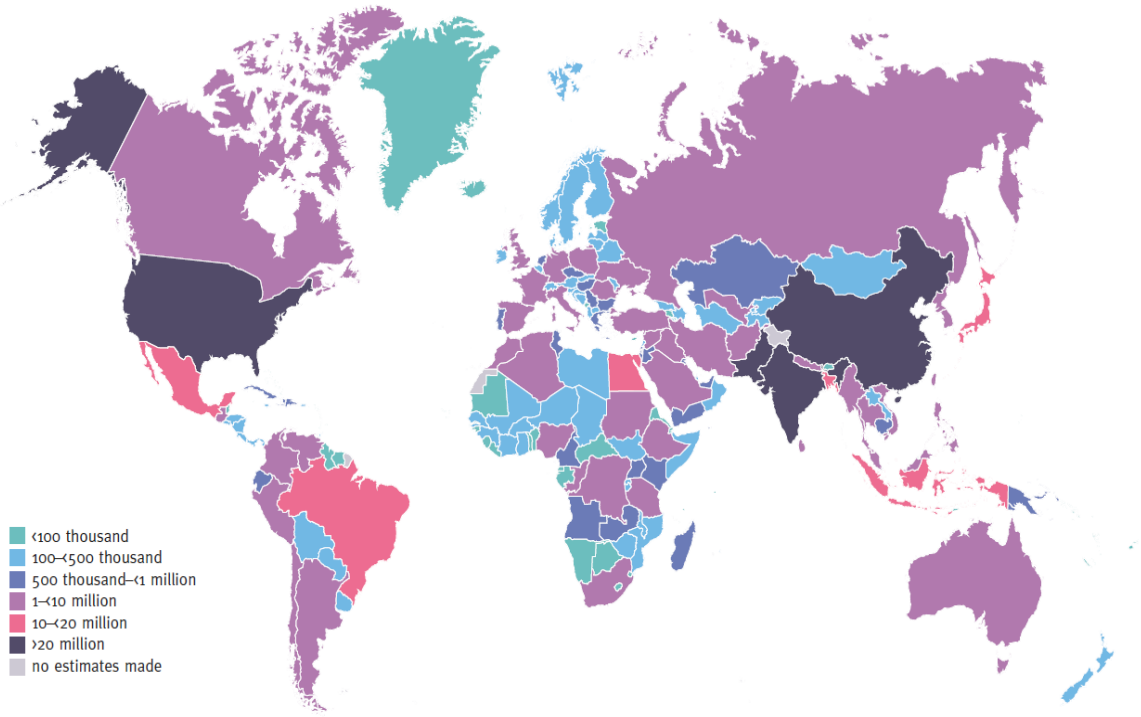


**Figure 1.1** Estimated total number of adults (20–79 years) with diabetes in 2021. Accessed from IDF Diabetes Atlas 2021 (www.diabetesatlas.org/atlas/tenth-edition) on 15th Nov 2023. [1]

Hyperglycemia (elevated blood sugar level), which arises from deficiencies in either insulin secretion, insulin action, or both, is the hallmark of the group of metabolic diseases known as diabetes. Long-term injury, dysfunction, and failure of various organs, particularly the eyes, kidneys, nerves, heart, and blood vessels, are linked to chronic hyperglycemia resulting due to diabetes. The etiology of diabetes involves multiple pathogenic mechanisms. These include anomalies that lead to resistance to the action of insulin, as well as autoimmune destruction of the pancreatic β-cells, which result in an insulin deficiency. Insufficient insulin secretion and/ or reduced tissue response to insulin at one or several stages in the intricate hormone action pathway causes insufficient insulin action. Diabetes can lead to a range of enduring complications, such as retinopathy, which carries the risk of vision impairment; nephropathy, ultimately resulting in renal failure; peripheral neuropathy, which increases the likelihood of foot ulcers, amputations, and Charcot joints; and autonomic neuropathy, which can manifest as gastrointestinal, genitourinary, cardiovascular symptoms, and sexual dysfunction. Individuals with diabetes also experience a higher prevalence of atherosclerotic cardiovascular disease, peripheral arterial disease, and cerebrovascular issues. Hypertension and disruptions in lipoprotein metabolism are commonly observed in diabetic individuals.

### 1.2 Etiology of DM

The vast majority of diabetes cases can be broadly classified into two primary etiopathogenic categories. In the first category, known as type 1 diabetes mellitus (T1DM), the root cause is a complete deficiency of insulin secretion. Those at an elevated risk of developing T1DM can often be diagnosed through serological markers indicating an autoimmune process affecting the pancreatic islets, along with genetic indicators. In the second category, a much more prevalent category, type 2 diabetes mellitus (T2DM), the cause is a combination of resistance to the action of insulin and insufficient compensatory insulin secretion. In T2DM, individuals may experience hyperglycemia that is significant enough to induce pathological and functional changes in various target tissues, even though they may not exhibit clinical symptoms. This hyperglycemia can persist for an extended period before diagnosis for diabetes could be made. During this asymptomatic phase, detecting abnormalities in carbohydrate metabolism is feasible by measuring fasting plasma glucose levels, conducting an oral glucose challenge test, or assessing HbA1C levels. [2, 3]

The assignment of a specific type of diabetes to an individual often hinges on the circumstances prevailing at the time of diagnosis. Many individuals with diabetes do not neatly fit into a single category. For instance, someone diagnosed with gestational DM (GDM) may continue to

experience high blood sugar levels after giving birth and may ultimately be reclassified as having T2DM. On the other hand, an individual who develops diabetes due to prolonged use of high doses of external steroids may return to normal blood glucose levels once glucocorticoids are discontinued. However, they may later develop diabetes many years after experiencing recurrent episodes of pancreatitis. Another scenario involves a person treated with thiazide diuretics may develop diabetes several years later, since thiazides themselves might induce severe hyperglycemia, although rarely, it is likely that such individuals already have underlying T2DM that is exacerbated by the medication. Therefore, for both healthcare professionals and patients, the emphasis should be less on categorizing the precise type of diabetes and more on comprehending the causes of elevated blood sugar and effectively managing it. Diabetic kidney disease (DKD) is spreading more prominently in developed countries as well, which is linked with microvascular complications developed by both T1DM and T2DM. A progressive decrease in the glomerular filtration rate and persistent albuminuria are the early signs of the disorder. There is a significant proof that the progression can be stopped or delayed with an early treatment. In individuals with T2DM, albuminuria may be evident when diabetes is initially diagnosed. However, diabetic nephropathy (DN) typically manifests in T1DM approximately 15 to 20 years later. Diabetes triggers structural and functional alterations in the kidneys, leading to the development of proteinuria, hypertension, and a gradual decline in kidney function. These characteristics collectively define the hallmark features of DN. [4]

### 1.3 DN: A global epidemic

DN affects 30 to 40 percent of people suffering from DM and its emergence is strongly associated with poor blood sugar level control, prolonged hypertension, and chronicity of DM. A common incidence of high blood pressure and cardiovascular problems in close family members is a potential cause for DN. High cholesterol, smoking and obesity are risk factors that, when paired with familial patterns aggravate risk of DN. [5] According to projections from the World Health Organization (WHO), 439 million people, or 7.7 percent of the world's population, will have diabetes by 2030. Over the past three decades, the number of diabetic patients has increased globally by a factor of three, as a result of the radically altered lifestyles, rising elderly population, and rapid urbanization. [6, 7] China, India, Pakistan, Indonesia, and Bangladesh are among the top 10 nations where DM prevalence is expected to be highest by 2030, making Asia the "diabetes epicentre of the world." [8, 9]

Numerous studies have shown that over the past few decades, diabetes has become more widespread worldwide. Till few years, the presence of albuminuria in DM patients equal to or greater than 300 mg/day was considered the hallmark of renal disorder, and marked the incidence of DN. This clinical condition was typically associated with hypertension and diabetic retinopathy, which resulted in loss of kidney function. [10] There are stages of DN in T1DM which could be different than T2DM, as it is many a times linked with hypertension, renal failure and/or proteinuria or a combination of these.

In DN induced by T1DM, a novel categorization of diabetic kidney lesions was presented by Tervaert et al. in 2010 **(Table 1.1)**. This classification underscored the existence of renal damage that is mostly associated with tubules, the interstitium, and/or arteries. This classification deviated from the conventional patterns of global or nodular glomerulosclerosis, which are frequently linked to kidney problems associated with diabetics.

**Table 1.1**
Pathophysiologic assessment of DN. [10]

| Glomerular lesions | Description |
|---|---|
| Class I | Thickening of glomerular basement membrane |
| Class II | Expansion of mesangial cells, [mild (IIa) or severe (IIb)] |
| Class III | Nodular sclerosis (Kimmelstiel-Wilson lesions) |
| Class IV | Advanced diabetic glomerulosclerosis |

The role of fibrosis, inflammation, and oxidative stress in the progression of DN is becoming more and more clear. *In-vivo* specimens of DN, the build-up of macrophages, lymphocytes, mast cells, inflammatory cells (e.g., neutrophils), and dendritic cells across the renal tissue is closely associated with DN. [11] In the local microenvironment, inflammatory cells play a pivotal role in synthesizing and releasing fibrogenic cytokines like tumor necrosis factor-α (TNF-α), interleukin-1 (IL-1), and reactive oxygen species (ROS). These substances can directly damage the kidney architecture or initiate the epithelial-to-mesenchymal transition (EMT) process, ultimately leading to the accumulation of extracellular matrix (ECM). [12] Another component involved in the initiation and progression of DN is chemokine C-C motif ligand 2 (CCL2), also known as monocyte chemotactic protein 1 (MCP-1). Renal fibrosis is a common consequence of kidney disease, leading to a substantial loss of the normal structure and function of the kidney, irrespective of whether the injury is induced by oxidative stress or inflammation. Key pathogenic factors in kidney fibrosis, also observed in DN, include the thickening of the glomerular basement membrane (GBM), glomerular hypertrophy, and an increase in the mesangial matrix. Prolonged stimulation by cytokines results in the excessive

production of ECM, thereby resulting in hindrance of its breakdown. Under normal circumstances, a moderate amount of ECM is generated to maintain regular cellular structure and function. However, in the case of persistent injury, triggered by inflammation or oxidative stress, profibrotic cytokines are excessively released. [13, 14]

Stress factors including increased blood pressure and raised level of glucose in the blood, especially as diabetes progresses, cause generation of high amounts of ROS in the renal tissues. Oxidative stress results from disruption in the oxidation-reduction equilibrium, which affects the autoregulatory system. Several investigations have shown that ROS from persistent hyperglycemia may cause both immediate and secondary injury to the kidney interstitium. In this situation, the polyol pathway contributes to increased advanced glycation end products (AGE) formation, and the activation of PKC and nicotinamide adenine dinucleotide phosphate oxidases (NOX) that are the main contributors towards the production of ROS. [15-18] These result in elevated vascular permeability, renal vascular sclerosis, both physiological and structural disabilities, and the induction of downstream facilitators such as extracellular regulated protein kinases (ERK), nuclear factor kappa B (NF-kB), activator protein-1 (AP-1), and p38 mitogen-activated protein kinases (p38 MAPK). Subsequently, a cascade of cellular responses is initiated that plays a vital role in the development of DN as illustrated in **Figure 1.2**.

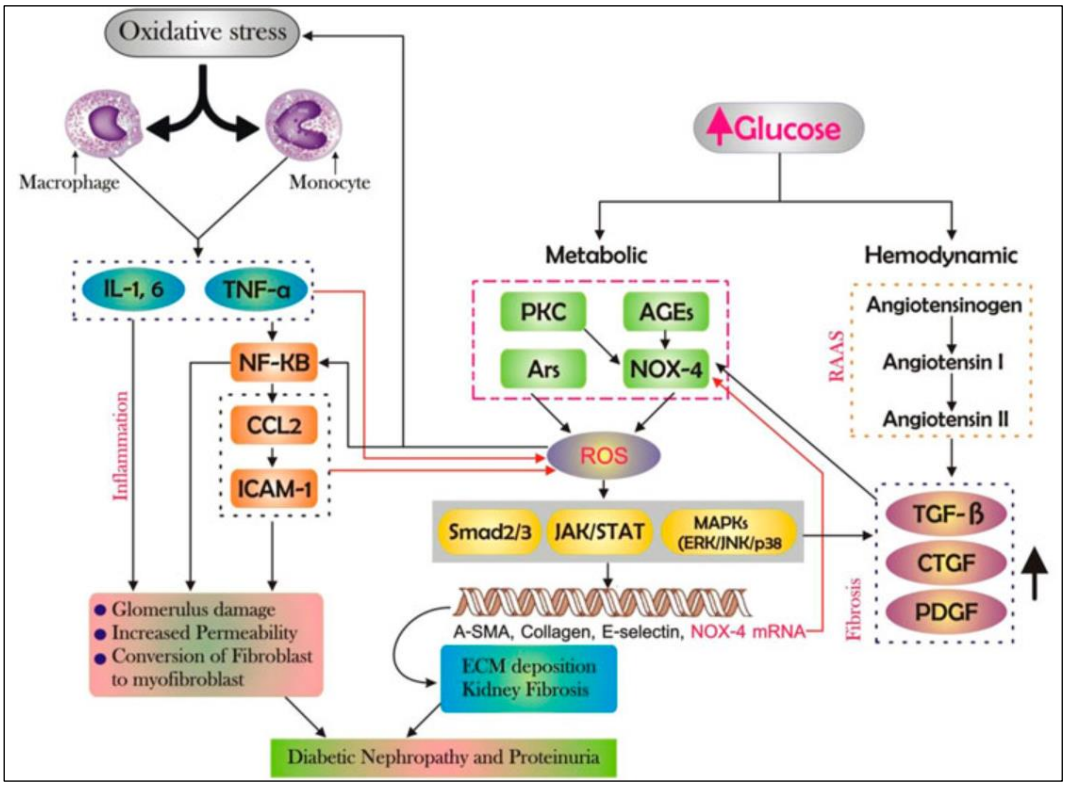


**Figure 1.2** Pathogenesis of DN, adapted from Lin B. *et al.* Front. Bioeng. Biotechnol. 2022. [13]

### 1.3.1 DN: Treatment and challenges

The existing treatment options for DN are primarily centred around the management of blood pressure, glycaemic control, and reduction of triglycerides. However, the molecular progression of DN has historically been overlooked, despite fibrosis, oxidative stress, and inflammation being consistently identified as key factors. [13]

Recent research in the field of DN has focussed towards multiple mechanisms, including the disruption of cell signal transduction pathways, targeting interrelated enzymes, and reducing ECM aggregation. [19-21] Emerging therapeutic strategies for DN encompass a diverse range of options, including endothelin receptor antagonists, Vitamin D receptor agonists, anti-inflammatory therapies; such as pentoxifylline (PTX) and lisofylline (LSF), antioxidants (like resveratrol), *Nrf2* activators (such as Bardoxolone methyl), and various peptides. This list has been further enriched by the inclusion of peptides that have demonstrated potential in slowing down the progression or treating DN. Peptides that normalize hyperglycemia include insulin and insulin analogs, as well as GLP1 agonists like exenatide, lixisenatide, liraglutide, exenatide, dulaglutide, semaglutide, and others. Promising peptides for DN treatment include C-peptide, Apelin, and Keratinocyte growth factor (KGF). [22] However, a significant drawback in applying these promising molecules is their very short half-life ($t_{1/2}$), rapid clearance, and often insufficient efficacy.

The altered vascularity of the kidney further complicates the treatment of DN. Kidneys with compromised tubular secretion and glomerular filtration require higher doses of drugs for effective delivery and sustained presence. However, this increased dosage raises concerns about dose-dependent toxicity in DN treatment. [23] In response to these challenges, the development of drug-loaded nanoparticles (NPs) has emerged as a promising area. This approach offers advantages such as sustained drug release, enhanced $t_{1/2}$, improved bioavailability, targeted delivery, and mechanism-based activity in the treatment of DN. [24] The complexities in treating DN are compounded by the altered physiology of the kidney, which sets specific criteria for effective nano-formulation development. Achieving kidney targeting is crucial for the successful treatment of DN, contingent upon nanoparticles' ability to cross the glomerular filtration unit and remain there for an extended period.

The glomerular filtration unit comprises glomerular endothelial cells (GECs), the glomerular basement membrane (GBM), and podocytes. GECs have fenestrations of 60-80 nm, preventing the entry of plasma constituents into the endothelial cell membrane. The GBM is a continuous

membrane approximately 300 nm wide, with pores ranging from 2-8 nm and containing negatively charged heparan sulfate and other proteins that facilitate filtration. [25, 26] Podocytes, tightly attached to the GBM, form filtration slits of 20-30 nm in width. [27] Thus, particle size emerges as a pivotal factor in site-specific targeting for DN treatment. Small particles (5-7 nm) can easily traverse the glomerular filtration barrier and be reabsorbed in the proximal tubule. However, ultra-small particles (~2 nm) may be eliminated by the liver as they cannot pass the glycocalyx. Particles ranging from 30-150 nm are unable to pass through glomerular filtration, but those below 80 nm exhibit the greatest glomerular retention. Additionally, Mesoscale NPs (MNPs) with a size of 400 nm were observed in proximal tubular cells, indicating endocytosis as their mechanism of uptake due to their larger size compared to fenestrations. These considerations underscore the critical importance of particle size in achieving effective and targeted DN treatment. [28]

### 1.4 Small molecules for diabetes treatment

Management of diabetes involves a combination of lifestyle modifications, including regular exercise and dietary control. This includes adhering to a diet that is low in trans and saturated fats, reducing the intake of added sugars, limiting sodium intake, and exercising control over excessive alcohol and tobacco consumption. These lifestyle changes play a crucial role in maintaining blood sugar levels and overall health in individuals with diabetes. It's important for individuals with diabetes to work closely with healthcare professionals to develop a personalized and effective management plan that aligns with their specific needs and health goals. [29, 30] Insulin-producing pancreatic β-cells are destroyed by the body's defence system in T1D, an autoimmune disease that results in a lifelong deficiency of insulin in the patient. For patients with T1D, lifelong external insulin replacement treatment is the accepted standard of care. Although elementary pancreatic islets or complete pancreas implantation is a viable treatment option for autoimmune T1D patients, logistical obstacles prevent its widespread use. These difficulties include the lack of islet cells, the difficulty of obtaining sufficient vascularization of islets after transplantation, the requirement for protracted immune suppression, and the scarcity of volunteers.

Investigating novel strategies to maintain inherent insulin secretion and prevent pancreatic β-cell death is imperative in order to control the level of glucose in the blood. [31] Currently, the treatment approach for T2DM predominantly relies on various conventional methods aimed at mitigating hyperglycemia. These include sulfonylureas and related insulin secretagogues, which boost insulin release from pancreatic islets; biguanides like metformin, which reduce

hepatic glucose production; peroxisome proliferator-activated receptor-γ (PPARγ) agonists, specifically thiazolidinediones, enhancing insulin action; α-glucosidase inhibitors, disrupting gut glucose absorption; and insulin itself, suppressing glucose production while augmenting glucose utilization. In cases where monotherapy falls short, a combination of these hypoglycemic agents is often prescribed. [32] Nevertheless, if the combined oral hypoglycemic approach fails to achieve the targeted blood glucose levels (BGL), insulin therapy becomes the recommended course of action. Insulin may also be administered in conjunction with metformin when the latter alone is insufficient in maintaining the desired BGL. Additionally, insulin therapy is initiated for patients newly diagnosed with T2DM and presenting elevated glucose levels (≥300-350 mg/dl) or HbA1C (≥10-12 %). [33, 34]

The conventional treatments currently available for DN encompass blood pressure control through the use of angiotensin-converting enzyme inhibitors (ACEIs), angiotensin II receptor blockers (ARBs), and aldosterone antagonists. Glycaemic control is achieved through lifestyle changes and the use of dipeptidyl peptidase-4 inhibitors (DPP4I), glucagon-like peptide (GLP1) receptor agonists, and sodium glucose cotransporter 2 (SGLT 2) inhibitors. Additionally, lipid metabolism is regulated using statins, and in some cases, haemodialysis may also be employed. This broader approach aims to address the multifaceted nature of DN progression. [13]

The present therapies for diabetes encounter obstacles pertaining to their restricted efficacy, tolerability, and substantial mechanism-based adverse reactions such as increased body weight and hypoglycemic attacks. Moreover, very few of these treatments effectively address underlying issues such as obesity and/or insulin resistance. Regarding sulfonylureas in particular, a major problem is that a large number of patients who respond to treatment initially, but develop resistance to them subsequently, resulting in what are known as "secondary failures." The search for novel and more potent therapeutics is still essential to overcome the shortcomings of existing diabetic treatments. [33, 35]

### 1.4.1 Lisofylline (LSF)

LSF, also known as l-(5-R-hydroxyhexyl)-3,7-dimethylaxanthine, is a derivative of methyl xanthine with two enantiomers (R and S) that are proven to have immunomodulatory and anti-inflammatory properties. [36, 37] Initially, LSF was designed and investigated to treat-reperfusion, hypoxia, and autoimmune damage to the cells. LSF regulates the release of inflammatory cytokines, blocks stress-activated lipid breakdown, and enhances responsiveness

of patients to radiation and chemotherapy. [38-40] LSF is one of the major active metabolites of pentoxifylline (PTX) which is used since the past three decades to treat intermittent claudication. Although it has a tendency to interconvert into PTX *in-vivo*, LSF is an active metabolite of PTX. This interconversion of LSF is mainly attributed to the presence of free hydroxyl group present in the side chain. Metabolic pathways of PTX and its metabolite LSF are depicted in **Figure 1.3** wherein, PTX forms several metabolites, among these, LSF (metabolite 1) is found to be active in diabetes as well as other autoimmune diseases. Cytochromes (CYPs) are mainly found in liver, and primarily involved in LSF and PTX interconversion. After initial metabolism into LSF, it is further converted to metabolite 2, 3 and 4. [41, 42] Also, previously our lab and other scientists have confirmed that PTX and LSF undergo metabolic interconversion. [43, 44] Since the past two decades, PTX and LSF are being tested in preclinical studies for inflammatory and autoimmune disorders including T1DM. [45]

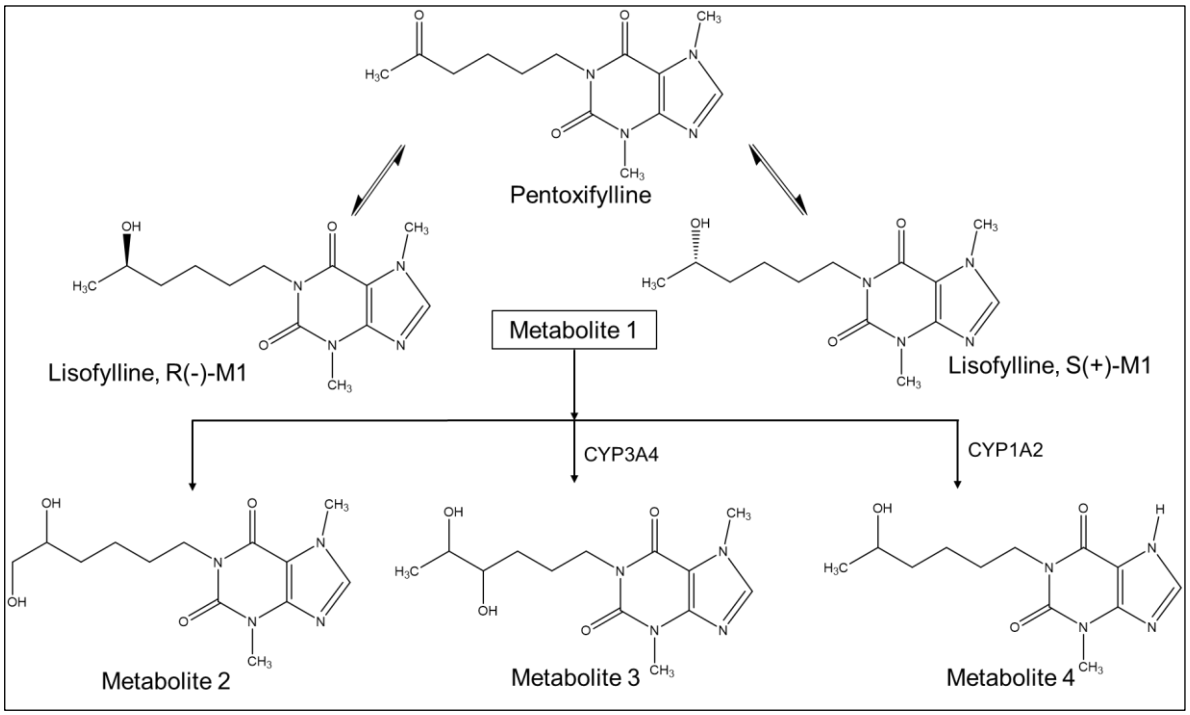


**Figure 1.3** PTX metabolism showing its interconversion to LSF (metabolite 1).

### 1.4.1.1 Mechanism of action

Although the primary mechanism of the action that LSF exhibits are still unclear, some likely processes have been identified hereunder based on existing literature. LSF is clinically useful in preventing T1DM and T2DM due to its broad range of activities. The enzyme phosphodiesterase 4 (PDE4) inhibitors are known to decrease the release of pro-inflammatory cytokines and help in the synthesis of some anti-inflammatory cytokines, LSF primarily acts

by inhibiting the above enzyme, thereby increasing the intracellular cyclic adenosine monophosphate (cAMP) levels and phosphorylation of protein kinase A, along with activating many transcription factors that control the generation of inflammatory cytokines, thus help in regaining the equilibrium that has been lost in autoimmune and inflammatory conditions. [46-49] In addition, LSF inhibits the cAMP response factor binding (CREB) protein activation, membrane oxidation, and generation of pro-inflammatory cytokines, thereby preventing hyperoxia-induced lung damage. [50] Strong inflammatory agents have the ability to initiate a variety of interrelated biological processes in different cell types. In response to particular inflammatory stimuli, phosphoric acid (PA) appears as a possible secondary messenger involved in intracellular signaling responses. [51] Intracellular PA variations are rapidly induced by inflammatory mediators such as interleukin 1 beta (IL-1β), endotoxins (lipopolysaccharide; LPS), and tumor necrosis factor-alpha (TNF-α). [52, 53] LSF effectively hinders the formation of PA, which reduces the activity of the enzyme lysophosphatidate acyltransferase (LPAT), which is connected with the cell membrane. The potential reduction in PA production and LPAT function also reduces the host's response to inflammatory stimuli such as TNF-α and IL-1β. [54, 55] LSF has demonstrated strong protective benefits in preclinical studies against a range of acute inflammatory diseases, including acute lung damage and acute respiratory distress syndrome. These advantageous effects are probably caused by LSF's ability to block the common PA secondary messenger channel. [37, 48, 56]

The systemic immune defence is mostly controlled by the signal transducer and transcription factor (STAT4). The expression of STAT4 is observed in humans at the sites of inflammation and is produced by various immune cells, including peripheral blood monocytes, dendritic cells (DC), and macrophages. [57-59] Its main job is to regulate the signaling of IL-12, which is essential for the establishment of protective immunity against infections within cells. Inhibition of T cell activation and a reduction in T cell-driven cytokine production results from alterations in the STAT4 gene. [60] LSF, on the other hand, obstructs IL-12's biological effects, which lowers IFN-γ production and controls T-cell activation and differentiation. [61, 62] An experimental model of multiple sclerosis called mouse allergic encephalomyelitis (EAE) has shown evidence of this interference with IL-12 signaling (**Figure 1.4**). [55, 63] As a result, LSF has a potential for use in clinical settings for immune modulation in an array of autoimmune disorders.

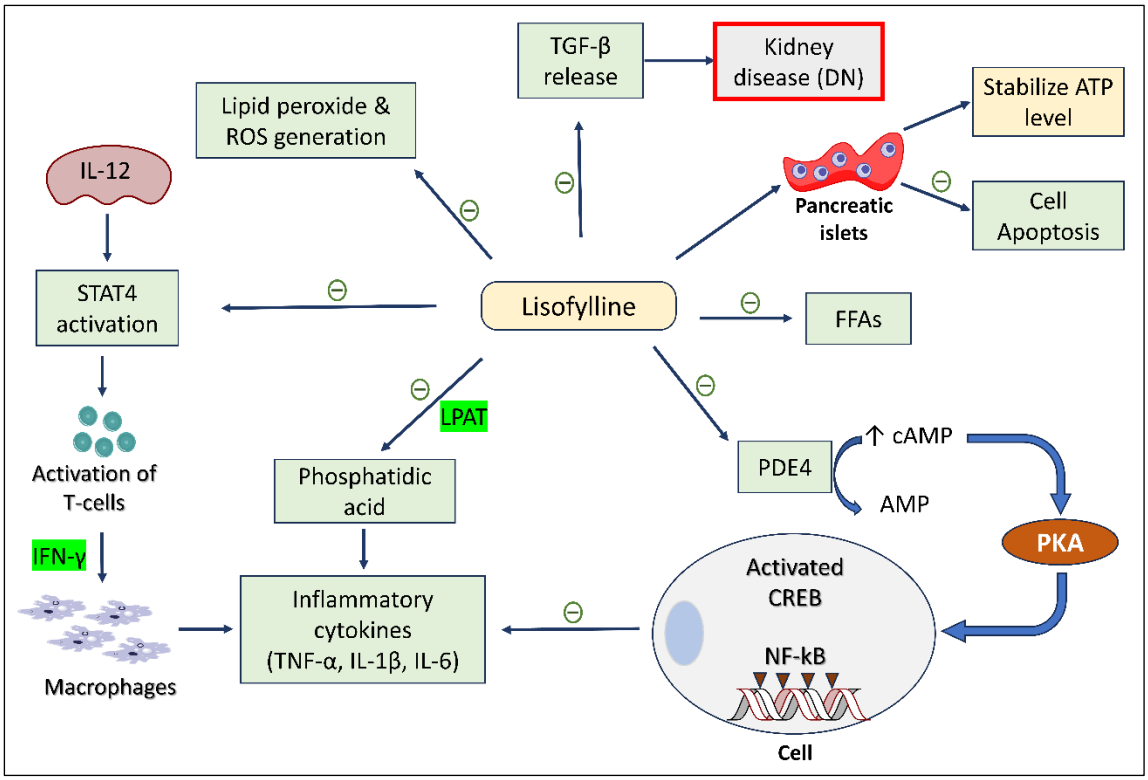


**Figure 1.4** Mechanism of action of LSF in diabetes.

### 1.4.1.2 LSF as a potential lead for treatment of diabetes

Cui and colleagues conducted a study wherein 32 derivatives were synthesized based on the chemical structure of LSF; however, only two of these analogues have been demonstrated to be efficient in preserving insulin secretory function and shielding β-cells from cytokine-induced damage in cell culture-based evaluations. [64] Pancreatic cells undergo damage as a result of the up-regulation of Th1-type responses, which is facilitated by immune cells such as T cells, B cells, macrophages, DC, and natural killer (NK) cells as well as cytokines. [65] Since cytotoxicity to β cells is caused by activated T cells, IL-12 may also contribute, either directly or indirectly, towards the onset of T1D. [66] It has been observed through experiments that IL-1β, TNF-α, and IFN-γ can prevent islets and rat insulinoma cells (INS-1) from secreting insulin. Further, Striffler and Nadler proved that LSF has the ability to delay the progression of diabetes in animal models by inhibiting the action of these cytokines. Additionally, LSF effectively recovered insulin secretion by stimulating mitochondrial metabolism in β cells and enhancing the glucose-stimulated insulin secretion by enhancing the ATP production for oxidative phosphorylation within the mitochondria of β cells, when LSF was co-incubated with insulin-secreting INS-1 cells, in the presence of pro-inflammatory cytokines. [36, 67] LSF therapy successfully delayed the development of diabetes in the non-obese diabetic (NOD) T1D mouse model. Intraperitoneal administration of 25 mg/kg of LSF twice a day was shown to improve

glucose-triggered insulin production in prediabetic animals with T2D, apparently through an improvement in the activity of surviving β cells. [68]

#### 1.4.1.3 Delivery challenges associated with LSF

In spite of the aforementioned potential, LSF has not received much attention from researchers; only a few studies have been reported elucidating its physicochemical and pharmacokinetic characteristics. Being a potent molecule, LSF exhibits an extensive range of activity, which indicates its substantial clinical promise. Even after participating in numerous clinical studies for testing, LSF is still in the developmental and experimental stages owing to shortcomings in its therapeutic effectiveness attributed primarily to its physicochemical and pharmacokinetic limitations. The considerable aqueous solubility of LSF, approximately 60 mg/mL in water, poses a challenge in its encapsulation into various delivery systems. [36] It is attributed to its hydrophilic nature, and demonstrates a short $t_{1/2}$ (approximately 0.75-1.17 h), rapid clearance, suboptimal distribution, and poor pharmacokinetics. Also, the bioavailability of LSF in humans is notably low, ranging from minimal to negligible (approximately 5.9%), primarily attributed to its high first-pass metabolism. [69] Because of its instantaneous conversion to PTX and other metabolites, LSF needs to be administered at elevated doses in order to have a therapeutic effect. [42] In clinical trials, LSF has been administered at a dose of 9 mg/kg by continuous i.v. infusion or at 12 mg/kg dose by subcutaneous infusion over a period of 10 h alternatively every week for the treatment of T1DM, which makes treatment non-patient compliant and therefore, these limitations restrict the molecule's potential for clinical use.

In order to overcome the associated barriers of LSF, our team developed a drug-fatty acid conjugate. These conjugates were synthesized through an esterification reaction, aiming to augment the pharmacokinetic performance of LSF. Our group has already synthesized and reported a prodrug of LSF with linoleic acid (LSF-LA), which was administered to treat streptozotocin (STZ)-induced T1DM in animals. The self-assembled micelles of the LSF-LA prodrug demonstrated enhanced therapeutic effects in inflammation-induced murine insulinoma cells MIN-6, with improved cell uptake. The $t_{1/2}$ of LSF was extended by the prodrug, and the interconversion with LSF-PTX was reduced, leading to a decrease in both the dose of LSF (from 25mg/kg to 15 mg/kg) and its frequency of administration, resulting in better efficacy in diabetic animal model. [44] Further, to protect the ester linkage of the LSF-LA prodrug and delay LSF metabolism, LSF-LA was encapsulated in self-assembled polymeric micelles (LSF-LA PLM). [70] To enhance the oral bioavailability of the developed LSF-LA

PLM, it was lyophilized and compressed into a tablet formulation which exhibited a 5.9-fold increase in permeability compared to free LSF in *in situ* SPIP permeability studies. [71]

### 1.5 Peptides used to manage diabetic complications

Treatment options for diabetes encompass insulin and various small drug molecules. In the case of T1D, insulin remains the primary and reliable therapy. However, newer insulin analogues with varied onset of action and duration of effect are now available in the market, offering more choices to patients. To emulate normal physiological insulin levels, a multiple-dose regimen is often necessary for maintaining optimal glucose levels. However, Pramlintide is used in combination with insulin medication approved by the US Food and Drug Administration (USFDA) for improving glycemic control. For emergency situations, glucagon is available as a kit for severe cases of hypoglycemia, which can however, lead to seizures or loss of consciousness. [72, 73] Pharmaceutical research is actively focused on developing therapeutics that can effectively manage the symptoms of micro and macrovascular complications associated with diabetes. A pivotal approach involves treatments capable of reversing or correcting these defects. Peptides, due to their broad range of action and target-selectivity, present a promising avenue for managing diabetic complications. **Table 1.2** outlines peptides used for diabetic management, along with strategies to enhance their stability.

However, peptide drugs face a significant limitation in clinical application due to their instability, proteolytic vulnerability and quick clearance by the kidneys with short circulation half-lives. Significant efforts have been made to address these issues by prolonging the half-lives of peptides in blood and introducing controlled delivery systems. The $t_{½}$ of peptides has been extended by a number of methods, such as fatty acylation, coupling of the immunoglobulin Fc segment, and PEGylation. These strategies have been successful in generating long-acting GLP-1 and insulin analogues that are intended for controlled release of peptide to manage the levels of glucose in clinical setting. A controlled release of peptide has been accomplished with the use of biopolymers such as polysaccharides and elastin like-polypeptides (ELP). Remarkably, in diabetic animal models, a single subcutaneous injection of polysaccharide-based biopolymer-conjugated peptides has demonstrated prolonged release of GLP-1, FGF21, and C-peptide from 5 to 19 days. Nevertheless, no clinically useful controlled release peptide medication is currently in the market. [74]

**Table 1.2**
Non-insulin peptides for the prevention and treatment of diabetic complications.

| Agent | Mechanism of action | Strategy for increased stability | Reference |
|---|---|---|---|
| GLP-1 receptor agonist | - Anti-inflammatory<br>- β–cell stress relief | - Amino acid modification<br>- Conjugation with nano-carrier system<br>- PEGylation | [75-77]<br>[78-80]<br>[81-85] |
| Amylin analogues/ Pramlintide | - Adjunct to insulin therapy | - Nanocarrier system<br>- Biodegradable silica depot formation | [86]<br>[87, 88] |
| C-peptide | - Targets mitogen-activated protein kinase (MAPK) pathways<br>- $Na^+/K^+$-ATPase activation<br>- Stimulation of Nitric Oxide synthase | - PEGylation<br>- Nanocarrier system<br>- Biopolymer conjugation (K9-C-peptide) | [89, 90]<br>[91]<br>[92, 93] |
| INGAP Peptide | - Regrowth of neurites in dorsal root ganglia (T1DM) | - Amino acid modification | [94, 95] |
| Monoclonal antibodies (Adalimumab, Golimumab, Infliximab, Rituximab. Tocilizumab) | - Anti-inflammatory | - PEGylation | [96-98] |
| N-acetyl-aspartyl-glutamate/ glutamate carboxypeptidase II (GCP-II)- Inhibitor | - Reduces the excitotoxic damage caused by glutamate | - Peptidase inhibition | [99-101] |
| Glutamic acid decarboxylase (GAD 65) | - Prevents autoimmune mediated destruction of pancreatic beta cells | - Nasal administration<br>- Adjuvant-formulated vaccine<br>- Genetically modified bacterial carrier | [102]<br>[103]<br>[104] |

### 1.5.1 C-peptide (CPep)

CPep is a bio-molecule with distinct physiological role in renal micro-vascular repair as well in anti-inflammatory immune responses in pancreas. CPep is a biogenic peptide (31- amino acids) secreted from the pancreas as a connecting peptide between the insulin chains A and B, in an equimolar concentration to insulin. There is a difference between human and rat C-peptide amino acid sequences. At human C-peptide positions 2, 5, 8, 10, 17, 20, 23, 28, 29 and 30, where changes to Ala→Val, Leu→Pro, Gly→Pro, Val→Leu, Gly→Glu, Ser→Asp,

Pro→Thr, Gly→Val, Ser→Ala and Leu→Arg amino acids are present. The present research work was performed on diabetic Wistar rats and therefore we have utilized rat C-peptide sequence in the research. It has approximately 5-6 times longer half-life than insulin (30-40 vs. 3–5 min) with a selective fate in renal metabolism wherein, renal uptake outlies the renal excretion almost by 7 folds. [105, 106] A short-term effect of CPep infusion was reported in 11 T1D patients who showed a significant decrease in glomerular filtration rate and increased renal blood flow with improved plasma glucose profile in the diabetic patients. In one of these studies, urinary excretion of albumin decreased by 40 and 55% after 2 and 4 weeks of CPep administration respectively, while no change was seen in patients taking insulin alone. [107] The underlying therapeutic benefits imparted by CPep could be described as improvement in renal insufficiency by suppressing TGF-β mediated inflammatory pathway and increased EGFR phosphorylation which ultimately increased the epithelial nitric oxide synthase (eNOS) and activation of the physiological antioxidants. [108-111] Recently, a study also reported that the CPep suppressed high glucose induced EMT and renal fibrosis thus combating the podocyte injury in STZ-induced mice. [111, 112] Although, CPep was not able to modulate the insulin secretion, it demonstrated an anti-apoptotic effect on the islet cells which might additionally aid its efficacy. [113] Despite its possible therapeutic excellence, CPep has not been used clinically in diabetes and diabetic complications because of its short biological half-life and lack of smart delivery systems. It is a well-known fact that peptide formulations face physical instability because of the extreme conditions employed during the development stages (pH, temperature, freeze drying, pressure, chemical reactions etc.), resulting in agglomeration and degradation. Yet, peptide-based therapeutics are considered as a promising genre of drugs as these provide a safe, efficient and targeted therapy for different pathological conditions. [112, 114] As reported, Ersatta™ by Cebix is a long-acting C-peptide in PEGylated form used to successfully treat functional disorders in DN. Administration of CPep in PEGylated form in T1D mice model (s.c.) for 20 weeks at a dose of 0.1–1.3 mg/kg twice a week showed higher plasma concentration as compared to native CPep administration at a higher dose of 0.4-1.3 mg/kg twice a day for the treatment of functional disorders in peripheral neuropathy including slowing of motor and sensory nerve conduction. [89] Recently, we came across a formulation of CPep by Z. Nataliya et al. that is, self-assembled nano spores wherein, C-peptide was bound onto novel nanospheres fabricated using random amphiphilic polypeptides to make it long acting and stable. It also exhibited a more pronounced biological effect by stimulating the activity of Na+/K+-ATPase in erythrocytes compared to the native peptide. [91]

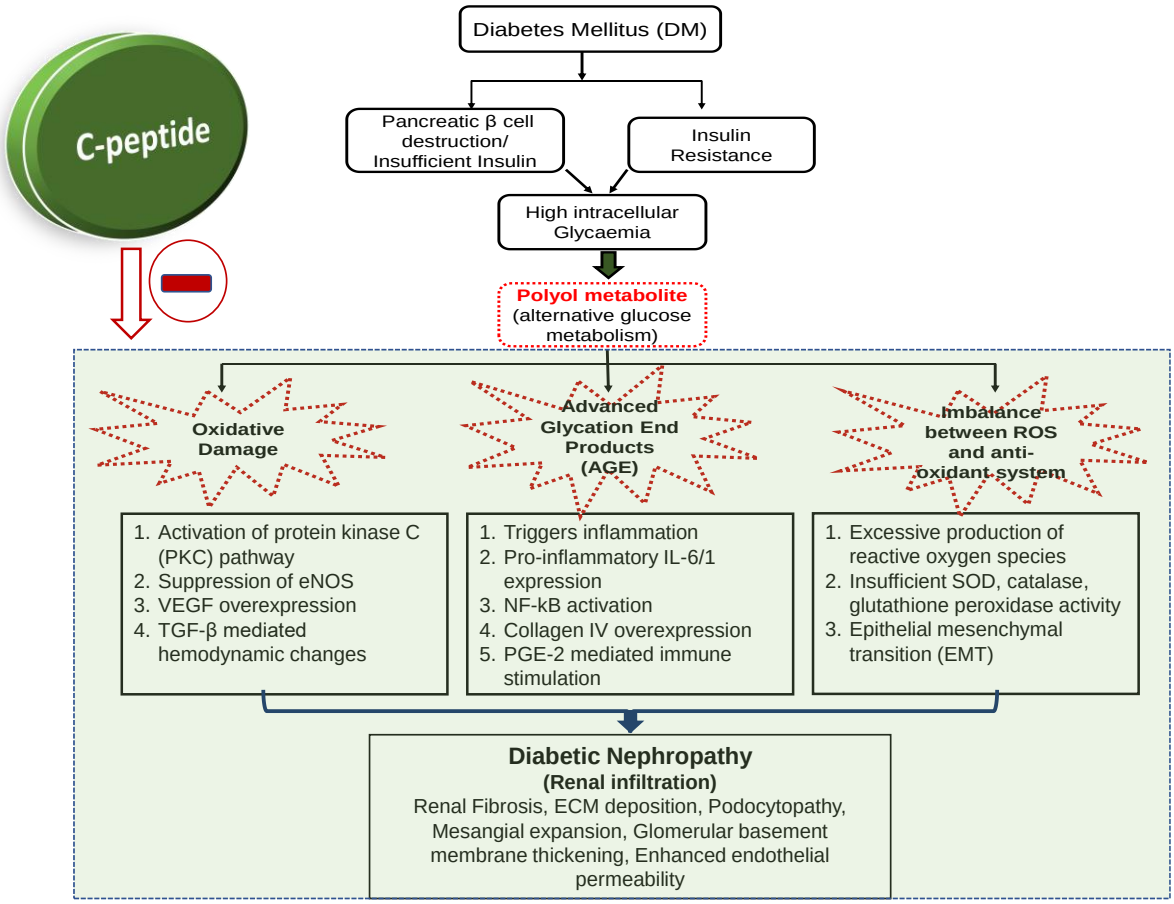


**Figure 1.5** Role of CPep in DN.

## 1.6 Combination delivery of small molecule drug and peptide

Various strategies have been employed to encapsulate therapeutics for treatment of DN, including the prodrug approach, polymeric nanoparticles, ligand or antibody-based formulations, liposomes, and inorganic nanoparticles. [13, 24] Prodrugs modified with amino acids, folate, and sugar moieties have demonstrated potential renal targeting activity. For instance, the Prednisolone succinate–glucosamine (PSG) conjugate showed 2.2 times higher uptake in human proximal renal tubular epithelial (HK-2) cells. [115] Reports on the co-delivery of small molecules for the treatment of DN included the use of hyaluronic acid (HA)-functionalized chitosan nanoparticles (CS-NPs) for efficient topical co-delivery of curcumin (CUR) and resveratrol (REV). Ionic-crosslinking techniques were employed to fabricate HA-functionalized co-loaded nanoparticles (HA-CUR-REV-CS-NPs), effectively entrapping both CUR (98.6 ± 1.8 %) and REV (51.9 ± 1.9 %). [116] In another study, a coaxial electrospray synthesis method was utilized to co-load the SGLT2 inhibitor dapagliflozin and thiazide diuretics indapamide into elliptical tri-layer PLGA nanoparticles. This demonstrated sustained and prolonged release of dapagliflozin and indapamide from trilayer structure compared to monolayer nanoparticles. In the most effective trilayer structures, 90 % of dapagliflozin and

indapamide were released after 120 and 144 h respectively. This release rate was notably 5–6 times slower compared to monolayer particles. [117] In a study by Yang et al., the combination of exendin-4 (Ex-4; 18 nM/day) and LSF (27 mg/kg/day) administered subcutaneously by Alzet osmotic minipumps was examined for its ability to create a stable systemic delivery over 14 days. The goal of this combination therapy was to stimulate β-cell function and to prevent cytokine damage to pancreas in the NOD mice model and reverse T1DM. The specific mechanism underlying the synergistic action of LSF and Ex-4 was not outlined in the study. However, it has been found that LSF enhanced mitochondrial activity and prevented the emergence of STAT-4 activation in tissues of interest, whereas Ex-4 acted as an activator of the GLP-1 receptor by inducing cyclic AMP and protein kinase A stimulation. The outcomes showed that insulin-dependent autoimmune diabetes was effectively reversed in the NOD mice model by combined therapy using LSF and Ex-4. [118] While these studies highlight innovative co-delivery approaches, the overall impact of these formulations on diabetes or its complications has not been extensively emphasized. Biologically active low-molecular-weight proteins (LMWP) with a molecular weight less than 30 kDa are considered promising to deliver the drugs to kidney. These proteins are readily reabsorbed in the renal tubules after being filtered by the glomerulus. In a recent study, a lipo-nanoparticle was developed, consisting of a polycaprolactone-polyethyleneimine (PCL-PEI) nanoparticle of rhein layered with kidney-targeting peptide (KTP)-modified DSPE-PEG lipids (DSPE-PEG-KTP). This formulation exhibited excellent kidney-targeted distribution and low urinary excretion in mice with STZ-induced DN. [119] In summary, several strategies have been devised for the targeted delivery of therapeutics for the treatment of DN, and polymer-based peptide delivery is an extensively explored domain in this context. [74]

The beneficial effects of native CPep have been reported in various diabetic complications, such as diabetic retinopathy, nephropathy, and neuropathy. [120, 121] Ha and colleagues conjugated recombinant CPep with a lysine-containing elastin-like polypeptide (K9-C-peptide) to obtain controlled release. It was demonstrated that a single subcutaneous injection of this CPep-conjugated biopolymer slowly released human CPep into the bloodstream for 19 days, providing protection against diabetic aortic dysfunction in T1DM mice. [93] Another noteworthy report discusses the co-delivery of CPep with insulin in a poly-L-lysine-coated oral water-in-oil-in-water (w/o/w) nano-emulsion formulation. This protective coating helped shield insulin and CPep from the harsh gastrointestinal environment, facilitating transcellular transport of macromolecules. This approach improves the pharmacokinetic profile of insulin after oral administration, offering a potential strategy for enhanced therapeutic efficacy. [122]

In the present thesis work, co-delivery strategies are explored for their potential benefits in the treatment of DN. However, there is a pressing need to accord greater significance to the assessment of the therapeutic effects of combination of potent molecules in diseased animal models. Notably, the combined therapy involving CPep and the anti-inflammatory agent LSF is yet to be thoroughly evaluated, both in terms of formulation development and its effectiveness in treating DN. Further investigation in this area is warranted to gauge the potential synergistic effects and to enhance our understanding of the therapeutic efficacy of this combination approach for DN treatment.

**1.7 Gaps in existing research**

DN stands as one of the predominant causes of end-stage renal disease globally. As the prevalence of diabetes continues to escalate, the incidence of DN is poised to reach pandemic proportions. Current treatment approaches for DN primarily target the control of blood pressure, hyperglycemia, and cholesterol levels, yet often overlook the progression mechanisms underlying the disease at the molecular level. The prolonged renal deterioration resulting due to either T1DM or T2DM can trigger DN and other diabetic complications. Initially characterized by hyperglycemia, this condition gradually leads to the deterioration of kidney function, marked by inflammation, fibrosis, and oxidative stress. Emerging strategies for the treatment of DN involve innovative approaches such as targeting interrelated enzymes and interrupting cell signaling pathways. Among these strategies, CPep, a therapeutic agent, plays a crucial role in modulating intracellular signaling pathways, offering a potent renoprotective effect in DN. However, a significant limitation of this promising peptide is its very short half-life, rapid clearance, and suboptimal efficacy. Additionally, the treatment of DN faces challenges due to the altered vascularity of the kidney; compromised tubular secretion and glomerular filtration requiring administration of higher doses of drugs to effectively reach and sustain itself within the kidney.

There is a pressing need for transition from conventional treatment with small molecules to advanced therapies facilitated by modified drug delivery systems. Small molecules pose challenges including, hydrophilicity, susceptibility to rapid metabolism, short half-life, rapid clearance, and poor oral bioavailability. Given the necessity for combination delivery to target multiple sites in diabetic patients, we propose a delivery system that combines both a small molecule (LSF) and a macromolecule (CPep). This integrated approach offers a broad range of action and has the potential to form a robust therapeutic combination for the treatment of DN. Currently, there are no reported studies on combination of CPep with a small molecule drug

like LSF for the treatment of diabetes and DN. Further, no initiatives have been undertaken to formulate these molecules into a drug delivery system.

To deliver these two potent molecules fraught with physicochemical and PK challenges, a suitable nanocarrier system was designed. Among the various nanocarriers available, a polymeric system was chosen due to its numerous advantages, including biocompatibility, potential for surface modification, availability in a wide range of molecular weight, cost-effectiveness, and the ability to protect active ingredients from the harsh *in-vivo* environment and the ultimate goal is to ensure the delivery of these molecules at the target site without compromising their pharmacological activity. Subsequently, the work involved selecting a strategy to load these molecules into the polymeric nanocarrier with an aim to achieve high encapsulation and particle size in nano-range for optimal effectiveness. The proposed strategy for combination delivery (CPep + LSF) involved, (i) the conjugation of a fatty acid to LSF to reduce its hydrophilicity and metabolism; (ii) synthesis of a high molecular weight cationic polymer to complex CPep; (iii) formulate the components into nano-sized system with an optimum zeta potential; (iv) ensure the integrity and activity of CPep in physiological microenvironment; and finally, (v) ensuring the simultaneous delivery of both the therapeutic molecules, LSF and CPep, for DN treatment.

### 1.8 Outline of current research work

The current thesis work is focused on the synthesis, characterization, and evaluation of CPep peptide and LSF-fatty acid conjugated prodrug within a cationic polymeric nano-formulation. This approach is designed for the treatment of DN with CPep playing a pivotal role in both the prevention and treatment of DN. Simultaneously, the drug component (LSF) aids in controlling blood glucose levels by preserving the insulin secretory function of β-cells.

Initially, a variety of fatty acids were carefully chosen for screening based on their carbon chain length and degree of unsaturation (double bond) in their chemical structure. These fatty acids were intended for conjugation to LSF to observe any physicochemical and pharmacological alterations in the LSF molecule. The synthesized LSF-fatty acid prodrugs were then subjected to comprehensive characterization and evaluation of their self-assembling nature. Subsequent steps involved *in-vitro* analyses of all the prodrugs in mouse insulinoma cells exposed to inflammatory conditions and *in-vivo* evaluation in a STZ-induced T1D animal model. Following the study, a LSF-oleic acid prodrug (LSF-OA) exhibiting superior *in-vitro*,

pharmacokinetic, and *in-vivo* activities as compared to other LSF-FA prodrugs was selected for further exploration in combination delivery as illustrated in **Figure 1.6**.

To determine the entrapment efficiency, release and stability studies, an analytical method was developed for the synthesized prodrug and CPep. A convenient and versatile reverse-phase high-pressure liquid chromatography (RP-HPLC) method, using a photodiode array detector, was devised and subsequently validated for quantification of both the molecules.

To facilitate the delivery of CPep and LSF-OA prodrug through a polymeric nanocarrier system, a high molecular weight cationic polymer was synthesized and characterized. Subsequently, positively charged blank nanospheres were prepared using single emulsion solvent evaporation method. Initially, the cationic polymeric nanocarrier was employed to electrostatically complex CPep and evaluated for its stability and sustained delivery. This was followed by an *in-vitro* cell-based evaluation under metabolically stressed conditions, pharmacokinetic evaluation, and *in-vivo* efficacy testing conducted in the STZ-induced DN animal model.

Utilizing the aforementioned strategy, a combination delivery system was further developed to co-load LSF-OA prodrug with CPep in a single polymeric nanocarrier system. This system was hypothesized to demonstrate effective antioxidant and anti-inflammatory effects in *in-vitro* cell culture studies and improved parameters in pharmacokinetic evaluation. Subsequently, its *in-vivo* efficacy in preventing and treating damaged renal conditions in a STZ-induced DN animal model was assessed.

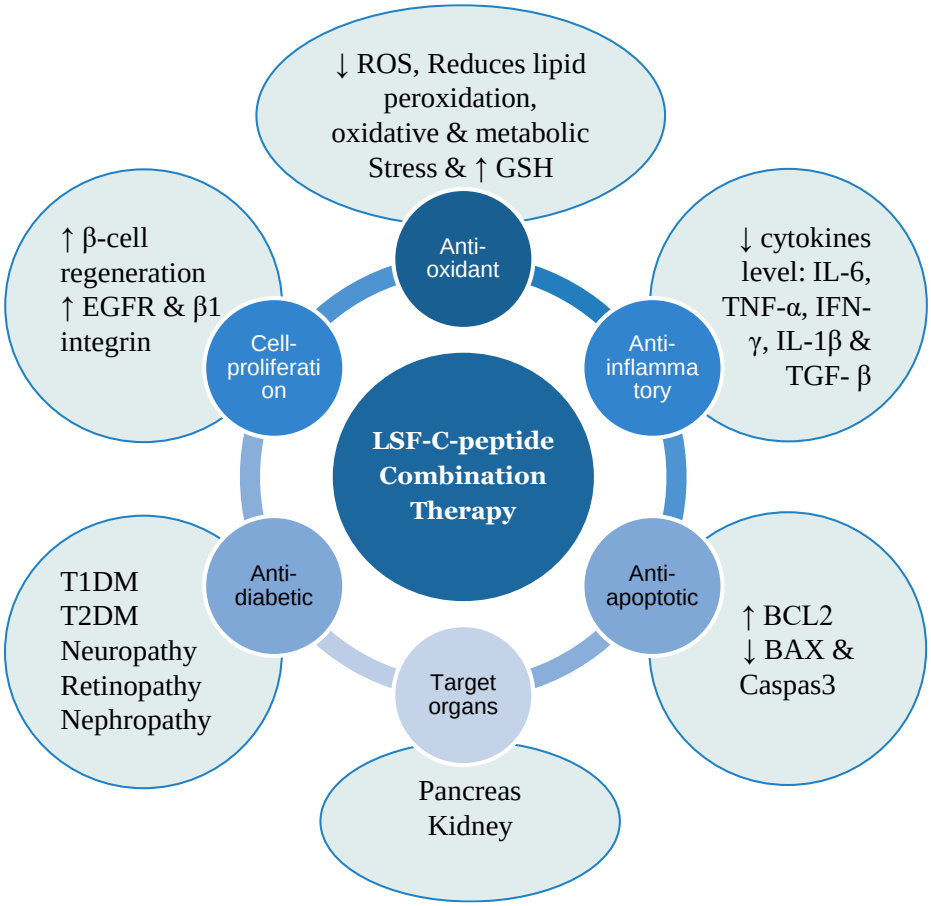


**Figure 1.6** Proposed therapeutic benefits of CPep and LSF combination therapy.

## 1.9 Objectives of proposed work

1. Synthesis, characterization and evaluation of different prodrugs of Lisofylline-fatty acid
    i. Synthesis and characterization of LSF-FA prodrugs (LSF-ALA, LSF-LA, LSF-OA and LSF-PA)
    ii. *In-vitro* cell culture studies of LSF-FA micelles
    iii. *In-vivo* pharmacokinetic study
    iv. *In-vivo* efficacy studies of LSF-FA micelles in STZ-induced T1DM animal model
2. Synthesis, characterization and evaluation of polymeric CPep nano-complexes
    i. Synthesis and characterization of cationic polymer
    ii. Development and evaluation of CPep nano-complexes
    iii. *In-vitro* cell culture-based evaluations of CPep nano-complexes
    iv. *In-vivo* pharmacokinetic study
    v. *In-vivo* efficacy studies of CPep nano-complexes in STZ-induced diabetic nephropathy

3. Development and evaluation of polymeric nano-formulation of LSF-OA prodrug and CPep combination
    i. Formulation development and evaluation of polymeric mPLM-LSF-OA-CPep nanoparticles
    ii. *In-vitro* cell culture studies of mPLM-LSF-OA-CPep nanoparticles
    iii. *In-vivo* pharmacokinetic study
    iv. *In-vivo* efficacy study of mPLM-LSF-OA-CPep nanoparticles in STZ-induced diabetic nephropathy

## 1.10 Bibliography

[1] K. Ogurtsova, L. Guariguata, N.C. Barengo, P.L.-D. Ruiz, J.W. Sacre, S. Karuranga, H. Sun, E.J. Boyko, D.J. Magliano, IDF diabetes Atlas: Global estimates of undiagnosed diabetes in adults for 2021, Diabetes research and clinical practice 183 (2022) 109118.

[2] A.D. Association, Diagnosis and classification of diabetes mellitus, Diabetes care 37(Supplement_1) (2014) S81-S90.

[3] M. Yau, N.K. Maclaren, M.A. Sperling, Etiology and pathogenesis of diabetes mellitus in children and adolescents, Endotext [Internet] (2021).

[4] R.T. Varghese, I. Jialal, C. Doerr, Diabetic nephropathy (nursing), StatPearls [Internet], StatPearls Publishing2022.

[5] K. Umanath, J.B. Lewis, Update on diabetic nephropathy: core curriculum 2018, American journal of kidney diseases 71(6) (2018) 884-895.

[6] S.E. Inzucchi, R.M. Bergenstal, J.B. Buse, M. Diamant, E. Ferrannini, M. Nauck, A.L. Peters, A. Tsapas, R. Wender, D.R. Matthews, Management of hyperglycemia in type 2 diabetes: a patient-centered approach: position statement of the American Diabetes Association (ADA) and the European Association for the Study of Diabetes (EASD), Diabetes Care 35(6) (2012) 1364-79.

[7] N.G. Forouhi, N.J. Wareham, Epidemiology of diabetes, Medicine (Abingdon) 42(12) (2014) 698-702.

[8] L. Chen, D.J. Magliano, P.Z. Zimmet, The worldwide epidemiology of type 2 diabetes mellitus—present and future perspectives, Nature reviews endocrinology 8(4) (2012) 228-236.

[9] P.Z. Zimmet, K.G.M. Alberti, Epidemiology of diabetes—status of a pandemic and issues around metabolic surgery, Diabetes care 39(6) (2016) 878-883.

[10] A. Martínez-Castelao, J.F. Navarro-González, J.L. Górriz, F. De Alvaro, The concept and the epidemiology of diabetic nephropathy have changed in recent years, Journal of clinical medicine 4(6) (2015) 1207-1216.

[11] Y. Wen, S.D. Crowley, The varying roles of macrophages in kidney injury and repair, Current opinion in nephrology and hypertension 29(3) (2020) 286.

[12] A. Qaseem, T.J. Wilt, D. Kansagara, C. Horwitch, M.J. Barry, M.A. Forciea, C.G.C.o.t.A.C.o. Physicians*, Hemoglobin A1c targets for glycemic control with pharmacologic therapy for nonpregnant adults with type 2 diabetes mellitus: a guidance statement update from the American College of Physicians, Annals of internal medicine 168(8) (2018) 569-576.

[13] B. Lin, Y.-Y. Ma, J.-W. Wang, Nano-technological approaches for targeting kidney diseases with focus on diabetic nephropathy: recent progress, and future perspectives, Frontiers in Bioengineering and Biotechnology 10 (2022) 870049.

[14] L.S. Gewin, TGF-β and diabetic nephropathy: Lessons learned over the past 20 years, The American journal of the medical sciences 359(2) (2020) 70-72.

[15] M. Lv, Z. Chen, G. Hu, Q. Li, Therapeutic strategies of diabetic nephropathy: recent progress and future perspectives, Drug Discovery Today 20(3) (2015) 332-346.

[16] J. Yabuuchi, S. Ueda, S.-i. Yamagishi, N. Nohara, H. Nagasawa, K. Wakabayashi, T. Matsui, H. Yuichiro, T. Kadoguchi, T. Otsuka, Association of advanced glycation end products with sarcopenia and frailty in chronic kidney disease, Scientific Reports 10(1) (2020) 17647.

[17] C.-F. Lien, S.-J. Chen, M.-C. Tsai, C.-S. Lin, Potential role of protein kinase C in the pathophysiology of diabetes-associated atherosclerosis, Frontiers in pharmacology 12 (2021) 716332.

[18] V. Thallas-Bonke, S.M. Tan, R.S. Lindblom, M. Snelson, C. Granata, J.C. Jha, K.C. Sourris, A. Laskowski, A. Watson, M. Tauc, Targeted deletion of nicotinamide adenine dinucleotide phosphate oxidase 4 from proximal tubules is dispensable for diabetic kidney disease development, Nephrology Dialysis Transplantation 36(6) (2021) 988-997.

[19] L. Wu, M. Chen, H. Mao, N. Wang, B. Zhang, X. Zhao, J. Qian, C. Xing, Albumin-based nanoparticles as methylprednisolone carriers for targeted delivery towards the neonatal Fc receptor in glomerular podocytes, International journal of molecular medicine 39(4) (2017) 851-860.

[20] J.E. Zuckerman, A. Gale, P. Wu, R. Ma, M.E. Davis, siRNA delivery to the glomerular mesangium using polycationic cyclodextrin nanoparticles containing siRNA, Nucleic acid therapeutics 25(2) (2015) 53-64.

[21] N. Raval, P. Gondaliya, V. Tambe, K. Kalia, R.K. Tekade, Engineered nanoplex mediated targeted miRNA delivery to rescue dying podocytes in diabetic nephropathy, International Journal of Pharmaceutics 605 (2021) 120842.

[22] N. Samsu, Diabetic nephropathy: challenges in pathogenesis, diagnosis, and treatment, BioMed research international 2021 (2021).

[23] C.C. Betônico, S.M. Titan, M.L.C. Correa-Giannella, M. Nery, M. Queiroz, Management of diabetes mellitus in individuals with chronic kidney disease: therapeutic perspectives and glycemic control, Clinics 71 (2016) 47-53.

[24] S. Uppal, K.S. Italiya, D. Chitkara, A. Mittal, Nanoparticulate-based drug delivery systems for small molecule anti-diabetic drugs: an emerging paradigm for effective therapy, Acta Biomater. 81 (2018) 20-42.

[25] S.C. Satchell, F. Braet, Glomerular endothelial cell fenestrations: an integral component of the glomerular filtration barrier, American Journal of Physiology-Renal Physiology 296(5) (2009) F947-F956.

[26] S. Ogawa, Z. Ota, K. Shikata, K. Hironaka, Y. Hayashi, K. Ota, M. Kushiro, N. Miyatake, N. Kishimoto, H. Makino, High-resolution ultrastructural comparison of renal glomerular and tubular basement membranes, American journal of nephrology 19(6) (1999) 686-693.

[27] A.-T. Lahdenkari, K. Lounatmaa, J. Patrakka, C. Holmberg, J. Wartiovaara, M. Kestila, O. Koskimies, H. Jalanko, Podocytes are firmly attached to glomerular basement membrane in kidneys with heavy proteinuria, Journal of the American Society of Nephrology 15(10) (2004) 2611-2618.

[28] K. Manna, S. Mishra, M. Saha, S. Mahapatra, C. Saha, G. Yenge, N. Gaikwad, R. Pal, D. Oulkar, K. Banerjee, Amelioration of diabetic nephropathy using pomegranate peel extract-stabilized gold nanoparticles: assessment of NF-κB and Nrf2 signaling system, International journal of nanomedicine (2019) 1753-1777.

[29] D. Care, Standards of medical care in diabetes 2019, Diabetes Care 42(Suppl 1) (2019) S124-38.

[30] M. Shomali, Diabetes treatment in 2025: can scientific advances keep pace with prevalence?, Therapeutic advances in endocrinology and metabolism 3(5) (2012) 163-173.

[31] S. Rathod, Novel insights into the immunotherapy-based treatment strategy for autoimmune type 1 diabetes, Diabetology 3(1) (2022) 79-96.

[32] R. Kumar, D. Kerins, T. Walther, Cardiovascular safety of anti-diabetic drugs, European Heart Journal-Cardiovascular Pharmacotherapy 2(1) (2016) 32-43.

[33] A. Chaudhury, C. Duvoor, V.S. Reddy Dendi, S. Kraleti, A. Chada, R. Ravilla, A. Marco, N.S. Shekhawat, M.T. Montales, K. Kuriakose, Clinical review of antidiabetic drugs: implications for type 2 diabetes mellitus management, Frontiers in endocrinology 8 (2017) 6.

[34] P. Zimmet, K. Alberti, J. Shaw, Global and societal implications of the diabetes epidemic, Nature 414(6865) (2001) 782-787.

[35] D.E. Moller, New drug targets for type 2 diabetes and the metabolic syndrome, Nature 414(6865) (2001) 821-827.

[36] J.S. Striffler, J.L. Nadler, Lisofylline, a novel anti-inflammatory agent, enhances glucose-stimulated insulin secretion in vivo and in vitro: studies in prediabetic and normal rats, Metabolism 53(3) (2004) 290-296.

[37] A. Świerczek, E. Wyska, K. Pociecha, S. Baś, J. Mlynarski, Influence of inflammatory disorders on pharmacokinetics of lisofylline in rats: implications for studies in humans, Xenobiotica (2018).

[38] J.W. Singer, S.L. Rursten, G.C. Rice, W. Perry Gordon, J.A. Bianco, Inhibitors of intracellular phosphatidic acid production: novel therapeutics with broad clinical applications, Expert Opinion on Investigational Drugs 3(6) (1994) 631-644.

[39] K. Waxman, K. Daughters, S. Aswani, G. Rice, Lisofylline decreases white cell adhesiveness and improves survival after experimental hemorrhagic shock, Critical care medicine 24(10) (1996) 1724-1728.

[40] E. Abraham, S. Bursten, R. Shenkar, J. Allbee, R. Tuder, P. Woodson, D.M. Guidot, G. Rice, J.W. Singer, J.E. Repine, Phosphatidic acid signaling mediates lung cytokine expression and lung inflammatory injury after hemorrhage in mice, The Journal of experimental medicine 181(2) (1995) 569-575.

[41] E. Wyska, Pharmacokinetic interaction between verapamil and methylxanthine derivatives in mice, Drug Metabolism Letters 4(1) (2010) 15-24.

[42] E. Wyska, E. Pękala, J. Szymura-Oleksiak, Interconversion and tissue distribution of pentoxifylline and lisofylline in mice, Chirality: The Pharmacological, Biological, and Chemical Consequences of Molecular Asymmetry 18(8) (2006) 644-651.

[43] K.S. Italiya, S. Sharma, I. Kothari, D. Chitkara, A. Mittal, Simultaneous estimation of lisofylline and pentoxifylline in rat plasma by high performance liquid chromatography-photodiode array detector and its application to pharmacokinetics in rat, Journal of Chromatography B 1061 (2017) 49-56.

[44] K.S. Italiya, S. Mazumdar, S. Sharma, D. Chitkara, R.I. Mahato, A. Mittal, Self-assembling lisofylline-fatty acid conjugate for effective treatment of diabetes mellitus, Nanomedicine: Nanotechnology, Biology and Medicine 15(1) (2019) 175-187.

[45] Z. Yang, M. Chen, J.L. Nadler, Lisofylline: a potential lead for the treatment of diabetes, Biochemical pharmacology 69(1) (2005) 1-5.

[46] V. Lagente, C. Martin-Chouly, E. Boichot, M.A. Martins, P.M. Silva, Selective PDE4 inhibitors as potent anti-inflammatory drugs for the treatment of airway diseases, Memórias do Instituto Oswaldo Cruz 100 (2005) 131-136.

[47] A. Świerczek, E. Wyska, S. Baś, M. Woyciechowska, J. Mlynarski, PK/PD studies on non-selective PDE inhibitors in rats using cAMP as a marker of pharmacological response, Naunyn-schmiedeberg's Archives of Pharmacology 390 (2017) 1047-1059.

[48] E. Bischoff, Potency, selectivity, and consequences of nonselectivity of PDE inhibition, International journal of impotence research 16(1) (2004) S11-S14.

[49] A. Jankowska, A. Swierczek, G. Chlon-Rzepa, M. Pawlowski, E. Wyska, PDE7-selective and dual inhibitors: advances in chemical and biological research, Current medicinal chemistry 24(7) (2017) 673-700.

[50] C.L. George, G. Fantuzzi, S. Bursten, L. Leer, E. Abraham, Effects of lisofylline on hyperoxia-induced lung injury, American Journal of Physiology-Lung Cellular and Molecular Physiology 276(5) (1999) L776-L785.

[51] P. Jones, Development of second generation epigenetic agents, MedChemComm 3(2) (2012) 135-161.

[52] I. Pokotylo, V. Kravets, J. Martinec, E. Ruelland, The phosphatidic acid paradox: too many actions for one molecule class? Lessons from plants, Progress in Lipid Research 71 (2018) 43-53.

[53] S. Bursten, R. Weeks, J. West, T. Wilson, D. Porubek, J. Bianco, J. Singer, G. Rice, Potential role for phosphatidic acid in mediating the inflammatory responses to TNF alpha and IL-1 beta, Circulatory shock 44(1) (1994) 14-29.

[54] D. Bleich, S. Chen, S.L. Bursten, J.L. Nadler, Lisofylline, an inhibitor of unsaturated phosphatidic acid generation, ameliorates interleukin-1 beta-induced dysfunction in cultured rat islets, Endocrinology 137(11) (1996) 4871-4877.

[55] Y. Oka, N. Hasegawa, M. Nakayama, G.A. Murphy, H.H. Sussman, T.A. Raffin, Selective downregulation of neutrophils by a phosphatidic acid generation inhibitor in a porcine sepsis model, Journal of Surgical Research 81(2) (1999) 147-155.

[56] A. Świerczek, K. Pociecha, M. Ślusarczyk, G. Chłoń-Rzepa, S. Baś, J. Mlynarski, K. Więckowski, M. Zadrożna, B. Nowak, E. Wyska, Comparative assessment of the new PDE7 inhibitor–GRMS-55 and lisofylline in animal models of immune-related disorders: a PK/PD modeling approach, Pharmaceutical Research 37 (2020) 1-21.

[57] Z. Yang, M. Chen, J.D. Ellett, L.B. Fialkow, J.D. Carter, M. McDuffie, J.L. Nadler, Autoimmune diabetes is blocked in Stat4-deficient mice, Journal of autoimmunity 22(3) (2004) 191-200.

[58] G.R. Stark, H. Cheon, Y. Wang, Responses to cytokines and interferons that depend upon JAKs and STATs, Cold Spring Harbor perspectives in biology 10(1) (2018) a028555.

[59] C. Ferreli, C. Lai, S. August, Y. Buggy, P. Kumar, N. Brownlow, P. Parker, P.S. Friedmann, M. Ardern-Jones, C. Pickard, STAT 4 expression and activation is increased during mitosis in vitro and in vivo in skin-and mucosa-derived cell types: implications in neoplastic and inflammatory skin diseases, Journal of the European Academy of Dermatology and Venereology 31(10) (2017) 1663-1673.

[60] D.V. Sawant, H. Yano, M. Chikina, Q. Zhang, M. Liao, C. Liu, D.J. Callahan, Z. Sun, T. Sun, T. Tabib, Adaptive plasticity of IL-10+ and IL-35+ Treg cells cooperatively promotes tumor T cell exhaustion, Nature immunology 20(6) (2019) 724-735.

[61] E. Wyska, A. Świerczek, K. Pociecha, K. Przejczowska-Pomierny, Physiologically based modeling of lisofylline pharmacokinetics following intravenous administration in mice, European Journal of Drug Metabolism and Pharmacokinetics 41 (2016) 403-412.

[62] Z. Yang, M. Chen, L.B. Fialkow, J.D. Ellett, R. Wu, J.L. Nadler, Inhibition of STAT4 activation by lisofylline is associated with the protection of autoimmune diabetes, Annals of the New York Academy of Sciences 1005(1) (2003) 409-411.

[63] J.J. Bright, C. Du, M. Coon, S. Sriram, S.J. Klaus, Prevention of experimental allergic encephalomyelitis via inhibition of IL-12 signaling and IL-12-mediated Th1 differentiation: an effect of the novel anti-inflammatory drug lisofylline, The Journal of Immunology 161(12) (1998) 7015-7022.

[64] P. Cui, T.L. Macdonald, M. Chen, J.L. Nadler, Synthesis and biological evaluation of lisofylline (LSF) analogs as a potential treatment for Type 1 diabetes, Bioorganic & medicinal chemistry letters 16(13) (2006) 3401-3405.

[65] J.H. Chang, Y. Jiang, V.G. Pillarisetty, Role of immune cells in pancreatic cancer from bench to clinical application: an updated review, Medicine 95(49) (2016).

[66] M. Campbell-Thompson, A. Fu, J.S. Kaddis, C. Wasserfall, D.A. Schatz, A. Pugliese, M.A. Atkinson, Insulitis and β-cell mass in the natural history of type 1 diabetes, Diabetes 65(3) (2016) 719-731.

[67] S.A. Tersey, J.D. Carter, L. Rosenberg, D.A. Taylor-Fishwick, R.G. Mirmira, J.L. Nadler, Amelioration of type 1 diabetes following treatment of non-obese diabetic mice with INGAP and lisofylline, Journal of diabetes mellitus 2(2) (2012) 251.

[68] Z. Yang, M. Chen, L.B. Fialkow, J.D. Ellett, R. Wu, J.L. Nadler, The novel anti-inflammatory compound, lisofylline, prevents diabetes in multiple low-dose streptozotocin-treated mice, Pancreas 26(4) (2003) e99-e104.

[69] S.L. Bursten, D. Federighi, J. Wald, B. Meengs, W. Spickler, E. Nudelman, Lisofylline causes rapid and prolonged suppression of serum levels of free fatty acids, Journal of Pharmacology and Experimental Therapeutics 284(1) (1998) 337-345.

[70] K.S. Italiya, M. Basak, S. Mazumdar, D.K. Sahel, R. Shrivastava, D. Chitkara, A. Mittal, Scalable self-assembling micellar system for enhanced oral bioavailability and efficacy of lisofylline for treatment of type-I diabetes, Molecular Pharmaceutics 16(12) (2019) 4954-4967.

[71] K.S. Italiya, A.K. Singh, D. Chitkara, A. Mittal, Nanoparticulate tablet dosage form of lisofylline-linoleic acid conjugate for type 1 diabetes: in situ single-pass intestinal perfusion (SPIP) studies and pharmacokinetics in rat, AAPS PharmSciTech 22 (2021) 1-12.

[72] A.L. Peters, A.J. Ahmann, T. Battelino, A. Evert, I.B. Hirsch, M.H. Murad, W.E. Winter, H. Wolpert, Diabetes technology—continuous subcutaneous insulin infusion therapy and continuous glucose monitoring in adults: an Endocrine Society clinical practice guideline, The Journal of Clinical Endocrinology & Metabolism 101(11) (2016) 3922-3937.

[73] M.W. Haymond, M.J. Redondo, S. McKay, M.J. Cummins, B. Newswanger, J. Kinzell, S. Prestrelski, Nonaqueous, mini-dose glucagon for treatment of mild hypoglycemia in adults with type 1 diabetes: a dose-seeking study, Diabetes Care 39(3) (2016) 465-468.

[74] H.-Y. Jeon, A.-J. Lee, K.-S. Ha, Polymer-based delivery of peptide drugs to treat diabetes: Normalizing hyperglycemia and preventing diabetic complications, BioChip Journal 16(2) (2022) 111-127.

[75] S. Pechenov, J. Revell, S. Will, J. Naylor, P. Tyagi, C. Patel, L. Liang, L. Tseng, Y. Huang, A.I. Rosenbaum, Development of an orally delivered GLP-1 receptor agonist through peptide engineering and drug delivery to treat chronic disease, Scientific Reports 11(1) (2021) 22521.

[76] M.i.E. Doyle, N.H. Greig, H.W. Holloway, J.A. Betkey, M. Bernier, J.M. Egan, Insertion of an N-terminal 6-aminohexanoic acid after the 7 amino acid position of glucagon-like peptide-1 produces a long-acting hypoglycemic agent, Endocrinology 142(10) (2001) 4462-4468.
[77] M.V. Hager, L.M. Johnson, D. Wootten, P.M. Sexton, S.H. Gellman, β-Arrestin-biased agonists of the GLP-1 receptor from β-amino acid residue incorporation into GLP-1 analogues, Journal of the American Chemical Society 138(45) (2016) 14970-14979.
[78] J.-G. Kim, L.L. Baggio, D.P. Bridon, J.-P. Castaigne, M.F. Robitaille, L. Jetté, C. Benquet, D.J. Drucker, Development and characterization of a glucagon-like peptide 1-albumin conjugate: the ability to activate the glucagon-like peptide 1 receptor in vivo, Diabetes 52(3) (2003) 751-759.
[79] J. Han, Y. Fei, F. Zhou, X. Chen, W. Zheng, J. Fu, Micellar nanomedicine of novel fatty acid modified Xenopus glucagon-like peptide-1: improved physicochemical characteristics and therapeutic utilities for type 2 diabetes, Molecular Pharmaceutics 14(11) (2017) 3954-3967.
[80] R. Ismail, T.N.Q. Phan, F. Laffleur, I. Csóka, A. Bernkop-Schnürch, Hydrophobic ion pairing of a GLP-1 analogue for incorporating into lipid nanocarriers designed for oral delivery, European journal of pharmaceutics and biopharmaceutics 152 (2020) 10-17.
[81] S.-H. Lee, S. Lee, Y.S. Youn, D.H. Na, S.Y. Chae, Y. Byun, K.C. Lee, Synthesis, characterization, and pharmacokinetic studies of PEGylated glucagon-like peptide-1, Bioconjugate chemistry 16(2) (2005) 377-382.
[82] Y. Youn, J. Jeon, S. Chae, S. Lee, K. Lee, PEGylation improves the hypoglycaemic efficacy of intranasally administered glucagon-like peptide-1 in type 2 diabetic db/db mice, Diabetes, Obesity and Metabolism 10(4) (2008) 343-346.
[83] F. Selis, R. Schrepfer, R. Sanna, S. Scaramuzza, G. Tonon, S. Dedoni, P. Onali, G. Orsini, S. Genovese, Enzymatic mono-pegylation of glucagon-like peptide 1 towards long lasting treatment of type 2 diabetes, Results in Pharma Sciences 2 (2012) 58-65.
[84] Y.S. Youn, S.Y. Chae, S. Lee, J.E. Jeon, H.G. Shin, K.C. Lee, Evaluation of therapeutic potentials of site-specific PEGylated glucagon-like peptide-1 isomers as a type 2 anti-diabetic treatment: Insulinotropic activity, glucose-stabilizing capability, and proteolytic stability, biochemical pharmacology 73(1) (2007) 84-93.
[85] P. Li, J. Zhang, Y. Jia, Y. Zhang, Novel mono-PEGylated dimeric GLP-1 conjugate with enhanced receptor activation and prolonged anti-diabetes efficacies, Life sciences 254 (2020) 117752.
[86] C. Zuglianello, A.F. Chamorro, V.A.d. Oliveira, F.H. Xavier Júnior, E. Lemos-Senna, Dextran sulfate/pramlintide polyelectrolyte nanoparticles as a promising delivery system: optimization, evaluation of supramolecular interactions and effect on conformational stability of the peptide drug, Journal of the Brazilian chemical society 32 (2021) 1642-1653.
[87] P. Tyagi, M. Koskinen, J. Mikkola, S. Sarkhel, L. Leino, A. Seth, S. Madalli, S. Will, V.G. Howard, H. Brant, Injectable Biodegradable Silica Depot: Two Months of Sustained Release of the Blood Glucose Lowering Peptide, Pramlintide, Pharmaceutics 14(3) (2022) 553.

[88] D.C. da Silva, L.M.T. Lima, Physico-chemical properties of co-formulated fast-acting insulin with pramlintide, International Journal of Pharmaceutics 547(1-2) (2018) 621-629.

[89] C. Jolivalt, M. Rodriguez, J. Wahren, N. Calcutt, Efficacy of a long-acting C-peptide analogue against peripheral neuropathy in streptozotocin-diabetic mice, Diabetes, Obesity and Metabolism 17(8) (2015) 781-788.

[90] J. Wahren, H. Foyt, M. Daniels, J.C. Arezzo, Long-acting C-peptide and neuropathy in type 1 diabetes: a 12-month clinical trial, Diabetes care 39(4) (2016) 596-602.

[91] N. Zashikhina, V. Sharoyko, M. Antipchik, I. Tarasenko, Y. Anufrikov, A. Lavrentieva, T. Tennikova, E. Korzhikova-Vlakh, Novel formulations of C-peptide with long-acting therapeutic potential for treatment of diabetic complications, Pharmaceutics 11(1) (2019) 27.

[92] S.H. Jung, J.Y. Lee, S.H. Lee, M.H. Kwon, E.T. Han, W.S. Park, S.H. Hong, Y.M. Kim, K.S. Ha, Preventive Effects of Thermosensitive Biopolymer-Conjugated C-Peptide against High Glucose-Induced Endothelial Cell Dysfunction, Macromolecular Bioscience 19(9) (2019) 1900129.

[93] A.J. Lee, Y.J. Lee, H.-Y. Jeon, M. Kim, E.T. Han, W.S. Park, S.H. Hong, Y.M. Kim, K.S. Ha, Application of elastin-like biopolymer-conjugated C-peptide hydrogel for systemic long-term delivery against diabetic aortic dysfunction, Acta Biomaterialia 118 (2020) 32-43.

[94] L. Rosenberg, M. Lipsett, J.-W. Yoon, M. Prentki, R. Wang, H.-S. Jun, G.L. Pittenger, D. Taylor-Fishwick, A.I. Vinik, A pentadecapeptide fragment of islet neogenesis-associated protein increases beta-cell mass and reverses diabetes in C57BL/6J mice, Annals of surgery 240(5) (2004) 875.

[95] F. Francini, H. Del Zotto, M.L. Massa, J.J. Gagliardino, Selective effect of INGAP-PP upon mouse embryonic stem cell differentiation toward islet cells, Regulatory peptides 153(1-3) (2009) 43-48.

[96] I. Wakefield, S. Stephens, R. Foulkes, A. Nesbitt, T. Bourne, The use of surrogate antibodies to evaluate the developmental and reproductive toxicity potential of an anti-TNFα PEGylated Fab′ monoclonal antibody, Toxicological Sciences 122(1) (2011) 170-176.

[97] E.P. Araújo, C.u.T. De Souza, M. Ueno, D.E. Cintra, M.B. Bertolo, J.B. Carvalheira, M.r.J. Saad, L.c.A. Velloso, Infliximab restores glucose homeostasis in an animal model of diet-induced obesity and diabetes, Endocrinology 148(12) (2007) 5991-5997.

[98] A.P. Chapman, PEGylated antibodies and antibody fragments for improved therapy: a review, Advanced drug delivery reviews 54(4) (2002) 531-545.

[99] W. Zhang, Y. Murakawa, K. Wozniak, B. Slusher, A. Sima, The preventive and therapeutic effects of GCPII (NAALADase) inhibition on painful and sensory diabetic neuropathy, Journal of the neurological sciences 247(2) (2006) 217-223.

[100] E.R. Garrido Sanabria, K.M. Wozniak, B.S. Slusher, A. Keller, GCP II (NAALADase) inhibition suppresses mossy fiber-CA3 synaptic neurotransmission by a presynaptic mechanism, Journal of neurophysiology 91(1) (2004) 182-193.

[101] C. Zhong, Q. Luo, J. Jiang, Blockade of N-acetylaspartylglutamate peptidases: a novel protective strategy for brain injuries and neurological disorders, International Journal of Neuroscience 124(12) (2014) 867-873.

[102] J. Tian, M.A. Atkinson, M. Clare-Salzler, A. Herschenfeld, T. Forsthuber, P.V. Lehmann, D.L. Kaufman, Nasal administration of glutamate decarboxylase (GAD65) peptides induces Th2 responses and prevents murine insulin-dependent diabetes, The Journal of experimental medicine 183(4) (1996) 1561-1567.

[103] A.E. Morales, K.M. Thrailkill, GAD-alum immunotherapy in Type 1 diabetes mellitus, Immunotherapy 3(3) (2011) 323-332.

[104] S. Robert, C. Gysemans, T. Takiishi, H. Korf, I. Spagnuolo, G. Sebastiani, K. Van Huynegem, L. Steidler, S. Caluwaerts, P. Demetter, Oral delivery of glutamic acid decarboxylase (GAD)-65 and IL10 by Lactococcus lactis reverses diabetes in recent-onset NOD mice, Diabetes 63(8) (2014) 2876-2887.

[105] B.L. Johansson, K. Borg, E. Fernqvist-Forbes, A. Kernell, T. Odergren, J. Wahren, Beneficial effects of C-peptide on incipient nephropathy and neuropathy in patients with Type 1 diabetes mellitus, Diabetic medicine 17(3) (2000) 181-189.

[106] K. Polonsky, J. Licinio-Paixao, B. Given, W. Pugh, P. Rue, J. Galloway, T. Karrison, B. Frank, Use of biosynthetic human C-peptide in the measurement of insulin secretion rates in normal volunteers and type I diabetic patients, The Journal of clinical investigation 77(1) (1986) 98-105.

[107] B.L. Johansson, A. Kernell, S. Sjöberg, J. Wahren, Influence of combined C-peptide and insulin administration on renal function and metabolic control in diabetes type 1, The Journal of Clinical Endocrinology & Metabolism 77(4) (1993) 976-981.

[108] J. Wahren, K. Ekberg, J. Johansson, M. Henriksson, A. Pramanik, B.-L. Johansson, R. Rigler, H. Jörnvall, Role of C-peptide in human physiology, American Journal of Physiology-Endocrinology And Metabolism 278(5) (2000) E759-E768.

[109] A. Kamikawa, T. Ishii, K. Shimada, K. Makondo, O. Inanami, N. Sakane, T. Yoshida, M. Saito, K. Kimura, Proinsulin C-peptide abrogates type-1 diabetes-induced increase of renal endothelial nitric oxide synthase in rats, Diabetes/metabolism research and reviews 24(4) (2008) 331-338.

[110] L. Sheng, G. Bayliss, S. Zhuang, Epidermal growth factor receptor: a potential therapeutic target for diabetic kidney disease, Frontiers in Pharmacology (2021) 2232.

[111] J. Luo, J. Jiang, H. Huang, F. Jiang, Z. Xu, Z. Zhou, H. Zhu, C-peptide ameliorates high glucose-induced podocyte dysfunction through the regulation of the Notch and TGF-β signaling pathways, Peptides 142 (2021) 170557.

[112] H. Nakamoto, K. Nakayama, N. Emoto, F. Kajiya, The Short-Term Effects of C-Peptide on the Early Diabetes-Related Ultrastructural Changes to the Podocyte Slit Diaphragm of Glomeruli in Rats, Microcirculation 22(2) (2015) 122-132.

[113] M. Bugliani, S. Torri, R. Lupi, S. Del Guerra, M. Grupillo, M. Del Chiaro, F. Mosca, U. Boggi, S. Del Prato, P. Marchetti, Effects of C-peptide on isolated human pancreatic islet cells, Diabetes/metabolism research and reviews 23(3) (2007) 215-219.

[114] K.L. Zapadka, F.J. Becher, A. Gomes dos Santos, S.E. Jackson, Factors affecting the physical stability (aggregation) of peptide therapeutics, Interface focus 7(6) (2017) 20170030.

[115] Y. Lin, X. Sun, T. Gong, Z.R. Zhang, Prednisolone succinate–glucosamine conjugate: Synthesis, characterization and in vitro cellular uptake by kidney cell lines, Chinese Chemical Letters 23(1) (2012) 25-28.

[116] Z. Hussain, M. Pandey, H. Choudhury, P. Ying, T. Xian, T. Kaur, Hyaluronic acid functionalized nanoparticles for simultaneous delivery of curcumin and resveratrol for management of chronic diabetic wounds: Fabrication, characterization, stability and in vitro release kinetics. J Drug Deliv Sci Technol 2020; 57: 101747, 2020.

[117] Y. Zhang, P.-L. Tremblay, T. Zhang, Electrosprayed trilayer poly (d, l-lactide-co-glycolide) nanoparticles for the controlled co-delivery of a SGLT2 inhibitor and a thiazide-like diuretic, Journal of Drug Delivery Science and Technology 81 (2023) 104311.

[118] Z. Yang, M. Chen, J.D. Carter, C.S. Nunemaker, J.C. Garmey, S.D. Kimble, J.L. Nadler, Combined treatment with lisofylline and exendin-4 reverses autoimmune diabetes, Biochemical and Biophysical Research Communications 344(3) (2006) 1017-1022.

[119] G. Wang, Q. Li, D. Chen, B. Wu, Y. Wu, W. Tong, P. Huang, Kidney-targeted rhein-loaded liponanoparticles for diabetic nephropathy therapy via size control and enhancement of renal cellular uptake, Theranostics 9(21) (2019) 6191.

[120] Y.C. Lim, M.P. Bhatt, M.H. Kwon, D. Park, S. Lee, J. Choe, J. Hwang, Y.-M. Kim, K.-S. Ha, Prevention of VEGF-mediated microvascular permeability by C-peptide in diabetic mice, Cardiovascular research 101(1) (2014) 155-164.

[121] K. Ekberg, T. Brismar, B.-L. Johansson, B. Jonsson, P. Lindstrom, J. Wahren, Amelioration of sensory nerve dysfunction by C-peptide in patients with type 1 diabetes, Diabetes 52(2) (2003) 536-541.

[122] R.K. Harsiddharay, A. Gupta, P.K. Singh, S. Rai, Y. Singh, M. Sharma, V. Pawar, A.S. Kedar, J.R. Gayen, M.K. Chourasia, Poly-L-lysine Coated Oral Nanoemulsion for Combined Delivery of Insulin and C-Peptide, Journal of Pharmaceutical Sciences 111(12) (2022) 3352-3361.

XXXXXXXXXXXXXXXXX

# CHAPTER 2

# Development and validation of HPLC based analytical method for quantification of Lisofylline prodrugs and C-peptide

## 2.1 Introduction

Pharmaceutical formulations are developed for treating various diseases using a variety of synthetic and naturally obtained chemical constituents. Various qualitative and quantitative analytical techniques are needed to identify each active ingredient in these dosage forms. Determining the entrapment efficiency, conducting release and stability studies, and other critical investigations are dependent upon the development and validation of analytical techniques for analyzing the active ingredient. [1] Reverse-phase high-performance liquid chromatography (RP-HPLC) with a photodiode array detector (PDA) is usually the technique of first choice for the development of analytical methods; the convenience and versatility of HPLC have led to its popularity as one of the most useful techniques for the analysis of drugs and peptides. In the current investigation, two distinct methods using the high-resolution RP-HPLC method have been developed to determine the concentrations of LSF-OA prodrug and CPep.

LSF is an immunomodulatory and anti-inflammatory drug that has demonstrated efficacy in treating severe infections linked to cancer, acute lung injury caused by hyperoxia, autoimmune diseases such as T1DM, and islet rejection following islet transplantation. [2-5] Additionally, it has proven to exhibit therapeutic potential in the early management and treatment of diabetes by improving the secretion of glucose-stimulated insulin. The fundamental explanation for protective effect rendered by LSF in diabetes is that it normalizes the membrane potential of mitochondria and stimulates energy generation by promoting the metabolic process of mitochondria in β-cells. [6] In spite of the potent activity of LSF, it has major challenges, including high hydrophilicity, short half-life, and is easily metabolized into PTX, resulting in poor oral bioavailability. [7] To overcome the limitations associated with LSF, we have designed an LSF-oleic acid (LSF-OA) prodrug which helps to increase its hydrophobicity and prevents its rapid metabolism thus enhancing its therapeutic efficacy in T1DM and DN.

The analytical and bioanalytical method for LSF have already been reported by our lab. [8] Briefly, an analytical method for simultaneous estimation of LSF and PTX was developed and validated using Inertsil ODS® (C18) column (250 × 4.6 mm, 5 µ) with a mobile phase consisting of methanol: water (65:35 % v/v) run in isocratic mode at a flow rate of 1 ml/min and detected at 273 nm. The above method has been extensively used to determine the concentration of LSF in *in-vitro* release samples and storage stability studies. The bioanalytical method was also developed to analyze pharmacokinetic study samples by modifying the above mobile phase to methanol:water (50:50 % v/v). The samples were prepared by liquid-liquid

extraction method to extract PTX and LSF from rat plasma wherein, 3-isobutyl 1-methyl xanthine (IBMX) was used as an internal standard. [9]

C-peptide (CPep; 31 amino acids, EVEDPQVPQLELGGGPEAGDLQTLALEVARQ, M.W.: 3299.8 g/mol), a structural polypeptide forming a bridge between A and B chains of pro-insulin molecule is released in an equimolar concentration as insulin in the body. [10] C-peptide like various other peptides has a limited in-vivo stability, it has a plasma half-life of 30 min in normal adults and around 40 min in diabetic patients. It also undergoes fast degradation upon storage at 37 °C and above in plasma. It is most unstable at room temperature and stable at 2-8 °C for 7 days. [11] Thus, to maintain a steady concentration in plasma, C-peptide is delivered continuously in its native form until it attains a therapeutic concentration in plasma. [10] It has an isoelectric point at pH 3.0, is negatively charged, and does not show an ordered tertiary structure under normal physiological conditions. [12] Functional aspects of C-peptide have been examined in numerous studies. In an investigation, the C-terminal pentapeptide of rat C-peptide was reported to activate Na+/K+-ATPase activity in renal tubular segments to the same extent as that of a full-length C-peptide. [13] It has a promising anti-inflammatory and renoprotective role in improving diabetic conditions and, hence could be a promising therapeutic molecule for treating DN because of an abundance of its receptor in the renal tissues. RP-HPLC, a technique employed for separating proteins based on relative hydrophobicity is possibly the most commonly utilized analytical technique for peptide and protein separation as well as analysis in a wide range of applications. [14] Initially, HPLC methods were established for separating and measuring insulin and CPep from protein mixtures; however, these typically need long run time and use buffers as mobile phases, which are frequently responsible for salt precipitation and pressure fluctuation in HPLC. [15]

In the current chapter, we aim to design an easy-to-use, sensitive, reproducible, and selective RP-HPLC-based analytical technique for the quantification of analytes. In order to quantify LSF-OA and CPep in nanoparticulate carriers, the current chapter outlines the method development and validation according to ICH guideline Q2R(1), the analytical techniques validated in terms of linearity, calibration curve, accuracy, precision, and specificity. [16]

## 2.2 Materials

Lisofylline-oleic acid (LSF-OA) prodrug was synthesized *in house*. CPep of rat origin was custom synthesized and procured from LifeTien, NJ, USA. Tri-flouroacetic acid (TFA) was purchased from SRL Pvt. Ltd. (India). Acetonitrile (ACN; HPLC grade) and sodium acetate

were procured from Merck Ltd. (Mumbai, India). Milli-Q water used to prepare buffers (mobile phase) for method development was obtained using Milli-Q® Reference water purification system. After passing through a 0.22 µ Millipore™ membrane filter (Merck, Darmstadt, Germany), the obtained solvents and buffers were degassed in an ultrasonic bath for a duration of 30 min.

## 2.3 Methods

### 2.3.1 Chromatographic conditions for analysis of LSF-OA prodrug

A Thermo Scientific Ultimate 3000 UHPLC system (Thermo Fisher Scientific, USA) equipped with a pump (LPG-3400SD), diode array detector (DAD 3000) and auto sampler (ACC-3000T) were used with 200 µL sample loop to develop the analytical method. The experimental run was started after the HPLC system was stabilized for about 60 min. LSF-OA chromatogram was generated using Inertsil ODS® (C18) column (250 × 4.6 mm, 5 µm) with mobile phase consisting of ACN: sodium acetate buffer (10mM; pH 3.5) in the ratio 95:05 (% v/v) run in isocratic mode at a flow rate of 1 mL/min and detected at 273 nm. Chromeleon software version 7.2 SR4 was used to manage the hardware and for data interpretation.

*Preparation of stock solution, calibration curve standards and quality control (QC) samples*

To make the primary stock solution of 1 mg/mL, precisely weighed amount of LSF-OA was dissolved in ACN (HPLC grade). Secondary stock solution (100 µg/mL) was prepared from the above stock solution, which was further utilized to prepare calibration samples (1, 10, 20, 50 and 100 µg/mL) by stepwise dilution with ACN. Similarly, the working QC standard samples were prepared by diluting the main stock solution to three concentration levels, i.e. low QC (LQC, 5 µg/mL), medium QC (MQC, 30 µg/mL) and high QC (HQC, 80 µg/mL). Before being used for analysis, all the stock and working solutions were stored in a refrigerator at -20 °C.

### 2.3.2 Chromatographic conditions for analysis of CPep

A Shimadzu HPLC system (Shimadzu, Japan) equipped with a pump (LC-20AD), SPD-M40 PDA detector and auto sampler (SIL-20AC HT) loop was used to develop the analytical method. The experimental runs were started after the HPLC system was stabilized for about 60 min. CPep chromatogram was generated using C18 InertSustain® (GL sciences) column (250 × 4.6 mm, 5 µm) with mobile phase consisting 0.1 % TFA in ACN: 0.1 % TFA in water (solvent B: solvent A) at varying ratios of ACN: 0.01min- 30 %, 21 min- 60 %, 25 min- 100 %, 29 min- 30 % and 34 min- 30 % ( v/v) run in a gradient mode at a flow rate of 1 mL/min

and detected at 220 nm. LC solution software version 7.2 SR4 was used to manage the hardware and for data interpretation.

*Preparation of stock solution, calibration curve standards and QC samples*

To make the primary stock solution of 1 mg/mL, a precisely weighed amount of CPep was dissolved in MQ water (freshly filtered with 0.22 µ membrane). A secondary stock solution (100 µg/mL) was prepared from the above stock solution, which was further utilized for calibration samples (0.5, 1, 10, 20 and 50 µg/mL) preparation by serial dilution with water. Similarly, different concentrations of working QC standard samples were prepared using the stock solution at three concentration levels, i.e. LQC (0.75 µg/mL), MQC (5 µg/mL) and HQC (30 µg/mL). All of the stock and working solutions were stored in a refrigerator at -20 °C till used.

### 2.3.3 Validation of analytical methods for LSF-OA and CPep

#### 2.3.3.1 Linearity and range

Five calibration curves were generated over the course of three days, and least square linear regression analysis was used to assess the linearity of analytical method. Analyte peak areas were plotted against analyte concentrations in the calibration curves.

#### 2.3.3.2 Accuracy and precision

Accuracy and precision were determined by calculating percentage deviation (% Bias) and percentage coefficient of variation (% RSD) of the peak areas of three different QC level concentrations (LQC, MQC and HQC) for both LSF-OA and CPep for intra-day and inter-day assay. Six replicates of each QC sample were used to check the accuracy of the developed method, and the result was represented as % recovery. For intra-day, samples were analysed within one day in triplicate, while inter-day assay were performed for three consecutive days in triplicate for each curve.

#### 2.3.3.3 LOD and LOQ

The signal to noise ratio approach was used to calculate LOD and LOQ for both LSF-OA and CPep. The definition of LOD is the lowest concentration at which the signal-to-noise (S/N) ratio is more than 3, whereas LOQ is the lowest concentration at which the S/N ratio is more than 10. The following formule (**Equation 2.1 and 2.2**) were used to determine the LOD and LOQ.

$$LOD = \frac{3.3\sigma}{s} \quad \text{....Equation 2.1}$$

$$LOQ = \frac{10\sigma}{s}$$ ….**Equation 2.2**

Wherein, $\sigma$ is the standard deviation of the response and s is the slope of the calibration curve.

#### 2.3.3.4 Specificity

The specificity was examined for the developed analytical method in the presence of formulation excipients. The QC samples were spiked with known concentration of excipients such as polymer and tween 80 to carry outspecificity analysis. After dissolving/dispersing the excipients in the mobile phase and sonicating them for 15 min, the QC samples of LSF were spiked with these solutions, and the validated HPLC method was employed for analysis. Any evidence of interference of any of the formulation ingredients at the retention time of the analyte was recorded.

#### 2.3.3.5 System suitability

To verify the suitability of the chromatographic system for intended analysis, a system suitability test was performed by running six replicate injections of a standard solution of LSF-OA (30 µg/mL), CPep (5 µg/mL) and % RSD between retention time was determined along with tailing factor, number of theoretical plates (N) and height equivalent to a theoretical plate (HETP).

## 2.4 Results

### 2.4.1 LSF-OA: RP-HPLC method development and validation

The HPLC method for LSF-OA prodrug was successfully developed using the chromatographic parameters shown in **Table 2.1**. **Figure 2.1 A** shows the representative chromatogram with the retention time (Rt) of 19.69 min for LSF-OA. Validation of the method was performed for accuracy, precision, specificity and system suitability as per the guidelines.

**Table 2.1**
Chromatographic conditions for analytical method of LSF-OA prodrug.

| **Chromatographic conditions** | |
|---|---|
| Instrument | Ultimate HPLC 3000, Thermo Fisher Scientific |
| Column | Inertsil® ODS (C18), (250 × 4.6 mm, 5 µ) |
| Mobile Phase (Isocratic mode) | Acetonitrile: sodium acetate buffer pH 3.5 (95:05 % v/v) |
| Flow rate | 1 mL/min |
| Column Temperature | 30 ± 0.5°C |
| Injection Volume | 20 µL |
| Wavelength | 273 nm |

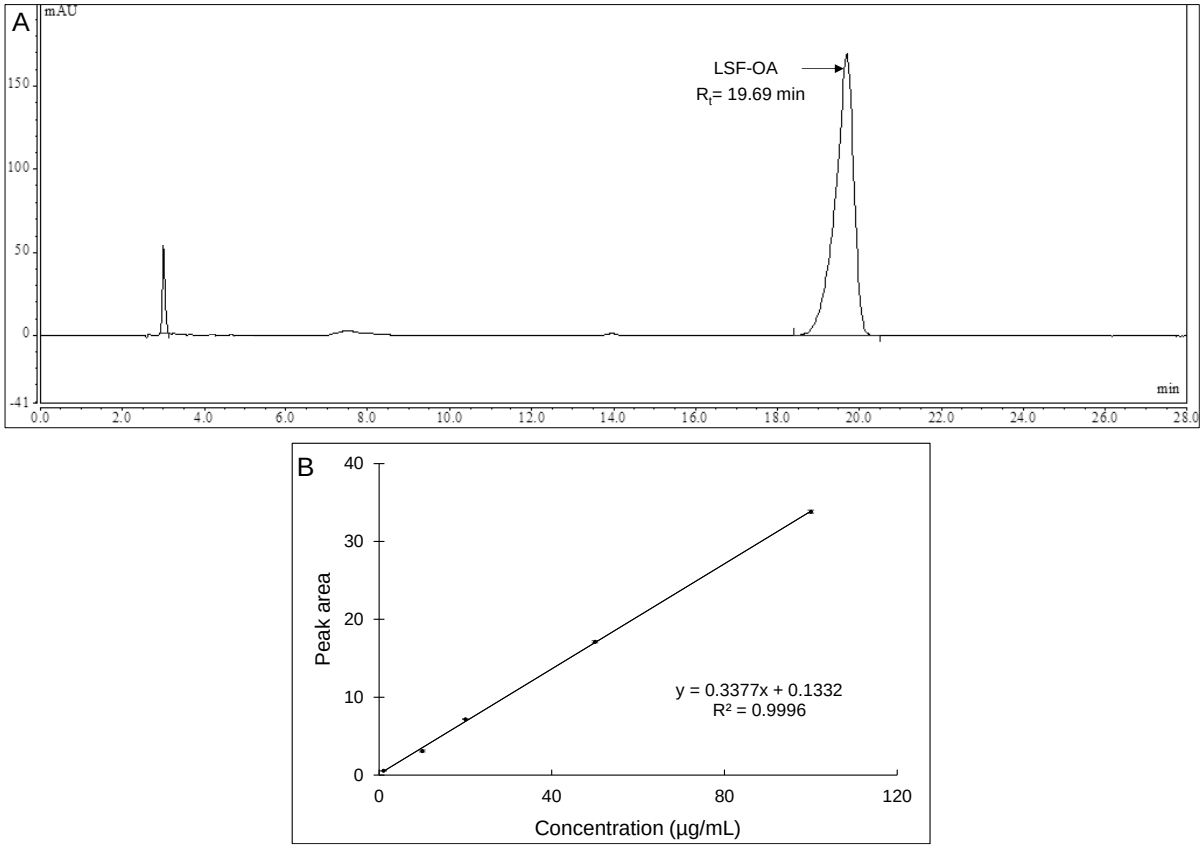


**Figure 2.1** A) Representative chromatogram of LSF-OA using the developed method. B) Calibration curve for LSF-OA prodrug.

### 2.4.1.1 Linearity and range

The calibration curve of LSF-OA prodrug prepared using five working standards in the 1 to 100 µg/mL concentration range exhibited good linearity with an $R^2$ value of 0.9996 **(Figure 2.1 B)**.

### 2.4.1.2 Accuracy and precision

Intra-day and inter-day samples of accuracy and precision of both the analytes were run and analyzed in triplicate **(Table 2.2)**. The precision represented as intra-day and inter-day % RSD of QC samples was found to be ≤ 3.73 and ≤ 3.41 % respectively for LSF-OA. % Bias of QC samples in intra-day and inter-day samples was ≤ 3.41 and ≤ 2.27 %. It was seen that both were within the range of ±5 %.

### 2.4.1.3 LOD and LOQ

The LOD and LOQ of the developed RP-HPLC method for LSF-OA prodrug were found to be 52.54 ng/mL and 159.24 ng/mL, respectively, when calculated from the standard deviation of the y-intercept and slope of the calibration curve using **Equations 2.1 and 2.2**.

**Table 2.2**
Accuracy and precision of QC samples of LSF-OA prodrug by the developed analytical method.

| | Level | Nominal conc. (µg/mL) | Measured conc. (Mean ± SD, µg/mL) | % Accuracy (% Bias) | % Precision (% RSD) |
|---|---|---|---|---|---|
| **Intra day** | LQC | 5 | 4.81 ± 0.01 | 3.73 | 3.41 |
| | MQC | 30 | 30.15 ± 0.21 | -0.50 | 0.70 |
| | HQC | 80 | 79.22 ± 0.80 | 0.98 | 1.01 |
| **Inter day** | LQC | 5 | 4.70 ± 0.11 | 3.35 | 2.27 |
| | MQC | 30 | 29.79 ± 0.23 | 0.68 | 0.77 |
| | HQC | 80 | 77.13 ± 1.61 | 3.59 | 2.09 |

### 2.4.1.4 Specificity

For specificity, the developed method for LSF-OA prodrug was verified with a sample prepared by spiking QC sample with excipients (tween 80 and cationic polymer) dissolved in mobile phase. It was observed that the developed method was specific for LSF-OA.

### 2.4.1.5 System suitability

All the system performance parameters obtained from the system suitability samples indicated that the developed method was suitable for the analysis of LSF-OA prodrug **(Table 2.3)**.

**Table 2.3**
System suitability parameters for LSF-OA analytical method.

| Parameter | Acceptance limit | Result |
|---|---|---|
| Retention time (min) | - | 19.82 ± 0.35 |
| HETP | - | 5.75 ± 0.09 |
| N | > 2000 | 7263.32 ± 345.81 |
| Tailing factor | < 1.5 | 0.96 ± 0.01 |

### 2.4.2 CPep: RP-HPLC method development and validation

For quantification of CPep, an analytical method was developed and validated as per the guidelines for accuracy, precision, specificity and system suitability. Herein, 0.1 % TFA was added to ACN and water as ion-pairing reagent to enable rapid equilibration of the system in gradient method. The method eluted out CPep efficiently at a mobile phase ratio of 45:55 (B:A; 0.1 % TFA in ACN: 0.1 % TFA in water) at 10.87 min retention time in the gradient mode. The total run time was set to 34 min for effective system equilibration **(Table 2.4)**. Followed by method validation.

**Table 2.4**
Chromatographic conditions for analytical method development of CPep.

| **Chromatographic conditions** | |
|---|---|
| Instrument | Shimadzu HPLC, Japan |
| Column | C18 InertSustain® (GL sciences), (250 × 4.6 mm, 5 µ) |
| Mobile Phase (Gradient mode) | A- 0.1 % TFA in water<br>B- 0.1 % TFA in Acetonitrile |
| Gradient program | Solvent B: 0.01min- 30 %, 21 min- 60 %, 25 min- 100 %, 29 min- 30 % & 34 min- 30 %. |
| Flow rate | 1 mL/min |
| Column Temperature | 30 ± 0.5 °C |
| Injection Volume | 20 µL |
| Wavelength | 220 nm |

### 2.4.2.1 Linearity and range

The calibration curve of CPep exhibited linearity in the concentration range of 0.5 to 50 µg/mL by the ordinary least square method with $R^2$ value of 0.9999 **(Figure 2.2)**.

### 2.4.2.2 Accuracy and precision

The percent accuracy for QC sample was calculated as % Bias for intra-day and inter-day samples and found to be in range of -3.65 to 0.26 % and -5.50 to -0.40 %, respectively. The % accuracy was calculated as % RSD which was in range of 1.63 to 4.41 % and 2.23 to 3.45 % for intra-day and inter-day, respectively **(Table 2.5)**, which was within the recommended range of ± 5 %.

### 2.4.2.3 LOD and LOQ

The LOD and LOQ of the developed RP-HPLC technique for CPep were found to be 38.19 ng/mL and 115.74 ng/mL respectively, when calculated from the standard deviation of the y-intercept and slope of the calibration curve using **Equations 2.1 and 2.2**.

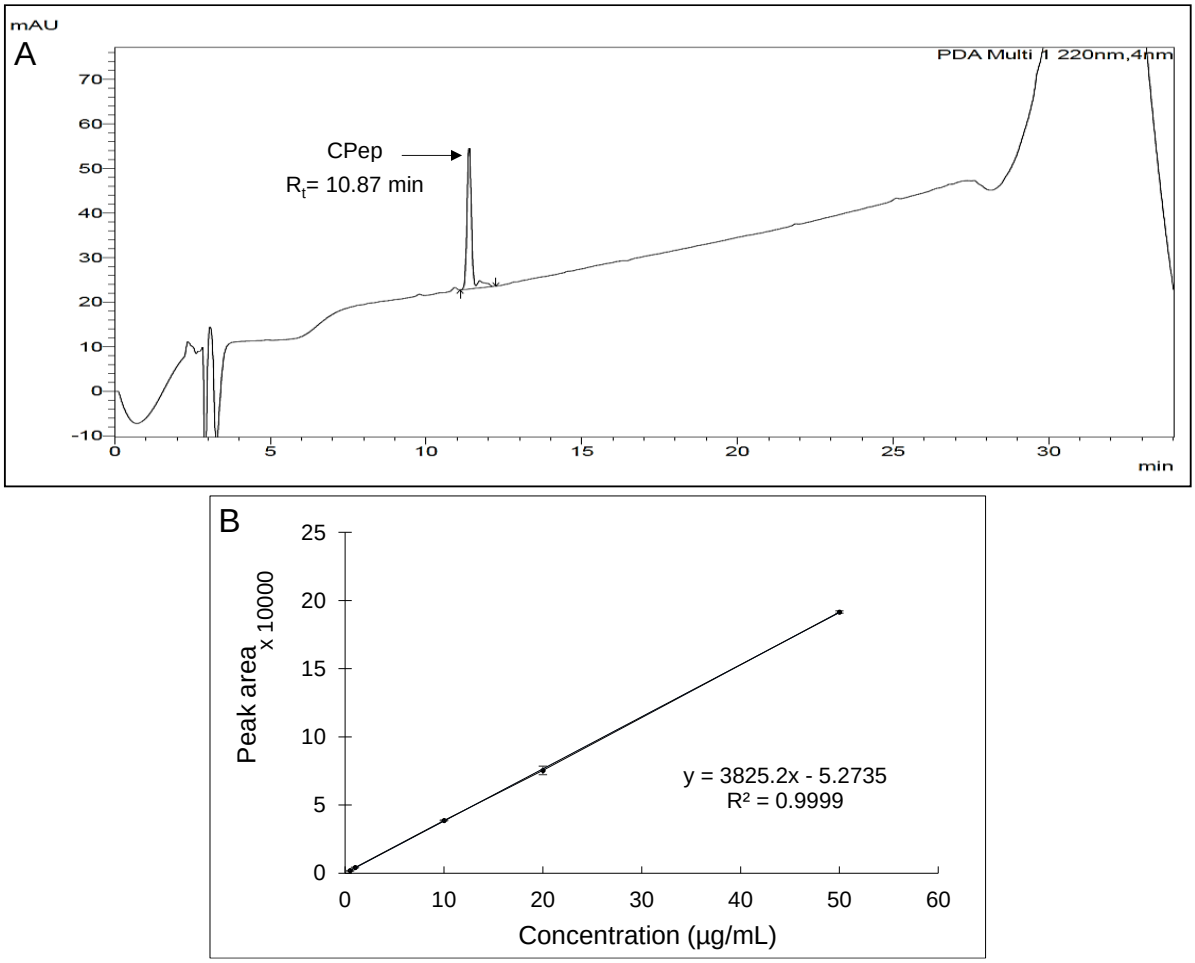


**Figure 2.2** A) Representative chromatogram of CPep using the developed RP-HPLC method and, B) calibration curve of CPep.

**Table 2.5**
Intra-day and inter-day accuracy and precision of QC samples of CPep.

| | Level | Nominal concentration (µg/mL) | Measured conc. (Mean ± SD, µg/mL) | % Accuracy (% Bias) | % Precision (% RSD) |
|---|---|---|---|---|---|
| **Intra day** | LQC | 0.75 | 29.92 ± 0.49 | 0.26 | 1.63 |
| | MQC | 5 | 5.18 ± 0.32 | -3.65 | 4.41 |
| | HQC | 30 | 0.76 ± 0.03 | -1.89 | 3.70 |
| **Inter day** | LQC | 0.75 | 29.77 ± 0.67 | -1.25 | 2.23 |
| | MQC | 5 | 5.02 ± 0.17 | -0.40 | 3.45 |
| | HQC | 30 | 0.79 ± 0.02 | -5.50 | 2.27 |

### 2.4.2.4 Specificity

The method was found to be specific for CPep (in the presence of formulation excipients), with a peak purity index of 0.9998 indicating a pure peak **(Figure 2.3 A and B)**.

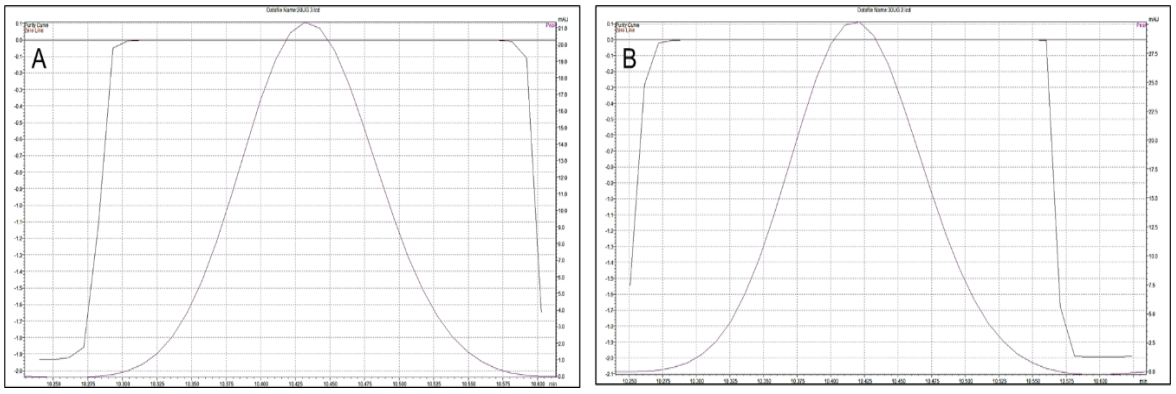


**Figure 2.3** Peak purity curves of A) standard CPep solution, and B) NPX formulation.
NPX: CPep nano-complexes.

### 2.4.2.5 System suitability

The system suitability of developed method was performed using six replicates of the QC sample (5 µg/mL). All the system performance parameters obtained from the system suitability samples indicated that the developed method was suitable for the analysis of CPep **(Table 2.6)**.

**Table 2.6**
System suitability parameters for CPep analytical method.

| Parameter | Acceptance limit | Result |
|---|---|---|
| Retention time (min) | - | 10.77 ± 0.15 |
| HETP | - | 3.98 ± 0.05 |
| N | > 2000 | 37809 ± 455.58 |
| Tailing factor | < 1.5 | 1.04 ± 0.01 |

## 2.5 Discussion

Two distinct RP-HPLC analytical methods were developed and validated for the identification and quantification of an *in-house* synthesized LSF-OA prodrug and a 31 amino acid chain, CPeptide. There were no degradation peaks observed throughout the method development of either of the molecules. Initially, at 1:1 ratio of organic: aqueous phase ratio run at a 1mL/min flow rate, LSF-OA did not elute out even in 30 min of run time. As LSF-OA is very hydrophobic, an increase in the amount of ACN in the mobile phase from 50% to 95% eluted out LSF-OA with a retention time of 23.6 min. However, when MQ water was used as the aqueous phase, tailing and a slight increase in the retention time of LSF-OA peak were observed which was gradually improved to 19.69 min after using sodium acetate buffer (10 mM, pH 3.5). Therefore, ACN: sodium acetate buffer (10 mM, pH 3.5) at 95:05 %v/v with 1.0 mL/min flow rate was selected as the mobile phase for LSF-OA to exhibit the best sensitivity. Further, the selection of sodium acetate buffer over water prevented a drastic change in pH upon

addition of acidic or basic molecules. The above developed method was applied for the analysis of the other synthesized LSF-fatty acids as well.

The gradient method for CPep was developed and validated. For heterogeneous macromolecules, gradient elutions are generally employed for effective resolution of peptide peak, which aims to reduce the analysis time by gradually increasing the concentration of organic solvent (ACN) in mobile phase. [17] Also, TFA was incorporated in the mobile phase for ionizing of peptide molecules and equilibrating the system. The mobile phase gradient elution was adjusted to prevent unwanted disturbances arising due to changes in the concentration of the mobile phase during the gradient elution. To prevent the C18 column deterioration from the acidic pH of mobile phase (0.1% TFA; pH 2.0), a special InertSustain® C18 column was employed to deveop the method under highly acidic condition. With optimization of all the parameters as discussed above, the resolution and intensity of CPep detection and quantification was enhanced and further utilized for generating the calibration curve and validation of the method.

## 2.6 Conclusion

Simple, effective, rapid, sensitive and accurate RP-HPLC based analytical methods were developed and validated for efficient quantification of LSF-OA prodrug and CPep. In accordance with ICH recommendations, this work established new, quick, and validated RP-HPLC methods for determining LSF-OA prodrug and CPep with retention times of 19.8 and 10.8 min, respectively. All parameters were within the range recommended by the ICH guidelines indicating that the methods were specific, precise, and accurate, with sensitive detection and quantification limits. The recommended methods were utilized to analyze the specificity, stability, and release profile of LSF-OA prodrug and CPep released from self-assembled nanoparticulate system in the subsequent experiments.

## 2.7 Bibliography

[1] S. Bonde, C. Bonde, B. Prabhakar, Quality by design based development and validation of HPLC method for simultaneous estimation of paclitaxel and vinorelbine tartrate in dual drug loaded liposomes, Microchemical Journal 149 (2019) 103982.

[2] J.S. Striffler, J.L. Nadler, Lisofylline, a novel anti-inflammatory agent, enhances glucose-stimulated insulin secretion in vivo and in vitro: studies in prediabetic and normal rats, Metabolism 53(3) (2004) 290-296.

[3] K. Waxman, K. Daughters, S. Aswani, G. Rice, Lisofylline decreases white cell adhesiveness and improves survival after experimental hemorrhagic shock, Critical care medicine 24(10) (1996) 1724-1728.

[4] E. Abraham, S. Bursten, R. Shenkar, J. Allbee, R. Tuder, P. Woodson, D.M. Guidot, G. Rice, J.W. Singer, J.E. Repine, Phosphatidic acid signaling mediates lung cytokine expression and lung inflammatory injury after hemorrhage in mice, The Journal of experimental medicine 181(2) (1995) 569-575.

[5] Z. Yang, M. Chen, J.D. Ellett, J.D. Carter, K.L. Brayman, J.L. Nadler, Inflammatory blockade improves human pancreatic islet function and viability, American Journal of Transplantation 5(3) (2005) 475-483.

[6] M. Chen, Z. Yang, R. Wu, J.L. Nadler, Lisofylline, a novel antiinflammatory agent, protects pancreatic β-cells from proinflammatory cytokine damage by promoting mitochondrial metabolism, Endocrinology 143(6) (2002) 2341-2348.

[7] P. Cui, T.L. Macdonald, M. Chen, J.L. Nadler, Synthesis and biological evaluation of lisofylline (LSF) analogs as a potential treatment for Type 1 diabetes, Bioorganic & medicinal chemistry letters 16(13) (2006) 3401-3405.

[8] K.S. Italiya, S. Sharma, I. Kothari, D. Chitkara, A. Mittal, Simultaneous estimation of lisofylline and pentoxifylline in rat plasma by high performance liquid chromatography-photodiode array detector and its application to pharmacokinetics in rat, Journal of Chromatography B 1061 (2017) 49-56.

[9] K.S. Italiya, S. Mazumdar, S. Sharma, D. Chitkara, R.I. Mahato, A. Mittal, Self-assembling lisofylline-fatty acid conjugate for effective treatment of diabetes mellitus, Nanomedicine: Nanotechnology, Biology and Medicine 15(1) (2019) 175-187.

[10] H. Yaribeygi, M. Maleki, T. Sathyapalan, A. Sahebkar, The effect of C-peptide on diabetic nephropathy: A review of molecular mechanisms, Life sciences 237 (2019) 116950.

[11] E. Leighton, C.A. Sainsbury, G.C. Jones, A practical review of C-peptide testing in diabetes, Diabetes therapy 8(3) (2017) 475-487.

[12] M. Landreh, J. Johansson, J. Wahren, H. Jörnvall, The structure, molecular interactions and bioactivities of proinsulin C-peptide correlate with a tripartite molecule, Biomolecular concepts 5(2) (2014) 109-118.

[13] Z. Zhong, O. Kotova, A. Davidescu, I. Ehren, K. Ekberg, H. Jörnvall, J. Wahren, A. Chibalin, C-peptide stimulates Na+, K+-ATPase via activation of ERK1/2 MAP kinases in human renal tubular cells, Cellular and Molecular Life Sciences CMLS 61(21) (2004) 2782-2790.

[14] M.I. Aguilar, HPLC of peptides and proteins: basic theory and methodology, HPLC of peptides and proteins: methods and protocols 251 (2004) 3-8.

[15] B. Sarmento, A. Ribeiro, F. Veiga, D. Ferreira, Development and validation of a rapid reversed-phase HPLC method for the determination of insulin from nanoparticulate systems, Biomedical Chromatography 20(9) (2006) 898-903.

[16] Guideline ICH Harmonized tripartite, Validation of analytical procedures: text and methodology, Q2 (R1) 1(20) (2005) 05.

[17] N.M. González-López, D.S. Insuasty-Cepeda, K.A. Huertas-Ortiz, J.E. Reyes-Calderón, J.A. Martínez-Ramírez, R. Fierro-Medina, Z. Jenny Rivera-Monroy, J.E. García-Castañeda, Gradient Retention Factor Concept Applied to Method Development for Peptide Analysis by Means of RP-HPLC, ACS omega 7(49) (2022) 44817-44824.

XXXXXXXXXXXXXXXXX

# CHAPTER 3

## Synthesis, characterization and evaluation of different prodrugs of Lisofylline-fatty acid

# {LSF-FA Prodrug}

## 3.1 Introduction

DM is a widespread chronic metabolic disorder classified into autoimmune insulin-dependent T1DM mainly diagnosed in young people and non-insulin dependent T2DM more prevalent in the middle-aged and older population. [1] T1DM develops owing to inflammation in the islet of Langerhans of pancreas in patients due to the pro-inflammatory cytokine-mediated β cells dysfunction which leads to chronic complications like kidney failure, blindness and, limb amputation. [2, 3]

Numerous studies have been reported wherein, a drug is covalently bound to a lipid moiety, i.e. phospholipids, glycerides or fatty acids (FAs), particularly for oral and intravenous (i.v.) administration for the treatment of cancer or other diseases and these drug-FA conjugates have shown increased efficacy and permeability, improved oral bioavailability, reduced toxicity, and could also be actively targeted along with enhancing the stability of the compound in biological fluids. [4-11] FAs generally contain a linear chain of carbon atoms with a reactive carboxyl end group that can form a strong ester or amide bond with a drug having α-hydroxyl or amine group. Prodrugs like Capecitabine-palmitic acid and gemcitabine-LA being amphiphilic in nature have been reported to exhibit self-assembling property to form micelles and efficiently target the cancer cells in pre-clinical xenograft model. [12, 13]

FAs are obtained from plants, animals and marine sources and are present in very small amount in the human body. These are endogenous biosynthetic products and are also involved in metabolic pathways like *de novo* synthesis of blood secreted triglycerides. [14] Chemically, these are carboxylic acids with long hydrocarbon chains but differ in carbon chain length and degree of saturation/ unsaturation which defines their physical properties. The hydrophobicity of these molecules' favours translocation of unionized FA through the phospholipid bilayer of the gastro-intestinal membrane. Membrane fluidity and transportation across the membrane is reported to significantly increase as the degree of unsaturation and chain length increases. [15, 16] The translocation of FAs across the membrane is also facilitated by intracellular enzymes and proteins present in the membrane. FAs are classified as saturated and unsaturated FA (SFA and USFA), among these, USFA are further designated according to the positions of double bonds like n-3, 6 and 9 (indicates the number of carbon atoms after double bond). Long chain polyunsaturated fatty acids (PUFA; containing two or more double bonds) play an important role in cholesterol metabolism, blood clotting, immune system regulation and also constitute an important component of most of the biological phospholipidic membranes. [17] Few studies in literature have demonstrated the positive effect of PUFA especially omega-3 FA (ω-3 or n-

3) in improving control over glycaemic levels and insulin sensitivity however, require at least 1-2 g/day dose. [18] Pre-clinical studies have also revealed that FAs like ω-3 and ω-6 play a significant role in reversing or improving the vascular and neural deficit in DN. [19] Epidemiological evidence shows that ingestion of some SFAs unlike USFAs promote insulin resistance. [20] However, unlike other long-chain SFAs, C16 and C18 (FAs with 16 and 18 carbon atoms) are not associated with insulin resistance, β-cell mass reduction and incidents of T2DM. [21] These are derived from food supplements and are also involved endogenously in the de novo lipogenesis pathway. [22] It has earlier been reported that higher the number of double bonds in a FA, greater are the chances of interference in the physiological activities of cells. This has been exemplified in a study on understanding the alteration in cardiolipin (CL), a dimeric phospholipid present in the inner membrane of mitochondria. Different 18-carbon FAs were administrated orally and it was observed that among these FAs, oleic acid (OA; C18:1, 18 carbons with 1 double bond) remained stable whereas, linoleic acid (LA; C18:2) and α-linoleic acid (C18:3) exhibited instability and underwent chain length elongation (up to C20) along with increase in the number of double bonds before getting incorporated into mitochondrial CL thus imparting a significant change in the structure and function of CL. [23]

In the present study, the drug of choice is Lisofylline (LSF) which is a broad-spectrum drug bearing significant clinical utility in preventing both T1DM and T2DM. It regulates the immune cell function to suppress autoimmunity and also retains insulin secretory function of β-cells in the presence of inflammatory cytokines. [2] It is however, known to be non-bioavailable by oral route of administration because it has an extremely short half-life. Also, in pre-clinical studies, it has been administered parenterally, twice daily in T1D animals at a high dose of 25 mg/ kg because of its high metabolism and conversion into pentoxifylline (PTX). [24] LSF has a free hydroxyl group in its structure which is responsible for its high solubility and fast metabolism. Considering this, our group has reported a hydrophobic conjugate of LSF with a FA, LA, LSF-LA; it exhibited self-assembly to form micelles in nano size range and displayed improved anti-diabetic efficacy at a reduced dose of 15 mg/ kg once daily compared to that of free LSF (25 mg/ kg, twice daily). [25] Choice of FA in liposomes is reported to influence the encapsulation efficiency and cytotoxicity of the payload depending upon the carbon chain length of the FA selected. [4, 26] The major focus of our study was to explore different FA that could be conjugated to LSF to obtain LSF-FA prodrugs and to investigate the impact of carbon chain length and degree of unsaturation of the FAs on self-assembling nature of the prodrug, pharmacokinetic behaviour of LSF prodrugs and their anti-diabetic activity.

Among the different FAs selected for the study, LA is an omega-6 FA with an 18 carbon long chain and two double bonds (ω-6 FA). LA is mainly present in vegetable and fish oil. Oleic acid (OA) is also an 18-carbon chain length FA and liquid in nature but has a single double bond (ω-9) which imparts the fluidic nature to cell membrane. SFA like palmitic acid (PA) contains 16 carbon chain without any double bond making cell membrane structure straight and rigid. [27] A functional FA, α-lipoic acid (ALA) was also chosen for the study; it is also known as thioctic acid as it comprises of pentanoic acid with 1,2-dithiolan-3-yl at $5^{th}$ position. It is a heterocyclic FA derived from an octanoic acid. [28]

In the present study, different FA prodrugs, LSF-ALA, LSF-PA, LSF-OA and LSF-LA were synthesized and analysed for self-assembling behaviour by determination of critical micellar concentration (CMC) and micelle aggregation number. The stability and release of free LSF from these prodrugs in plasma was also studied. The non-toxicity of the FAs and synthesized prodrugs was initially confirmed in MIN-6 cells. These cells were then exposed to inflammatory conditions similar to those observed in diabetes to study the protective effect of micelles of LSF prodrugs followed by cell uptake study. All the prodrugs were examined for their pharmacokinetic behaviour in Wistar rats at a single dose of ~15 mg/kg of free LSF. Anti-diabetic activity was monitored by administering the prodrugs by i.p. route daily for 35 days in streptozotocin (STZ) induced T1DM rat model. Post-treatment, evaluation of efficacy was carried out by measuring blood glucose level, plasma insulin level and determining biochemical parameters like SGPT, SGOT, cholesterol, triglyceride, uric acid and total protein. The excised pancreatic tissues of the experimental animals were also studied for histopathological changes by haematoxylin/ eosin (H&E) staining and expression of CD4+ and CD8+ T-cells.

### 3.2 Materials and Reagents

LSF (purity > 98%, HPLC) was synthesized *in house*. As a reference standard, LSF was also procured from Cayman Chemical (Michigan, USA). IBMX as internal standard; HPLC ≥ 99%, 3-[4,5-dimethylthiazol-2-yl]-2,5-diphenyltetrazolium bromide (MTT) and STZ were bought from Sigma Aldrich (St. Louis, MO). 4-dimethylaminopyridine (DMAP) and N-(3-dimethylaminopropyl)-N-ethylcarbodiimide hydrochloride (EDC.HCl) were procured from Spectrochem Ltd. Dulbecco's modified eagle medium (DMEM), TrypLE, fetal bovine serum (FBS) and recombinant proteins (TNF-α, IL-1β and IFN-γ) were obtained from Invitrogen (USA); bovine serum albumin (BSA), dimethyl sulfoxide (DMSO, molecular biology grade) and phosphate buffered saline (PBS) pH 7.4 were purchased from Hi-media laboratories

(Mumbai, INDIA). Fatty acids, LA and OA (99%) were purchased from Acme synthetic chemicals (Mumbai, INDIA) and PA (98%) from Suvidhinath laboratories (Vadodara, Gujarat) and ALA (>99%) from TCI (Tokyo, Japan). Accucheck active glucometer was purchased from Roche diabetes care India Pvt. Ltd. (Mumbai, INDIA). Biochemical parameters were estimated using kits purchased from Coral clinical systems (INDIA). All other chemicals and reagents were of analytical grade and used as obtained. MIN-6 cells were procured from NCCS, Pune (INDIA). Wistar rats (male; 8–10 weeks, 200–220 g) were procured from Central Animal Facility, BITS-PILANI (Pilani, India). All animal experiments were performed in accordance with the guidelines laid down by CPCSEA and the protocols were approved by institutional animal ethics committee (IAEC), BITS-Pilani.

## 3.3 Methods

### 3.3.1 Synthesis of LSF and LSF- FA prodrugs

LSF was synthesized in house as reported earlier. [29] Briefly, in the presence of $NaBH_4$ (reducing agent) and protic solvent methanol, the carbonyl group present in the PTX was reduced to a secondary alcohol. The reaction mixture was stirred at room temperature wherein, the reaction progress was monitored by thin layer chromatography (TLC, toluene: acetone in 1:1 ratio). The resultant product that is, LSF was characterized by HPLC, HR-MS, $^1$H NMR and FT-IR and it was compared to the commercially available LSF (Cayman Chemical).

LSF was chemically conjugated to various FAs namely ALA, LA, PA and OA to obtain prodrugs- LSF-ALA, LSF-LA, LSF-PA and LSF-OA (**Figure 3.1**), using our previously reported method. [25] In brief, the coupling reaction of carbodiimide/DMAP was used to conjugate FAs to the LSF hydroxyl pendant group. At RT and under $N_2$, different FAs including ALA, LA, OA and PA (21.6, 22, 19.2 and 21.1 mmol) were mixed with DMAP (1.2 eq., 21.6 mmol) and EDC.HCl (1.5 eq., 27 mmol) to form a uniform mixture in anhydrous DCM (250 mL). To the reaction mixture, LSF (19.8 mmol) was added and left on stirring in dark for next 36 h. After completion of the reaction (as monitored by TLC using ethyl acetate: hexane in 90:10 ratio), the reaction mixture was washed twice with water and saturated solution of salt, dried over $Na_2SO_4$ and then DCM was evaporated under vacuum. The crude prodrugs so obtained from the above reaction were semi-solid in texture. These crude prodrugs were then purified using flash chromatography (Bonna-Agela Technologies, USA) using ethyl acetate: hexane as mobile phase in different ratios ranging from 45:55 to 95:5 depending upon the lipophilicity of the prodrug (**Table 3.1**). The instrumental parameters for all the prodrugs were set constant; $\lambda_{max}$ 273 nm and 20 ml/min flow rate using a standard packed column (40 g;

dimensions 3.1*14 cm) with silica gel (40-60 µm). The purified prodrugs LSF-ALA, LSF-LA, LSF-PA and LSF-OA were characterized by HPLC, HR-MS, $^{1}$H NMR and FTIR.

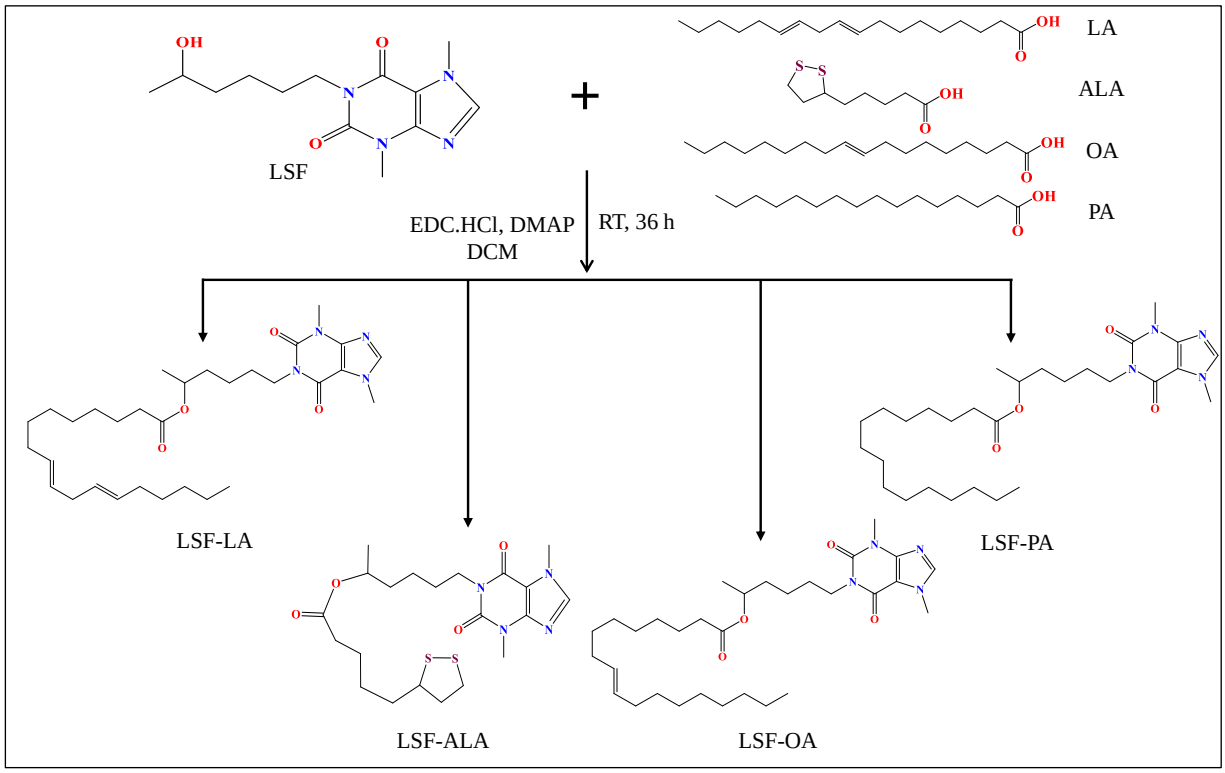


**Figure 3.1** Reaction scheme of synthesized LSF-FA prodrugs using LSF and different FAs.

**Table 3.1**
Mobile phase ratios optimized for elution of purified prodrugs using flash chromatography.

| S. No. | Prodrugs | Mobile Phase | | Elution time (min) |
|---|---|---|---|---|
| | | Hexane | Ethyl acetate | |
| 1 | LSF-ALA | 45 % | 55 % | 71 |
| 2 | LSF-LA | 22 % | 78 % | 102 |
| 3 | LSF-PA | 5 % | 95 % | 140 |
| 4 | LSF-OA | 8 % | 92 % | 125 |

### 3.3.2 Stability of prodrugs in plasma

Each prodrug was dissolved in DMSO (20 mg/mL) and 10 µL of aliquot was spiked in rat plasma (1 mL) and maintained at 37 °C. At predetermined time points, 100 µL aliquots were withdrawn from each prodrug sample. To each of the aliquots, 50 µL IBMX (IS, 2 µg/mL) and 1.8 mL DCM were added and mixed, the mixture was then centrifuged at 3500 rpm, 4°C for 15 min. The organic phase was then transferred into another tube and DCM was evaporated under nitrogen stream. Using 200 µL mobile phase, the dried samples were reconstituted and analysed using our previously reported HPLC based method. [30]

### 3.3.3 Self-assembly of prodrugs

Hydrophilic nature of LSF and hydrophobic nature of FAs, imparted an amphiphilic nature to all the prodrugs leading to their self-assembly into micelles. To study this, solution of prodrugs in DCM was evaporated under vacuum to obtain a thin film which was allowed to undergo self-assembly in aqueous media. The micelles so formed were sonicated for 3 min to enable size reduction. The size and zeta-potential were then recorded for all the prodrug micelles with a scattering angle of 173° using Zetasizer Nano-ZS (Malvern, UK).

### 3.3.4 CMC of prodrugs

The self-assembling ability of the prodrugs was confirmed by fluorescence spectroscopy (RF-5301 Shimadzu, Japan). The CMC value of each prodrug was estimated by using pyrene in aqueous solution. Pyrene dissolved in acetone ($6 \times 10^{-7}$ M) was incubated with different concentrations of prodrugs ($1.0 \times 10^{-5}$ mg/ mL to 1.0 mg/ mL) and kept on stirring at RT under dark conditions for 24 h. The fluorescence intensity of each sample was measured at an excitation range of 300–360 nm and emission at 390 nm with slit width of 5 nm. The ratio of intensities of peaks at $I_1$ and $I_3$ corresponding to wavelengths of 333 nm and 337 nm were recorded, and a graph was plotted between I3/I1 versus log concentrations of prodrugs.

### 3.3.5 Micelle aggregation number ($N_{agg}$) of the prodrugs

Determination of micellar aggregation number of prodrugs was performed by fluorescence steady state method at an excitation wavelength of 318 nm ensuring that no Raman scattering will occur near to the emission peaks projected from 320 nm to 450 nm at 5 nm bandwidth. The probe and quencher (pyrene and cetylpyridinium chloride (CPC), respectively) were used here, wherein, the sample preparation was done by dissolving pyrene ($10^{-4}$ M) in 2 mL ethanol which was then evaporated under nitrogen leaving a thin film of pyrene. This film was reconstituted with 100 mL aqueous solution of micelles of prodrugs at 30 times CMC value of the respective prodrug, with overnight stirring at room temperature (this was named as *solution 1* containing, 2 x $10^{-6}$ M pyrene in 100 mL of micellar solution). Solution 2 was prepared by taking 110.05 mg of CPC in 10 mL of solution 1 (CPC concentration 2.8 x $10^{-3}$ M). The molar concentration of quencher was further varied from 0 to 1.12 x $10^{-3}$ M by diluting it with solution 1 and probe intensities were thereafter recorded.

$$\ln \frac{F_0}{F_Q} = \frac{Q}{M} \qquad \text{…. } \textbf{Equation 3.1}$$

$$\text{where, } M = \frac{C - CMC}{N_{agg}} \qquad \text{.... Equation 3.2}$$

Here, M= micellar concentration, $F_Q$ and $F_0$ = fluorescence intensities of probe with and without quencher, Q = concentration of quencher in micelle solution, C = concentration of prodrug, CMC = critical micelle concentration of prodrug and $N_{agg}$ = aggregation number.

### 3.3.6 Protein interaction of prodrug micelles

BSA was selected here as a model protein which undergoes a change in its UV absorption spectra when incubated with different concentrations of prodrugs micelles. With the help of fluorescence quenching method, the change in protein's fluorescence spectra was recorded after incubating it with micelles using Scatchard equation **(Equation 3.3)**. The binding site present per BSA molecule represents the binding of prodrugs on the vacant sites of the protein.

$$\log \frac{F_0 - F_Q}{F_Q} = \log K_b + n\log[Q] \qquad \text{.... Equation 3.3}$$

where, $F_0$ and $F_Q$ as in the above formula represent the fluorescence intensities in the absence and presence of quencher at any particular concentration (Q), n denotes the number of binding sites per protein molecule and $K_b$ is the apparent binding constant.

Preparation of samples was done by making a series of different concentrations of prodrug micelles (0 to 100 μM) and spiking with a constant amount of BSA (2 μM). Fluorescence intensities were recorded after 30 min of incubation of each sample at excitation and emission wavelength of 280 nm and 343 nm respectively. For the determination of number of binding sites and binding constant, a graph was plotted between log $(F_0\text{-}F_Q)/F_Q$ vs. log of quencher concentration (LSF or prodrug). Further, the mechanism of quenching of BSA molecule by LSF or prodrug was studied by UV-visible spectrophotometer (JASCO V-650) using a 1 cm path length quartz cell.

### 3.3.7 *In-vitro* hemocompatibility study

The interaction of prodrugs' micelles with blood was studied *in-vitro* with modification in the previously reported method. [41] Blood was collected from Wistar rats and mixed with EDTA solution (10% w/v) to prevent coagulation. It was washed 3 times with normal saline solution followed by centrifugation at 1500 rpm for 10 min at 4 °C. The red blood cells (RBCs) so obtained were then diluted in 1:5 ratio with a normal saline solution. Free LSF (20 μM) and prodrugs' micelles (~ 20 μM LSF) were dispersed in 1 mL of RBC suspension with negative and positive control groups (normal saline and 0.1% triton X solution, respectively). After

incubation for 1 h at 37 °C, each sample was centrifuged at 2000 rpm for 5 min and 200 µL of the supernatant was analysed for optical density (OD) at 540 nm using Epoch microplate spectrophotometer (BioTek Instruments, VT, USA). The percentage hemolysis was determined by using **Equation 3.4**.

$$\% \text{ Hemolysis} = \frac{\text{OD}_{\text{Sample}} - \text{OD}_{\text{Negative control}}}{\text{OD}_{\text{Positive control}} - \text{OD}_{\text{Negative control}}} \times 100 \qquad \text{.... Equation 3.4}$$

### 3.3.8 *In-vitro* cell culture studies of self-assembled micelles of LSF-FA prodrugs

Efficacy of LSF prodrug micelles was evaluated in MIN-6 cells (originated from insulinoma cells of mouse). These cells were cultured in DMEM media supplemented with 10% FBS and incubated in 5% $CO_2$ at 37 °C.

#### 3.3.8.1 Cell internalization of prodrugs micelles

The internalization of free drug and micelles of self-assembled LSF-prodrugs into the cells was studied. In this study, micelles of all four types of prodrugs (~20 µM free LSF) and free LSF (20 µM) were added to the MIN6 cells for 6 h. The cells without treatment served as control. After incubation, media was collected from each well and centrifuged for 10 min at 1200 rpm to remove any cells/ debris. Extraction of the prodrugs and LSF from the media (0.5 mL) was carried out using DCM (1.3 mL) followed by centrifugation at 3500 rpm. DCM was transferred in a fresh tube and dried under nitrogen. The residue was then redispersed into 100 µL of mobile phase and analysed for LSF/prodrugs by HPLC, this concentration when subtracted from the initial drug/conjugate added provided the amount of drug internalized by the cells.

#### 3.3.8.2 Cell viability assay (under normal and inflammatory conditions)

MIN-6 cells (5000 cells/well) were seeded and allowed to adhere for 24 h in a 96-well culture plate under normal growth conditions. Different treatments were given to the cells including the prodrug micelles, free LSF and free FAs (LA, OA, PA and ALA) at 20 µM concentration and incubated at 37 °C. After 48 h, MTT assay was performed and the inhibition in cell growth was determined with respect to untreated cells (media only).

$$\% \text{ Cell viability} = \frac{\text{Absorbance}_{\text{Sample wells}}}{\text{Absorbance}_{\text{Untreated wells}}} \times 100 \qquad \text{.... Equation 3.5}$$

Once the cell compatibility was confirmed, freshly seeded MIN6 cells (5000 cells/well) were further exposed to a mixture of 03 different pro-inflammatory cytokines (TNF-α; 10 ng/mL, IL-1β; 5 ng/mL and IFN-γ; 100 ng/mL) to induce inflammation [31] followed by treatment

with free LSF and synthesized LSF prodrugs (~20 μM free LSF). Post 48 h, cell viability was analysed by MTT assay.

### 3.3.9 *In-vivo* evaluation of LSF-FA prodrugs

All the experiments were carried out in compliance with CPCSEA guidelines and protocols were approved by IAEC, BITS Pilani, Pilani. The rats were housed in well-ventilated cages with periodic light/dark periods for 12 h and fed within standard laboratory conditions with routine *ab libitum* diet.

#### 3.3.9.1 Pharmacokinetic study of prodrugs

The micelles of LSF prodrugs and free LSF were injected intravenously into the Wistar rats (200-220 g) at a dose of 30 mg/kg (~15 mg/kg of LSF) and 15 mg/kg respectively. Blood samples were collected by retro-orbital route at pre-set time points till 24 h. Plasma was retrieved from the collected blood followed by sample extraction and sample analysis (previously described in the stability of the prodrugs in plasma section). Using non-compartmental model, plasma concentration-time profile was plotted for free LSF and its prodrugs employing Phoenix 2.1 WinNonlin (Pharsight Corporation, USA).

#### 3.3.9.2 Efficacy studies in STZ-induced T1DM model

STZ-induced diabetes model was created in Wistar rats (200-220 g) with a standard dose of STZ (55 mg/ kg) prepared in cold citrate buffer (0.01M, pH 4.5) using the i.p. route, while control rats were administered only buffer. Fasting glucose level (FGL) was measured after 72 h of STZ injection, and animals exhibiting a blood glucose level of 250 mg/dL or greater were labeled as diabetic. The rats were randomly grouped into normal control (NC), diabetic control (DC), free LSF treated and self-assembled prodrug micelles treated rats. Treatment was initiated on the 3rd day after the hyperglycaemic state was verified.

For the daily treatment regimen, one of the groups was treated with 15 mg/kg i.p. injection of free LSF solution in water. The self-assembled micelles of the respective four prodrugs were delivered at 30 mg/kg dose (~15 mg/kg of free LSF) once daily to each of the groups. The blood glucose levels were measured using Accu-Check active glucometer by tail bleeding method on every 3$^{rd}$ day till 5 weeks. Plasma was collected after 21 and 35 days and used for estimating the insulin levels and biochemical parameters for lipid and protein profiling of liver and kidney functions.

#### 3.3.9.3 Histopathology and immunohistochemical analysis

After giving treatment to the animals for 5 weeks, they were sacrificed for the assessment of pancreatic islet morphology with the help of H&E staining. Standard protocol was followed for immunohistochemical (IHC) analysis of expression of CD4+ and CD8+ T-cells in the pancreatic samples. The primary antibodies used were CD4 Rabbit mAb (1:400) and CD8a Mouse mAb (1:20). As a secondary antibody, signal stain IHC boost reagent and anti-mouse IgG antibody were used at 1:1 and 1:500 dilutions, respectively.

### 3.3.10 Statistical analysis

All of the data have been expressed as mean ± standard deviation and analyzed using GraphPad prism 7.0 software (GraphPad software, San Diego, CA). Statistical analysis was performed using one-way ANOVA by Tukey's multiple comparison test with 95% confidence interval for confirming the difference between the groups. A p-value $< 0.05$ was considered statistically significant.

## 3.4 Results

### 3.4.1 Synthesis and Characterization of LSF and LSF-FA prodrugs

LSF was successfully synthesized with >98% purity as determined by HPLC (UHPLC, ThermoFisher Scientific, USA) and a complete reduction of the ketone group present in PTX was seen, giving a high % yield. LSF-FA prodrugs were then successfully synthesized (**Figure 1**) and purified by flash chromatography using varying ratios of hexane and ethyl acetate as mobile phase for different prodrugs (**Table 3.1**) with approximately 50% yield except for LSF-LA (41.91 % yield) **(Table 3.2)**. The physical appearance of the purified prodrugs was quite different from each other wherein, LSF-LA and LSF-OA were colourless and semi-solid, but LSF-PA was white coloured and LSF-ALA was light yellow in colour; both were solid in nature. LSF and its FA prodrugs exhibited the following attributes when characterized by different spectroscopic and analytical techniques.

**Table 3.2**
HPLC and HR-MS analysis of synthesized LSF and LSF prodrugs.

| S. No. | Drug/ Prodrugs | Molecular Formula | % Yield | Retention time ($R_t$ min) | Purity (%) | Expected mass (g/mol) | $(M+H)^+$ peak (g/mol) |
|---|---|---|---|---|---|---|---|
| 1 | Free LSF | $C_{13}H_{20}N_4O_3$ | 92 | 6.21 | 99.7 | 280.1535 | 281.161 |
| 2 | LSF-ALA | $C_{21}H_{32}N_4O_4S_2$ | 52 | 4.19 | 95.1 | 468.1865 | 469.1933 |
| 3 | LSF-LA | $C_{31}H_{32}N_4O_4$ | 41.91 | 13.84 | 95.8 | 542.3832 | 543.3994 |
| 4 | LSF-PA | $C_{29}H_{50}N_4O_4$ | 55.75 | 18.82 | 98.1 | 518.3832 | 519.3889 |
| 5 | LSF-OA | $C_{31}H_{52}N_4O_4$ | 49.25 | 19.69 | 96.8 | 544.3989 | 545.4044 |

$^{1}$H NMR (400 MHz, $CDCl_3$) of the synthesized LSF drug showed a peak at chemical shift value of 3.75 ppm (-CH-OH) corresponding to the hydroxyl group in the side chain of LSF formed by the reduction of ketone group of PTX. Further, the successful conjugation of FA with LSF was confirmed, wherein all the prodrugs exhibited a peak at 4.9 ppm corresponding to the formation of an ester (-CH-$COO^-$) group and removal of peak for hydroxyl proton (–CH-OH) signifying a complete reaction between LSF and FAs and absence of any free drug in the purified products **(Figure 3.2)**. In HPLC analysis, lab synthesized LSF exhibited retention time ($R_t$) of 6.21 min, indicating its hydrophilic nature, no additional peak was detected in the chromatogram of LSF indicating absence of any impurity/ reaction byproducts (**Figure 3.3**). The spectrum of the synthesized LSF was similar to that of the commercially available LSF (Cayman chemical). For quantification of prodrugs, HPLC analysis was carried out as mentioned in our previous report. [25] Here, LSF showed $R_t$ value of 3.01 min, whereas the prodrugs showed an increased $R_t$ compared to the drug alone **(Figure 3.6)**. Among all, the minimum $R_t$ was observed for LSF-ALA (4.19 min) followed by other prodrugs as shown in **Table 3.2**, indicating enhanced hydrophobicity of the prodrugs. All the prodrugs were obtained with a purity >95% with negligible amount of free LSF present in final product **(Figure 3.3)**. A peak corresponding to any other impurity was also not observed in any of the chromatograms. HR-MS showed $(M+H)^+$ ion peaks (expected mass of the drug/prodrug + Mass of $^{1}$H) **(Figure 3.4)** which were found to be closely matching with the molecular formula of the respective prodrug and exactly calculated mass of LSF/ prodrugs **(Table 3.2)**. In FTIR, the LSF spectra showed peak at 3380 $cm^{-1}$ corresponding to –CH-OH group that was absent in the spectra of all the prodrugs as it was consumed in ester bond (–C=O) formation as depicted by presence of the –COOH peak at 1700-1650 $cm^{-1}$ in the FTIR spectra of the prodrugs **(Figure 3.5).**

### 3.4.2 Stability of prodrugs in plasma

Due to the conjugation of LSF to FAs, its stability in rat plasma increased and the prodrugs released LSF in a sustained manner for 72 h, wherein LSF-ALA exhibited maximum release of 60% in 72 hours followed by other prodrugs (**Figure 3.7**).

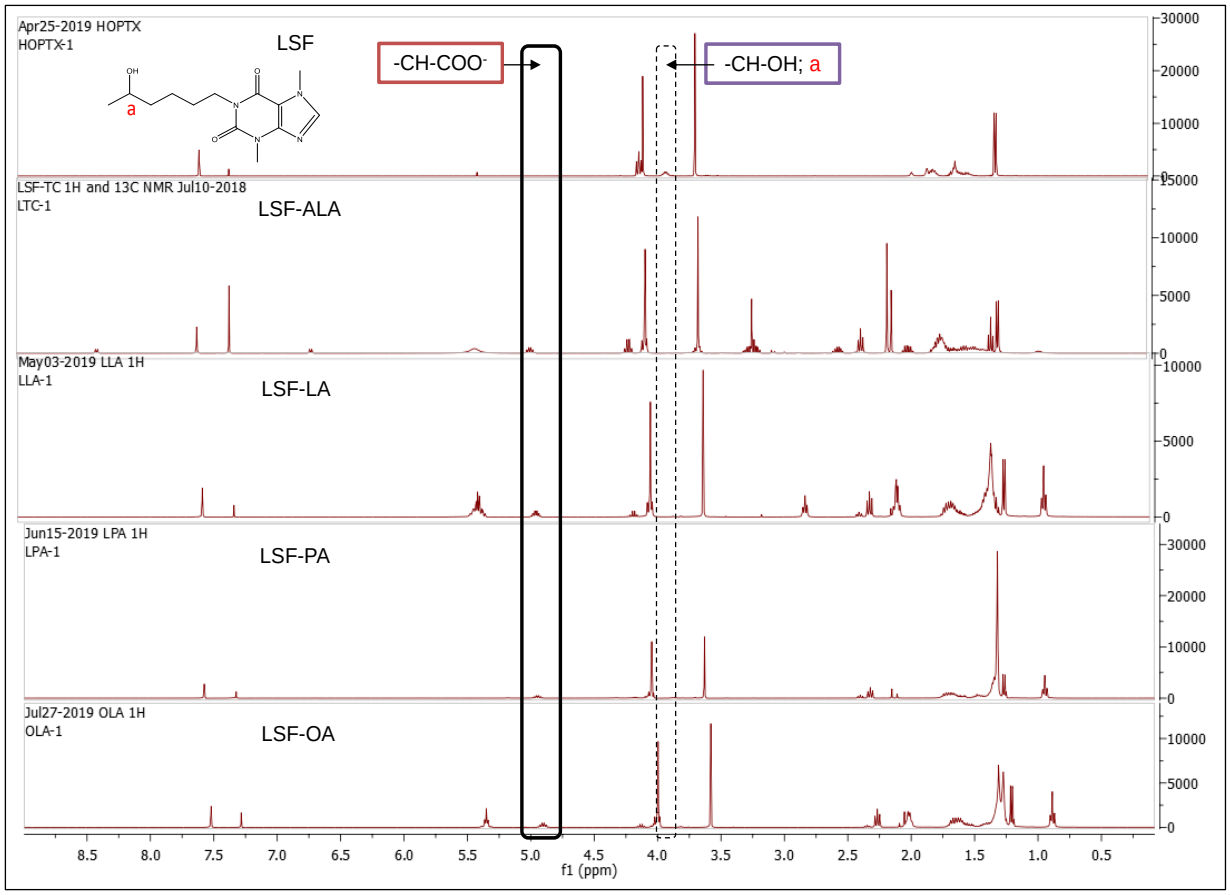


**Figure 3.2** Stacked $^{1}H$ NMR spectra of LSF and prodrugs in $CDCl_3$ solvent.

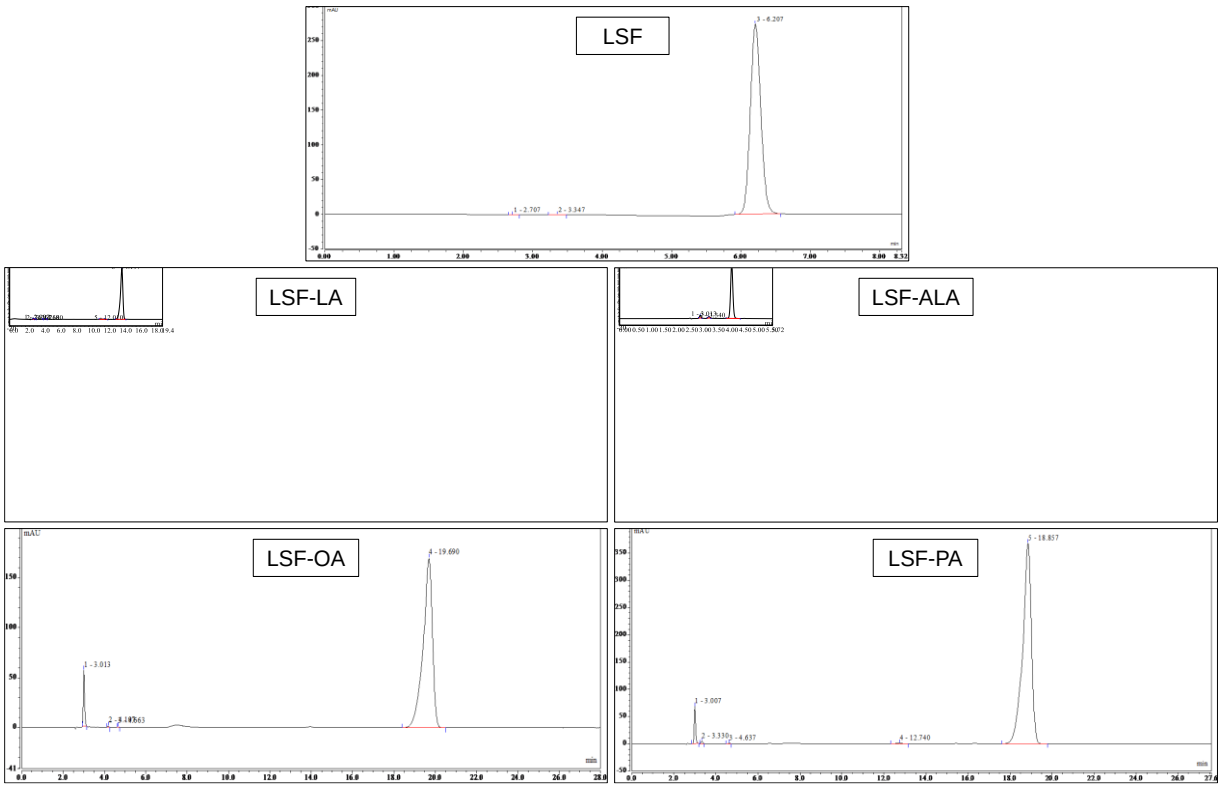


**Figure 3.3** HPLC purity spectra of synthesized LSF, LSF-ALA, LSF-LA, LSF-OA and LSF-PA.

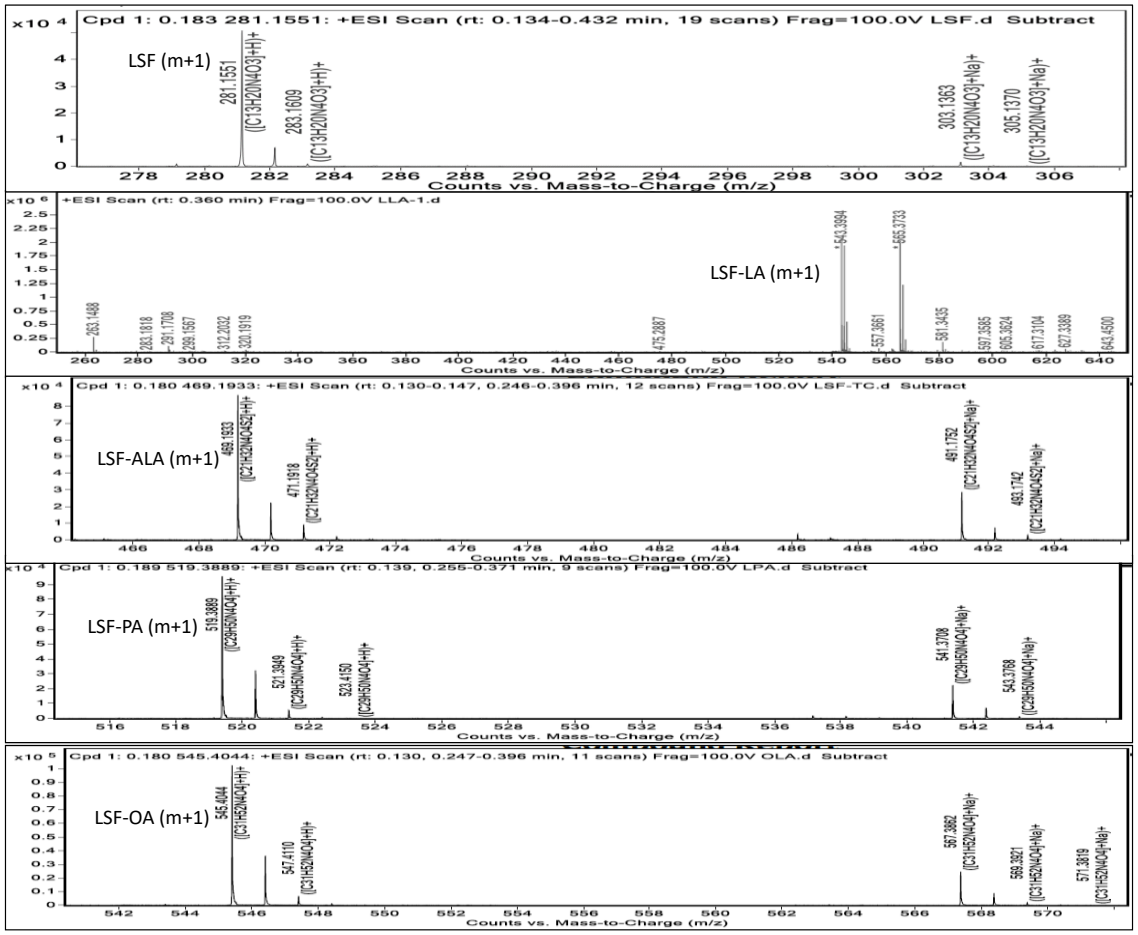


**Figure 3.4** Stacked mass spectra of LSF and its prodrugs.

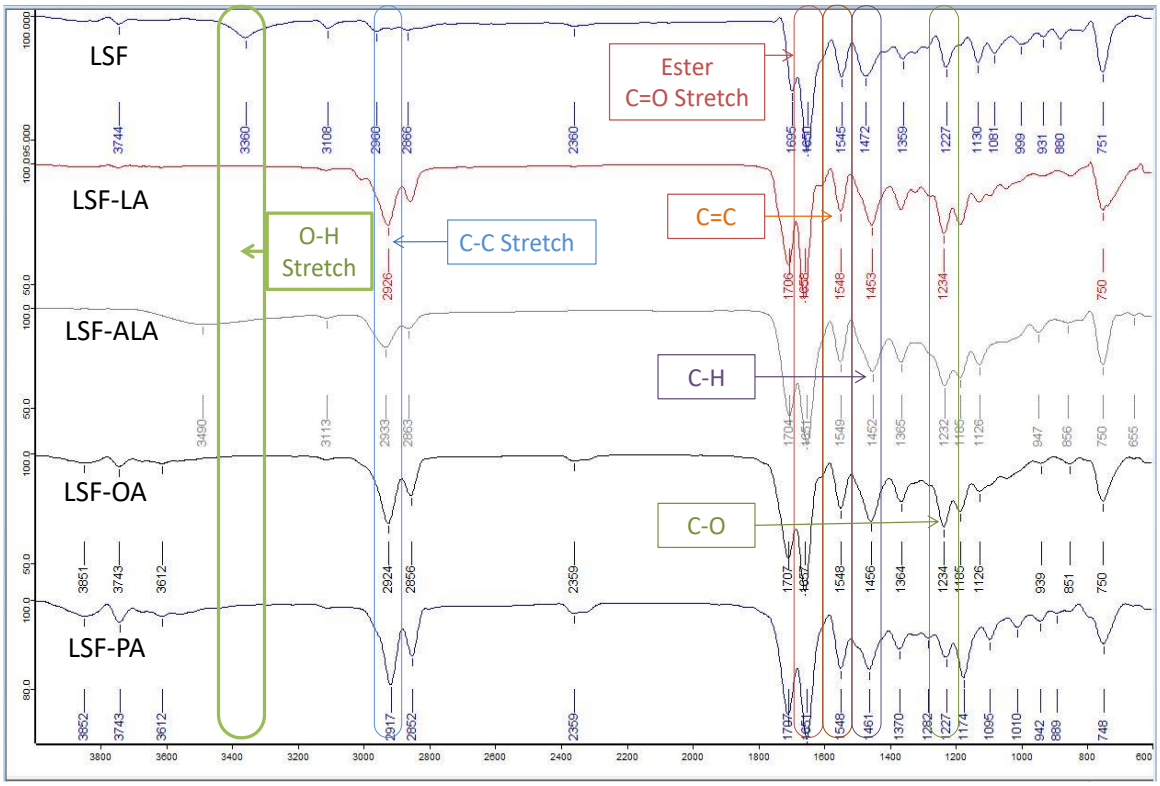


**Figure 3.5** Stacked FTIR spectra of LSF and its prodrugs.

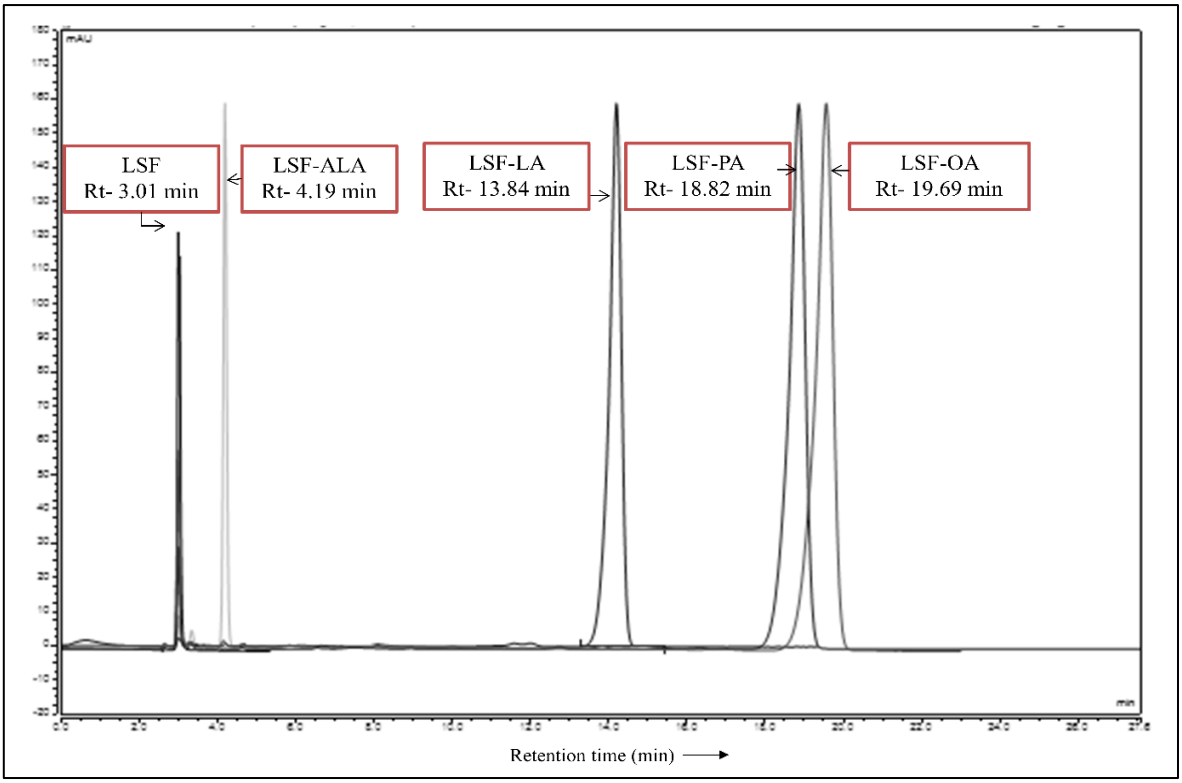


**Figure 3.6** Stacked representative HPLC chromatograms of LSF prodrugs.

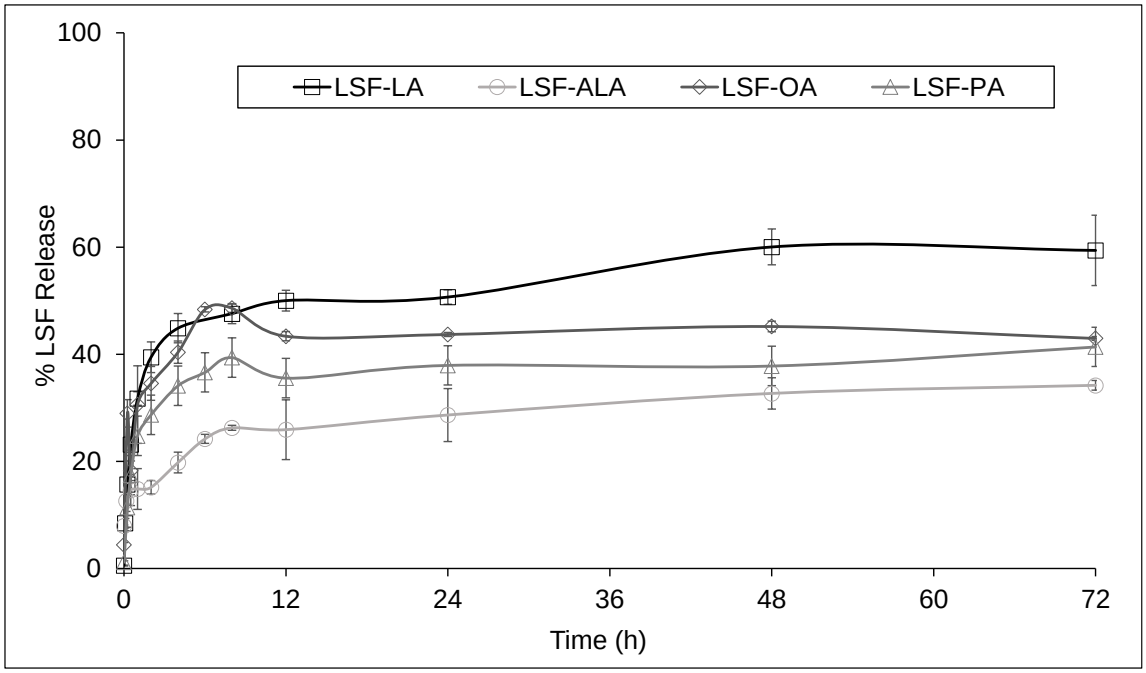


**Figure 3.7** Stability of LSF prodrugs and the rate of release of free LSF from the prodrugs in rat plasma. Data represents mean (n=3) ± SD.

### 3.4.3 Self-assembly of prodrugs

These prodrugs are amphiphilic in nature as these comprise of hydrophilic (LSF) and hydrophobic components (FAs) in a 1:1 ratio (on mole basis), which imparts self-assembling property to them, enabling the formation of micelles in the presence of water. The self-

assembled micelles were characterized for particle size and zeta potential using a Malvern dynamic light scattering system (**Table 3.3**). The micelle size ranged from 70.4 nm to 170.5 nm and zeta potential values -4.3 mV to -22.6 mV for different prodrugs. For confirming self-assembly of micelles, CMC value was obtained for each of the prodrugs and was found to be in range of 0.81-7.58 µg/ mL (**Figure 3.8 A**).

**Table 3.3**
Characterization of self-assembled LSF-fatty acid micelles.

| S. No. | Prodrugs | Particle size (nm) | PDI | Zeta potential (mV) | CMC (µg/mL) | LSF (µg/mL ~20 µM) | $N_{agg}$ | $K_b$ ($L.mol^{-1}$) | n |
|---|---|---|---|---|---|---|---|---|---|
| 1 | LSF-ALA | 170.50 | 0.257 | -13.0 | 6.31 | 9.36 | 47 | $2.05 \times 10^4$ | 1.18 |
| 2 | LSF-LA | 92.67 | 0.326 | -22.6 | 0.81 | 10.85 | 52 | $2.70 \times 10^4$ | 1.03 |
| 3 | LSF-PA | 71.74 | 0.268 | -4.3 | 7.4 | 10.37 | 69 | $5.55 \times 10^4$ | 0.85 |
| 4 | LSF-OA | 70.4 | 0.232 | -15.6 | 7.58 | 10.88 | 61 | $6.34 \times 10^4$ | 0.92 |

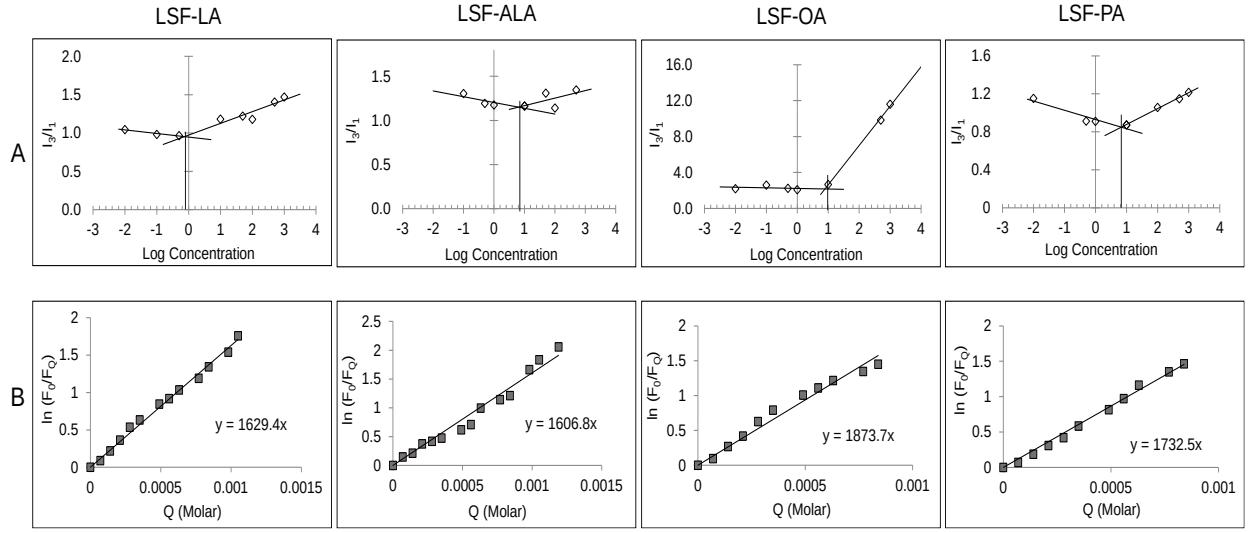


**Figure 3.8** Study of self-assembling nature of LSF prodrugs by (A) critical micelle concentration (CMC) and, (B) micelles aggregation number.

### 3.4.4 Estimation of aggregation number

The $N_{agg}$ was determined after estimating the micelles (M) concentration by the steady-state fluorescence, and the intensities were compared with and without quencher. So, the decrease in the intensity of pyrene with prodrug micelles in the presence of various concentrations of CPC (quencher) was recorded. A straight line was obtained when a graph was plotted between $\ln(F_0/F_Q)$ and Q (concentration of quencher in micelles), where M was determined by the slope of the graph using equation 1 and then $N_{agg}$ was calculated using **Equation 3.2 (Figure 3.8 B)**.

### 3.4.5 Protein interaction of prodrugs with BSA

This study was performed to check the interaction of protein with prodrugs by fluorescence quenching method, wherein the emission spectra of BSA were recorded before and after interaction of BSA with free LSF and prodrugs. A decrease in relative intensity of BSA with an increase in concentration of prodrugs was observed, revealing an interaction between BSA and prodrugs. A bathochromic peak shift was observed only in the case of LSF-PA, which itself showed fluorescence (**Figure 3.9**). After plotting the graph of $\log(F_0\text{-}F_Q)/F_Q$ and log Q, the binding constant $K_b$ and number of binding sites (n) present on BSA were determined (**Table 3.6**). The $K_b$ and n values for free LSF were estimated to be $6.32 \times 10^4$ and 1.16, respectively.

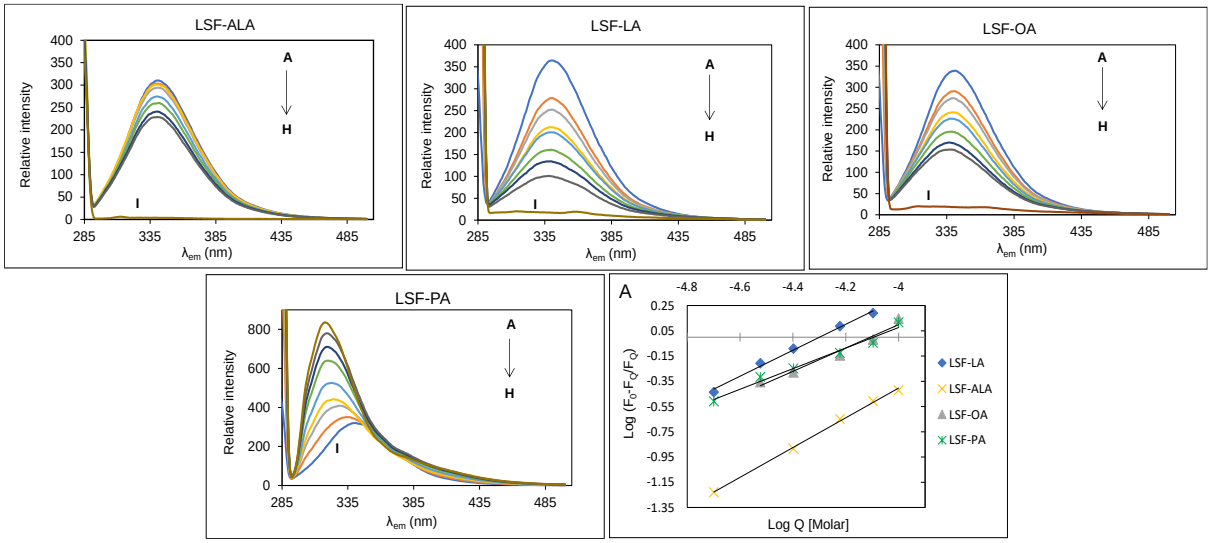


**Figure 3.9** Protein interaction study between LSF prodrugs and BSA. Emission spectra of BSA ($\lambda_{ex}$ = 280 nm) at 2.0 µM concentration in the presence of different concentrations of prodrug micelles that is 0, 10, 20, 30, 40, 60, 80 and 100 µM, corresponding to curves A–H. Plot I correspond to the emission spectrum of respective prodrug micelle only (500 µM). A) Plot of Log ($F_0\text{-}F_Q/F_Q$) against log (Q) at different concentrations of the prodrugs at room temperature.

### 3.4.6 *In-vitro* studies of prodrugs

#### 3.4.6.1 Hemocompatibility study

To understand if the micelles can cause hemolysis during systemic circulation, % hemolysis was calculated. Hemolysis exhibited by the different prodrugs was very less as compared to the lysis caused by the positive control (Triton X) (**Figure 3.10 A and B**).

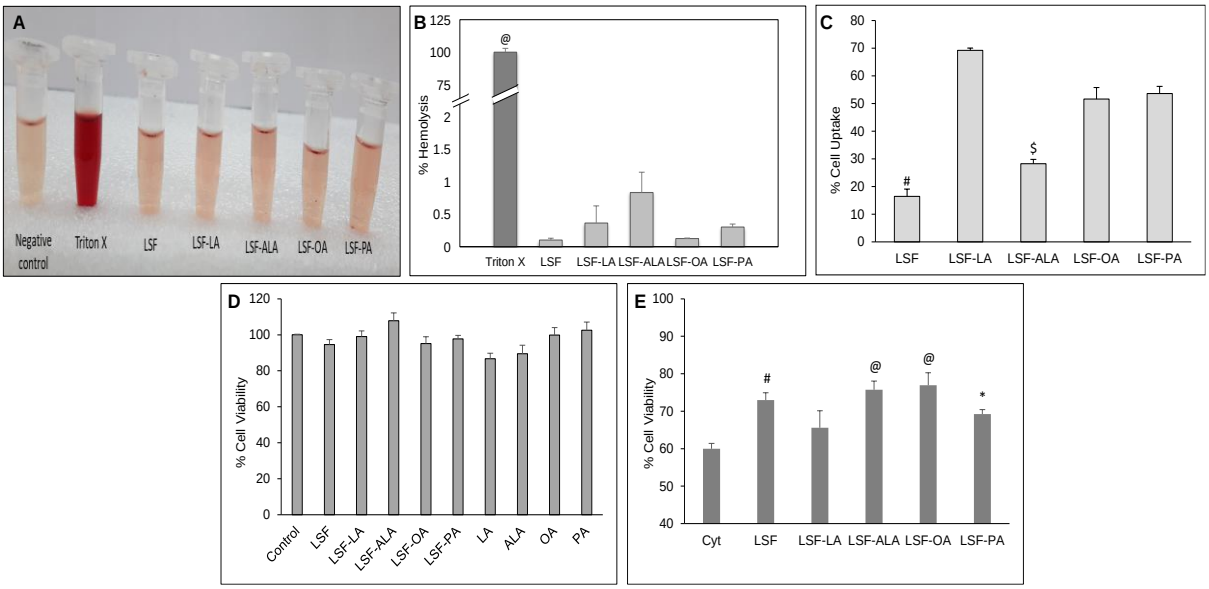


**Figure 3.10** *In-vitro* evaluation of the LSF prodrugs. (A) and (B) *In-vitro* hemocompatibility study $^{@}$Triton X vs. all ($^{@}$P<0.0001), (C) cell uptake study in MIN-6 cells after 6h of incubation $^{@}$LSF vs. LSF-OA ($^{@}$P<0.0001); $^{\#}$LSF vs. LSF-LA and LSF-PA ($^{\#}$P<0.001), (D) cytotoxicity study of FAs, LSF (20 µM) and prodrugs (~20 µM free LSF) under normal conditions $^{@}$Positive control vs. all groups ($^{@}$P<0.0001) and, (E) cell viability in presence of cytokine induced inflammation $^{@}$Cyt vs. LSF-ALA and LSF-OA ($^{@}$P<0.0001); $^{\#}$Cyt vs. LSF (P<0.001); $^{*}$Cyt vs. LSF-PA ($^{*}$P<0.05).
*In figure 4C, all the bars correspond to the amount of free LSF released from the corresponding prodrugs shown on x-axis.

### 3.4.6.2 Cell internalisation of prodrug micelles

As micelles are nano-sized systems, the prodrugs micelles exhibited higher cell uptake into MIN-6 cells than the free drug after 6 h, wherein LSF was analysed in the incubated media, washings, and after lysis of the cells. It was found that 56 ng of LSF was present in cell lysates treated with LSF-OA after 6h, followed by LSF-LA and LSF-PA prodrugs (**Figure 3.10 C**).

### 3.4.6.3 Cell viability under normal and inflammatory conditions

Under normal cell culture conditions, all of the prodrugs, free drug and FAs exhibited no cell death after 48 h, confirming that the synthesized prodrugs of LSF are non-toxic to the cells (**Figure 3.10 D**). As seen in **Figure 3.10 E**, upon exposure to the cytokine-mediated inflammatory conditions, a drastic reduction in cell viability was observed in all of the samples. However, the presence of LSF prodrugs with the cells under these conditions significantly preserved their viability compared to the control cells (in media alone).

## 3.4.7 *In-vivo* studies of prodrugs

### 3.4.7.1 Pharmacokinetic study

The non-compartmental estimation of pharmacokinetic (PK) parameters showed that the conjugation of LSF increased the half-life of LSF by 2 to 6 fold (from 0.752±0.03 h to

4.44±0.47 h), and the apparent volume of distribution ($V_d$) of prodrugs also increased from 3 to 15 fold. The mean residence time (MRT) of prodrug elevated to 9 h as compared to 0.8 h for free LSF (**Figure 3.11**). The clearance values of LSF-LA and LSF-ALA prodrugs were found to be lower than of free LSF but found to be much higher in LSF-OA and LSF-PA as shown in **Table 3.4**.

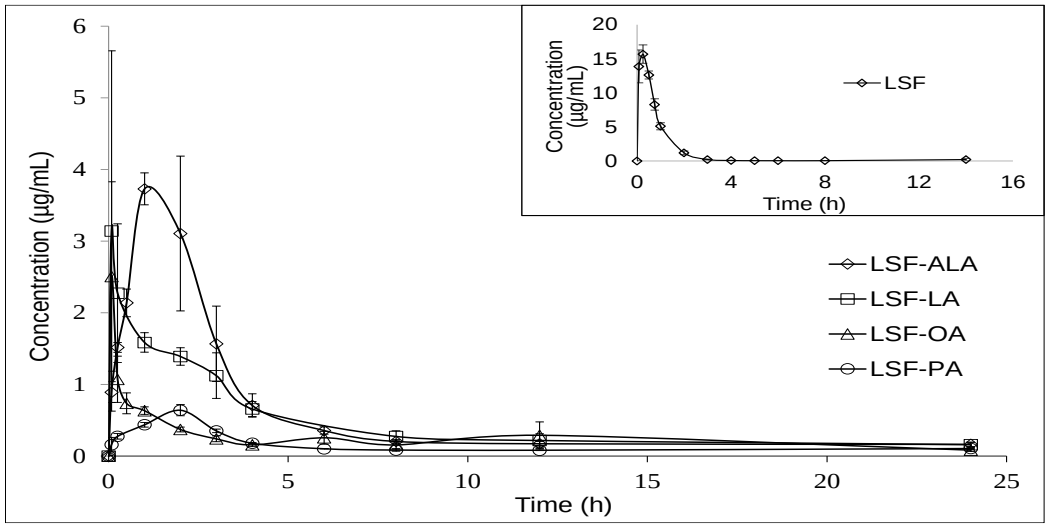


**Figure 3.11** Systemic pharmacokinetic study of LSF and LSF prodrugs in Wistar rats, IV administration. Each point represents mean (n = 4) ± SD at ~15 mg/ kg dose of free LSF.

**Table 3.4**
Pharmacokinetic study of LSF (15 mg/kg; i.v. dose) and LSF prodrug (30 mg/kg; i.v. dose) administered in rat and analysed by non-compartmental method.

| | **LSF** | **LSF-LA** | **LSF-ALA** | **LSF-OA** | **LSF-PA** |
|---|---|---|---|---|---|
| **$C_0$ (ng/mL)[a]** | 16395.65± 1630.78 | 4902.86±3223. 37 | 4117.86±588. 65 | 4747.3±3028. 56 | 266.75±110.19 |
| **$t_{1/2}$ (h)** | 0.752±0.03 | 3.12±0.29 | 1.26±0.13 | 4.44±0.47 | 3.59±0.51 |
| **Ke (1/h)** | 0.924±0.04 | 0.23±0.02 | 0.51±0.06 | 0.16±0.02 | 0.17±0.01 |
| **$AUC_{0-t}$ (ng.h/mL)** | 14692.73±60 3.55 | 16157.94±543 7.84 | 13467.82±153 8.58 | 6107.96±132 2.07 | 3491.96±145.5 5 |
| **$AUC_{0-\infty}$ (ng.h/mL)** | 14738.52±59 0.77 | 16984.11±536 5.74 | 13838.8±1439 .5 | 6635.59±127 0.95 | 3887.79±268.3 1 |
| **$AUMC_{0-t}$ (ng.h/mL)** | 12068.34±12 47.91 | 77115.13±131 61.58 | 67512.96±328 2.77 | 30549.55±74 09.28 | 29926.06±133 9.38 |
| **$AUMC_{0-\infty}$ (ng.h/mL)** | 12797.01±12 78.92 | 98737.84±182 77.97 | 77295.34±543 0.21 | 43158.66±14 430.4 | 24806.43±390 5.12 |
| **MRT (h)** | 0.818±0.06 | 6.55±0.55 | 5.16±0.67 | 7.91±0.93 | 9.07±0.33 |
| **$V_d$ (mL/kg)** | 961.55±79.1 6 | 2587.82±558.8 6 | 1769.5±395 | 14974.4±158 8.02 | 13774.62±250 1.16 |
| **Cl (mL/h/kg)** | 1020.9±39.4 6 | 634.05±191.99 | 951.84±107.2 2 | 2415.3±407.2 9 | 3894.14±260.6 5 |

[a]Refer to free LSF released in plasma from the prodrugs.

$C_0$: initial concentration, $t_{½}$: half-life, $K_e$: elimination rate constant, $AUC_{0-t}$: area under the curve from time 0 to t concentration $AUC_{0-\infty}$: area under the curve from time 0 to last measurable concentration, $AUMC_{0-\infty}$: area under the first moment curve from time 0 to last measurable concentration, $AUMC_{0-t}$ : area under the first moment curve from time 0 to t concentration, MRT: mean residence time, $V_d$: volume of distribution, Cl: clearance rate.

### 3.4.7.2 *In-vivo* efficacy studies in STZ induced T1D model

The LSF-FA self-assembled micelles were administered once daily intraperitoneal at a dose of 30 mg/kg (~15 mg/kg of LSF) over a period of 5 weeks and compared with free LSF dosed at 15 mg/kg, once daily. In this study, FGL of animals (mg/dL) were recorded every week. An overall FGL level at 3$^{rd}$ and 5$^{th}$ week exhibited decreased FGL levels. The DC group showed a significant increase in FGL level (555.5 ± 22.73 mg/dL) compared to NC animals (106.25 ± 4.77 mg/dL) as no treatment was given to this group except for saline. Free LSF also showed a significant increase in FGL in 3$^{rd}$ and 5$^{th}$ weeks. LSF-LA and LSF-PA demonstrated slight increase in FGL in 5$^{th}$ week compared to their 3$^{rd}$ week level. LSF-OA showed a better control of FGL than other prodrugs by maintaining a constant level throughout the study. In LSF-ALA group, FGL level exhibited significant increase in the 5$^{th}$ week as compared to the 3$^{rd}$ week **(Figure 3.12 A).** All of the prodrugs showed significantly increased insulin levels compared to DC and free LSF group (i.p.), among which LSF-OA and LSF-PA prodrugs showed higher insulin levels than LSF-LA and LSF-ALA, which indicates increased protection of the residual β cells owing to controlled blood glucose levels (**Figure 3.12 B)**.

In T1DM, progressive liver injury occurs due to an increase in oxidative stress which is further associated with higher levels of SGOT (ASAT) and SGPT (ALAT) as seen in DC group. Treatment with the prodrugs lowered the levels of ALAT and ASAT, with minimum levels of ASAT being observed in LSF-OA and LSF-LA showed the lowest ALAT level. All the groups exhibited similar total protein level. Due to persistent hyperglycaemia in the body, the renal functions get compromised, which increases the urea and uric acid levels in plasma. Here, all the prodrugs showed a significant reduction in uric acid level compared to DC and free LSF with the highest reduction being observed in LSF-OA. It has also been reported that cholesterol and triglyceride levels are significantly increased in patients with diabetes due to insulin resistance and dyslipidaemia. All of the prodrugs demonstrated a significant reduction in cholesterol and triglycerides levels compared to DC group **(Figure 3.12 C)**.

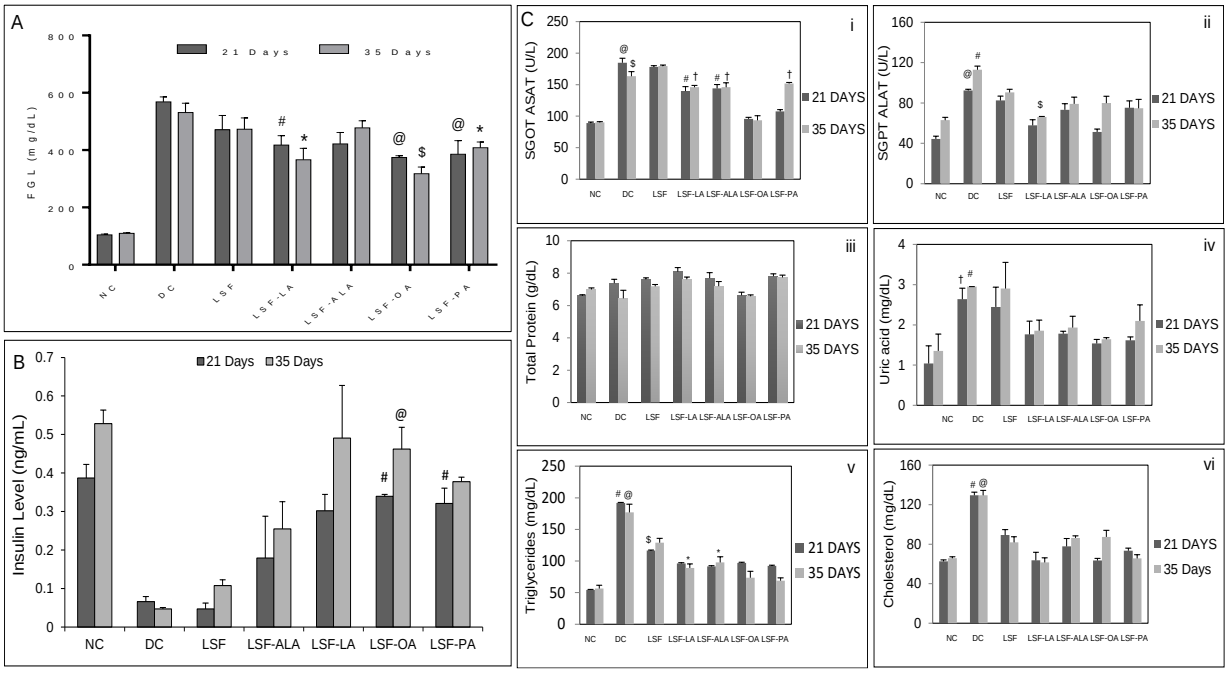


**Figure 3.12** *In-vivo* anti-diabetic activity of the LSF prodrugs evaluated in a STZ induced diabetic model. A) Fasting blood glucose levels after 35 days $^{\$}$DC *vs.* LSF-OA ($^{\$}P$<0.005); $^{@}$DC *vs*. LSF-OA and LSF-PA; *DC *vs.* LSF-LA and LSF-PA ($^{@*}P$<0.01); $^{\#}$DC *vs*. LSF-LA ($^{\#}P$<0.05), B) serum insulin level $^{\#}$DC *vs*. LSF-OA and LSF-PA; $^{@}$DC *vs*. LSF-OA ($^{\#@}P$<0.05), C) Biochemical analysis of plasma i) SGOT $^{@}$DC *vs*. LSF-OA and LSF-PA; $^{\$}$DC *vs*. LSF-OA ($^{@\$}P$<0.005); $^{\#}$DC *vs*. LSF-LA and LSF-ALA ($^{\#}P$<0.01); $^{\dagger}$DC *vs*. LSF-LA, LSF-ALA and LSF-PA ($^{\dagger}P$<0.05), ii) SGOT $^{@}$DC *vs*. LSF-LA and LSF-OA, $^{\$}$DC *vs.* LSF-LA ($^{@\$}P$<0.005); $^{\#}$DC *vs*. LSF-ALA, LSF-OA and LSF-PA ($^{\#}P$<0.05), iii) Total protein (non-significant), iv) Uric acid $^{\dagger}$DC *vs*. LSF-LA, LSF-ALA, LSF-OA and LSF-PA ($^{\dagger}P$<0.01); $^{\#}$DC *vs*. LSF-LA, LSF-ALA and LSF-OA ($^{\#}P$<0.005), v) Triglycerides $^{@}$DC vs. LSF-LA, LSF-ALA, LSF-OA and LSF-PA; $^{\#}$DC vs. LSF-OA and LSF-PA ($^{@\#}P$<0.001); $^{\$}$DC *vs.* LSF; $^{*}$DC vs. LSF-LA and LSF-ALA ($^{\$*}P$<0.05), vi) Cholesterol $^{\#}$DC vs. LSF-LA and LSF-OA ($^{\#}P$<0.005); $^{@}$DC vs. LSF-LA and LSF-OA ($^{@}$P<0.01).
NC: normal control, DC: diabetic control, FGL: fasting glucose level

### 3.4.7.3 Histopathology and Biochemical assay

The pancreatic islets isolated after sacrificing the experimental animals at the terminal time point were analysed for the morphology and immunohistochemical expression. The β cells in DC were distorted, and very few of these have visible islets after H&E staining compared to NC and other prodrugs. Although, LSF, LSF-ALA and LSF-PA exhibited proper arrangement of pancreatic islets however, number of β cells were lesser as compared to LSF-LA and LSF-OA treated groups. A higher population of CD4+ and CD8+ inflammatory cells was seen in DC, along with depletion of other cells in the vicinity. The presence of these inflammatory cells was significantly diminished in prodrug treated diabetic rat's pancreas (**Figure 3.13**).

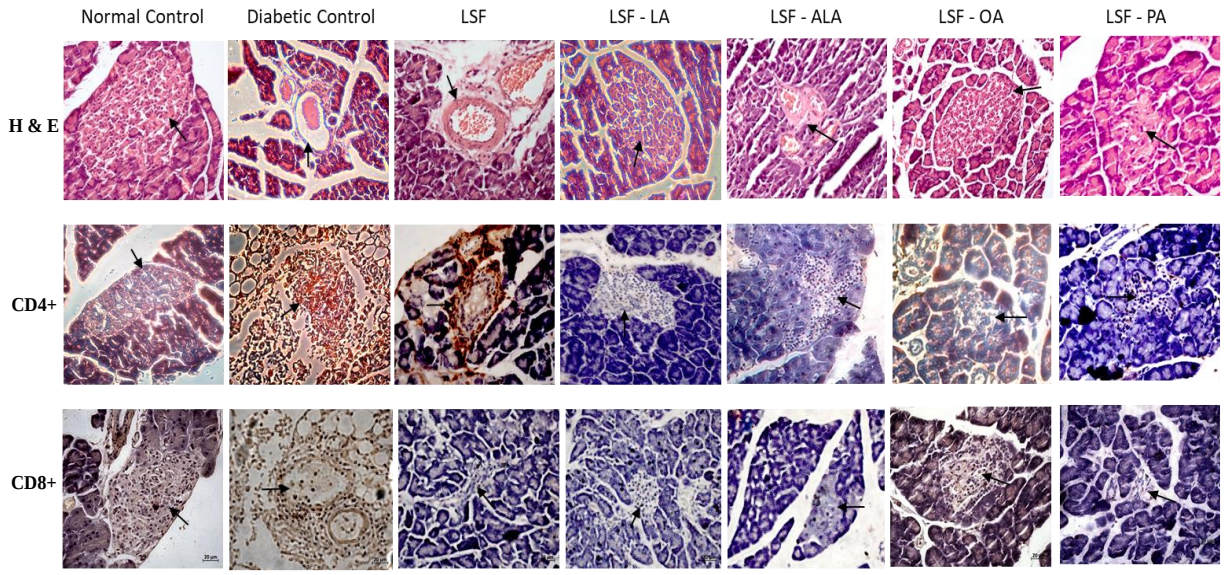


**Figure 3.13** Immunohistochemical study of pancreatic islets of control and treated groups after 35 days of treatment by Haematoxylin-eosin (H&E) staining and expression of CD4+ and CD8+ T-cells (indicated by brown colour and black arrows) (*under 400 × magnification; 20 µm scale bar).

### 3.5 Discussion

LSF is a synthetic drug molecule with potent anti-diabetic activity and its well-known immunomodulatory and anti-inflammatory activities. To improve its physicochemical and pharmacokinetic attributes, we conjugated it with different types of FAs, which are also endogenously present in the human body and are synthesized by de novo lipogenesis of triglycerides and lipids. These are also extracted from plant and animal sources and are extensively consumed in diet and food supplements. To reduce the solubility of hydrophilic LSF and to enhance its efficacy and bioavailability, we conjugated it with hydrophobic FAs belonging to different classes to form prodrugs with LSF with increased lipophilicity. LA has an 18-carbon chain and two double bonds (ω-6 FA; PUFA). OA also has an 18-carbon chain and is liquid in nature but with a single double bond (ω-9 FA; MUFA), which imparts fluidity to the cell membrane. SFA-like PA contains a 16-carbon chain without any double bond, making the cell membrane structure straight and rigid. [31] A functional short-chain FA, ALA, was also chosen for the study; it is a heterocyclic FA derived from an octanoic acid. [28]

Here, the objective was to elucidate the effect of the length of carbon chain in terms of short and long chains, presence or absence of double bonds, and degree of unsaturation on the LSF-FA prodrug properties and associated pharmacological activity. In spite of same carbon chain length, FAs can demonstrate a huge difference in their physiological behavior owing to their geometrical and conformational differences.

FAs have been used in diabetes, mainly omega-3 FAs employed for the treatment of diabetes, particularly type 2 diabetes mellitus (T2DM), as these are known to decrease insulin resistance along with reducing the triglycerides levels in the body. [32] Here, FAs have been used as a carrier to deliver drug to increase its bioavailability and enhance the rate and extent of distribution inside the body. Previously, FAs like lauric acid and palmitic acid have been explored for the treatment of T2DM by conjugating with GLP-1 analogue, i.e., exendin-4, wherein pharmacokinetic parameters such as mean residence time and elimination t1/2 were substantially improved compared with free exendin-4. [33] In another study, porcine zinc insulin was incorporated into mixed micelles of 30 mM bile salts and 40 mM linoleic acid for ileo-colonic delivery, and it exhibited 1.8% enhanced mean absolute bioavailability, leading to improved paracellular diffusion of the peptide. [34] As reported earlier by our group, LA conjugation to LSF also reduced the rapid conversion of LSF to PTX and increased the drug stability by offering protection to the hydroxyl group present in the side chain of LSF. [13] The nanosized micellar system generated due to the amphiphilic nature of prodrugs helps in bypassing the first-pass metabolism of LSF thus, increasing its bioavailability. It also enables RES escape prolonging its mean residence time in the body and reducing clearance.

First, LSF was synthesized in-house by reduction of the keto group of PTX using simple green chemistry followed by its purification. The synthesized drug was characterized by HPLC, FT-IR, and HR-MS analyses and compared with LSF procured from Cayman Chemical. The prodrugs were synthesized by conjugation of LSF with different categories of FAs, LA, OA, PA, and ALA, all having the same structural chemistry (−COOH) at one end of carbon facilitating a similar procedure for the synthesis for all of the prodrugs. The mechanism is based on carbodiimide coupling, where FAs having free −COOH group was dissolved in DCM followed by the addition of 4-dimethylaminopyridine (DMAP) to activate the −COOH group, which forms an anhydride form of FA. [35, 36] Thereafter, the N-(3-dimethylaminopropyl)-N-ethyl-carbodiimide hydrochloride (EDC·HCl) was added into the ongoing reaction to form the O-acylisourea intermediate via an ion pair transfer; this O-acylisourea intermediate then reacted with the already present catalytic amount of DMAP (strong nucleophile) to form an acyl pyridinium specie, which acts as an acyl-transfer reagent and reacts with the −OH group of LSF to form ester linkage (−COOR′) between the FA and LSF. [37] Herein, DMAP provided an appreciable yield of the product by preventing the formation of the byproduct (N-acylurea) during the reaction. This mechanism is also termed as the Steglich esterification. Then, the byproducts, unreacted EDC·HCl and DMAP, were washed out with water and brine solution

(**Figure 3.14**). [38, 39] There was a progressive increase in the hydrophobicity of the prodrugs as the alkyl chain length of the associated FA increased; this was reflected during the purification of the prodrugs in terms of the mobile phase ratio required and the elution time observed in flash chromatography; the same was further confirmed by the retention time of the prodrugs in HPLC **(Table 3.2)**. The purified prodrugs also exhibited different physical states: LSF-LA and LSF-OA were in liquid form, while LSF-PA and LSF-ALA were solid in nature; this might be attributed to the presence of cis double bond in the long alkyl carbon chain of LA and OA that generates kinks and bents and does not allow the resultant molecules to attain a tightly packed structure. [22] The calculated molecular weight of all the prodrugs matched the molecular weight obtained by HR-MS **(Table 3.2)**. The proton NMR and FTIR spectra of prodrugs confirmed the removal of the −CH−OH group from 3360 cm−1 in FTIR and 3.9 ppm in NMR of LSF and the formation of −CH−COO− ester bond as revealed by signals at 2917−2933 cm−1 (FTIR) and 4.85−5 ppm (NMR, **Figures 3.2**). The CMC value is important to determine the minimum media volume required to form micelles, wherein it depends on the hydrophobic chain length and varying structural properties of the compounds. It has been reported that with an increase in the carbon chain length, the CMC value decreases along with a low $N_{agg}$. [40, 41] Aggregation number represents the average monomers involved in the formation of spherical micelles at or beyond CMC. [42] In our study, the nanosized self-assembled prodrugs showed CMC values ranging from 0.8 to 7.6 μg/mL, wherein LSF-LA exhibits CMC lower than LSF-ALA and LSF-PA owing to the longer chain length of LA, and LSF-OA has a higher CMC value due to a different degree of unsaturation compared to LSF-LA. LSF-ALA showed the least $N_{agg}$, which might be attributed to the short carbon chain of ALA, resulting in higher relative aqueous solubility in comparison to micelles of other prodrugs. A higher $N_{agg}$ results in a low diffusion coefficient and reduced rate of transport from the interface to the bulk causing hindrance in the solubilization of the micelles. The prodrugs when evaluated for their stability and rate of release or cleavage of ester bond of free LSF from prodrugs in fresh rat plasma at 37 °C exhibited a sustained release of the drug up to 72 h **(Figure 3.7)**, wherein 100% release of LSF was observed in the case of LSF-ALA, followed by other prodrugs in 72 h of the study. We did not observe a complete release of LSF in other prodrugs, that is, LSF-LA, LSF-PA, and LSF-OA owing to the following two reasons: (1) with every sample that is withdrawn, along with the drug, the LSF-FA prodrug also gets sampled out and thus is no longer available in the study to release the drug; this is an experimental limitation (the amount of drug getting sampled out as intact prodrug was also quantified in the case of LSF-ALA and LSF-OA (n = 4) and was found to be 0.98 ± 0.66% (observed only at 5 min time

point) in LSF-ALA and 9.74 ± 2.3% (cumulative after 72 h) in LSF-OA). (2) Since plasma has been used here as the release media, the prodrugs and the released drug might have undergone metabolism. Overall, the experiment reconfirmed that conjugation of the FAs with small/large molecules enhances their *in-vivo* stability in comparison to LSF. [10, 43]

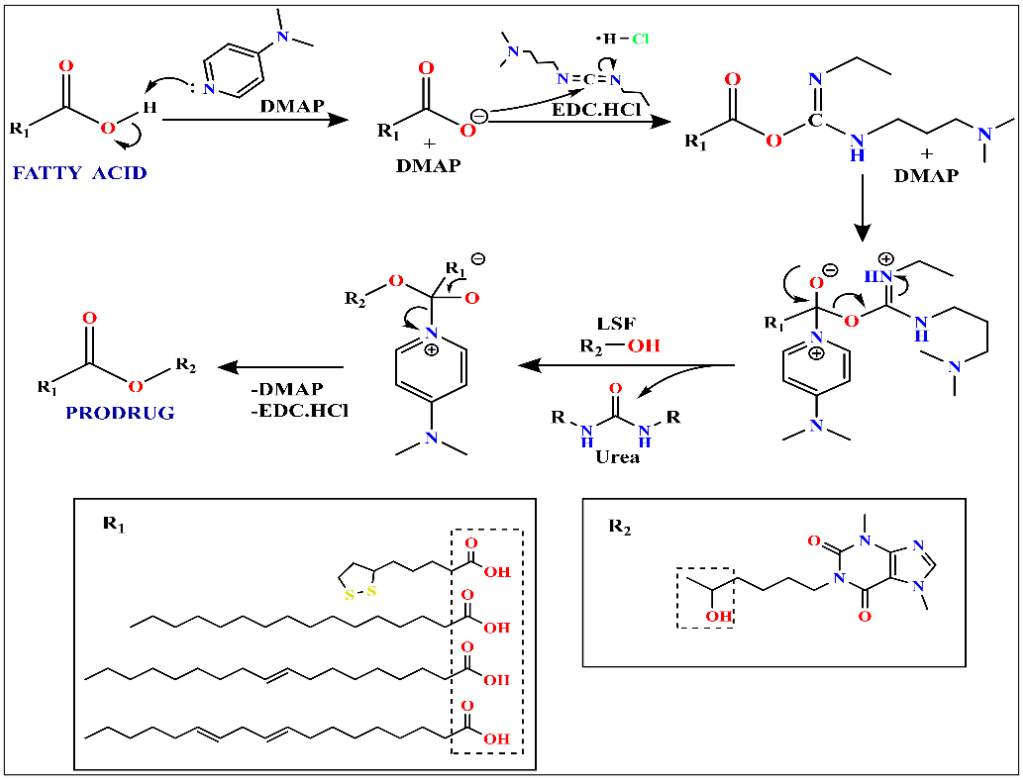


**Figure 3.14**. The mechanism involved in the formation of LSF-fatty acid prodrugs.

Adsorption and binding of the endogenous proteins on the surface of nanocarriers is a predominant factor affecting their behavior in the systemic circulation. To understand protein binding with the prodrugs, BSA was selected for the study owing to its structural similarity with human serum albumin (HSA) that is endogenously present and is majorly found in the circulatory system. It is well reported that the free FAs can easily bind to the HSA, which makes FAs and their conjugates potent and stable in the bloodstream. [44] Under normal physiological conditions, FA molecules bind to HSA in 1:1 or 1:2 ratio; this however increases by 4- to 5-fold under diabetic conditions, [45] further prolonging the mean residence time of the molecules in the circulation and thus supporting the choice of conjugating FAs with LSF to enhance its anti-diabetic potential. The binding site per BSA molecule was found to be slightly higher in free LSF and LSF-ALA compared to other micelles, indicating lesser affinity of these micelles toward endogenous proteins in contrast to LSF-PA and LSF-OA micelles, which show higher binding affinity possibly due to the fact that FAs like OA and PA are abundantly present

in the tissues and are known to bind firmly to albumin and use it as a carrier in the blood. [46] The *in-vitro* study showed a lower binding constant of LSF-ALA followed by LSF-LA; however, LSF-OA and LSF-PA exhibited a stronger interaction with the protein (revealed by a higher value of binding constant and lower aggregation number), indicating a probable increase in half-life and mean residence time of the prodrugs and hence controlled release with prolonged availability of the drug *in-vivo*. [47, 48]

The proof of hemocompatibility of prodrugs was established by the *in-vitro* study, wherein negligible hemolysis of RBCs was observed in the presence of prodrug micelles **(Figure 3.10 A and B)**. PUFAs, especially, are advantageous to the system because the presence of a long carbon chain increases the fluidity and flexibility of the membrane while maintaining the curvature of the membranes. [22, 49] This was reflected in the higher cell uptake and internalization of the micelles of LSF-OA compared to other prodrugs and free LSF, signifying its optimum lipophilicity attributed to the presence of a longer carbon chain followed by other prodrugs. Cell internalization of FA-conjugated drug increases with an increase in the degree of lipophilicity of the prodrug, which is dictated by the chain length of FA attached to LSF. As the chain length and degree of unsaturation of FA increase, the extent and rate of cell internalization increase. This is also reflected in the cellular uptake of LSF-ALA, which is almost similar to that of free LSF and minimum among all of the prodrugs attributed to its shorter carbon chain, rendering it less hydrophobic than other prodrugs and thus hindering its uptake. Further, this might have resulted in rapid cleavage of the ester bond in the growth media and release of free LSF before its internalization into the cells. Also, the prodrugs self-assembled into micelles, which offer the advantages of nano-size and thus exhibited a higher cell internalization compared to free drug. [50] Once the prodrugs are taken up by endocytosis, LSF gets cleaved from its FA prodrug in the presence of acidic endosomal environment. This further indicates that use of these FA-based prodrugs would enable a higher uptake of LSF into the cells as supported by the cell uptake data **(Figure 3.10 C)** and greater therapeutic efficacy. The cell viability study of prodrug micelles in MIN-6 cells demonstrated a close to 100% cell viability in the presence of FAs as well as prodrugs **(Figure 3.10 D)**. Although some inflammatory effects of FAs have been reported earlier, such as PA exhibits increased apoptosis and cytotoxicity in HepG2 cells at 300 μM or higher concentrations; [51, 52] however, these were found to be safe within the concentrations used in the present study. LSF prodrugs restored the cell viability in the presence of cytokines to a significant extent.

Conjugation of hydrophobic moieties like FAs to the drugs has been reported to improve the *in-vivo* performance significantly by us as well as by other groups. [10, 11, 13, 53] Conjugation of PA to the peptide, GLP-1 increased its $t_{½}$ from 5 min to 13 h providing it a sustained release. [43] Likewise, in this study, also the synthesized prodrugs exhibited 1.5 to 6-fold higher $t_{1/2}$ than free LSF with a simultaneous increase of 7 to 11-fold in MRT due to the increased hydrophobicity of the prodrugs attributed to the carbon chain present in FAs; MRT increases linearly with an increase in the chain length of the FA as shown in **Table 4**. The $V_d$ of prodrugs was found to be higher than that of free LSF, wherein LSF-PA and LSF-OA demonstrated a 15-times higher $V_d$, indicating distribution to peripheral organs attributed to their longer chain length and hence greater lipophilicity.

*In-vivo* efficacy of the prodrugs was evaluated in STZ-induced T1D model. The micelles used for treatment were formulated by the film hydration method and exhibited a particle size range of 70.4−170.5 nm with a narrow PDI. The FGL level was maintained at a significantly lower level than the diabetic control group in all of the treatment groups representing the anti-diabetic potential of LSF but among all of the prodrugs, LSF-PA and LSF-OA showed the best control of glucose level with decreased mortality compared to other prodrugs **(Figure 3.6 A)**. Among all of the prodrugs, LSF-ALA exhibited a comparatively higher FGL, which might be due to the inadequate hydrophobicity of shorter carbon chain length of ALA affecting the half-life and MRT of LSF as seen in the PK data. [13, 54] A remarkable increase in the insulin level was found on the 21$^{st}$ day (3$^{rd}$ week) of the study, which further improved on the 35$^{th}$ day (5$^{th}$ week) in all of the prodrugs compared to the diabetic control and free LSF-treated group with LSF-OA treatment showing the highest insulin levels in comparison to the diabetic control group.

Persistent hyperglycemia induces certain adverse effects in kidney, pancreas, and other organs. A study of different biochemical parameters known to undergo a drastic change under diabetic conditions revealed that the prodrugs (particularly LSF-LA and LSF-OA) showed reduced oxidative stress as seen by the reduced plasma ASAT and ALAT levels compared to DC. Renal function also gets compromised in T1DM as seen by the increased uric acid level in DC; LSF-OA showed a significantly reduced uric acid level than other prodrugs. Diabetes can cause hepatic dyslipidemia, wherein low-density lipoproteins, total cholesterol, and triglycerides increase with a significant decrease in high-density lipoproteins; the anti-inflammatory property of LSF adequately addresses these stress-induced lipid metabolism changes. [55] LSF prodrugs treatment also rapidly reduced the total cholesterol and triglyceride levels after 21

days that was maintained till the 35$^{th}$ day of the study. No significant difference was seen in total protein content in both DC and treatment groups.

The presence of pro-inflammatory cytokines induces the infiltration of CD4+ and CD8+ T lymphocytes in the pancreas, causing destruction and depletion of β-cells in the islets in the diabetic model. The effectiveness of LSF released from the prodrugs in protecting the β-cells from inflammation and hence T-cell infiltration was shown by H&E and IHC staining of pancreatic tissues collected after five weeks of the treatment. H&E staining confirmed the intactness of β cells in islets after treatment with the micelles of prodrugs compared to the diabetic control, most prominently visible in LSF-LA and LSF-OA prodrug-treated groups. Daily administration of LSF prodrugs also reduced the entry of T cells (CD4+ and CD8+) into the islets, which otherwise cause β-cell destruction compared to the DC group **(Figure 3.13)**.

## 3.6 Conclusion

The present study confirms the successful conjugation of LSF with different types of FAs and self-assembly into nanosized micelles along with improved *in-vitro* and *in-vivo* performance than the free drug itself. Among the different drug−FA prodrugs studied, LSF-OA showed comparatively better systemic pharmacokinetic and pharmacodynamic profiles in diabetes. OA, the FA *per se*, has also been proven to be significantly better than PA in terms of its anti-inflammatory action, improved β-cell survival, and increased insulin sensitivity. [56] LSF-OA exhibits greater and longer retention in the systemic circulation and efficiently treats diabetic condition with decreased mortality and stabilized FGL in diabetic Wistar rats. Overall, this research study presents OA as the most suitable FA among ALA, LA, PA, and OA for enhancing the stability and efficacy of LSF in diabetes treatment. The above displayed data in this chapter has already been published. Reprinted (adapted) with permission from {Singh, A. K., Italiya, K. S., Narisepalli, S., Chitkara, A. & Mittal, A. (2021). Role of chain length and degree of unsaturation of fatty acids in the physicochemical and pharmacological behavior of drug–fatty acid conjugates in diabetes. Journal of Medicinal Chemistry, 64(19), 14217-14229. doi.org/10.1021/acs.jmedchem.1c0039. Copyright {2021} American Chemical Society.

## 3.7 Bibliography

[1] B. Saberzadeh-Ardestani, R. Karamzadeh, M. Basiri, E. Hajizadeh-Saffar, A. Farhadi, A.M.J. Shapiro, Y. Tahamtani, H. Baharvand, Type 1 Diabetes Mellitus: Cellular and Molecular Pathophysiology at A Glance, Cell J 20(3) (2018) 294-301.

[2] M. Chen, Z. Yang, R. Wu, J.L. Nadler, Lisofylline, a novel antiinflammatory agent, protects pancreatic beta-cells from proinflammatory cytokine damage by promoting mitochondrial metabolism, Endocrinology 143(6) (2002) 2341-8.

[3] D.F. Sheehy, S.P. Quinnell, A.J. Vegas, Targeting type 1 diabetes: selective approaches for new therapies, Biochemistry 58(4) (2019) 214-233.

[4] M.L. Immordino, P. Brusa, F. Rocco, S. Arpicco, M. Ceruti, L. Cattel, Preparation, characterization, cytotoxicity and pharmacokinetics of liposomes containing lipophilic gemcitabine prodrugs, J Control Release 100(3) (2004) 331-46.

[5] H.J. Jung, M.J. Ho, S. Ahn, Y.T. Han, M.J. Kang, Synthesis and Physicochemical Evaluation of Entecavir-Fatty Acid Conjugates in Reducing Food Effect on Intestinal Absorption, Molecules 23(4) (2018).

[6] B. Sun, C. Luo, L. Li, M. Wang, Y. Du, D. Di, D. Zhang, G. Ren, X. Pan, Q. Fu, Core-matched encapsulation of an oleate prodrug into nanostructured lipid carriers with high drug loading capability to facilitate the oral delivery of docetaxel, Colloids and Surfaces B: Biointerfaces 143 (2016) 47-55.

[7] A.M. Bergman, A.D. Adema, J. Balzarini, S. Bruheim, I. Fichtner, P. Noordhuis, Ø. Fodstad, F. Myhren, M.L. Sandvold, H.R. Hendriks, Antiproliferative activity, mechanism of action and oral antitumor activity of CP-4126, a fatty acid derivative of gemcitabine, in in vitro and in vivo tumor models, Investigational new drugs 29(3) (2011) 456-466.

[8] D. Irby, C. Du, F. Li, Lipid–drug conjugate for enhancing drug delivery, Mol Pharm 14(5) (2017) 1325-1338.

[9] K. Breistøl, J. Balzarini, M.L. Sandvold, F. Myhren, M. Martinsen, E. De Clercq, Ø. Fodstad, Antitumor activity of P-4055 (elaidic acid-cytarabine) compared to cytarabine in metastatic and sc human tumor xenograft models, Cancer Research 59(12) (1999) 2944-2949.

[10] B.R. Sloat, M.A. Sandoval, D. Li, W.-G. Chung, D.S. Lansakara-P, P.J. Proteau, K. Kiguchi, J. DiGiovanni, Z. Cui, In vitro and in vivo anti-tumor activities of a gemcitabine derivative carried by nanoparticles, International journal of pharmaceutics 409(1-2) (2011) 278-288.

[11] M.O. Bradley, N.L. Webb, F.H. Anthony, P. Devanesan, P.A. Witman, S. Hemamalini, M.C. Chander, S.D. Baker, L. He, S.B. Horwitz, Tumor targeting by covalent conjugation of a natural fatty acid to paclitaxel, Clinical Cancer Research 7(10) (2001) 3229-3238.

[12] X. Gong, M.J. Moghaddam, S.M. Sagnella, C.E. Conn, S.J. Danon, L.J. Waddington, C.J. Drummond, Lamellar crystalline self-assembly behaviour and solid lipid nanoparticles of a palmityl prodrug analogue of Capecitabine—A chemotherapy agent, Colloids and Surfaces B: Biointerfaces 85(2) (2011) 349-359.

[13] L. Wu, F. Zhang, X. Chen, J. Wan, Y. Wang, T. Li, H. Wang, Self-assembled gemcitabine prodrug nanoparticles show enhanced efficacy against patient-derived pancreatic ductal adenocarcinoma, ACS Applied Materials & Interfaces 12(3) (2019) 3327-3340.

[14] D.M. Lambert, Rationale and applications of lipids as prodrug carriers, European journal of pharmaceutical sciences 11 (2000) S15-S27.

[15] J.A. Hamilton, F. Kamp, W. Guo, Mechanism of cellular uptake of long-chain fatty acids: Do we need cellular proteins?, Molecular and cellular biochemistry 239(1-2) (2002) 17-23.

[16] S. Leekumjorn, H.J. Cho, Y. Wu, N.T. Wright, A.K. Sum, C. Chan, The role of fatty acid unsaturation in minimizing biophysical changes on the structure and local effects of bilayer membranes, Biochimica et Biophysica Acta (BBA)-Biomembranes 1788(7) (2009) 1508-1516.

[17] B.P. Ander, C.M. Dupasquier, M.A. Prociuk, G.N. Pierce, Polyunsaturated fatty acids and their effects on cardiovascular disease, Experimental & Clinical Cardiology 8(4) (2003) 164.

[18] O.G.L. Coelho, B.P. da Silva, D.M.U.P. Rocha, L.L. Lopes, R.d.C.G. Alfenas, Polyunsaturated fatty acids and type 2 diabetes: impact on the glycemic control mechanism, Critical reviews in food science and nutrition 57(17) (2017) 3614-3619.

[19] M.A. Yorek, The potential role of fatty acids in treating diabetic neuropathy, Current diabetes reports 18(10) (2018) 86.

[20] J.S. Lee, S.K. Pinnamaneni, S.J. Eo, I.H. Cho, J.H. Pyo, C.K. Kim, A.J. Sinclair, M.A. Febbraio, M.J. Watt, Saturated, but not n-6 polyunsaturated, fatty acids induce insulin resistance: role of intramuscular accumulation of lipid metabolites, Journal of applied physiology 100(5) (2006) 1467-1474.

[21] L. Huang, J.-s. Lin, I.M. Aris, G. Yang, W.-Q. Chen, L.-J. Li, Circulating saturated fatty acids and incident type 2 diabetes: A systematic review and meta-analysis, Nutrients 11(5) (2019) 998.

[22] C.C. De Carvalho, M.J. Caramujo, The various roles of fatty acids, Molecules 23(10) (2018) 2583.

[23] H.-C. Ting, L.-T. Chen, J.-Y. Chen, Y.-L. Huang, R.-C. Xin, J.-F. Chan, Y.-H.H. Hsu, Double bonds of unsaturated fatty acids differentially regulate mitochondrial cardiolipin remodeling, Lipids in health and disease 18(1) (2019) 53.

[24] J.S. Striffler, J.L. Nadler, Lisofylline, a novel anti-inflammatory agent, enhances glucose-stimulated insulin secretion in vivo and in vitro: studies in prediabetic and normal rats, Metabolism 53(3) (2004) 290-296.

[25] K.S. Italiya, S. Mazumdar, S. Sharma, D. Chitkara, R.I. Mahato, A. Mittal, Self-assembling lisofylline-fatty acid conjugate for effective treatment of diabetes mellitus, Nanomedicine 15(1) (2019) 175-187.

[26] F. Castelli, M.G. Sarpietro, F. Rocco, M. Ceruti, L. Cattel, Interaction of lipophilic gemcitabine prodrugs with biomembrane models studied by Langmuir–Blodgett technique, Journal of colloid and interface science 313(1) (2007) 363-368.

[27] K. Nagy, I.-D. Tiuca, Importance of fatty acids in physiopathology of human body, Fatty acids, IntechOpen2017.

[28] F. Seifar, M. Khalili, H. Khaledyan, S. Amiri Moghadam, A. Izadi, A. Azimi, S.K. Shakouri, α-Lipoic acid, functional fatty acid, as a novel therapeutic alternative for central nervous system diseases: A review, Nutritional neuroscience 22(5) (2019) 306-316.

[29] K.S. Italiya, M. Basak, S. Mazumdar, D.K. Sahel, R. Shrivastava, D. Chitkara, A. Mittal, Scalable self-assembling micellar system for enhanced oral bioavailability and efficacy of lisofylline for treatment of type-I diabetes, Molecular Pharmaceutics 16(12) (2019) 4954-4967.

[30] K.S. Italiya, S. Sharma, I. Kothari, D. Chitkara, A. Mittal, Simultaneous estimation of lisofylline and pentoxifylline in rat plasma by high performance liquid chromatography-photodiode array detector and its application to pharmacokinetics in rat, J Chromatogr B Analyt Technol Biomed Life Sci 1061-1062 (2017) 49-56.

[31] K. Nagy, I.-D. Tiuca, Importance of fatty acids in physiopathology of human body, in: A. Catala (Ed.), Fatty acids, IntechOpen2017, pp. 3-22.

[32] A. IS Sobczak, C. A Blindauer, A. J Stewart, Changes in plasma free fatty acids associated with type-2 diabetes, Nutrients 11(9) (2019) 2022.

[33] S.Y. Chae, Y.G. Choi, S. Son, S.Y. Jung, D.S. Lee, K.C. Lee, The fatty acid conjugated exendin-4 analogs for type 2 antidiabetic therapeutics, Journal of Controlled Release 144(1) (2010) 10-16.

[34] J.C. Scott-Moncrief, Z. Shao, A.K. Mitra, Enhancement of intestinal insulin absorption by bile salt–fatty acid mixed micelles in dogs, Journal of pharmaceutical sciences 83(10) (1994) 1465-1469.

[35] A. Ramazani, F.Z. Nasrabadi, A. Rezaei, M. Rouhani, H. Ahankar, P.A. Asiabi, S.W. Joo, K. Ślepokura, T. Lis, Synthesis of N-acylurea derivatives from carboxylic acids and N, N′-dialkyl carbodiimides in water, Journal of Chemical Sciences 127(12) (2015) 2269-2282.

[36] N. Fattahi, K. Triantafyllidis, R. Luque, A. Ramazani, Zeolite-based catalysts: a valuable approach toward ester bond formation, Catalysts 9(9) (2019) 758.

[37] N. Fattahi, A. Ramazani, V. Kinzhybalo, Imidazole-Functionalized Fe 3 O 4/Chloro-Silane core-shell nanoparticles: An efficient heterogeneous organocatalyst for esterification reaction, Silicon 11(4) (2019) 1745-1754.

[38] M. Tsakos, E.S. Schaffert, L.L. Clement, N.L. Villadsen, T.B. Poulsen, Ester coupling reactions–an enduring challenge in the chemical synthesis of bioactive natural products, Natural product reports 32(4) (2015) 605-632.

[39] N. Fattahi, N. Varnaseri, A. Ramazani, A novel approach toward thioester bond formation mediated by N, N'-diisopropylcarbodiimide in water, Phosphorus, Sulfur, and Silicon and the Related Elements 196(1) (2020) 6-12.

[40] M.E. Mahmood, D.A. Al-Koofee, Effect of temperature changes on critical micelle concentration for tween series surfactant, Global Journal of Science Frontier Research Chemistry 13(4) (2013) 1-7.

[41] H. Luan, L. Gong, X. Yue, X. Nie, Q. Chen, D. Guan, T. Que, G. Liao, X. Su, Y. Feng, Micellar aggregation behavior of alkylaryl sulfonate surfactants for enhanced oil recovery, Molecules 24(23) (2019) 4325.

[42] N.J. Turro, A. Yekta, Luminescent probes for detergent solutions. A simple procedure for determination of the mean aggregation number of micelles, Journal of the American Chemical Society 100(18) (1978) 5951-5952.

[43] H. Agersø, L. Jensen, B. Elbrønd, P. Rolan, M. Zdravkovic, The pharmacokinetics, pharmacodynamics, safety and tolerability of NN2211, a new long-acting GLP-1 derivative, in healthy men, Diabetologia 45(2) (2002) 195-202.

[44] S. Curry, P. Brick, N.P. Franks, Fatty acid binding to human serum albumin: new insights from crystallographic studies, Biochimica et Biophysica Acta (BBA)-Molecular and Cell Biology of Lipids 1441(2-3) (1999) 131-140.

[45] B. Elsadek, F. Kratz, Impact of albumin on drug delivery—New applications on the horizon, Journal of Controlled Release 157(1) (2012) 4-28.

[46] A.A. Spector, K. John, J.E. Fletcher, Binding of long-chain fatty acids to bovine serum albumin, Journal of lipid research 10(1) (1969) 56-67.

[47] F. Keller, M. Maiga, H.-H. Neumayer, H. Lode, A. Distler, Pharmacokinetic effects of altered plasma protein binding of drugs in renal disease, Eur. J. Drug Metab. Pharmacokinet. 9(3) (1984) 275-282.

[48] X. Yu, R. Liu, D. Ji, F. Yang, X. Li, J. Xie, J. Zhou, P. Yi, Study on the synergism effect of lomefloxacin and ofloxacin for bovine serum albumin in solution by spectroscopic techniques, Journal of solution chemistry 40(3) (2011) 521-531.

[49] M. Pinot, S. Vanni, S. Pagnotta, S. Lacas-Gervais, L.-A. Payet, T. Ferreira, R. Gautier, B. Goud, B. Antonny, H. Barelli, Polyunsaturated phospholipids facilitate membrane deformation and fission by endocytic proteins, Science 345(6197) (2014) 693-697.

[50] F. Li, C. Snow-Davis, C. Du, M.L. Bondarev, M.D. Saulsbury, S.O. Heyliger, Preparation and characterization of lipophilic doxorubicin pro-drug micelles, J. Vis. Exp. (114) (2016) 54338.

[51] R.B. Sharma, L.C. Alonso, Lipotoxicity in the pancreatic beta cell: not just survival and function, but proliferation as well?, Current diabetes reports 14(6) (2014) 492.

[52] Y. Luo, P. Rana, Y. Will, Palmitate increases the susceptibility of cells to drug-induced toxicity: an in vitro method to identify drugs with potential contraindications in patients with metabolic disease, Toxicological Sciences 129(2) (2012) 346-362.

[53] K. Breistøl, J. Balzarini, M.L. Sandvold, F. Myhren, M. Martinsen, E. De Clercq, O. Fodstad, Antitumor activity of P-4055 (elaidic acid-cytarabine) compared to cytarabine in metastatic and sc human tumor xenograft models, Cancer Research 59(12) (1999) 2944-2949.

[54] Y. Li, Y. Wang, Q. Wei, X. Zheng, L. Tang, D. Kong, M. Gong, Variant fatty acid-like molecules conjugation, novel approaches for extending the stability of therapeutic peptides, Scientific reports 5(1) (2015) 1-9.

[55] S.L. Bursten, D. Federighi, J. Wald, B. Meengs, W. Spickler, E. Nudelman, Lisofylline causes rapid and prolonged suppression of serum levels of free fatty acids, Journal of Pharmacology and Experimental Therapeutics 284(1) (1998) 337-345.
[56] M. Nemecz, A. Constantin, M. Dumitrescu, N. Alexandru, A. Filippi, G. Tanko, A. Georgescu, The distinct effects of palmitic and oleic acid on pancreatic beta cell function: the elucidation of associated mechanisms and effector molecules, Frontiers in pharmacology 9 (2019) 1554.

XXXXXXXXXXXXXXXXX

# CHAPTER 4

# Synthesis, characterization and evaluation of polymeric C-peptide nano-complexes

# {NPX}

## 4.1 Introduction

DM is a universally prevalent metabolic syndrome causing chronic hyperglycemia due to excessive insulin deficiency caused by either destruction of pancreatic β-cells (T1DM) or insulin resistance (T2DM). [1] DM becomes life-threatening when it advances to diabetic complications wherein, multiple internal organs become metabolically compromised and thus result in microvascular damage, cardiovascular disorders, nephropathy, retinopathy and neuropathy. Among all the complications, DN is caused by both T1DM and T2DM and extends to DKD or progresses from normoalbuminuria to macroalbuminuria, persistent hypertension, and hematuria through multiple stages. Although proteinuria and declined glomerular filtration rate (GFR) are prominent indications in DN, T2DM patients rarely manifest proteinuria and predominantly show extensive glomerulopathy and interstitial damage. [2, 3] Among all the pathological interventions, oxidative stress and inflammation have unquestionable involvement in the manifestation and progression of DN. [4] It has been demonstrated that oxidative stress not only contributes towards metabolic modification but also alters renal hemodynamics. Increased generation of ROS and modulation of NAD(P)H oxidase, nitric oxide synthase (NOS), mitogen-activated kinase (MAPK), and advanced glycation end products (AGE) contributes to the cytokine and growth factors generation, responsible for pathogenesis of DN. [5] Evidently, ROS production induces renal complications via cell membrane peroxidation, protein oxidation, renal vasoconstriction, DNA damage, AGEs formation and elevated transforming growth factor-β (TGF-β) expression. TGF-β was found to induce overexpression of mesangial matrix and formation ofECM, an inevitable step in manifestation of renal fibrosis. [6] Alike TGF-β, each cytokine and growth factor eventually contributes towards the progression of the DN slowly and steadily. [7]

C-peptide (CPep; 31 amino acids, EVEDPQVPQLELGGGPEAGDLQTLALEVARQ, M.W.: 3299.8 g/mol g/mol), a structural polypeptide from rat origin forming a bridge between A and B chains of pro-insulin molecule is released in an equimolar concentration as insulin in the body. [8] It was evident that the C-terminal pentapeptide (EVARQ) of CPep is responsible for its biological activity by interacting through specific receptors present in the renal tubular cells. The renoprotective role elicited by CPep could be linked with $Na^+/K^+$ ATPase activation, epithelial NOS (eNOS) expression, MAPK activation, and suppression of TGF-β mediated pathway, strong anti-apoptotic and anti-fibrotic effects elicited by suppressing TNF-α mediated pathway. [9] Evidently, external administration of CPep can only impart significant physiological changes under diabetic conditions wherein the basal level of CPep is found

compromised. In healthy subjects, complete saturation of CPep receptors is reached by the physiologically formed CPep at the concentration of 0.9 nmol/l, which could not be attained under diabetic conditions. In fact, a clinical trial reported that 60 min infusion of CPep in diabetic patients was accompanied by a significant 7% fall in GFR from 143±3 to 133±4 ml $min^{-1}$/1.73 $m^2$, whereas the GFR in healthy individuals showed no change. CPep could be a promising therapeutic molecule for treating DN because of abundance of its receptor in the renal tissues. Despite its promising anti-inflammatory and renoprotective role in improving diabetic conditions, CPep could not be utilized for therapeutic application because of its short circulation half-life (20-30 min in healthy subjects) and rapid elimination from the body. [10, 11]

The conventional therapy of DM including sulphonylureas, thiazolidinediones, biguanides, etc., helps to elevate insulin release along with decreased blood glucose levels and related metabolic dysfunction. [12] Apart from these small molecules, biological molecules like insulin analogs, long-acting insulins, GLP-1 receptor agonists, sodium-glucose cotransporter 2 (SGLT2) inhibitors and gastric inhibitory polypeptide (GIP) have also been found beneficial to control both DM and DKD in the long term. [13-15] However, the drawbacks of current treatment regimens include incompliant route of application, off-target activity, short half-life, rapid elimination, solubility complications, and immunogenicity. Nanotechnology bears enormous promise to provide sustained release, reduced dose, enhanced half-life, improved bioavailability, and enhanced patient compliance for the treatment of DM and DKD. [16]

Recently, nanotechnology has been explored for the delivery of CPep wherein a delayed release formulation of CPep has been reported. In this study, CPep was embedded into an absorbable PLGA polymeric matrix administered subcutaneously that slowed down the peptide release upto 5 days. [17] In another study, the effectiveness of PEGylated CPep has been reported against peripheral neuropathy and microvascular complications in T1DM and compared with native CPep in a 12-month long clinical trial. Here, 250 patients with T1DM and peripheral neuropathy received 0.8 to 2.4 mg per week dose of PEGylated CPep for 52 weeks; vibration perception threshold (VPT) showed improvement while no improvement was observed in Sciatic Nerve Conduction Velocity (SNCV). [18] Jun Lee *et. al.* have also reported K9-C-Peptide (CPep conjugated to a lysine-containing Elastin Like Peptide) hydrogel formulation for reducing hyperglycemia-induced vascular dysfunction including ROS generation, inflammation, and apoptosis in the diabetic mouse aorta. Herein, a sustained release of CPep from hydrogel was achieved for 19 days resulting in restoration of diabetic aortic dysfunction.

[19] These studies make it evident that CPep is able to prevent and treat several diabetes-linked complications efficiently. Since the maximum abundance of CPep receptors is seen in renal tubular tissues and pancreas,[20] we hypothesize that it would treat DN efficiently.

In this study, *in-house* synthesized cationic polymer was employed to form cationic blank nanospheres onto which CPep was electrostatically complexed at neutral pH to formulate CPep nano-complexes (NPX). Considering the isoelectric point of CPep (pI=3.77), the carboxylic groups of CPep undergo deprotonation in phosphate buffer (pH 7.4), attaining a negative charge at higher pH than the pI. This strategy of complexing CPep with the cationic nanospheres bypasses the need for covalent conjugation of peptide along with increasing its stability and availability under physiological conditions. The safety of the prepared NPX was also evaluated by conducting hemocompatibility assay. Also, normal rat kidney tubular epithelial (NRK-52E) cells exhibited efficient cellular uptake of NPX as compared to free CPep resulting in promising anti-oxidant and anti-apoptotic effects under high glucose-induced metabolic-stress conditions. Furthermore, *in-vivo* efficacy studies in (STZ-induced DN model demonstrated effective anti-diabetic and anti-inflammatory effects in terms of improved renal and pancreatic histology, reduced interleukin-6 (IL-6) level with reduced FGL.

**4.2 Materials**

CPep was custom synthesized and procured from LifeTien, NJ, USA. Bis(hydroxymethyl) propionic acid, tin(II) 2-ethylhexanoate, methoxy poly(ethylene glycol) (mPEG, 5000 Da), 5,5′-dithiobis-(2-nitrobenzoic acid) and N,N-dimethyldipropylenetriamine were purchased from Sigma-Aldrich (St. Louis, MO). D, L-Lactide and N,N-diisopropylethylamine (DIPEA) were purchased from TCI Chemicals (Japan). STZ was purchased from MP Biomedicals. TFA (HPLC grade), sulphanilamide, fluorescein isothiocyanate (FITC) and reduced glutathione (GSH) were purchased from SRL Pvt. Ltd. (India). FBS, DMEM, Spectra Multicolor low range protein ladder (1.7 to 40 kDa) and Rat IL-6 mini ABTS ELISA development kit (Peprotech) were purchased from Thermo Fisher Scientific, USA. Benzyl bromide, palladium charcoal, N-hydroxybenzotriazole, tetrahydrofuran and triphosgene were procured from Spectrochem. Hydrogen peroxide, dichloromethane, acetonitrile for HPLC were purchased from Merck. Rat C-Peptide ELISA kit was procured from FineTest, China. All other chemicals and reagents were of analytical grade and purchased from local vendors. For cell culture studies, NRK-52E cells were acquired from NCCS, Pune, India. The animal protocol has been approved by the IAEC with protocol number: IAEC/RES/28/17.

## 4.3 Methods

### 4.3.1 Synthesis of cationic polymer (mPEG-b-P(CB-{g-DMDP chain}-co-LA))

#### 4.3.1.1 Synthesis of cyclic carbonate monomer

A multi-step reaction was performed to synthesize cyclic carbonate monomer 2-methyl-2-benzyloxycarbonylpropylene carbonate (MBC) to facilitate the grafting of cationic chain after the polymerization. As reported earlier by our group, briefly MBC was synthesized in a two step reaction where 2,2-bis (hydroxymethyl) propionic acid was mixed with potassium hydroxide in dimethylformamide (DMF) followed by the addition of benzyl bromide and kept on stirring at 100°C for 15h. [21] The crude product was then washed with ice-cooled water to remove DMF and recrystallized with toluene to yield an intermediate benzyl 2,2-bis (methylol) propionate (product 1) as illustrated on **Figure 4.1**. The second step consisted of the addition of product 1 in a mixture of pyridine: dichloromethane (DCM) in a ratio of 1:6 and then reacted with triphosgene for 1 h at -78°C, followed by stirring for 2 h at room tempaerature (RT). The reaction was quenched with saturated ammonium chloride solution to yield crude MBC. The crude product was purified by 1M Hydrochloric acid (HCl), saturated Sodium bicarbonate, and dried over sodium sulfate. The white crystals of MBC (product 2) were obtained after recrystallization of the crude product with ethyl acetate and characterized by proton Nuclear Magnetic resonance spectrometer ($^1$H NMR, 400 MHz, Bruker).

#### 4.3.1.2 Synthesis of polycarbonate cationic polymer

*Step 1*- To synthesize hydrophobic copolymer, polyethylene glycol poly(carbonate-co-lactide) (**mPEG-b-P(CB-co-LA)**; product 3) by ring-opening polymerization method as shown in **Figure 4.1**, instead of previously used conventional synthesis method, microwave synthesis (Monowave 300, Anton Paar) has been used to reduce the reaction time and enhance the polymer yield. Here, stannous 2-ethylhaxanoate (10 mol percent relative to mPEG) was used as catalyst and added to the mixture of calculated amount of mPEG, DL-Lactide and inhouse synthesized MBC (product 2) into the dried monowave vial. The reaction mixture was placed under vacuum and heated at 130°C for 1 h in microwave synthesizer. The obtained polymer was cooled at RT to stop the polymerization reaction and dissolved in chloroform to purify in an ample amount of chilled isopropyl alcohol and diethyl ether. The polymer precipitates were dried at RT under vacuum to remove solvent traces and characterized by $^1$H NMR.

*Step 2*- To synthesize a polymer with free carboxyl pendant groups (–COOH) from product 3, by the reduction of benzyl group present at polycarbonate backbone. Here, the catalytic hydrogenation technique was employed, where product 3 was dissolved in tetrahydrofuran:

methanol (1:1) in hydrogenation flask with palladium charcoal (Pd/C) as a catalyst, and the reaction was performed under 60 psi pressure for 6 h to yield **mPEG-b-P(CB-{g-COOH}-co-LA)** (product 4). In post-reaction, reaction mixture was centrifuged at 8000 rpm for 10 min to separate fine Pd/C particles, followed by the elimination of solvent mixture by rota vapor (Buchi) and characterized by $^{1}$H NMR.

*Step 3*- To synthesize a cationic chain grafted polymer, where N, N-dimethyldipropylenetriamine (DMDP, cationic chain) was utilized to coupled over free carboxyl groups on product 4 polymer backbone by carbodiimide/ N-hydroxybenzotriazole (HOBt) coupling reaction. Initially, product 4 polymer was dissolved in DMF for atleast 1 h followed by addition of N,N-diisopropylethylamine and HOBt as soon as all material present in dissolved form 1-ethyl-3-(3-dimethylaminopropyl) carbodiimide hydrochloride (EDC.HCl) was added at 0 °C and kept on stirring for 1 h in presence of Nitrogen ($N_2$) environment. Further, DMDP was added into the reaction mixture with continued stirring for 24 h at RT under $N_2$ atmosphere. To purify the synthesized polymer **mPEG-b-P(CB-{g-DMDP}-co-LA)** (Product 5), the reaction mixture was dialysed with dialysis membrane (SnakeSkin, M.W. cut-off 3.5 kDa, ThermoScientific) against water for 6 h, wherein the water was replaced with fresh water every at 1 h to remove unreacted compounds and DMF. The content of the dialysis bag was then freeze-dried and characterized for $^{1}$H NMR.

### 4.3.2 Development and characterization of NPX

#### 4.3.2.1 Formulation development strategy

The blank nanospheres (BNP) were prepared by single emulsion solvent evaporation method wherein, the polymer was weighed and dissolved in chloroform, followed by making a primary emulsion (O/W) in 1:10 ratio of organic:aqueous media followed by probe sonication at 25 % amplitude for 2 min. Then the organic solvent was removed from the system by evaporation under reduced pressure. Centrifugation at 5000 rpm for 5 min at 4 °C was performed to separate the larger particles. The supernatant containing BNP was then separated and analyzed for particle size and zeta potential (ZP). The NPX was prepared using CPep and BNP in the ratio 1:10 w/w in deionized water followed by incubation for 1 h at room temperature (RT) as shown in **Figure 4.6 A**. After incubation, uncomplexed CPep was separated from the NPX by ultracentrifugation (Sorvall MX150+, Thermo Scientific) and the pellet so obtained was redispersed in deionized water.

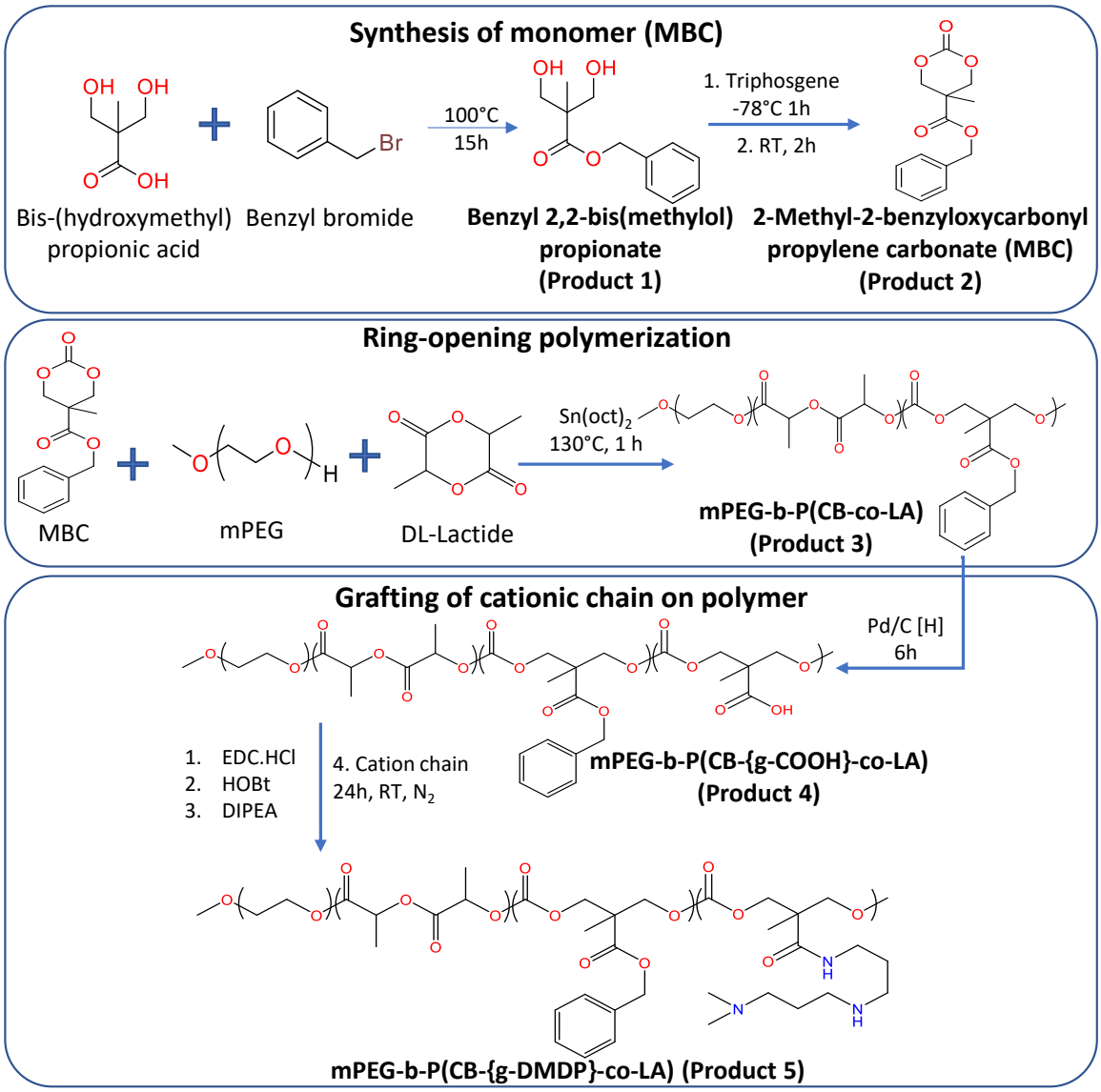


**Figure 4.1** Synthesis scheme of cationic polymer.

### 4.3.2.2 Characterization of the formulation

BNP and NPX were characterized for particle size (nm) and zeta potential (mV) using the dynamic light scattering (DLS) technique (25 °C, 173° backscattering, and total number of runs 10) using Litesizer 500 (Anton Paar, Germany). The morphological characterization was carried out by high-resolution transmission electron microscopy (HR-TEM, Tecnai G2 20 (FEI) S-Twin TEM, MRC, MNIT Jaipur) with an acceleration voltage of 200 kV, wherein the sample was prepared by putting drop of the NPX (suspended in deionized water) on carbon-coated copper grid followed by overnight drying.

Complexation efficiency of the CPep and BNP in NPX was confirmed by utilizing an *in-house* developed analytical method for quantification of CPep using reverse phase-high pressure liquid chromatography (RP-HPLC) method. The chromatographic parameters are mentioned

in **Table 4.2** and a calibration curve of CPep has been provided. The amount of CPep complexed with BNP was reconfirmed by carrying out a competition assay using 10 mM sodium acetate buffer (pH 3.0) resulting in dissociation of CPep from the NPX. The dissociated CPep in supernatant was separated from the BNP-acetate complex by ultracentrifugation, analysed and quantified using **Equation 4.1.** Assuming complete dissociation of CPep from NPX, the amount of peptide dissociated was considering equivalent to the amount initially complexed in NPX.

$$\% \text{ Peptide dissociated} = \frac{CPep\ (\mu g)\ in\ the\ supernatant}{Total\ amount\ of\ CPep\ initiallly\ added\ (\mu g)} \times 100 \quad \ldots. \textbf{Equation 4.1}$$

### 4.3.3 Synthesis and Characterization of FITC-labeled-CPep (FCP)

For making fluorescent CPep, FITC was selected for labeling wherein, the carboxyl groups of FITC undergo reaction with the amine groups present on the CPep chain as illustrated in **Figure 4.3**. FCP was purified over Vivaspin column (MWCO 2kDa, Sartorius, Germany) and extracted by repeated washings with deionised water, the FCP residue was then lyophilized and stored at -20°C. Further, FCP was redispersed in deionized water to determine the concentration and zeta potential using HPLC and DLS method.

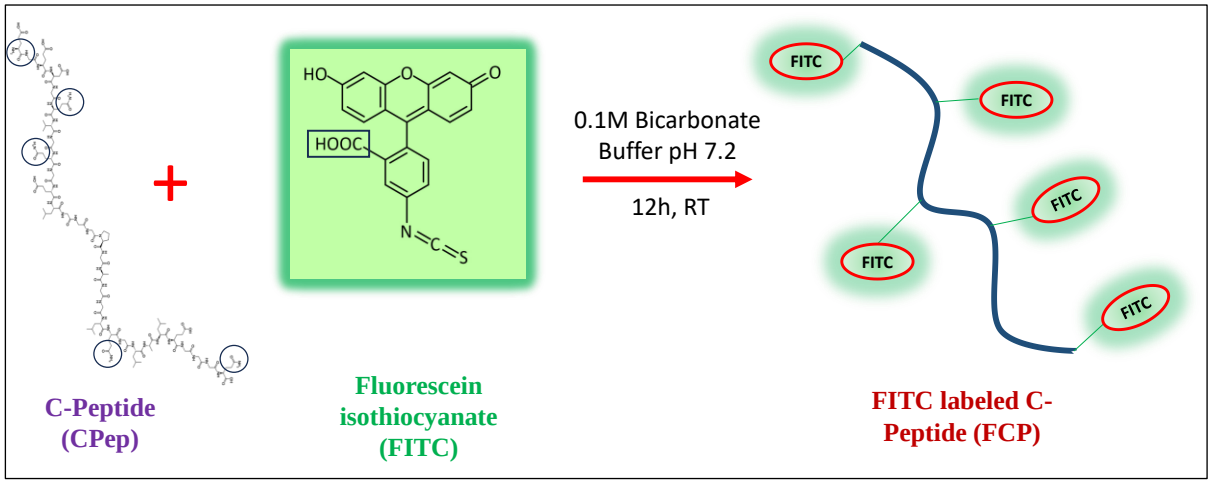


**Figure 4.2** Schematic diagram showing labeling of CPep with FITC to yield FITC labeled CPep (FCP).

#### 4.3.3.1 Gel retardation assay

The tris/tricine native polyacrylamide (PAGE) gel electrophoresis technique was utilized to confirm the complexation CPep with BNP. For this purpose, FITC labeled CPep (FCP) was synthesized *in-house* as illustrated in **Figure 4.2**. In this assay, the complexation ability of FCP with BNP was screened at different FCP:BNP ratios ranging from 2.5:1 to 10:1 and the ratio at which a restricted mobility of FCP was observed indicated as successful complexation.

### 4.3.4 CPep release study from NPX

In this study, 50 µg of free CPep and NPX containing an equivalent amount of CPep were transferred in a dialysis bag of MWCO 12,000-14,000 Da and immersed in 0.01 M phosphate buffer (pH 7.4) at a temperature of 37 °C. A time-dependent release study was performed by replacing complete 2 ml of release media at each time-point, i.e., 15 and 30 min, 1, 2, 4, 6, 12, 24, 36, 48, 72, 96, 120, 144 and 168 h. Samples were collected at each time point, centrifuged and analyzed using HPLC based analytical method to determine the CPep released at each time point. The samples were also analyzed for the structural integrity of the released CPep by circular dichroism (CD). CD is most widely used to study the secondary structure of peptides and proteins. For CD analysis, the samples were dispersed in deionized water and scanned at 25 °C at a 50 nm/min speed using a cell length of 1 cm in the CD (J-815 spectropolarimeter, JASCO) instrument. Here, free CPep and CPep released from NPX (*as detailed in section 3.3*) were analyzed for their secondary structure.

### 4.3.5 Stability study of NPX

The stability study was performed by incubating free CPep and NPX (~20 µg/mL CPep) in deionized water at 25 °C for 30 days. The samples were analyzed for change in CPep concentration using HPLC based method. Further, stability samples of NPX were also characterized for their particle size, PDI and zeta potential by DLS.

### 4.3.6 Cell culture based efficacy studies

NRK-52E cells were grown in DMEM supplemented with 10 % FBS and 1 % antibiotic solution (100 IU/mL penicillin/streptomycin) and maintained at 5 % $CO_2$ and 37 °C as reported in Chapter 3 (section 3.3.8). Herein, the free CPep and NPX were evaluated for their efficacy in the NRK-52E cells under normal as well as under metabolic and oxidative stress-induced conditions.

#### 4.3.6.1 Cell uptake studies of FCP nano-complex

##### 4.3.6.1.1 Qualitative uptake

After the initial passage of cells in cell culture flasks, $4\times10^4$ NRK-52E cells were seeded onto the coverslips placed inside 6-well plates and kept in complete media for surface adherence. The cells were further incubated with free FCP and FCP-NPX for 6h. Post-treatment, the cells were sequentially washed with phosphate buffer saline (PBS) thrice, fixed with paraformaldehyde, and stained with DAPI for nuclei staining. Further, the cellular uptake of

FCP and FCP nano-complexes was observed and compared using confocal microscopy (CLSM, Carl Zeiss, Germany).

#### 4.3.6.1.2 Quantitative uptake

In 6 well plates, $0.15 \times 10^6$ NRK-52E cells were seeded and allowed overnight to adhere to the culture plate. After the cell attachment, cells were treated with only either FCP or FCP-NPX for 6h. After 6 h, the cells were trypsinized, followed by washing with PBS (twice) and resuspended in 0.5 mL PBS to be run in flow cytometer (Cytoflex, M/s Beckman, Coulter, USA).

### 4.3.6.2 Cell viability under normal, oxidative stress and metabolic stressed conditions

Initially, $5\times10^3$ NRK-52E cells were seeded in 96 well plates and allowed to adhere to the surface overnight. The cytoprotective effect of CPep was evaluated in cells under normal conditions and in cells under stress conditions (both oxidative and metabolic stress). The metabolic and oxidative stress were induced by exposing the cells to high glucose (100 mM) containing media for 24 h or to hydrogen peroxide ($H_2O_2$; 250 μM) for 2 h as pre-treatment, respectively. After the induction of stress for the stipulated time period, media was replaced with the fresh media containing 50 nM free CPep, NPX (~ 50 nM CPep) and BNP for the next 48 h followed by MTT assay. The percent cell viability under different experimental conditions was analyzed using **Equation 3.5**.

### 4.3.6.3 Anti-oxidant effect under high glucose-mediated metabolic stress

The anti-oxidant effect of NPX on metabolically stressed NRK-52E was confirmed by quantifying nitrite (a marker of oxidative stress) by Griess's assay and GSH assay as an anti-oxidative marker. The cells ($5\times10^5$) were seeded in 100 mm petri plates, incubated in phenol red free DMEM complete media, and allowed to adhere. The cells were further challenged with glucose (100 mM) for 24 h, followed by initiating the treatment with free CPep and NPX for the next 48h. After treatment, the conditioned cell media was collected and cells were scrapped and washed thrice with PBS and then lysed in Tris/Triton-X-100 lysis buffer supplemented with 1X protease inhibitor. Further, the protein concentration of the cell lysate was ascertained by the Pierce™ BCA protein assay (as per the manufacturer's protocol). For estimation of nitrite and GSH concentrations in the conditioned media, it was further centrifuged at 5000 rpm for 5 min to remove dead cells and cellular debris. The prepared cell lysates and conditioned media were then subjected to anti-oxidant assays as per the details mentioned below.

#### 4.3.6.3.1 Nitrite estimation

Alteration of nitric oxide metabolism promotes renal oxidative stress. [22] For this, Griess reagent (1 % p-amino-benzene sulphonamide and 0.01 % naphthylethylenediamine in 2.5 % v/v phosphoric acid) was freshly prepared under dark conditions and stored at 4 °C. 100 µl of the prepared cell lysate or the conditioned media was taken into a microplate and mixed with 100 µl of Griess reagent and incubated for 30 min at 37 °C. After completion of the incubation period, absorbance was measured at 540 nm using a microplate reader. The corresponding concentration of nitrite present in the cell lysate was determined using the previously prepared standard curve of sodium nitrite.

#### 4.3.6.3.2 GSH assay

5,5′-dithiobis-(2-nitrobenzoic acid) (DTNB, also known as Ellman's reagent) forms adduct (GSH-TNB adduct) with GSH present in the cell lysate, giving a yellowish color. Herein, 100 µl of prepared cell lysate and the conditioned media were incubated with an equal volume of the DTNB solution at 37 °C for 30 min and the absorbance was measured at 412 nm utilizing microplate reader.

#### 4.3.6.3.3 Immunoblot assay for exploring the mechanism of action of CPep

The comparative anti-oxidative and cytoprotective effect of CPep and NPX were evaluated by immunoblot assay. Herein, cell lysate (~50 µg protein) from each treatment group was resolved on 12 % SDS-PAGE, transferred to the activated 0.22 µm PVDF membrane, and blocked with 3 % w/v BSA in TBST solution. The blots were probed with rabbit primary antibodies, β-actin, β1-integrin, EGFR, BAX, BCL2, TGF-β and Caspase3 (at 1:1000 ratio) overnight at 4 °C. The blots were then washed thrice in TBST and then re-probed with an anti-rabbit secondary antibody at 1:2000 ratio. Before visualization by Chemi-doc (Bio-Rad), the blots were developed using an ECL kit (Bio-Rad). The intensity of the protein band was quantified by densitometric analysis using ImageJ software.

### 4.3.7 Hemocompatibility study

As the study proposes the use of cationic polymer to formulate the nano-complexes, an overall positive surface charge might impart some cytotoxicity to the polymer. Hence, hemocompatibility of the BNP and NPX was evaluated.

Using a previously reported method in Chapter 3 (section 3.3.7), RBCs were separated from the animal blood using 10% ethylenediaminetetraacetic acid at 4500 rpm for 5 min. The cells were washed thrice, and diluted with normal saline (1:5), followed by incubation with normal saline (negative control), 0.1 % TritonX solution (positive control), 50 nM NPX and BNP (equivalent to NPX) for 1 h at RT. Further, each sample was centrifuged at 1500 rpm for 5 min and 200 µL of supernatant was analysed for OD at 540 nm. % Haemolysis was calculated for BNP and NPX using **Equation 3.4.**

Additionally, morphological changes in RBCs were also studied by field-emission scanning electron microscopy (FESEM). The RBCs (pelleted down) were fixed with 4% paraformaldehyde (PFA) and smeared on the coverslips. The cells were sequentially dehydrated with ascending ethanol concentrations from 30% to 100% and left overnight for air-drying. The samples were prepared by gold sputtering over the coverslips and then analysed by FESEM.

### 4.3.8 *In-vivo* pharmacokinetic study

Pharmacokinetic studies of CPep and NPX were carried out by intravenous (i.v.) injection of CPep (1 µg/kg) to the Wistar rats (200-220 g) and blood samples were withdrawn at predetermined time points. Plasma was retrieved from the blood immediately by centrifugation and stored at -80°C until required for assay. The plasma concentration of CPep was determined using commercially available CPep ELISA quantification kit (Rat C-peptide ELSA, FineTech). Using non-compartmental model, plasma concentration-time profile was plotted for CPep and NPX employing Phoenix Winonlin 8.3 version.

### 4.3.9 *In-vivo* efficacy study in diabetic nephropathy animal model

The STZ-induced nephropathy model was developed in Wistar rats (180-200g) by administering a single dose of STZ (42 mg/kg, intraperitoneal injection, i.p.) dissolved in ice-cold citrate buffer (0.01 M, pH 4.5). After 72 hours of STZ administration, fasting glucose levels were measured; animals with FGL greater than 250 mg/dL were considered diabetic and included in the study. After 4 weeks of STZ injection, renal functional parameters, i.e., microalbumin and creatinine levels were analysed in animal urine samples. For the urine collection, rats were housed separately in metabolic cages for 24 h and volume of urine collected was recorded as ml of urine/24 h. The animals were randomly divided into four groups: non-diabetic control/ healthy (NC), diabetic control (DC), diabetic/treated with free CPep and diabetic/treated with NPX. As treatment, the free peptide group received CPep

dispersed in deionized water at a dose of 1µM/kg/day and the NPX group received an equivalent dose of CPep once daily. NC and DC groups received i.p injections of sterile saline daily. The treatment was continued for 4 weeks and FGL was measured weekly by tail bleeding method using Accu-Check active glucometer **(Figure 4.3)**.

At the terminal study point (completion of the 8th week), animals from the DC group exhibited apparent renal failure with an increase in the microalbumin and creatinine amount, indicating worsening of the symptoms and complications of DN. The aggravation of the diseased condition was also confirmed by plasma IL-6 cytokine level measurement. At terminal time point, urine and plasma were collected for biochemical parameter estimation (measured using Coral clinical system kits) followed by euthanization of animals. Kidney was removed, washed, blotted dried and kept at -80 °C for immunoblotting studies. Further, pancreas and kidney were isolated and stored in 10% formalin solution, processed and stained for Hematoxylin & Eosin (H&E) and Periodic acid-Schiff (PAS) analysis.

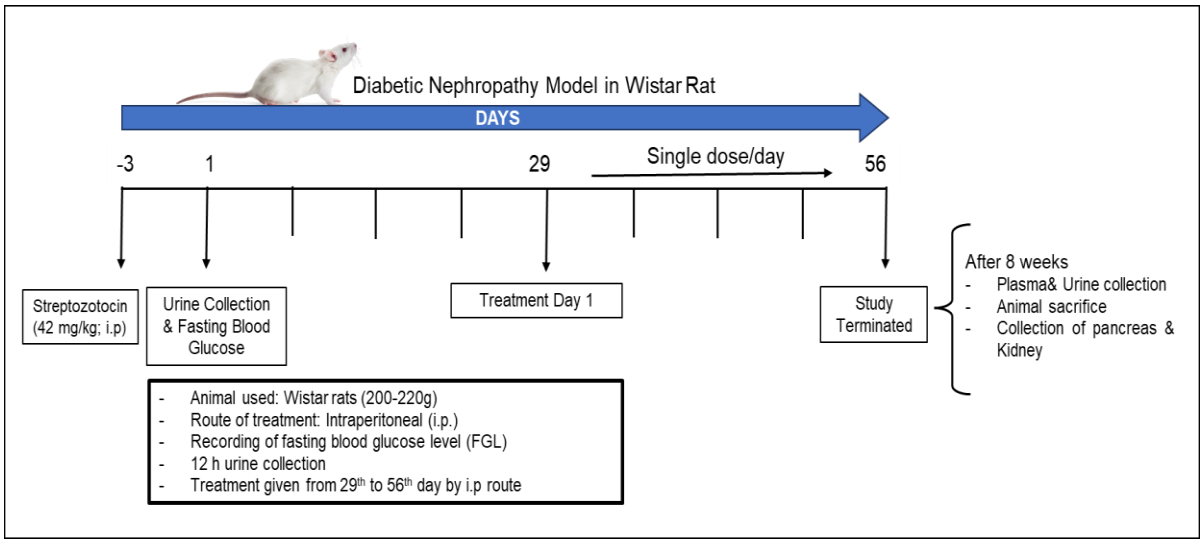


**Figure 4.3** *In-vivo* animal model development and study plan in STZ-induced DN.

### 4.3.10 Statistical analysis

All the data have been expressed as mean ± standard deviation and *in-vivo* data points as mean ± standard error of the mean, where the statistical significance of the data was analyzed using GraphPad Prism 8.0.1 software (GraphPad Software, San Diego, CA). Statistical analysis was performed using one-way ANOVA with non-parametric anaylsis by Tukey's multiple comparison test with a 95% confidence interval to confirm the difference between the groups. A p-value $< 0.05$ was considered statistically significant.

## 4.4 Results

### 4.4.1 Synthesis and characterization of monomers and cationic polymer

For peptide delivery, a cationic copolymer (**mPEG-b-P(CB-{g-DMDP}-co-LA**), Product 5) was synthesized **(Figure 4.1)** to impart a positive charge to BNP for electrostatic coupling with CPep to formulate NPX. As reported before, a cyclic carbonate( MBC; Product 2) was synthesized and characterized by $^{1}$H NMR (400MHz, $CDCl_3$) and showed proton peaks at δ 1.2 ($CH_3$, s, 1H), 4.3 ($CH_2$, d, 2H) and 4.7 ($CH_2$, d, 2H), δ 5.2 ($CH_2$, s, 2H) and δ 7.3 ($C_6H_5$, m, 5H) with 92% product yield (**Figure 4.4**). The polymerization was initiated by ring-opening polymerization reaction of MBC and D, L-Lactide with mPEG in the presence of tin(II) 2-ethylhexanoate results in Product 3 co-polymer with 42625 Da molecular weight estimated from the monomers present in co-polymer. Here, the $^{1}$H NMR showed the absence of two MBC peaks (δ 4.3 and δ 4.7) and after polymerization a single peak at δ 4.3 ($CH_2$, m, 4H) of 2-methyl-2-benzyoxycarbonyl-propylene carbonate (CB) appeared with δ 1.24 ($CH_3$, s, 3H), δ 5.2 ($CH_2$, s, 2H), δ 7.3 ($C_6H_5$, m, 5H) peaks, LA proton peaks at δ 1.6 ($CH_3$, s, 3H) and δ 5.2 (CH, q, 1H) and mPEG at δ 3.56 ($CH_2$, m, 4H) with yield of 88%. Co-polymer product 3 was then hydrogenated to reduce benzyl group protons to generate free carboxylic acid pendant group for coupling at δ 13 (COOH, s, 1H) on product 4 co-polymer backbone ($^{1}$H NMR 400mHz, d-DMSO) with a yield of 82%. Further, in the final step for producing a cationic polymer, DMDP cationic chain was grafted by the EDC-HOBt coupling reaction on the free carboxyl group on product 4 co-polymer to yield product 5-mPEG-b-P(CB-{g-DMDP}-co-LA). Through 1H NMR (400MHz, d-DMSO) DMDP peaks found at δ 2.1 (NH, s, 1H) and δ 8.4 (NH, s, 1H) by disappearing of COOH peak (**Figure 4.5**), where the molecular weight and % yield was mentioned in **Table 4.1**.

### 4.4.2 Preparation and characterization of C-peptide nano-complexes (NPX)

Using cationic copolymer, BNPs were prepared with an average particle size of 158.5±5.8 nm with polydispersity index (PDI) of 0.19±0.008 and zeta potential of +27.3±2.07 mV. NPX were prepared by an electrostatic interaction between positive charged BNPs and negatively charged CPep (it has an pI of 3.77; at pH greater than 3, CPep attains a negative charge -6.2 mV) as illustrated in **Figure 4.6 A**. The morphology of NPX was found to be spherical with 162 nm diameter under HR-TEM **(Figure 4.6 B)**. Upon formation of NPX, a slight increase in the particle size was observed (167.7 nm with PDI 0.2, **Figure 4.6 C**) as compared to BNP with a CPep complexation efficiency of 87.50 % and an overall reduction in ZP to +10.3 mV was evident **(Figure 4.6 D)** as per CPep HPLC method **(Table 2.4)**. Competition assay performed

by incubating the NPX in 10mM sodium acetate buffer (pH 3.0) exhibited 85.70 % dissociation of CPep from NPX, reconfirming similar complexation efficiency **(Table 4.2).**

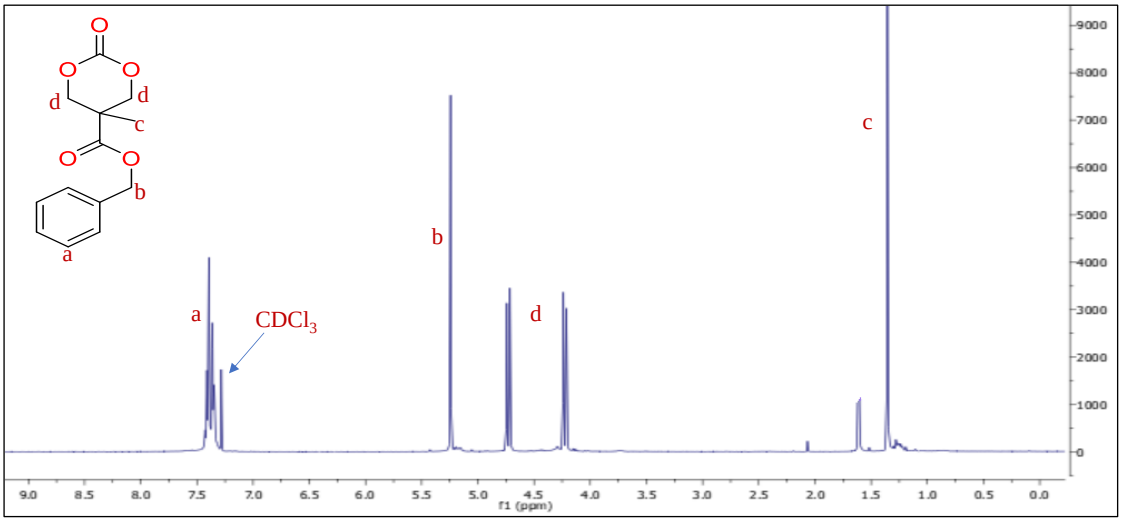


**Figure 4.4** $^{1}$H-NMR spectrum of MBC monomer.

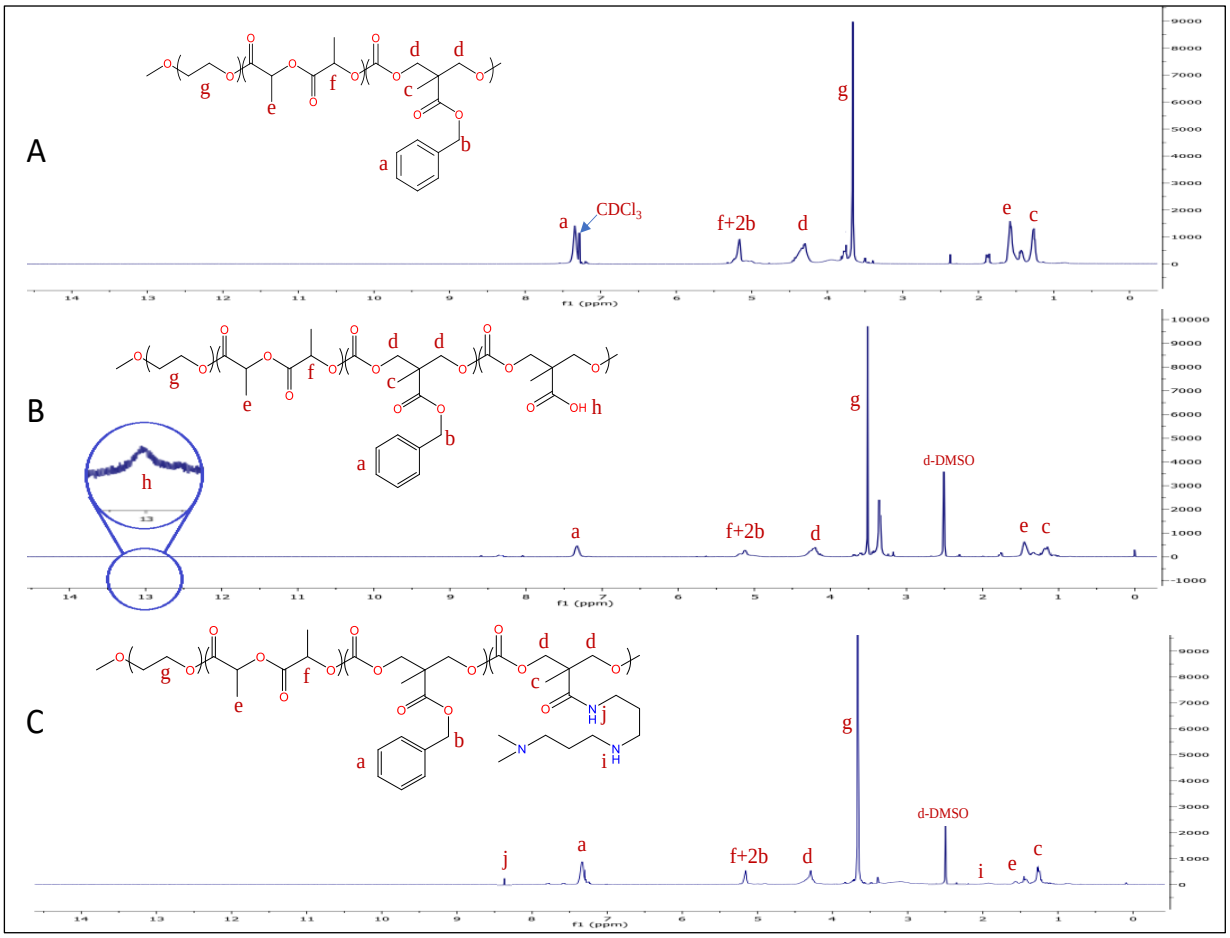


**Figure 4.5** Stacked $^{1}$H-NMR spectra of A) mPEG-b-P(CB-co-LA), B) mPEG-b-P(CB-{g-COOH}-co-LA) and, C) mPEG-b-P(CB-{g-DMDP}-co-LA).

**Table 4.1**
Estimation of monomer amount in cationic polymer by $^{1}H$ NMR.

| Product No. | Polymer | Copolymer units | Molecular weight (Da) | Yield (%) |
|---|---|---|---|---|
| 5 | mPEG-b-P(CB-[g-DMDP]-co-LA) | LA= 125<br>MBC= 42<br>CB-DMDP= 36 | 44,767 | 74 |

mPEG: methoxy polyethylene glycol, CB: carbonate chain, LA: lactic acid, MBC: 2-Methyl-2-benzyloxycarbonyl propylene carbonate.

**Table 4.2**
Characterization of NPX by DLS and HPLC.

| | C-peptide NPX | | | | | Dissociation of CPep from NPX | | | | |
|---|---|---|---|---|---|---|---|---|---|---|
| | DLS Characterization | | | % of CPep (HPLC) | | DLS Characterization of NPX left after CPep dissociation | | | % of CPep (HPLC) | |
| | Size (nm) | PDI | ZP (mV) | Super natant | NPX | Size (nm) | PDI | ZP (mV) | Super natant | NPX |
| **BNP** | 158.5± 5.8 | 0.19± 0.008 | 27.3±2.07 | - | - | - | - | - | - | - |
| **NPX** | 167.7± 2.5 | 0.2±0.007 | 10.3±4.5 | 11.3±4.4 | 87.5 ±2.9 | 168.1± 11.5 | 0.22±0.01 | 35.3±10.8 | 85.7±3.4 | 1.3± 2.1 |

DLS: dynamic light scattering, HPLC: high-performance liquid chromatography, PDI: poly-dispersity index, ZP: zeta potential, CPep: C-peptide, NPX: CPep nano-complexes, BNP: blank nanospheres.

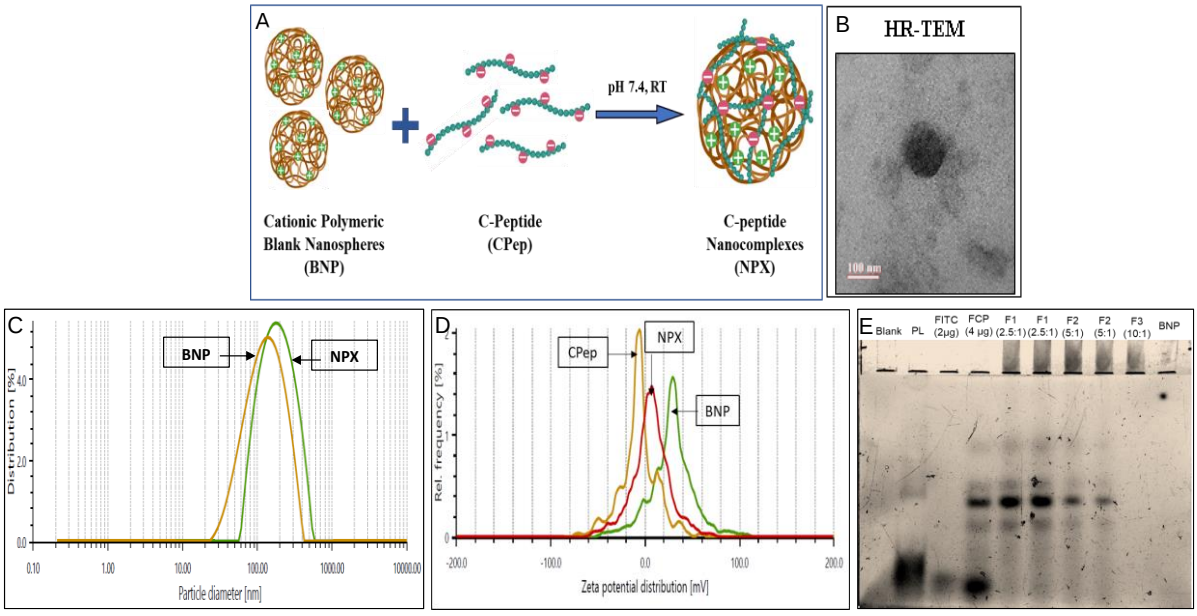


**Figure 4.6** Preparation and characterization of NPX. A) Schematic diagram of peptide complexation with cationic BNP at neutral pH. B) Morphological characterization of NPX by HR-TEM. C & D) Particle size and zeta potential of BNP and NPX. E) Gel retardation assay at different ratios of BNP:FCP (w/w; in µg) by native PAGE.
HR-TEM, high resolution transmission electron microscopy; PL, protein ladder; FITC, fluorescein isothiocyanate; BNP, blank nanospheres; FCP, FITC labeled CPep; F1, BNP:FCP::2.5:1; F2, BNP:FCP::5:1; F3, BNP:FCP::10:1.

### 4.4.3 Synthesis and characterization of FCP

FITC was successfully labeled to CPep to obtain fluorescent FCP wherein, the purity of FCP was analyzed by HPLC-based analytical method **(Table 2.4)**. Among various peaks, three peaks corresponds to free FITC were observed with FCP peak at 10.55 min **(Figure 4.7)**. After labeling CPep to FITC, the zeta potential of FCP was found to be similar to the free CPep (-4.5 mV at neutral pH).

#### 4.4.3.1 Gel retardation assay

FCP was employed to confirm the electrostatic complexation of CPep to the cationic BNPs using 15 % Tris-tricine Native PAGE technique. It was found that free FCP exhibited 2 intense fluorescence bands at 14 and 4 kDa and 3 faint bands at 42, 17 and 12 kDa when compared with multicolor low range protein ladder (PL), whereas after complexation, FCP bands were diminished in F1 & F2 (at ratios, 2.5:1 & 5:1) and disappeared completely at BNP:FCP ratio of 10:1 w/w (in µg) in F3 indicating effective complexation (**Figure 4.6 E**). Additionally, at all the ratios of BNP:FCP tested, NPX were seen to be retarded in the loading wells of the gel**,** indicating retarded mobility of CPep post-complexation with BNP.

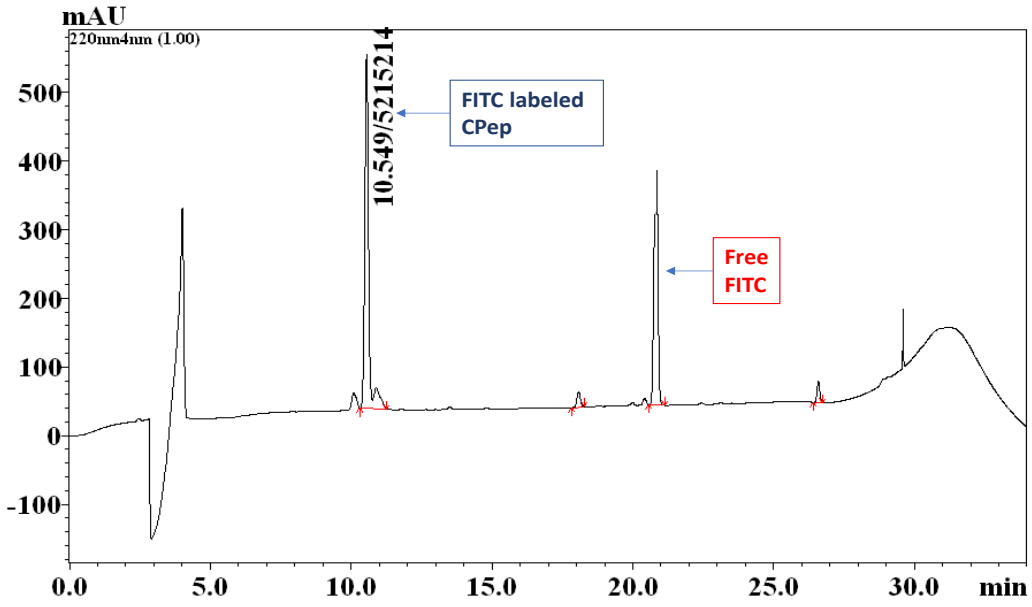


**Figure 4.7** HPLC characterization of FCP.

### 4.4.4 *In-vitro* release studies

#### 4.4.4.1. Cumulative release of Cpep

*In-vitro* release study of CPep from NPX in 0.01 M phosphate buffer pH 7.4 at 37 °C revealed release pattern similar to that of free CPep from the dialysis bag for the initial 6 h. However, free CPep could not be detected after 24 h, whereas NPX exhibited sustained release of CPep

for seven days **(Figure 4.8 A)**. While only a cumulative release of 40 % of CPep was observed from NPX which might be attributed to the degradation of C-peptide at pH 7.4 at 37 °C, only 20 % of free CPep was observed to be released indicating ~80 % of degradation of CPep in free form. This clearly demonstrates enhanced stability and steady release of the peptide after complexation with NPX.

### 4.4.4.2. Structural integrity of CPep released from NPX by Circular dichroism

The secondary structure of free CPep and its structure after getting released from NPX was determined by JASCO CD instrument. CD spectra of free CPep showed α-helix structure with three minima at 202, 208 and 222 nm. CD analysis of the CPep released from the NPX ($7^{th}$ day sample) exhibited a similar α-helix minima (**Figure 4.8 C)** as seen in case of free CPep (**Figure 4.8 B**), confirming the intactness of the CPep after complexation with BNP as well as under *in-vitro* release conditions till 7 days.

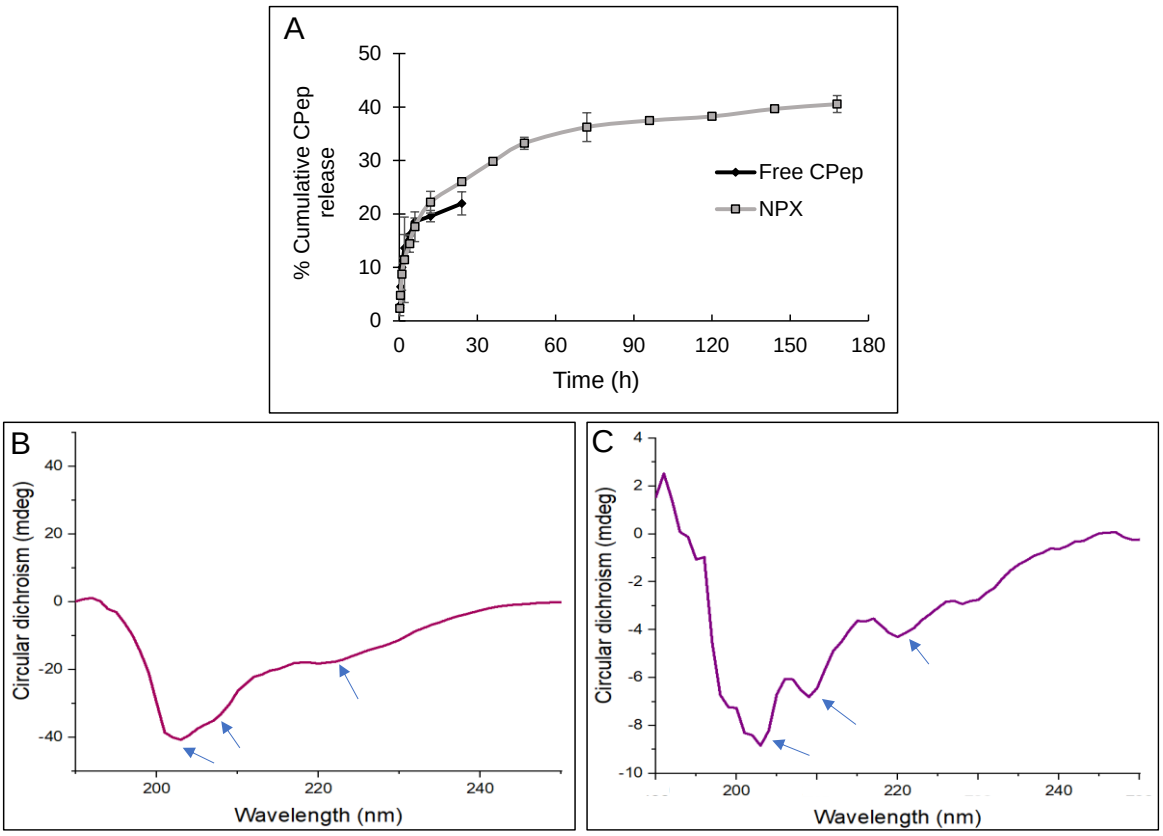


**Figure 4.8** *In-vitro* release of CPep from NPX. A) Release in 0.01M PBS at 37°C. Circular dichroism spectra of B) free CPep and, C) CPep released from NPX on day 7.
CPep, C-peptide; NPX, CPep nano-complexes.

### 4.4.5 Stability of NPX

The stability study of CPep and NPX was conducted to check the benchtop stability at 25 °C. Free CPep started degrading rapidly as seen by a decrease in concentration (**Figure 4.9 A)** and

could not be detected after 8 days. However, CPep in NPX was found to exhibit 100 % stability till 8 days of the study period, while 60 % of CPep could still be detected till 30 days. No significant differences were found in particle size and zeta potential of NPX till 20 days of incubation at 25 °C as compared to the day 1 sample **(Figure 4.9 B).**

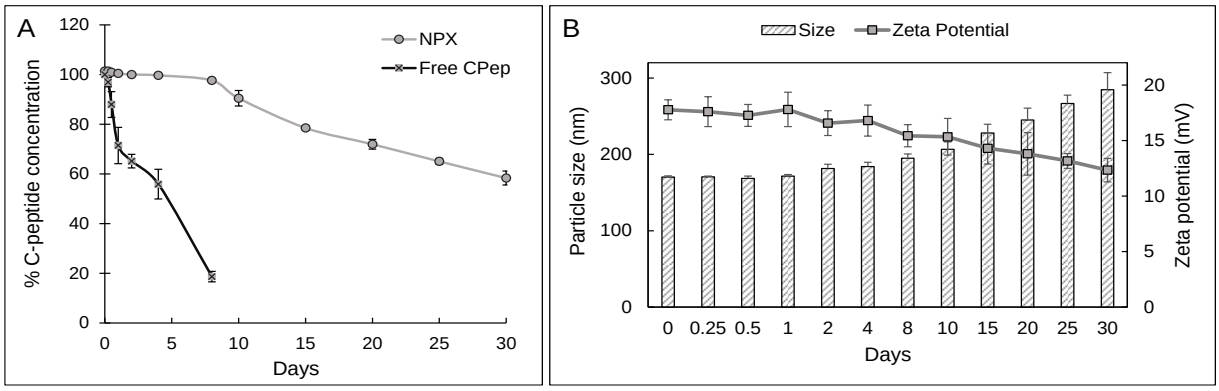


**Figure 4.9** Stability study of NPX at 25°C till 30 days. A) Concentration of CPep remaining intact. B) Particle size & zeta potential. Each data point represents mean (n=3) ± SD.

### 4.4.6 Cell culture studies

#### 4.4.6.1 Cell uptake study

The cellular uptake of FCP-NPX was confirmed by both qualitative and quantitative analysis using confocal microscopy and flow cytometry respectively (**Figure 4.10)**. In comparison to FCP treated NRK-52E cells, FCP-NPX treated cells showed intense green fluorescence surrounding the nucleus after 6 h of incubation **(Figure 4.10 A)**. Attributed to the efficient complexation between FCP and polymeric BNPs, enhanced FITC signal was observed in FCP-NPX treated cells confirming higher cell uptake (95.61 %) and longer residence time inside the cells by flow-cytometric analysis (**Figure 4.10 B and C**).

#### 4.4.6.2 Cell viability studies

The NRK-52E were treated with CPep and NPX for 48 h under three different conditions- normal condition (without stress), oxidative stress and metabolic stress. Under normal conditions (**Figure 4.11 A**), BNP demonstrated 96.32 ± 4.45 % cell viability. Under metabolic and oxidative stress conditions, the cell viability of NRK-52E cells decreased to 81.6 ± 6.79 % and 68.3 ± 3.54 %, which upon treatment with NPX, increased to 111.9 ± 5.2 % and 89.3 ± 2.25 %, respectively (**Figure 4.11 B and C**). Free CPep showed 100.64 ± 7.6 % and 80.24 ± 3.5 % viability of the cells under metabolic and oxidative stress conditions, respectively. Thus, the NPX exhibited better cell protection than free CPep, and enabled the cells to survive under the high glucose and $H_2O_2$ mediated stress conditions wherein more than 20 % & 15 % higher cell viability has been observed in NPX treated group as compared to cells under stress.

### 4.4.6.3 Nitrite estimation

The corresponding concentration of nitrite in the cell lysate of all the above samples was determined using a previously prepared standard curve of sodium nitrite. From **Figure 4.11 D1 and D2**, it can be concluded that the 50 nM concentration of CPep showed considerable anti-oxidant response by reducing nitrite concentration in cell-conditioned media and cell lysate. The cells treated with NPX exhibited nitrite concentration of 0.84 µM in cell lysate and 4.23 µM in cell-conditioned media as compared to the cells under stress (2.16 µM and 11.99 µM respectively).

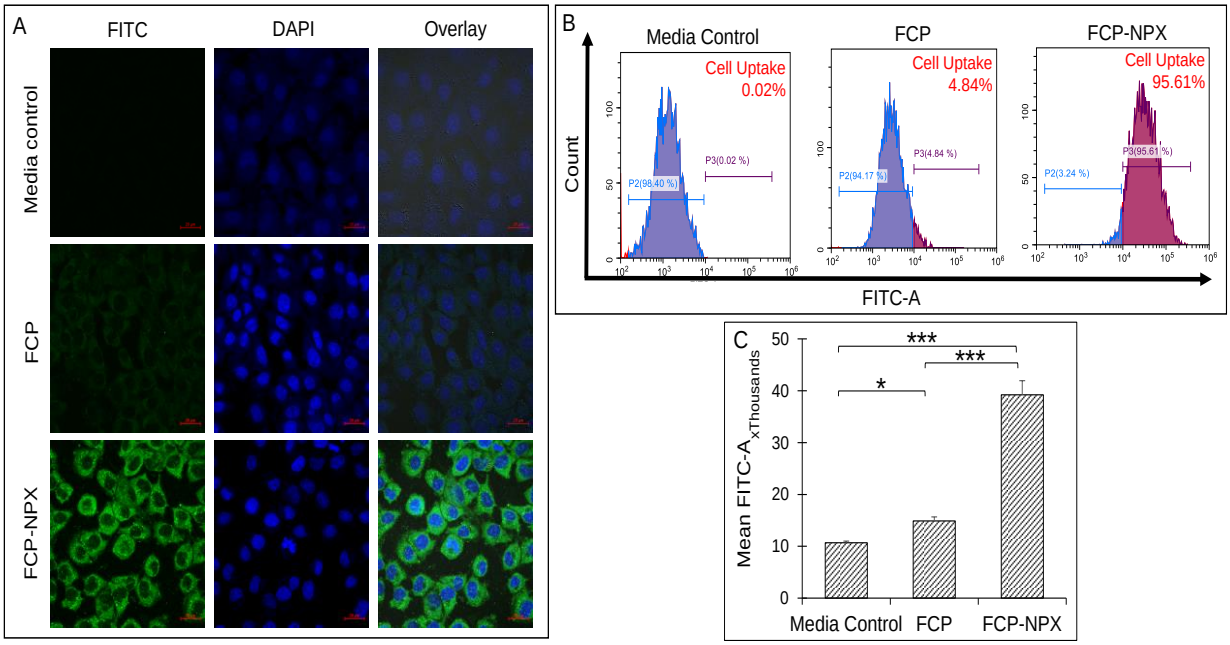


**Figure 4.10** Cell uptake study of FITC labeled CPep. A) Qualitative cell uptake by confocal microscopy. B) Quantitative cell uptake study by flow cytometry. C) Mean fluorescence intensity analyzed by flow cytometry after 6 h of incubation. *p<0.05; ***p<0.005. Each data point represents mean (n=3) ± SD.
FITC, fluorescein isothiocyanate; FCP, FITC labeled CPep; FCP-NPX, FCP nano-complexes; DAPI, 4′,6-diamidino-2-phenylindole fluorescent staining dye; FITC-A, FITC cytogram area.

### 4.4.6.4 GSH estimation

**Figures 4.11 E1 and E2** showed that CPep at 50 nM effectively demonstrated anti-oxidative response and elevated GSH concentration in cell conditioned media and cell lysate. Also, the cells treated with NPX demonstrated 1.8 and 1.4 fold higher response in cell conditioned media [equivalent to the normal cells in media control (MC) group] than the cells treated with PBS and free CPep.

### 4.4.6.5 Protein expression by western blotting

Oxidative stress elevates with increase in glucose concentration in the cell culture media, triggers ROS generation, leads to vasoconstriction, apoptosis, and cell death. However, CPep

has been reported to prevent and treat above mentioned problems. Here, housekeeping gene, β-actin has been used as a loading control to normalize protein levels of targeted protein. As indicated by the **Figure 4.12**, high glucose (HG)+NPX group showed reduced expression of apoptotic marker proteins (Caspase3 and BAX), increased expression of the cellular growth marker proteins (EGFR and β1-integrin), decreased expression of DN marker (TGF- β) and anti-apoptotic marker protein (BCL2). NPX upregulated EGFR and β1-integrin expression by 2.28 and 3.40 folds (**Figure 4.12 B)** and downregulated TGF-β expression by 1.67 folds **(Figure 4.12 C)** in comparison to HG control group. This proved the growth stimulatory effect of the NPX in NRK-52E cells even under high glucose-mediated metabolic stress conditions. In case of apoptotic marker proteins, BAX, BCL2 and caspase3 (**Figure 4.12 C and 4.12 D)** NPX treatment depicted 3.54 folds increase in BCL2, 2.7 folds decline in BAX and almost 2 times reduced expression of Caspase-3 in comparison to HG pre-treated NRK-52E cells. Additionally, NPX showed 1.65 and 1.19 fold reduction in apoptotic protein BAX and Caspase 3 expression respectively in comparison to the free CPep treated group. These observations clearly indicated enhanced cytoprotective activity of NPX in metabolically stressed NRK-52E cells.

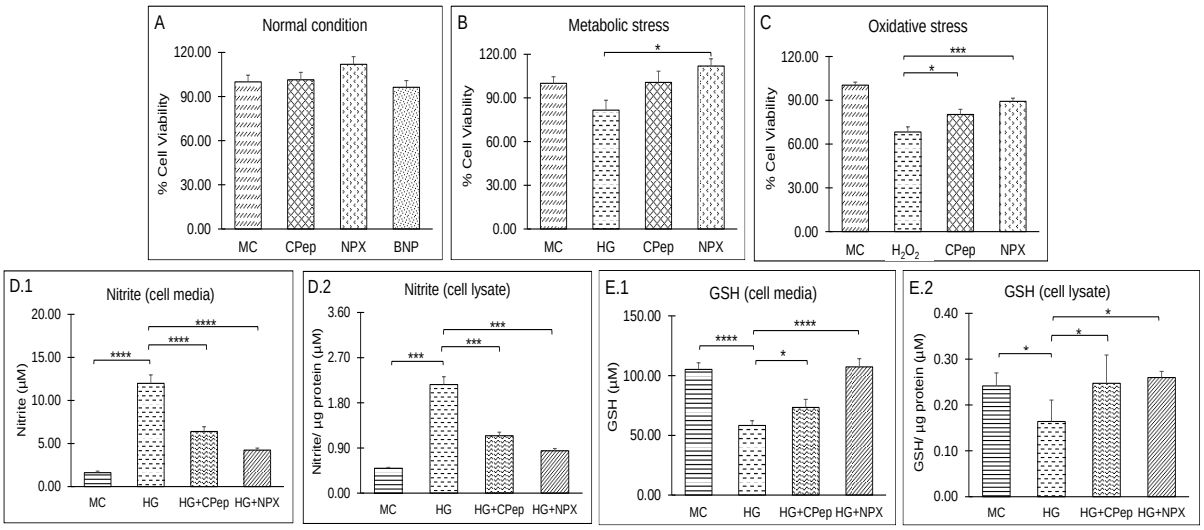


**Figure 4.11** Cytoprotective ability of free CPep/NPX under A) normal condition, B) metabolic stress condition (100 mM glucose) and C) oxidative stress condition (250 µM hydrogen peroxide). D1 & D2) Estimation of nitrite under metabolic stress in both cell conditioned media and cell lysate. E1 & E2) GSH determination under metabolic stress in both cell conditioned media and cell lysate. *p<0.05; ***p<0.005; ****p<0.0001. Each data point represents mean (n=3) ± SD.

MC, media control; CPep, C-peptide; NPX, CPep nano-complexes; BNP, blank nanospheres; HG, high glucose; $H_2O_2$, hydrogen peroxide; GSH, glutathione; HG+CPep, cells grown in high glucose media treated with C-peptide; HG+NPX, cells grown in high glucose media treated with CPep nano-complexes.

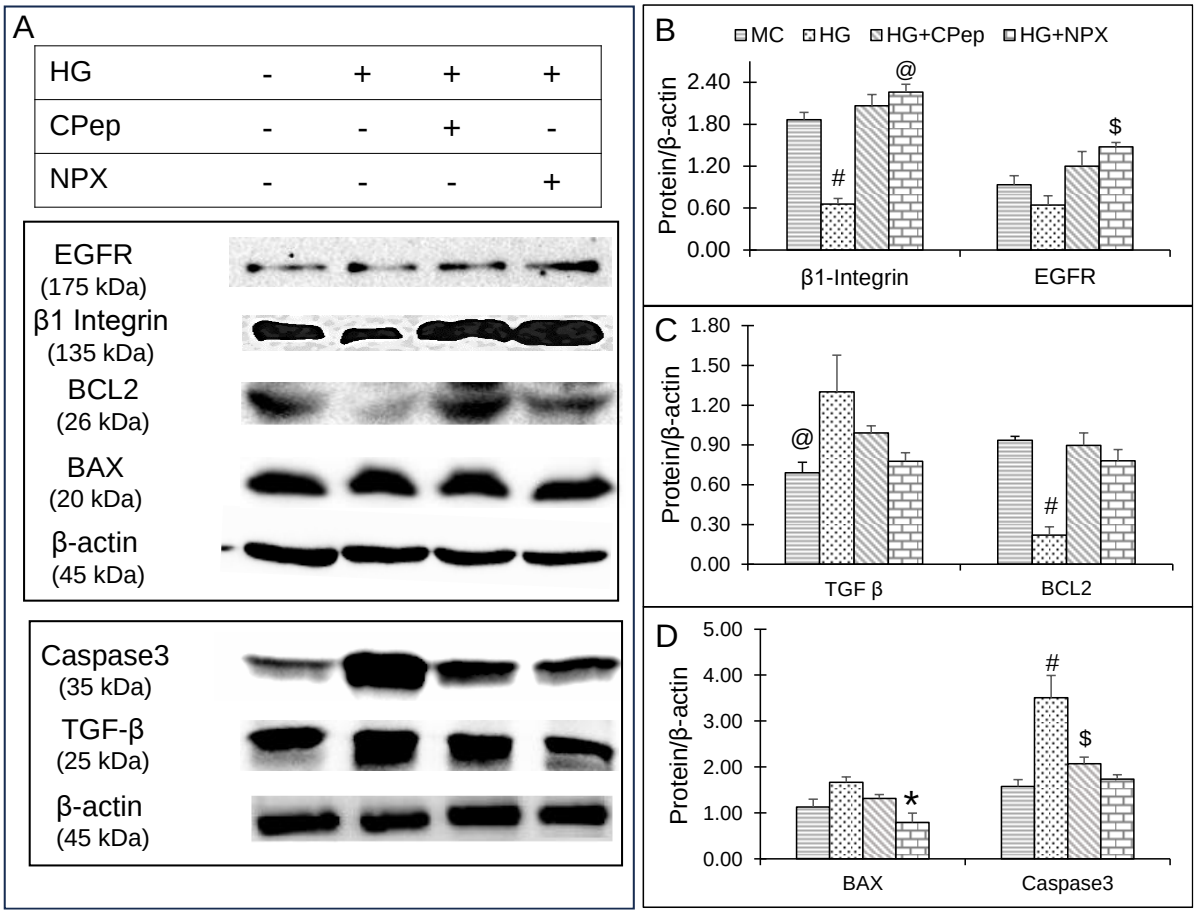


**Figure 4.12** Expression of marker proteins in NRK-52E cells. A) Relative protein expression upon incubation with MC, HG, HG+CPep and HG+NPX. Fold change in protein expression of B) β1-integrin and EGFR $^{\#}$HG *vs* MC and HG+CPep ($^{\#}p<0.01$), $^{@}$HG *vs* HG+NPX ($^{@}p<0.001$), $^{\$}$HG *vs* HG+NPX ($^{\$}p<0.05$); C) TGF-β and BCL2 $^{@}$HG *vs* MC ($^{@}p<0.05$), $^{\#}$HG *vs* MC, HG+CPep and HG+NPX ($^{\#}p<0.005$); D) BAX and Caspase-3 *HG *vs* HG+NPX, $^{\$}$HG *vs* HG+CPep ($^{*\$}p<0.05$), $^{\#}$HG *vs* MC and HG+NPX ($^{\#}p<0.01$). Each data point represents mean (n=3)±SD.
MC, media control; HG, high glucose; CPep, C-peptide; NPX, CPep nano-complexes; HG+CPep, cells grown in high glucose media treated with C-peptide; HG+NPX, cells grown in high glucose media treated with CPep nano-complexes.

### 4.4.7 Hemocompatibility study

This visual evaluation of the integrity of RBCs confirmed the hemocompatibility of BNP and NPX as shown in **Figure 4.13 A**. OD values of different treatment groups were compared with positive control group (0.1% triton X causing 100% cell lysis) in **Figure 4.13 B** wherein, NPX and BNP demonstrated negligible hemolysis i.e., 0.35±0,14 % and 1.4±3.7 %, respectively. Therefore, NPX proved to be safe for use in *in-vivo* animal models for further studies. Morphological analysis of RBCs incubated with various test samples provided additional support to the haemocompatibility of BNP and NPX. As indicated in **Figure 4.13 C**, positive control group depicted clear rupture of RBCs, while BNP and NPX showed negligible impact on the RBC morphology which resembled the RBCs in negative control group.

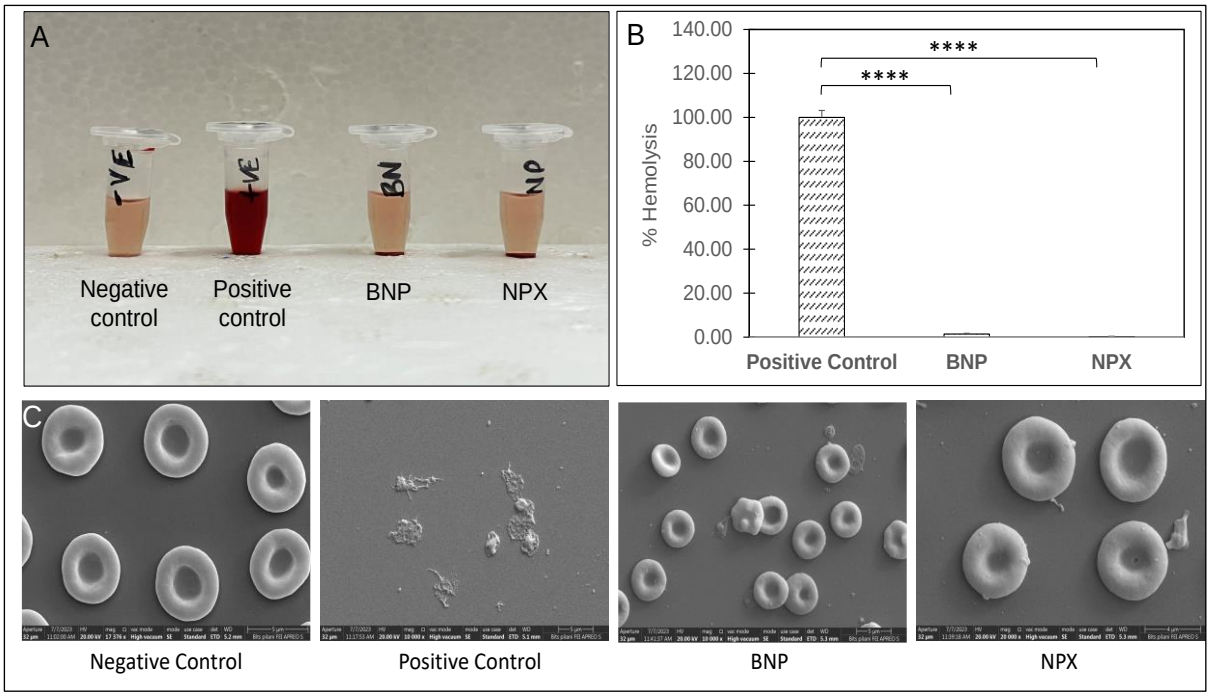


**Figure 4.13** Hemocompatibility study of BNP and NPX particles. A) Visual illustration of *Wistar* blood supernatant after 1 h of incubation. B) Hemolysis assay. C) Scanning electron microscopy of RBCs after 1 h of incubation. ****p<0.0001. Each data point represents mean (n=3)±SD.
BNP, blank nanospheres; NPX, CPep nano-complexes; RBCs, red blood cells.

### 4.4.8 Pharmacokinetic studies

The non-compartmental estimation of pharmacokinetic parameters showed that the half-life of CPep was increased by 6.34 folds when administered as NPX compared to free CPep. After i.v. injection, NPX exhibited $T_{max}$ within an hour followed by a controlled release of CPep as illustrated in **Figure 4.14**. As summarised in **Table 4.3**, the $t_{1/2}$ and MRT of NPX were 21.95±2.63 h and 25.90±2.99 h, respectively. Moreover, apparent volume of distribution ($V_d$) and apparent clearance (Cl) of CPep decreased by 1.7 and 12.3 fold in NPX compared to free CPep which clearly proved prolonged *in-vivo* retention of NPX. This further would enable overcoming the limitations of short half-life and rapid elimination of CPep *in-vivo*.

### 4.4.9 *In-vivo* efficacy study

The animals were monitored for FGL and body weight weekly and sacrificed after 8 weeks as shown in **Figure 4.3.** The induction of diabetes by STZ is commonly determined by a significant increase in the FGL wherein, DC demonstrated 526±16.22 mg/dL of FGL, which was 6.26 folds higher than the NC group after 8 weeks of diabetic induction. Further, NPX played significantly better role in lowering FGL to 407.5±18.17 mg/dL compared to free CPep (504.5±6.02 mg/dL) and DC group (**Figure 4.15 A**). DN also causes a decrease in animal body weight; here, the average body weight was kept similar within each group at the beginning of

the treatment. As shown in **Figure 4.15 B**, DC showed significantly lower body weight than NC. In contrast, after four weeks of diabetes induction, all animals exhibited reduced body weight attributed to the diabetic condition as compared to their initial weights however, by the end of the study, NPX treated animals gained substantial weight.

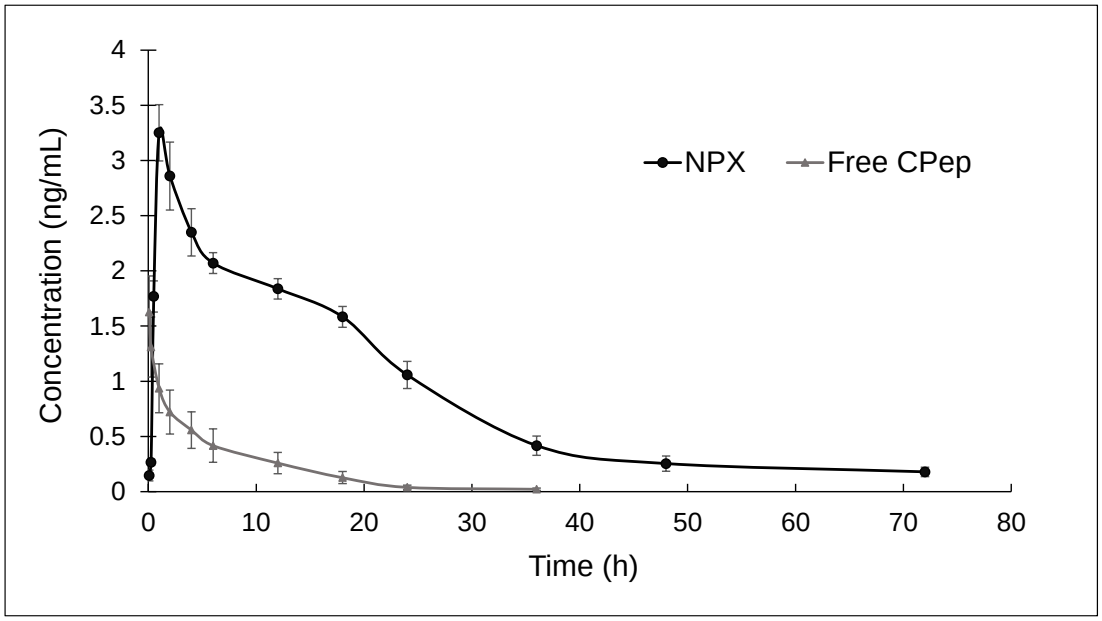


**Figure 4.14** Plasma concentration-time profile of free CPep and NPX in Wistar rats at ~1µg/kg dose of CPep after i.v. adminstration. Each point represents mean (n=3) ± SEM.
CPep, C-peptide; NPX, CPep nano-complexes.

**Table 4.3**
*In-vivo* pharmacokinetic parameters of CPep.

| Parameters | Free CPep | NPX |
|---|---|---|
| $C_{max}$ (ng/mL) | 1.627±0.326 | 3.217±0.255 |
| $T_{max}$ (h) | 0.083±0.00 | 1.0±0.00 |
| $t_{½}$ (h) | 3.468±0.65 | 21.951±2.631 |
| $K_e$ (1/h) | 0.213±0.035 | 0.032±0.004 |
| $AUC_{0-\infty}$ (h*ng/mL) | 8.145±2.651 | 68.091±5.53 |
| MRT (h) | 6.175±0.765 | 25.90±2.995 |
| $V_d$ (mL/kg) | 793.047±283.663 | 462.31±17.374 |
| Cl (mL/h/kg) | 178.98±86.332 | 14.875±1.167 |

*CPep and NPX (1 µg/kg; i.v.) were administered to rats and analyzed by non-compartmental method; mean (n=3) ±SEM.

$C_{max}$: maximum concentration, $T_{max}$: time taken to reach maximum concentration, $t_{½}$: half-life, $K_e$: elimination rate constant, $AUC_{0-\infty}$: area under the curve from time 0 to last measurable concentration, MRT: mean residence time, $V_d$: volume of distribution, Cl: clearance, CPep: C-peptide, NPX: CPep nano-complexes.

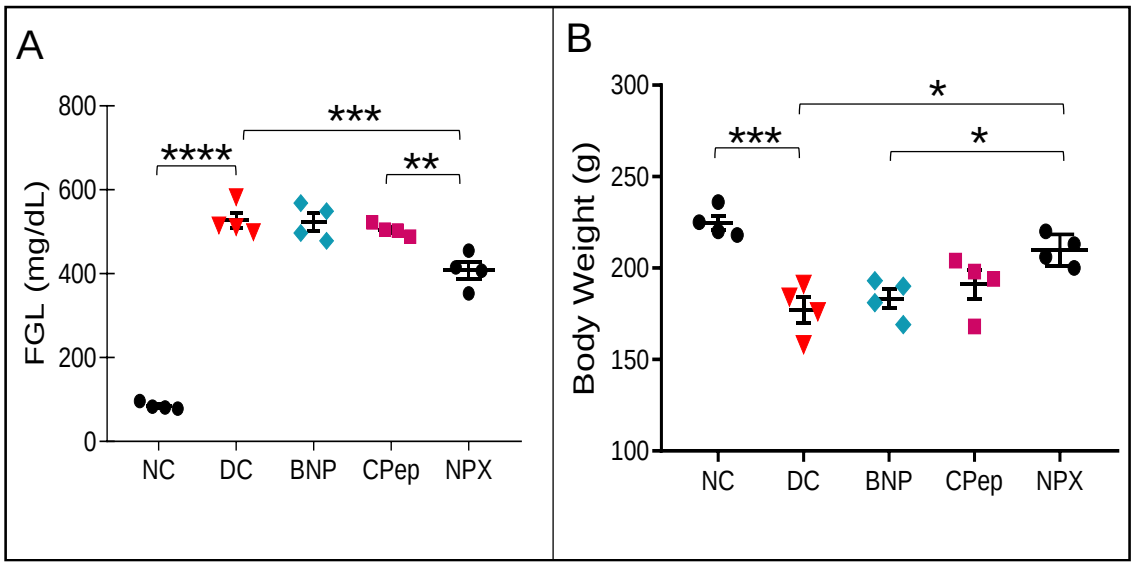


**Figure 4.15** *In-vivo* efficacy study in STZ-induced DN animal model. A) Terminal fasting blood glucose level (FGL) after 8 weeks. B) Animal body weight after 8 weeks. *p<0.05; **p<0.01; ***p<0.005; ****p<0.0001. Each data point represents mean (n=4)±SEM.
FGL, fasting glucose level; NC, normal control; DC, diabetic control; BNP, blank nanospheres; CPep, C-peptide; NPX, CPep nano-complexes.

### 4.4.9.1 IL-6 cytokine estimation

IL-6 signaling is involved in the inflammatory responses that are central to the progression of DN. [23] The prevalence and severity of DN is also directly connected with level of pro-inflammatory cytokines in the body. The level of IL-6 in the plasma in DC group was 3421 pg/mL that was significantly decreased to 1336.67 pg/mL upon treatment with NPX (**Figure 4.16**). Normalizing the level of cytokines delays progression of diabetes to its associated complications. [7, 24, 25]

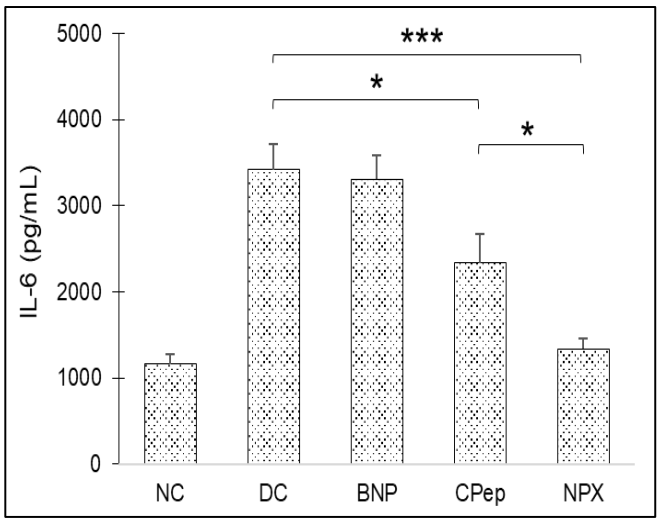


**Figure 4.16** Estimation of IL-6 cytokine level in plasma. *p<0.05; ***p<0.005. Each data point represents mean (n=4) ± SEM.
IL-6, interleukin-6; NC, normal control; DC, diabetic control; BNP, blank nanospheres; CPep, C-peptide; NPX, CPep nano-complexes.

#### 4.4.9.2 Biochemical assay

At the end of the study (8$^{th}$ week), urine and plasma samples exhibited marked increase in the levels of albumin and creatinine, indicating microalbuminuria and progression of DN. NPX treatment significantly reduced the urine creatinine and albumin levels by 5.8 and 2.3 fold compared to the DC group. The other two parameters, blood urea nitrogen (BUN) and uric acid were utilized to evaluate renal functions and indicated effectiveness of NPX towards decreasing BUN and uric acid accumulation in blood plasma (3.4 and 1.7 fold). Hyperlipidaemia is common in patients with DM, which leads to lipid accumulation in kidney causing vascular damage. Here, both plasma cholesterol and triglycerides (TG) were reduced by 1.6 fold by NPX compared to DC group (**Table 4.4**).

**Table 4.4**
Biochemical analysis of urine and plasma samples after 8 weeks of treatment (n=3).

| | Urine | | Plasma | | | |
|---|---|---|---|---|---|---|
| | **Creatinine (g/L)** | **Albumin (mg/L)** | **BUN (mg%)** | **Uric acid (mg/dL)** | **Cholesterol (mg/dL)** | **TG (mg/dL)** |
| **NC** | 0.23±0.05 | 8.92±1.99 | 22.61±0.43 | 3.19±0.21 | 113.04±3.37 | 137.46±3.42 |
| **DC** | 2.51±0.24 | 39.55±8.17 | 93.98±2.77 | 6.57±0.39 | 212.95±9.56 | 246.69±10.21 |
| **BNP** | 2.47±0.26 | 38.35±3.45 | 84.76±3.55 | 6.68±0.33 | 208.29±9.67 | 227.87±7.36 |
| **CPep** | 1.56±0.24 | 22.78±3.21 | 42.23±2.03 | 5.12±0.46 | 166.13±8.52 | 185.46±8.45 |
| **NPX** | 0.43±0.06 | 17.49±1.83 | 27.91±1.68 | 3.95±0.17 | 131.06±7.20 | 141.01±5.71 |

NC: Normal control, DC: diabetic control, BNP: blank nanospheres, CPep: C-peptide, NPX: CPep nano-complexes, BUN: blood urea nitrogen, TG: triglycerides.

#### 4.4.9.3 Immunoblotting study

The kidney samples collected from the animal groups were investigated for cytokines and apoptotic markers (**Figure 4.17 E**). **Figure 4.17 F** demonstrates an increased level of TGF-β expression in kidney samples of DC compared to NPX treated animals (2.3 folds reduction). Also, NPX elicited its action by inhibiting apoptosis as concluded by significantly lowered caspase3 protein level and increased BCL2 protein level in the kidney (~3 folds) when compared to DC group.

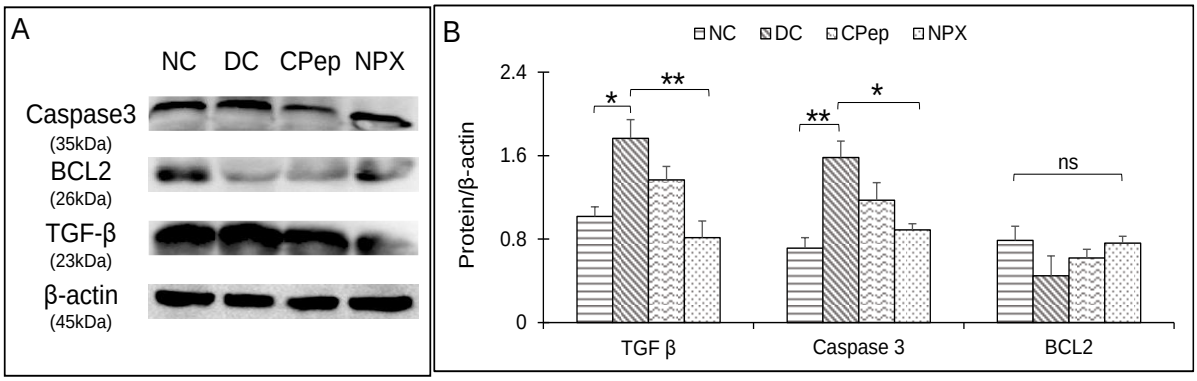


**Figure 4.17** A) Immunoblots quantified by densitometry analysis. A) Relative protein expressions of TGF-β, Caspase3 and BCL2. β-actin was used as a loading control to normalize the protein amount. *p<0.05; **p<0.01; ns, non-significant.

#### 4.4.9.4 Effect on pancreatic islets

After administering treatment for 4 weeks to the diabetic animals, these were sacrificed for the assessment of pancreatic islet morphology by H&E staining. The β-cells in DC after 4 weeks were found distorted, and very few of these were visible in islets of Langerhans (IL) after H&E staining compared to NC, CPep and NPX. In comparison to the NPX-treated group, the CPep treated group failed to prevent ROS attack on the cells as indicated by higher concentration of cytokines along with necrotic and cellular inflammatory islets. NPX demonstrated protection of β-cells from STZ-induced diabetic conditions and maintained cell integrity as illustrated in **Figure 4.18 A.** [20] **Figure 4.18 D** depicts the pancreatic damage score (0-4) indicating cell inflammation, necrosis and destruction of islets in the pancreatic tissue; a score of 4 indicates maximum damage while 0 indicates least damage. Among all the treatment groups, NPX showed significantly lesser necrosis and pancreatic damage with a score of 1.25. [26]

### 4.9.5 Effect on kidney

**Figure 4.18 B and C** indicate the histopathological changes in the kidney sections by H&E and PAS (Periodic-acid Schiff) staining evaluated by microscopy at 400 X magnification. The H&E staining in **Figure 4.18 B** showed normal glomerulus (G) and tubules in cortical region of kidney (PCT- Proximal Convoluted Tubule & DT-Distal tubule) without any pathological changes in NC group whereas, DC demonstrated severe glomerulosclerosis, vacuolation of tubular epithelial cell, shrinkage of glomerulus, thickening of Bowman's capsules and wide glomerular space of the nephron. The kidney sections of animals treated with CPep (1μM/kg/day) and NPX (equivalent to 1μM/kg/day of CPep) exhibited improvement in the kidney cyto-histology. Compared to the free CPep-treated group, NPX treatment significantly improved the nephron condition by reducing glomerular hypertrophy, tubular injury and mesangial expansion in kidney sections also supported by damage score of 1.16 compared to

2.83 in DN control group **(Figure 4.18 E)**. The glomerular and tubular necrosis are important parameters to be ascertained in DN, and therefore a blinded visual semiquantitative damage score ranging from 0 to 4 was used wherein, score 0 indicated minimal change in glomerular structure and integrity as seen in NC, while a score of 4 represented glomerular damage with hypertrophy and tubular injury. [27]

In **Figure 4.18 C,** the pathological condition of glomerulus in DN was assessed by PAS staining. In comparison to NC, DN depicted glycoprotein rich extracellular matrix components inside glomeruli that appear purple in the microscopy. In the case of DN, glomerular hypertrophy, mesangial cell (MC) proliferation, and renal tubular epithelial degeneration were observed. However, kidney sections of the free CPep and NPX treated groups indicated attenuated disease conditions along with reduction in PAS positive cells indicating reduced intracellular glycogen accumulation along with diminished infiltration of the inflammatory cells (blue nucleus). The condition improved further with mild mesangial expansion, lesser deposition of mesangial matrix and almost normal relative glomerular basement membrane (BS) thickness demonstrating a significantly reduced score in samples obtained from the NPX treated group **(Figure 4.18 F)**.

### 4.5 Discussion

DN is one of the most prevalent subtypes of complications associated with diabetes, characterized by the progression from microalbuminuria to macroalbuminuria and haematuria alongside impaired kidney function. The primary reason behind DN is attributed to the activation of several oxidative stress-related pathways involving physiological modulation by different growth factors and cytokines, i.e., TNF-α, NF-κB, TGF-β and many more. Long-term insulin can help achieve the normal blood glucose level but cannot suppress the progression of DN and other complications as mentioned in Diabetes Control and Complication Trials (DCCT).

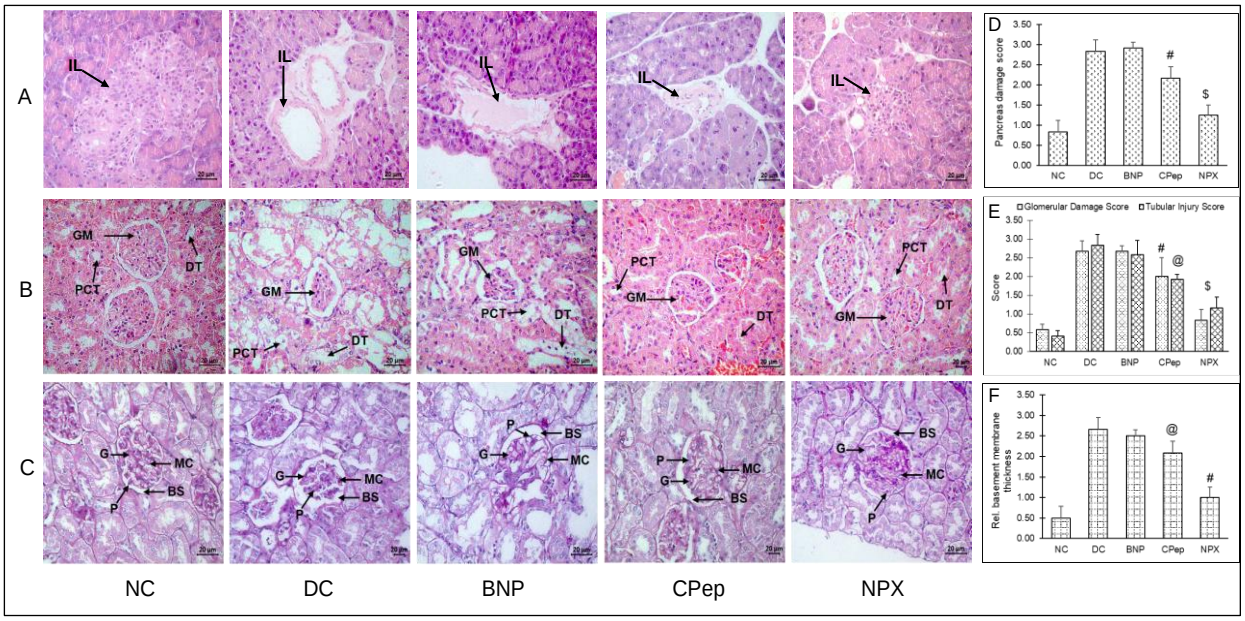


**Figure 4.18** Histopathological examination. A) H&E stained sections of pancreas, B) H&E stained sections of kidney and, C) PAS staining of kidney (400 × magnification; 20 µm scale). Scoring represents the extent of damage to, D) pancreas $^{\$}$HG *vs* HG+NPX ($^{\$}$p<0.0005), $^{\#}$HG+CPep *vs* HG+NPX ($^{\#}$p<0.01); E) glomerulus and tubules $^{\$}$HG *vs* HG+NPX ($^{\$}$p<0.0005), $^{\#}$HG+CPep *vs* HG+NPX ($^{\#}$p<0.01), $^{@}$HG+CPep *vs* HG+NPX ($^{@}$p<0.05); F) relative basement membrane thickness $^{@}$HG *vs* HG+NPX ($^{@}$p<0.005), $^{@}$HG+CPep *vs* HG+NPX ($^{@}$p<0.05) Each data point represents mean (n=3) ± SD.

NC, normal control; DC, diabetic control; BNP, blank nanospheres; CPep, C-peptide; NPX, CPep nano-complexes; IL, Islets of Langerhans; GM, Glomerulus; PCT, proximal convoluted tubule; DT, distal tubule; G, glomeruli; P, podocytes; MC, mesangial cells; BS, basement membrane.

In this context, we have designed a system to sustain the delivery of CPep, a cleavage product of pro-insulin, which has shown therapeutic potential for treating diabetes and is proven to be renoprotective in several recent studies. [7, 13, 28, 29] Despite having promising therapeutic implications, CPep faced odds for the treatment of DN due to its very short circulation half-life ($t_{1/2}$ 30 min), rapid metabolism and ease of elimination from the body. Recently, protein/ peptide therapeutics have demonstrated extraordinary and promising outcomes in the treatment of DM and DM linked complications. [30-32] In fact, a long acting CPep analog (PEG-CPep) administered once-weekly by subcutaneous route at doses of 0.8 mg and 2.4 mg over a 12 month period (tested on 250 patients) resulted in marked improvement of vibration perception threshold (VPT) in comparison to placebo injections. A cationic chitosan/pectin nanocarrier system has also been developed to complex insulin electrostatically and deliver it orally to avoid patient non-compliance and protect insulin in the GI environment. The current work aimed to develop a nano-complex formulation for CPep wherein, it was electrostatically conjugated to an *in-house* synthesized cationic polymer with an objective of prolonging its residence time inside the body thus enhancing its therapeutic efficacy. This polymeric NPX system further aimed controlled delivery of CPep by increasing its *in-vivo* stability, enabling

extended half-life. By shielding CPep from *in-vivo* degradation and by maintaining its structural integrity, it was further intended to enhance its antioxidant, cell-proliferative, and anti-inflammatory activity. The NPX so formulated also proved its anti-diabetic and reno protective effect in STZ-induced T1DN animal model.

Previously, our group had synthesized cationic amphiphilic copolymers to formulate biocompatible and biodegradable lipopolymeric nanoplexes to deliver negatively charged mi-RNA34a to breast cancer cells. [19] The present PEC-based polymer was prepared with the same strategy but with higher molecular weight (44,767 Da) and hydrophobicity (Product 5). The final units attached to the cationic polymer were, $mPEG_{114}$, $LA_{125}$, $MBC_{36}$ & PCB-g-$DMDP_{42}$, respectively wherein, LA and MBC units contribute to an increase in polymer hydrophobicity because of presence of long carbon chains in their structure resulting in increasing the retention time of nano-formulations in body. Therefore, a high molecular weight cationic polymer bears significant potential to complex more amount of biomolecule like CPep along with provding a sustained release. [33]

The disadvantages associated with the covalent conjugation of a peptide includes inactivity of the potent peptide molecule due to the use of various reagents in harsh reaction conditions. Additionally, hydrophilicity of peptides limits their encapsulation in nanoparticles, eventually resulting in low payload. To overcome these limitations, electrostatic interaction was employed in this study wherein, an *in-house* synthesized cationic polymer was utilized to formulate BNPs (positively charged) to complex with negatively charged CPep by incubation at physiological pH. After complexation, a slight increase in nano-sized NPX particles with decreased ZP was observed compared to BNP (**Figure 4.6 C and D**). The complexation efficiency of CPep in NPX was found to be 87.50 % by modified HPLC gradient method. To reconfirm the complexation, *in-vitro* dissociation of CPep from NPX was carried out using 10 mM sodium acetate buffer (pH 3.0; pH value less than its pI). Sodium acetate buffer caused protonation of CPep and dissociated it from the BNP; 85.70 % of the dissociated CPep was detected in the supernatant (**Table 4.3**). The structural integrity of CPep during the formulation process was confirmed when, NPX was found to release the CPep in a controlled manner for 180 h at RT, while free CPep was not detected after 24 h. Additionally, CD was employed to study the secondary structure of peptides and proteins, namely α-helix, β-sheet and random coiling. The conformational changes by amide present in the peptide absorb circularly polarized light in a far-UV region (190-230 nm). The CD analysis confirmed no confirmational change with identical α-helix minima at 202 nm, 208 nm and 222 nm, in free CPep and released CPep from

NPX, demonstrating the structural intactness of same throughout the release study. Further, high molecular weight of cationic polymer (due to the presence of long carbon chain) controlled the release of the CPep (~40 % release) upto 7 days in *in-vitro* release media. The stability study also revealed rapid degradation of free CPep within 24 h however, complexed CPep in NPX remained stable for 8 days due to high polymer molecular weight and its shielding effect. The stability of the NPX was further confirmed by insignificant changes in the particle size, zeta potential and CPep entrapment in initial 20 days; furthernext, 60 % of CPep was found intact after 30 days of storage of NPX at 25 °C (**Figure 4.9 A**).

Apart from the efficient complexation of peptide and its stability in media, another critical attribute is to enhance the cellular internalization of CPep to potentiate its therapeutic efficiency. A study reported that PEC-based nanoparticles bypass macrophage-mediated phagocytosis and show stealth effect without any additional PEGylation or further surface modification. Also, these polymers have shown efficient cell uptake through energy-dependent endocytic pathways, including clathrin and caveolae-mediated endocytosis. [34, 35] FITC has been extensively used in imaging, bioanalytical applications, and labeling of biomolecules such as insulin. [36] However, FITC labeling of CPep has been reported in this study for the first time (**Figure 4.2**), wherein, after synthesis and purification of FCP, it was quantified by modified CPep HPLC method (**Table 4.2**). FCP so obtained was utilized to prepare fluorescently tagged NPX to evaluate CPep complexation efficiency at different BNP:CPep ratios by gel retardation method. As indicated in **Figure 4.6 E**, F3 with BNP:CPep::10:1 (w/w; in µg) exhibited FCP retardation in the well after complexation and also demonstrated higher cellular internalization by both qualitative and quantitative methods (**Figure 4.10**). Further, this efficient uptake was correlated with cyto-protectiveness of the CPep under both induced metabolic and oxidative stress conditions (**Figure 4.11 A-C**). Physiologically, CPep has a specific binding affinity for its specific receptors at an optimum concentration of 0.9 nmol/l, beyond which external administration of CPep failed to show any improvement in its effect. [37] Hence, the prominent impact of CPep could only be observed under stressed/diabetic conditions. This is exemplified by the cyto-protective ability of CPep under metabolic and oxidartive stress as compared to the cells under normal conditions (**Figure 4.11 B and C vs. A)**, which further indicated that NPX might provide renoprotection as well under stressed conditions. BNP did not show any cytotoxicity in NRK-52E cells after 48 h incubation, proving that the cationic polymer (~10 µg/mL) is safe for cells. ROS is generated due to excessive protein metabolism when the cell is under extreme stress, resulting in detrimental effects on

cell structure and homeostasis leading to oxidative stress. Dysfunction of endothelial cells leads to enhanced production of superoxide which decreases the nitric oxide level. Ineffective suppression of ROS enhances vasoconstriction. The metabolic and oxidative stress cause excessive generation of ROS such as superoxide ions ($O_2^-$), reacting instantly with NO radicals to form peroxynitrite ion, which causes tissue injury and biomolecule damage. [38] This also encourages the release of proinflammatory cytokine TNF-α, vasoconstriction, thrombosis and apoptosis. Therefore, nitrite concentration increases with elevation of GFR and leads to oxidation and degulation of NO commonly in T1D and DN. However, CPep binds to G-protein coupled receptor to raise intercellular calcium levels, which triggers a rise in eNOS. The synthesis of NO lowers ROS levels and promotes vasodilation. [39] Through the adaptive cellular pathway, CPep detoxifies ROS by upregulating the activity of anti-oxidant enzymes such as superoxide dimutase, glutathione peroxidase and catalase to normalise the cellular functions. [20] **Figure 4.11 D and E** illustrates action of free CPep and NPX under oxidative stress and ROS to suppress the nitrite concentration and enhance the GSH level. For nitrite and GSH estimation, cell lysate and conditioned media of cells were utilized to confirm the amount of NO and GSH produced inside the cells and released out in media. In DM, ROS plays a key role in generating oxidative stress and destroying kidney and pancreatic β cells. It has already been reported that among multiple signaling effects, CPep also suppresses oxidative stress along with providing renoprotection. [8] This was observed in the present study also wherein, it downregulated apoptotic proteins by elevating anti-oxidant enzymes, like Caspase3 and BAX and upregulated anti-apoptotic protein, BCL2, EMT-linked EGFR and β1-integrin proteins (**Figure 4.12 A and B**). CPep has been reported to suppress TGF-β; [29] NPX downregulated TGF-β in metabolically stressed NRK-52E cells by 1.6 folds compared to HG control group. These results were calibrated with house-keeping gene, β-actin as loading control to normalize the target protein expression.

Cationic nano-carriers employed in drug and gene delivery are often known to cause toxicity and therefore these need to thoroughly tested before study. Previously, our group has also screened cationic PEC polymer in mice and found that 10 mg/kg dose showed no toxicity. [40] Here, BNP and NPX prepared using PEC polymer (10 µg/mL) demonstrated compatibility with RBCs in the *in-vitro* hemocompatibility study wherein, negligible hemolysis (0.2 % & 1.4 %) was observed after 1 h of incubation. According to American Society for Testing and Materials (ASTM F756-17), any material causing hemolysis less than 2% is considered non-hemolytic. [41] Further, the FESEM images of RBCs incubated with BNP and NPX did not

exhibit any cell lysis or morphological changes and therefore, the developed nano-complexes were proved safe for *in-vivo* use (**Figure 4.13 C**).

The hydrophobicity and sustained release of CPep from NPX were achieved due to the polymer's high molecular weight, along with being non-toxic and high biocompatible, as reported earlier by our group. [21, 42] A study has also reported that PEC based nanoparticles show stealth effect and low amount of plasma protein binding along with bypassing macrophage-mediated phagocytosis which eventually enhance the half-life of the PEC NPs significantly. [34] Also, CPep is inherently present in the body unless the patient is suffering from severe T1DM resulting in depletion of pancreatic β cells and maintenance of a minimum CPep level in body. NPX administration in Wistar rats (i.v.) revealed that the steady plasma concentration of CPep was maintained till 72 h above the normal CPep concentration (**Figure 4.14**) and demonstrated $t_{1/2}$ of ~22 h, permitting sufficient time to CPep to exhibit its action.

*In-vivo* free CPep and NPX efficacy was accessed in STZ-induced type 1 DN animal model wherein, it was found that after 8 weeks of study, FGL of DC group was 526±16.22 mg/dL which was significantly controlled by NPX (FGL 407.5±18.17 mg/dL) along with normalizing the weight of animals (**Figure 4.15 B**). The anti-inflammatory effect of NPX reduced the predominantly elevated proinflammatory cytokine, IL-6 in plasma to 3 fold lesser than the DC group along **(Figure 4.16)** with 2.3 fold reduction in the expression of TGF-β (**Figure 4.17)**. Increased TGF-β expression is a key factor in the development of DN (1.7 folds higher TGF-expression was observed in DC vs. NC animals) however, CPep has been shown to suppress the same [29, 43] which was also demonstrated by NPX in the present study. In addition, Caspase3 and BCL2 expression was consistent with the anti-apoptotic activity with NPX treatment group (**Figure 4.17**). High glucose leads to ROS generation, followed by extensive stress generation in kidney and pancreas, release of inflammatory cytokines, which further result in necrosis and destruction of pancreatic β-cells. [20] CPep is known to provide renoprotective effects by ameliorating histological damages such as glomerular hypertrophy, mesangial expansion, tubulointerstitial inflammation, tubular sodium reabsorption, and glomerular hyperfiltration. The histopathology of kidney section of DC group revealed severe glomerulosclerosis, vacuolation of tubular epithelial cells and shrinkage of glomerulus, which are well reported to be caused by DN. **Figure 4.18** clearly demonstrates that NPX treated and protected pancreatic islets, glomerulus, tubular structures and mesangial cells under conditions of DN.

## 4.6 Conclusion

In the present work, we have proficiently explored the efficiency of CPep and its nano-complexes through *in-vitro* and *in-vivo* studies. An *in-house* synthesized cationic polymer was employed to prepare cationic blank nanospheres, and on its surface CPep was complexed by electrostatic interaction at neutral pH to form NPX. This strategy of complexing Cpep on the cationic nanosphere was observed to have increased the stability and availability of peptide for 7 days under physiological conditions. The safety of the prepared NPX was also confirmed by RBC hemocompatibility assay. Also, normal rat kidney cells' exhibited efficient cellular uptake of NPX as compared to free CPep, resulting in promising anti-oxidant and anti-apoptotic effect under high glucose-induced metabolically-stressed conditions. Furthermore, a significant improvement of pharmacokinetic parameters compared to free CPep such as half-life and AUC was also observed. The *in-vivo* efficacy studies in STZ-induced DN model demonstrated effective anti-diabetic and anti-inflammatory effects in terms of reducing the FGL level, improved renal and pancreatic histology, reduced IL-6 level and TGF-β expression.

## 4.7 Bibliography

[1] K. Ogurtsova, L. Guariguata, N.C. Barengo, P.L.-D. Ruiz, J.W. Sacre, S. Karuranga, H. Sun, E.J. Boyko, D.J. Magliano, IDF diabetes Atlas: Global estimates of undiagnosed diabetes in adults for 2021, Diabetes research and clinical practice 183 (2022) 109118.

[2] M.C. Thomas, M. Brownlee, K. Susztak, K. Sharma, K.A. Jandeleit-Dahm, S. Zoungas, P. Rossing, P.-H. Groop, M.E. Cooper, Diabetic kidney disease, Nature reviews Disease primers 1(1) (2015) 1-20.

[3] Y. Chen, K. Lee, Z. Ni, J.C. He, Diabetic kidney disease: challenges, advances, and opportunities, Kidney diseases 6(4) (2020) 215-225.

[4] N. Kashihara, Y. Haruna, V. K Kondeti, Y. S Kanwar, Oxidative stress in diabetic nephropathy, Current medicinal chemistry 17(34) (2010) 4256-4269.

[5] L. Kubiczkova, L. Sedlarikova, R. Hajek, S. Sevcikova, TGF-β–an excellent servant but a bad master, Journal of translational medicine 10 (2012) 1-24.

[6] C.E. Hills, N. Al-Rasheed, N. Al-Rasheed, G.B. Willars, N.J. Brunskill, C-peptide reverses TGF-β1-induced changes in renal proximal tubular cells: implications for treatment of diabetic nephropathy, American Journal of Physiology-Renal Physiology 296(3) (2009) F614-F621.

[7] J. Haidet, V. Cifarelli, M. Trucco, P. Luppi, Anti-inflammatory properties of C-peptide, The review of diabetic studies: RDS 6(3) (2009) 168.

[8] H. Yaribeygi, M. Maleki, T. Sathyapalan, A. Sahebkar, The effect of C-peptide on diabetic nephropathy: A review of molecular mechanisms, Life sciences 237 (2019) 116950.

[9] C.E. Hills, N.J. Brunskill, Cellular and physiological effects of C-peptide, Clinical science 116(7) (2009) 565-574.

[10] C. Jolivalt, M. Rodriguez, J. Wahren, N. Calcutt, Efficacy of a long-acting C-peptide analogue against peripheral neuropathy in streptozotocin-diabetic mice, Diabetes, Obesity and Metabolism 17(8) (2015) 781-788.

[11] N. Zashikhina, V. Sharoyko, M. Antipchik, I. Tarasenko, Y. Anufrikov, A. Lavrentieva, T. Tennikova, E. Korzhikova-Vlakh, Novel formulations of c-peptide with long-acting therapeutic potential for treatment of diabetic complications, Pharmaceutics 11(1) (2019) 27.

[12] C.-H. Moon, A.-J. Lee, H.-Y. Jeon, E.-B. Kim, K.-S. Ha, Therapeutic effect of ultra-long-lasting human C-peptide delivery against hyperglycemia-induced neovascularization in diabetic retinopathy, Theranostics 13(8) (2023) 2424.

[13] G.L. Yosten, C. Maric-Bilkan, P. Luppi, J. Wahren, Physiological effects and therapeutic potential of proinsulin C-peptide, American Journal of Physiology-Endocrinology and Metabolism 307(11) (2014) E955-E968.

[14] Y. Qu, H. Shi, M. Liu, M. Zhang, H. Wang, L. Pang, C. Zhang, D. Kong, C. Li, In Vivo Insulin Peptide Autoantigen Delivery by Mannosylated Sodium Alginate Nanoparticles Delayed but Could Not Prevent the Onset of Type 1 Diabetes in Nonobese Diabetic Mice, Molecular Pharmaceutics 18(4) (2021) 1806-1818.

[15] Y. Zhuang, X. Yang, Y. Li, Y. Chen, X. Peng, L. Yu, J. Ding, Sustained release strategy designed for lixisenatide delivery to synchronously treat diabetes and associated complications, ACS applied materials & interfaces 11(33) (2019) 29604-29618.

[16] B. Lin, Y.-Y. Ma, J.-W. Wang, Nano-technological approaches for targeting kidney diseases with focus on diabetic nephropathy: recent progress, and future perspectives, Frontiers in Bioengineering and Biotechnology 10 (2022) 870049.

[17] D.S. Mohr, T., Delayed-release pharmaceutical formulations containing proinsulin c-peptide, US, 2001.

[18] J. Wahren, H. Foyt, M. Daniels, J.C. Arezzo, Long-acting C-peptide and neuropathy in type 1 diabetes: a 12-month clinical trial, Diabetes care 39(4) (2016) 596-602.

[19] A.-J. Lee, Y.-J. Lee, H.-Y. Jeon, M. Kim, E.-T. Han, W.S. Park, S.-H. Hong, Y.-M. Kim, K.-S. Ha, Application of elastin-like biopolymer-conjugated C-peptide hydrogel for systemic long-term delivery against diabetic aortic dysfunction, Acta Biomaterialia 118 (2020) 32-43.

[20] P. Luppi, P. Drain, C-peptide antioxidant adaptive pathways in β cells and diabetes, Journal of Internal Medicine 281(1) (2017) 7-24.

[21] S. Sharma, S. Mazumdar, K.S. Italiya, T. Date, R.I. Mahato, A. Mittal, D. Chitkara, Cholesterol and morpholine grafted cationic amphiphilic copolymers for miRNA-34a delivery, Molecular pharmaceutics 15(6) (2018) 2391-2402.

[22] D.K. Singh, P. Winocour, K. Farrington, Oxidative stress in early diabetic nephropathy: fueling the fire, Nature Reviews Endocrinology 7(3) (2011) 176-184.

[23] T. Petreski, N. Piko, R. Ekart, R. Hojs, S. Bevc, Review on inflammation markers in chronic kidney disease, Biomedicines 9(2) (2021) 182.

[24] S. Tsalamandris, A.S. Antonopoulos, E. Oikonomou, G.-A. Papamikroulis, G. Vogiatzi, S. Papaioannou, S. Deftereos, D. Tousoulis, The role of inflammation in diabetes: current concepts and future perspectives, European cardiology review 14(1) (2019) 50.

[25] V. Kothari, J.A. Galdo, S.T. Mathews, Hypoglycemic agents and potential anti-inflammatory activity, Journal of inflammation research (2016) 27-38.

[26] D.R.A.P. Sari, F.F. Ahmad, Y.Y. Djabir, R. Yulianty, Breadfruit leaves extract (Artocarpus altilis) effect on pancreatic damage in diabetic type II animal model induced by alloxan–nicotinamide, Medicina Clínica Práctica 3 (2020) 100099.

[27] P.-R. Wang, H. Kitamura, A. Shimizu, N. Yamanaka, Glomerular damage in experimental proliferative glomerulonephritis under glomerular capillary hypertension, Kidney and Blood Pressure Research 40(2) (2015) 188-199.

[28] C.E. Hills, N.J. Brunskill, P.E. Squires, C-peptide as a therapeutic tool in diabetic nephropathy, American journal of nephrology 31(5) (2010) 389-397.

[29] J. Luo, J. Jiang, H. Huang, F. Jiang, Z. Xu, Z. Zhou, H. Zhu, C-peptide ameliorates high glucose-induced podocyte dysfunction through the regulation of the Notch and TGF-β signaling pathways, Peptides 142 (2021) 170557.

[30] L. Wang, N. Wang, W. Zhang, X. Cheng, Z. Yan, G. Shao, X. Wang, R. Wang, C. Fu, Therapeutic peptides: Current applications and future directions, Signal Transduction and Targeted Therapy 7(1) (2022) 48.

[31] A.M. Curreri, J. Kim, M. Dunne, P. Angsantikul, M. Goetz, Y. Gao, S. Mitragotri, Deep Eutectic Solvents for Subcutaneous Delivery of Protein Therapeutics, Advanced Science 10(7) (2023) 2205389.

[32] M. Rekha, C.P. Sharma, Oral delivery of therapeutic protein/peptide for diabetes–future perspectives, International journal of pharmaceutics 440(1) (2013) 48-62.

[33] J. Wang, Z. Wang, G. Chen, Y. Wang, T. Ci, H. Li, X. Liu, D. Zhou, A.R. Kahkoska, Z. Zhou, Injectable biodegradable polymeric complex for glucose-responsive insulin delivery, ACS nano 15(3) (2021) 4294-4304.

[34] N. Bege, T. Renette, M. Jansch, R. Reul, O. Merkel, H. Petersen, C. Curdy, R.H. Müller, T. Kissel, Biodegradable poly (ethylene carbonate) nanoparticles as a promising drug delivery system with "stealth" potential, Macromolecular bioscience 11(7) (2011) 897-904.

[35] X. Jiang, H. Xin, Q. Ren, J. Gu, L. Zhu, F. Du, C. Feng, Y. Xie, X. Sha, X. Fang, Nanoparticles of 2-deoxy-D-glucose functionalized poly (ethylene glycol)-co-poly (trimethylene carbonate) for dual-targeted drug delivery in glioma treatment, Biomaterials 35(1) (2014) 518-529.

[36] D. Shah, Y. Guo, J. Ocando, J. Shao, FITC labeling of human insulin and transport of FITC-insulin conjugates through MDCK cell monolayer, Journal of Pharmaceutical Analysis 9(6) (2019) 400-405.

[37] Y.-H. Cho, Y. Lee, J.I. Choi, S.R. Lee, S.Y. Lee, Biomarkers in metabolic syndrome, Advances in Clinical Chemistry 111 (2022) 101-156.
[38] T.S. Assmann, L.A. Brondani, A.P. Boucas, J. Rheinheimer, B.M. de Souza, L.H. Canani, A.C. Bauer, D. Crispim, Nitric oxide levels in patients with diabetes mellitus: A systematic review and meta-analysis, Nitric Oxide 61 (2016) 1-9.
[39] R.L. Washburn, K. Mueller, G. Kaur, T. Moreno, N. Moustaid-Moussa, L. Ramalingam, J.M. Dufour, C-peptide as a therapy for type 1 diabetes mellitus, Biomedicines 9(3) (2021) 270.
[40] S. Sharma, S. Pukale, D.K. Sahel, P. Singh, A. Mittal, D. Chitkara, Folate targeted hybrid lipo-polymeric nanoplexes containing docetaxel and miRNA-34a for breast cancer treatment, Materials Science and Engineering: C 128 (2021) 112305.
[41] F. Committee, Practice for Assessment of Hemolytic Properties of Materials, ASTM International (2013).
[42] D.K. Sahel, M. Salman, M. Azhar, S.G. Goswami, V. Singh, M. Dalela, S. Mohanty, A. Mittal, S. Ramalingam, D. Chitkara, Cationic lipopolymeric nanoplexes containing the CRISPR/Cas9 ribonucleoprotein for genome surgery, Journal of Materials Chemistry B 10(37) (2022) 7634-7649.
[43] L. Wang, H.-L. Wang, T.-T. Liu, H.-Y. Lan, TGF-beta as a master regulator of diabetic nephropathy, International journal of molecular sciences 22(15) (2021) 7881.

XXXXXXXXXXXXXXXXX

# CHAPTER 5

# Development and evaluation of polymeric nano-formulation of LSF-OA prodrug and C-peptide combination

# {mPLM-LSF-OA-CPep}

## 5.1 Introduction

DM and its associated complications are a significant cause of various health risks, including infections, CKD, severe liver disease, cardiovascular issues, stroke, and cancer. While diabetes management involves preventive measures, lifestyle improvements, strict glycemic control, and the management of hypertensive and lipid profiles, complications arising from diabetes are deemed severe and necessitate appropriate medication and rigorous diabetes control. In all instances, the available treatment for diabetic complications, especially diabetic nephropathy (DN) needs more specific treatment options. The scarcity of treatment options makes the condition incurable and it becomes difficult to restrict the disease from further advancement. [1, 2]

The global prevalence of diabetes is experiencing a substantial increase, particularly in developing countries like India. Consequently, DN has already emerged as a significant contributor to end-stage kidney diseases, accounting for approximately one-third of cases. The main focus is now spotted on CKD treatment by both intensified glycaemic control and reduction in high blood pressure. [3, 4] LSF is a small molecule drug that possesses anti-inflammatory and immunomodulatory effects and is reported as a treatment intervention in T1DM in clinical trials, with the potential to prevent cell death along with the protection and regeneration of pancreatic beta cells. [5] The anti-diabetic activity of LSF is majorly attributed to its ability to a) inhibit the proinflammatory cytokines' (IL-1β, TNF-α and IFN-γ) production and, b) effective suppression of T-cell activation and differentiation via inhibition of the STAT4-mediated IL-12 signaling. [6] Most importantly, LSF can also maintain β-cell insulin secretory function in the presence of inflammatory cytokines and regulate immune cell function to suppress autoimmunity. LSF faces formulation challenges due to its physicochemical properties including high aqueous solubility (~60 mg/mL in water) which hinders its encapsulation in any delivery system and short biological half-life. LSF is reported to be orally non-bioavailable and needs to be administered at a high dose of 25 mg/kg twice daily in T1D animals and in clinical trials, at a single dose of 12 mg/kg by continuous subcutaneous (s.c.) or i.v. infusion over 24 h. [7] It also undergoes rapid metabolism to form metabolite PTX and this LSF-PTX interconversion is mainly responsible for the high dose of LSF. [8] In order to overcome the barriers associated with the effective delivery of LSF, our lab developed a drug-fatty acid conjugate. These conjugates were synthesized through an esterification reaction, aiming to augment the pharmacokinetic performance of LSF. Among the different prodrugs synthesized and reported by our lab, LSF-OA exhibited most promising *in-vitro* and *in-vivo*

performance. [9] Recently, a combination of LSF (27 mg/kg/day) has been reported with exendin-4 (Ex-4; 18 nM/day) administered subcutaneously by Alzet osmotic minipumps to create its stable systemic delivery over fourteen days. The specific mechanism underlying the synergistic action of LSF and exenatide-4 was not very clear, but LSF enhanced the mitochondrial activity and prevented STAT-4 activation in tissues of interest whereas, Ex-4 acted as an activator of the GLP-1 receptor by inducing cyclic AMP and protein kinase A stimulation. [10]

Another potent anti-diabetic molecule is CPep which plays a renoprotective role by suppressing TGF-β pathway and exhibits anti-apoptotic activity thus imparting significant improvement in microvascular system along with controlling the glomerular filtration rate (GFR). [11] It also shows anti-inflammatory activity and therefore has demonstrated decrease in the cytokines levels in DN models. CPep is a polypeptide composed of 31 amino acids; it was initially identified as a cleaved subunit of proinsulin. However, it is now well-known for its ability to mitigate microvascular complications in diabetes-induced kidney disorders due to its prominent anti-inflammatory effects. [12] Despite these therapeutic benefits, CPep faces challenges on the formulation front including low stability, a limited circulation half-life (30 min), and rapid elimination. Recently, nanotechnology has emerged as a promising avenue to overcome the limitations associated with peptide delivery including CPep as a therapeutic molecule. [13, 14] In a 12-month clinical trial, the efficacy of PEGylated CPep was evaluated in the context of peripheral neuropathy in T1D microvascular complications and compared with native CPep. Among 250 patients with T1D and peripheral neuropathy who received a weekly dose ranging from 0.8 to 2.4 mg for 52 weeks, the VPT improvement was noted. [15] In a separate study, Jun Lee et al. reported the development of a K9-C-peptide hydrogel formulation designed to mitigate hyperglycemia-induced vascular dysfunction, encompassing ROS generation, inflammation, and apoptosis in the aorta of diabetic mice. This formulation based on elastin-like polypeptide conjugation with CPep achieved a sustained release of CPep over 19 days. The hydrogel demonstrated the capability to restore diabetic aortic dysfunction. [16]

This suggests a strong rationale to design a co-delivery system for LSF and CPep for the treatment of DN. While LSF is anticipated to manage the diabetic condition, CPep is expected to contribute toward kidney protection. Herein, we combined the therapeutic advantages of LSF-OA prodrug with CPep by co-delivering them using an *in-house* synthesized high molecular weight cationic polymer. The strategy involved encapsulation of LSF-OA inside

polymeric nanoparticles, followed by its lyophilization and then complexation of CPep by electrostatic interaction. The combination formulation was further evaluated for its anti-oxidant, anti-apoptotic and proliferative activities on metabolically stressed kidney and insulinoma cells. After screening the nanoparticles for hemocompatibility, their pharmacokinetic profile was also generated and compared with our previously published data of free LSF and LSF-OA [9] and CPep nano-complexes. The efficacy of combination delivery was further evaluated for its effect on pancreatic islets and diabetic kidney complications in a STZ-induced DN model in Wistar rats.

## 5.2 Materials

LSF (purity >98 %, HPLC) and LSF-OA prodrug (purity >96.5 %, HPLC) were synthesized *in house*.[9] CPep was custom synthesized and procured from LifeTien, NJ, USA. IBMX (internal standard; HPLC ≥99 %), DMDP, MTT and mPEG (5000 Da) were purchased from Sigma Aldrich (St. Louis, MO). DMAP, EDTA, EDC.HCl were procured from Spectrochem Ltd (Mumbai, India). STZ was purchased from MP biomedicals LLC, Germany. Trifluoroacetic acid (HPLC grade), sulphanilamide and GSH were purchased from SRL Pvt. Ltd. (India). PTX, DIPEA and D, L-Lactide were purchased from TCI chemicals, Japan. Alexa Fluor 488 was purchased from Invitrogen, USA. OA was purchased from Acme synthetic chemicals (Mumbai, India). DMEM, FBS, IL-6 and TNF-α mini ABTS ELISA development kit (Peprotech) were purchased from Thermo Fisher Scientific, USA. Rat CPep ELISA kit was procured from FineTest (China). All other chemicals and reagents were of analytical grade. MIN-6 and NRK-52E cells were procured from NCCS, Pune (India). The animal protocol has been approved by the IAEC (protocol number IAEC/RES/28/17).

## 5.3 Methods

### 5.3.1 Synthesis and characterization of LSF-OA prodrug

As reported earlier by our group, LSF was synthesized from PTX by single step reaction with $NaBH_4$ in the presence of protic solvent (methanol). [17] It was characterized by HPLC (Shimadzu, Japan) and $^1$H NMR, 400 MHz (Bruker, Germany). Further, to prevent the conversion of LSF into PTX and to make LSF hydrophobic, it was converted to LSF-OA prodrug as reported earlier in Chapter 3 (section 3.3.1). [9] The prodrug was then characterized by $^1$H NMR and HPLC based analytical method reported in Chapter 2 (section 2.3.1).

### 5.3.2 Synthesis and characterization of cationic polymer (mPEG-b-Poly(carbonate-{grafted-DMDP}-co-lactide)

To facilitate the co-delivery, stability and sustained release of drug and peptide, a multi-step polymer synthesis was carried out *in-house* as reported earlier by our group and mentioned in Chapter 4 (section 4.3.1.2). [18] The DMDP was grafted onto the free carboxyl pendent groups present on the polymer backbone to synthesize the final copolymer (mPEG-b-P(CB-{g-DMDP}-co-LA) (mPLM). The polymer was characterized by $^{1}$H NMR for estimating its molecular weight by determining the number of units of each monomer present in the polymer.

### 5.3.3 Preparation of LSF-OA loaded polymeric nanoparticles (mPLM-LSF-OA)

The nano-formulation of LSF-OA was prepared by single emulsion evaporation method. The cationic polymer and LSF-OA prodrug were dissolved in DCM, followed by probe sonication in 1 % tween 80 aqueous solution at 25 % amplitude for 2 min under cold conditions to form the primary emulsion. To solidify the particle surface, organic solvent was removed from the formulation under vacuum. Any micron sized particles were separated from the formulation by centrifugation at 5000 rpm for 5 min at 4 °C. Further, LSF-OA nanoparticles (mPLM-LSF-OA) were obtained by ultracentrifugation (Sorvall MX150+, Thermo Scientific), and the nanoparticles pellet was redispersed in deionized water. Further, the particle size and zeta potential were measured using Litesizer (Anton Paar, Austria) and using **Equation 5.1 and 5.2**, entrapment efficiency and drug loading were calculated.

$$\text{Encapsulation efficiency (\% EE)} = \frac{Weight\ of\ entrapped\ drug}{Weight\ of\ drug\ initially\ taken} \times 100 \quad \text{….. } \mathbf{Equation\ 5.1}$$

$$\text{Drug loading (\% DL)} = \frac{Weight\ of\ entrapped\ drug}{Weight\ of\ lyophilized\ nanoparticles} \times 100 \quad \text{….. } \mathbf{Equation\ 5.2}$$

### 5.3.4 Lyophilization parameters

Trehalose and PEG 2000 at 5 % and 10 % concentration were screened as cryoprotectants for mPLM-LSF-OA and the lyophilized product was analyzed for particle size and zeta potential. Both the cryoprotectants were freshly prepared by mixing with mPLM-LSF-OA formulation and placed inside a batch lyophilizer (Freezone Triad System, LABCONCO, USA). The lyophilization parameters and RAMP cycles followed were optimized by our lab earlier. [19] The lyophilization efficiency was assessed by determining the $S_f/S_i$ ratio for each sample, where $S_f$ represents the particle size after lyophilization, and $S_i$ represents the particle size before freezing cycles. Samples with a $S_f/S_i$ ratio within the range of $1 \pm 0.3$ were chosen for subsequent studies. [20]

### 5.3.5 Preparation of mPLM-LSF-OA-CPep nanoparticles

For complexation, the mPLM-LSF-OA nanoparticles were incubated with CPep for 1 h at RT. Complexation between C-peptide and mPLM-LSF-OA occurred by electrostatic interaction at neutral pH wherein, CPep attained a negative charge above its isoelectric pH 3.0 while mPLM-LSF-OA was positively charged owing to the presence of a cationic chain on the polymer backbone, to achieve CPep complexed polymeric LSF-OA nanoparticles (mPLM-LSF-OA-CPep) as illustrated in **Figure 5.1**. After incubation, the uncomplexed peptide were separated with the help of ultracentrifugation at 40000 rpm for 20 min. The particle size, zeta potential and complexation efficiency (by indirect method) were evaluated by DLS, HPLC and **Equation 5.3**.

$$\% \text{ Complexation efficiency} = \frac{Initial\ concentration\ of\ CPep - concentration of\ CPep\ in\ supernatant}{Initial\ concentration\ of\ CPep} \times 100$$

…. **Equation 5.3**

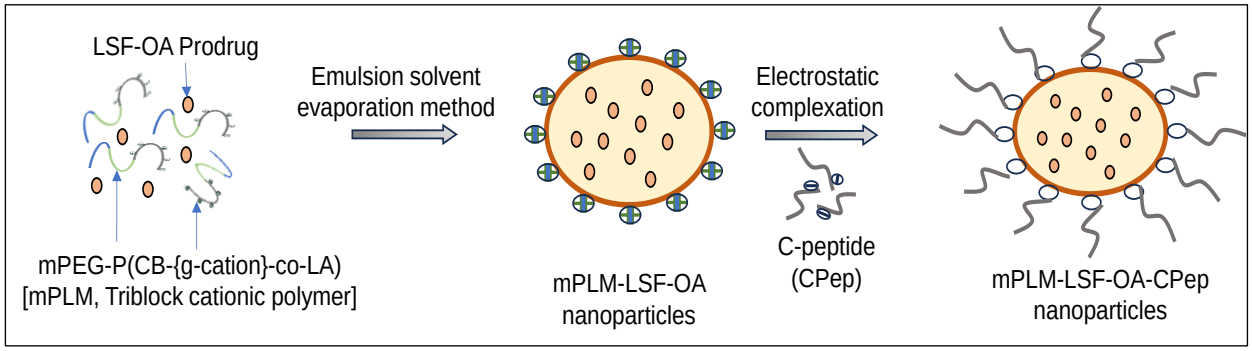


**Figure 5.1** Schematic illustration to formulate mPLM-LSF-OA-CPep nanoparticles.

#### 5.3.5.1 Complexation efficiency by direct method: heparin competition assay

The competition assay was performed to analyze the amount of CPep complexed to the cationic mPLM-LSF-OA nanoparticles with the help of heparin, known to carry polyanionic charge and used as a competitor to release complexed peptide from the cationic system. [21] Different concentrations of heparin (0.01 to 10 IU/mL) were incubated with mPLM-LSF-OA-CPep nanoparticles in deionized water at RT for 1 h. After incubation, the particles were collected and analyzed by DLS, whereas CPep released from the complexes was quantified by HPLC.

### 5.3.6 Stability Study

The benchtop stability study of the mPLM-LSF-OA-CPep nanoparticles was determined to check the integrity of nanoparticles in deionized water at 25 ºC for 30 days. The nanoparticles were analyzed for their particle size and zeta potential by DLS.

### 5.3.7 Hemocompatibility study

Using a previously reported method in Chapter 3 (section 3.3.7), the *in-vitro* interaction between nanoparticles and RBCs was investigated. [9] The mPLM-LSF-OA and mPLM-LSF-OA-CPep nanoparticles were dispersed in 1 mL of RBC suspension with negative and positive control groups (normal saline and 0.1 % Triton X solution). After 1 h of incubation at 37 °C, the samples were centrifuged at 2000 rpm for 5 min, the supernatant was analyzed using an Epoch microplate spectrophotometer (BioTek Instruments, VT) for optical density (OD) at 540 nm. Further, % hemolysis was calculated using **Equation 3.4**. Further, FESEM analysis of RBCs was performed to understand the morphological changes that occur due to incubation with various test samples. The RBCs were smeared on coverslips after fixing with paraformaldehyde solution in 1:1 ratio. The cells were dehydrated in ethanol at concentrations ranging from 30 % to 100 % and dried overnight. The samples were prepared by gold sputtering over the samples, followed by FESEM analysis.

### 5.3.8 Cell culture study

To evaluate the efficiency of the mPLM-LSF-OA and mPLM-LSF-OA-CPep nanoparticles under hyperglycemic conditions, MIN-6 and NRK-52E were employed. The cells were cultured with same protocol as reported in Chapter 3 (section 3.3.8) in DMEM media supplemented with 10 % FBS and 1 % antibiotic solution and incubated at 37 °C in a humidified atmosphere with 5 % $CO_2$.

#### 5.3.8.1 Cell viability study in metabolic stressed cells

The study was performed on two different cells, MIN-6 and NRK-52E, representing pancreatic and kidney cells. In a 96 well plate, approximately $5\times10^3$ cells were seeded and allowed to adhere overnight. The cytoprotective effect of treatment groups: mPLM-LSF-OA and mPLM-LSF-OA-CPep was evaluated on the cells under metabolic stress condition. The metabolic stress was induced by exposing the cells to media containing high glucose (HG; 100 mM dextrose) for 24 h. After stress induction, the media was replaced with fresh media containing mPLM-LSF-OA (40 µM LSF-OA) and mPLM-LSF-OA-CPep (40 µM LSF-OA and 50 nM CPep) nanoparticles and cells were incubated for another 48 h. Using MTT assay, the percentage of viable cells was analyzed by **Equation 3.5**.

#### 5.3.8.2 Anti-oxidant effect under high glucose-mediated metabolic stress

To assess the anti-oxidant impact of LSF, CPep and both in combination treatment groups, namely mPLM-LSF-OA and mPLM-LSF-OA-CPep nanoparticles, a comprehensive analysis

at the cellular level was conducted using appropriate methods. As reported earlier in Chapter (section 4.3.6.3), after post cell adhesion, the cells were incubated in phenol red-free media containing dextrose (100 mM) for 24 h followed by treatment given for next 48 h. The conditioned media was collected from each well separately and centrifuged at 5000 rpm for 5 min to eliminate cellular components for NO and GSH assay. This was followed by harvesting and washing of cells with PBS for apoptosis assay.

**5.3.8.2.1 GSH assay**

GSH is an anti-oxidative marker used to confirmed the anti-oxidant effect of treatment groups on metabolically stressed MIN-6 and NRK-52E cells. It serves as an antioxidant, employed to alleviate the damage caused by ROS. DTNB, commonly known as Ellman's reagent, reacts with GSH in the media, forming a yellowish-coloured adduct (GSH-TNB adduct). In this procedure, 100 µl of the prepared cell lysate and conditioned media were incubated with an equal volume of DTNB solution at 37 °C for 30 min, and the absorbance was subsequently measured at 412 nm using a microplate reader.

**5.3.8.2.2 Nitrite estimation**

ROS serves as an oxidative marker produced during intense protein metabolism when the cells are under significant stress. Therefore, a reduction in nitrite levels signifies the anti-oxidative impact of above mentioned treatment groups. For this assay, Griess reagent, comprising of 1 % p-amino-benzene sulphonamide and 0.01 % naphthylethylenediamine in 2.5 % v/v phosphoric acid, was freshly prepared and stored at 4 °C under dark condition. Subsequently, 100 µL of the above collected conditioned media was combined with 100 µL of Griess reagent and incubated for 30 min. Following incubation, absorbance was measured at 540 nm using a microplate reader. The concentration of nitrite in media was determined by using a previously established standard curve of sodium nitrite.

**5.3.8.2.3 Apoptosis assay**

The cells undergo apoptosis under metabolic stress conditions, and therefore this experiment was performed to quantify the extent of apoptosis induced by high glucose and evaluate the protection rendered by the treatment groups. The cells were centrifuged and resuspended in 1X binding buffer and stained with FITC labeled Annexin V (Annexin-FITC Conjugate) for 20 min in dark room, followed by addition propidium iodide. The cells were analyzed using flow cytometer (Beckman Coulter, USA) and the data were analyzed by CytExpert software.

### 5.3.9 Pharmacokinetic study

Previously our group has reported PK profile for free LSF and its prodrug LSF-OA at a dose of 30 mg/kg (~15 mg/kg LSF). [7, 9] The PK analysis of mPLM-LSF-OA nanoparticles was performed at the 30 mg/kg dose of LSF-OA and mPLM-LSF-OA-CPep nanoparticles at a dose of 30 mg/kg of LSF-OA with 1 µg/kg dose of CPep in Wistar rats (200 ± 20 g). After the i.v. administration of nanoparticles, blood samples were withdrawn from the retro-orbital plexus at preset time points of 15, 30 min, 1, 2, 4, 8, 12, 24, 48, 72, 96 h. Centrifugation was used to extract the plasma at 7000 rpm for 5 min and stored at –80 ºC for further examination. For determination of LSF concentration in plasma aliquots, a simple liquid-liquid extraction (LLE) method was used. The sample was prepared with 100 µL of plasma and 50 µL IS (IBMX, 2 µg/mL) extracted by dichloromethane, vortexed, centrifuged and evaporated overnight at 40 °C. The residue was reconstituted with 100 µL of mobile phase and examined by previously reported HPLC method. Briefly, LSF and IBMX was analysed with 80 µL injection volume on stationary phase, Inertsil ODS C18 column (250×4.6 mm, 5 µ) with methanol:water (1:1 v/v) mobile phase run in isocratic mode at a flow rate of 1mL/min and monitored at a wavelength of 273 nm. Additionally, commercially available CPep ELISA quantification kit (Rat C-peptide ELISA, FineTest) was used to measure the concentration of CPep in plasma. The plasma concentration- time profile was plotted and analysed by the non-compartmental model approach using Phoenix 8.3 WinNonline to determine various PK parameters.

### 5.3.10 *In-vivo* efficacy study

In Wistar rats (200 ± 20 g), STZ induced DN model was developed by injecting a single dose of STZ (42 mg/kg, intraperitoneal injection, i.p.) dissolved in cold citrate buffer (0.01 M, pH 4.5). The fasting blood glucose level (FGL) was determined after 72 h of STZ injection by tail bleeding method using Accu-Check active glucometer **(Figure 4.3)**. Animals with FGL above 250 mg/dL were considered diabetic and included in the study. After 4 weeks, animals were randomly divided into four groups: healthy/ non-diabetic (NC), diabetic control (DC), diabetic/treated with mPLM-LSF-OA nanoparticles and diabetic/treated with mPLM-LSF-OA-CPep nanoparticles. Animals in NC and DC groups received sterile saline, while mPLM-LSF-OA and mPLM-LSF-OA-CPep were administered daily at a dose of LSF-OA prodrug (30 mg/kg/day) and CPep (1 µg/kg/day) respectively by i.p. route. The treatment was continued for 4 weeks, where FGL and body weight were measured weekly.

Towards the end of the study ($8^{th}$ week of diabetes), animals from DC group started exhibiting apparent renal failure; confirmed by the renal functional parameters, i.e., microalbumin and

creatinine levels in animal urine. For the urine collection, rats were housed separately in metabolic cages for 24 h and volume of urine collected was recorded as ml of urine/24 h. An increase in these parameters indicated an escalation of DN symptoms and complications. The plasma IL-6 and TNF-α cytokine levels also confirmed the severity of the diseased condition. At terminal time point, animal was euthanized. Further, pancreas and kidney were isolated and stored in 10 % formalin solution, processed and stained by H&E, PAS analysis and immunohistochemistry (IHC) with Ki-67 staining.

### 5.3.11 Statistical analysis

The *in-vitro* data was processed by one-way ANOVA followed by Tukey's multiple comparison test (expressed as mean ± SD). For the animal study, statistical significance was assessed using one-way ANOVA (followed by Tukey's multiple comparison test using single variance), which was further numerically expressed as mean ± SEM through the use of Prism 8.0.1 software (GraphPad). Results were considered statistically significant if the *p*-value was <0.05, with significance levels denoted as **** for $p < 0.0001$, *** for $p < 0.001$, ** for $p < 0.01$ and * for $p < 0.05$.

## 5.4 Results

### 5.4.1 Synthesis and characterization of LSF-OA prodrug and cationic copolymer

*LSF-OA prodrug*: LSF with >98 % purity was synthesized and characterized by $^{1}$H NMR and HPLC (Shimadzu, Japan), followed by synthesis of LSF-OA prodrug with >96 % purity, 50 % yield and characterization by HPLC, HR-MS, FTIR and $^{1}$H NMR **(Figures 3.3, 3.4 and 3.5)**. The successful conjugation of OA with LSF was confirmed by the removal of hydroxyl (-CH-$OH^{-}$) group proton (at 3.75 ppm) from LSF and emergence of an ester group (-CH-$COO^{-}$) peak at 4.9 ppm in NMR signifying the complete absence of free LSF and formation of prodrug **(Figure 3.2)**. As reported earlier, LSF-OA prodrug exhibited increased retention time $R_t$=19.69 min as compared to free LSF ($R_t$=3.56 min) attributed to the enhanced hydrophobicity of the prodrug after conjugation with the fatty acid **(Figure 3.6)**.

*Cationic polymer*: For co-loading of LSF-OA prodrug and CPep in cationic copolymer (mPEG-b-P(CB-{g-DMDP}-co-LA) was synthesized, its NMR spectrum revealed that the attached number of monomers on mPLM copolymer were- lactic acid= 125 and carbonate units= 78 with 42 units DMDP with a molecular weight of 44,023 Da as reported earlier in Chapter 4 **(Figure 4.5 C)**.

### 5.4.3 Preparation and characterization of LSF-OA loaded polymeric nanoparticles (mPLM-LSF-OA)

The LSF-OA prodrug was encapsulated in cationic copolymer by single emulsion evaporation method to prepare mPLM-LSF-OA nanoparticles with an average particle size of 187 ± 10.76 nm (PDI 0.218) with a zeta potential of 18.3 ± 2.28 mV in deionized water. Furthermore, the encapsulation efficiency of LSF-OA was found to be 78.89 ± 3.63 % with a practical drug loading of 12.20 ± 2.26 % in mPLM-LSF-OA nanoparticles.

#### 5.4.3.1 Lyophilization of mPLM-LSF-OA nanoparticles

All the lyophilized formulations prepared using PEG 2000 and Trehalose (5 % and 10 % w/v) showed good appearance with an intact cake. Here, 5 % trehalose was found to be better since it provided cake with desired nano-size (203 ± 12.03 nm) and favourable positive zeta potential (14.2 ± 2.20 mV) compared to lyophilized formulation without cryoprotectant (named as, no cryo; 363.733 ± 41.71 nm) as illustrated in **Figure 5.2 A**. The cakes formed with trehalose redispersed in less than 30 s compared to PEG 2000 (86 s) and exhibited adequate Sf/Si value (1.22), while other formulations showed Sf/Si value more than 1 ± 0.3 **(Figure 5.2 B)**.

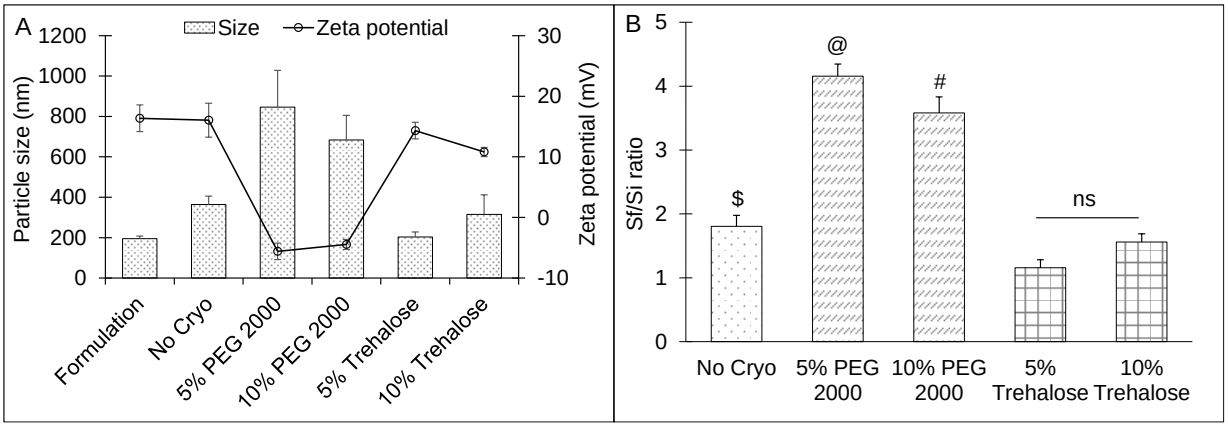


**Figure 5.2** Screening of a suitable cryoprotectant by characterization of lyophilized mPLM-LSF-OA nanoparticles for, A) size distribution and zeta potential and, B) Sf/Si ratio. $^{\$}$no cryo *vs* 5% trehalose ($^{\$}p<0.01$), $^{@}$5% PEG 2000 *vs* no cryo, 5% trehalose and 10% trehalose; $^{\#}$10% PEG 2000 *vs* no cryo, 5% trehalose and 10% trehalose ($^{@\#}p<0.0001$). Each data point represents mean (n=3) ± SD.
No Cryo: formulation without cryoprotectant, Sf: particle size after lyophilization, Si: particle size before freezing cycle.

### 5.4.4 Preparation of mPLM-LSF-OA-CPep nanoparticles

The lyophilized LSF-OA polymeric nanoparticles were covalently complexed with CPep and subjected to analysis by DLS, revealing an average particle size of 208.6 ± 7.4 nm with a PDI of 0.245 ± 0.06 and a zeta potential of 5.2 ± 2.37 mV **(Figure 5.3 A and B)**. Interestingly, the mPLM-LSF-OA-CPep nanoparticles exhibited a slightly larger particle size compared to mPLM-LSF-OA. The complexation efficiency of CPep was found to be 82.75 %. Furthermore,

a reduction in zeta potential was observed due to the process of complexation with negatively charged CPep. A competition assay using heparin was conducted to confirm and validate the efficiency of complexation of CPep with mPLM-LSF-OA nanoparticles. This assay involved heparin as a competing polyanion used to release complexed CPep (dissociation) which was covalently bound to the surface of the nanoparticles. After addition of 0.01 IU of heparin to the mPLM-LSF-OA-CPep nanoparticles, CPep started dissociating with a decrease in the zeta potential of nanoparticles, and it continued till 2 IU concentration of heparin. Addition of 2 IU of heparin provided maximum ~94 % of CPep decomplexation from nanoparticles with -19.3 mV zeta potential as illustrated in **Figure 5.3 C**. No further increase in CPep concentration and decrease in zeta potential was observed as heparin was further increased up to 10 IU.

### 5.4.5 Stability study of mPLM-LSF-OA-CPep nanoparticles

The stability of mPLM-LSF-OA-CPep nanoparticles was studied at 25 °C for 30 days. As seen in **Figure 5.3 D**, after 30 days, the particle size was found not to significantly differ from the initial particle size and zeta potential of nanoparticles.

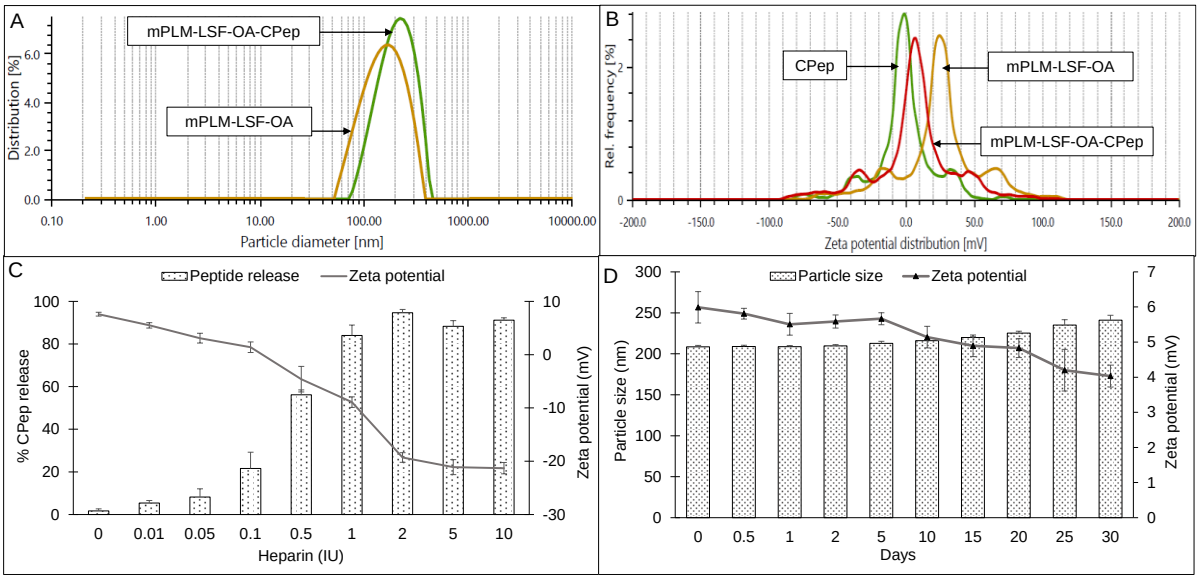


**Figure 5.3** Characterization of mPLM-LSF-OA and mPLM-LSF-OA-CPep nanoparticles for A) size and size distribution and, B) zeta potential. C) Heparin competition assay of mPLM-LSF-OA-CPep nanoparticles: % CPep release and zeta potential. D) Stability study of mPLM-LSF-OA-CPep at 25 °C for 30 days, particle size and zeta potential. Each data point represents mean (n=3) ± SD.

### 5.4.6 Hemocompatibility study

Visual assessment of the integrity of RBCs affirmed the hemocompatibility of mPLM-LSF-OA and mPLM-LSF-OA-CPep nanoparticles **(Figure 5.4 A)**. The positive control, containing a potent surfactant (0.1 % Triton X), resulted in the lysis of all the RBCs upon incubation for 1 h compared to other groups. Comparing the OD values of positive control with treatment

groups, mPLM-LSF-OA and mPLM-LSF-OA-Cep showed minimal hemolysis, i.e. 3.64 ± 1.27 % and 1.68 ± 0.52 %, respectively **(Figure 5.4 B)**.

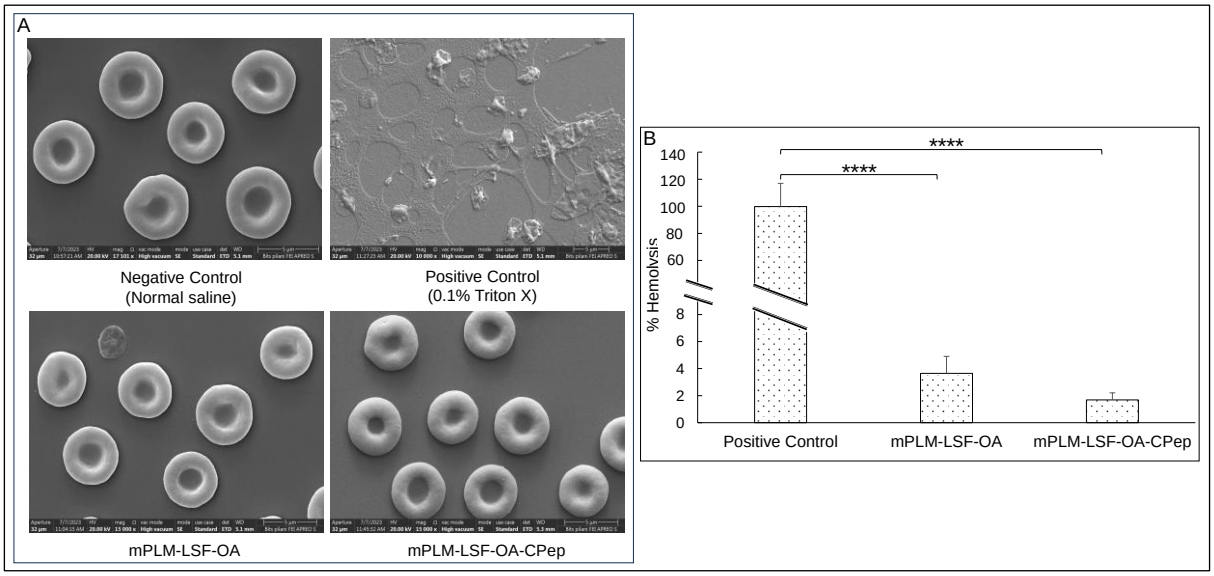


**Figure 5.4** Hemocompatibility study of mPLM-LSF-OA and mPLM-LSF-OA-CPep nanoparticles. A) Visual illustration of RBCs after 1 h of incubation with different control and treatment groups by FESEM and, B) hemolysis assay. ****$p<0.0001$. Each data point represents mean (n=3) ± SD.

### 5.4.7 Cell culture studies

#### 5.4.7.1 Cell viability study

In the experiment, metabolic stress conditions were induced in MIN-6 and NRK-52E cells by incubation with HG (100 mM) for 24 h. The MC (under normal glucose) and HG groups were treated as the control groups and some of the HG exposed cells were subsequently treated with mPLM-LSF-OA (LSF-OA: 40 µM), and mPLM-LSF-OA-CPep (LSF-OA: 40 µM, CPep: 50 nM) nanoparticles. Due to high glucose pretreatment, 34.92 ± 2.13 % and 38.17 ± 0.89 % cell death was seen in MIN-6 and NRK-52E cells respectively. As indicated in **Figure 5.5**, mPLM-LSF-OA resulted in 75.27 ± 1.8 % and 75.99 ± 2.83 % cell viability under metabolic stress conditions in MIN-6 and NRK-52E respectively. Interestingly, mPLM-LSF-OA-CPep exhibited 1.08 and 1.16 fold elevated cell viability in metabolic stress induced MIN-6 and NRK-52E cells in comparison to mPLM-LSF-OA.

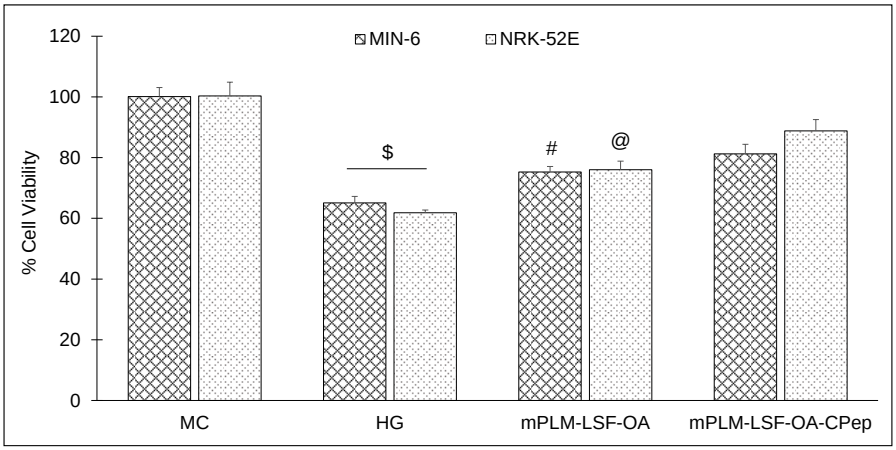


**Figure 5.5.** Cell viability study conducted in metabolically stressed cells, MIN-6 and NRK-52E, after 48 h of treatment. $^{\$}$HG *vs* mPLM-LSF-OA and mPLM-LSF-OA-CPep ($^{\$}p<0.0001$), $^{\#}$mPLM-LSF-OA *vs* mPLM-LSF-OA-CPep ($^{\#}p<0.05$), $^{@}$mPLM-LSF-OA *vs* mPLM-LSF-OA-CPep ($^{@}p<0.0001$). All data are represented as mean (n=3) ± SD.

### 5.4.7.2 GSH and Nitrite assay

Both, insulinoma cells, MIN-6 and kidney cells, NRK-52E showed reduced GSH production and increased nitrite concentration upon incubation with HG (100 mM) containing media (**Figure 5.6 A),** when compared to the media control. This observation clearly indicated the suppression of anti-oxidative pathways (GSH) resulting in dominance of oxidative stress (nitrite). Upon treatment with mPLM-LSF-OA, the GSH level increased by 1.62 and 1.27 fold in the MIN-6 and NRK-52E cells respectively. In **Figure 5.6 B**, the nitrite concentration was reduced by 1.6 and 1.72 fold in MIN 6 and NRK-52E after being treated with mPLM-LSF-OA. This elevation of GSH and reduction of nitrite level indicate the reduction of oxidative stress in the presence of LSF-OA nano-formulation. Comparatively, the combination formulation (mPLM-LSF-OA-CPep) elevated GSH by 2.06 and 1.80 fold with significant reduction in nitrite concentration to 7.1 ± 1.09 µM and 4.6 ± 0.77 µM in MIN-6 and NRK-52E cells respectively, clearly demonstrating the synergistic antioxidative effect of CPep in combination with LSF-OA in the treated cells. This study provided evidence of the *in-vitro* efficacy of the co-loaded formulation to reduce the oxidative stress.

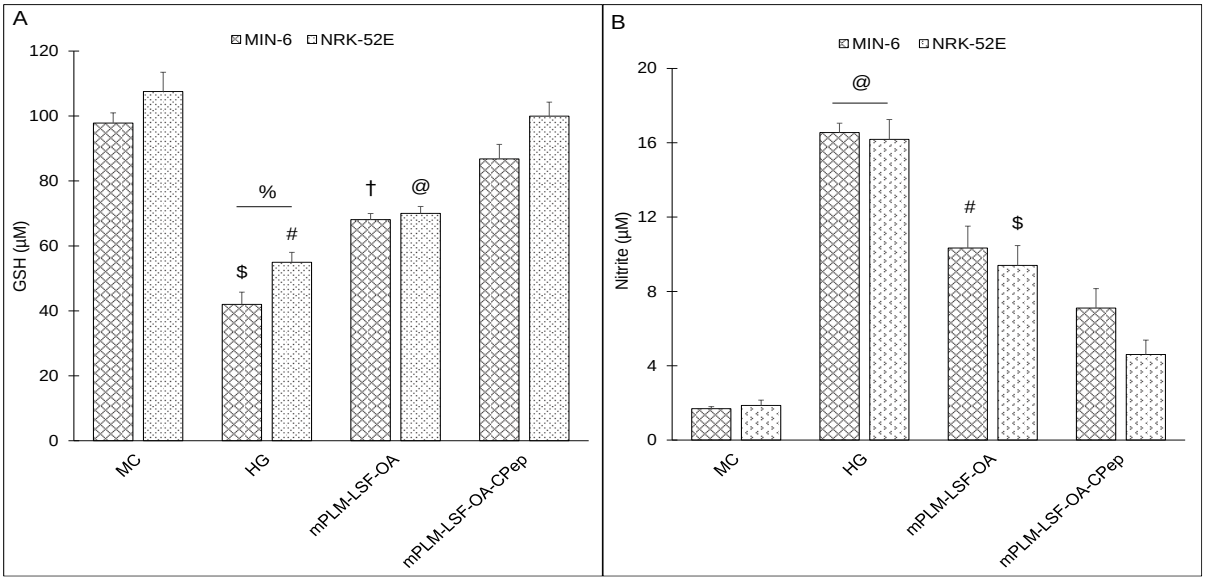


**Figure 5.6** Comparative estimation of GSH and nitrite levels in the conditioned media of metabolic stressed cells MIN-6 and NRK-52E: A) GSH. $^{\%}$HG *vs* mPLM-LSF-OA-CPep ($^{\$}p<0.0001$), $^{\$}$HG *vs* mPLM-LSF-OA ($^{\$}p<0.0001$), $^{\#}$HG *vs* mPLM-LSF-OA ($^{\#}p<0.01$), $^{\dagger}$mPLM-LSF-OA *vs* mPLM-LSF-OA-CPep ($^{\dagger}p<0.001$), $^{@}$mPLM-LSF-OA-CPep *vs* HG and mPLM-LSF-OA-CPep ($^{@}p<0.0001$) and, B) nitrite levels. $^{@}$HG *vs* mPLM-LSF-OA and mPLM-LSF-OA-CPep ($^{@}p<0.0001$), $^{\#}$mPLM-LSF-OA *vs* mPLM-LSF-OA-CPep ($^{\#}p<0.01$), $^{\$}$mPLM-LSF-OA *vs* mPLM-LSF-OA-CPep ($^{\$}p<0.001$). All data are represented as mean (n=3) ± SD.

### 5.4.7.3 Apoptosis assay

To assess the level of apoptosis induced by hyperglycemic conditioning of cell media and to evaluate the anti-apoptotic activity of the nanoparticles after 48 h of treatment, Annexin/PI dual staining technique was employed. In the early stages of apoptosis, Annexin V FITC serves as a probe to quantify the amount of phosphatidylserine on the cell surface due to its high affinity. In the flow cytometry plots depicting FITC-A vs PE-A, four distinct quadrants identified were lower left (LR- live cells), upper left (UL- necrotic cells), upper right (UR - late apoptotic cells) and lower right (LR - early apoptotic cells) wherein, the "apoptotic cells" are accessed by combining the percentage of cells present in UR & LR quadrants **(Figure 5.7 A)**. In MIN-6 cells after 48 h of incubation without treatment, the HG group has shown 11.56 % of apoptosis, which reduced by 6.26 fold after treatment with mPLM-LSF-OA-CPep. Consequently, cells treated with mPLM-LSF-OA developed 4.19 fold higher apoptotic cells than mPLM-LSF-OA-CPep treated group. Similarly, NRK-52E cells after treatment with mPLM-LSF-OA-CPep group demonstrated reduction in apoptotic cells by 5.78 and 2.90 fold in comparison to HG and mPLM-LSF-OA treated groups **(Figure 5.7 B)**.

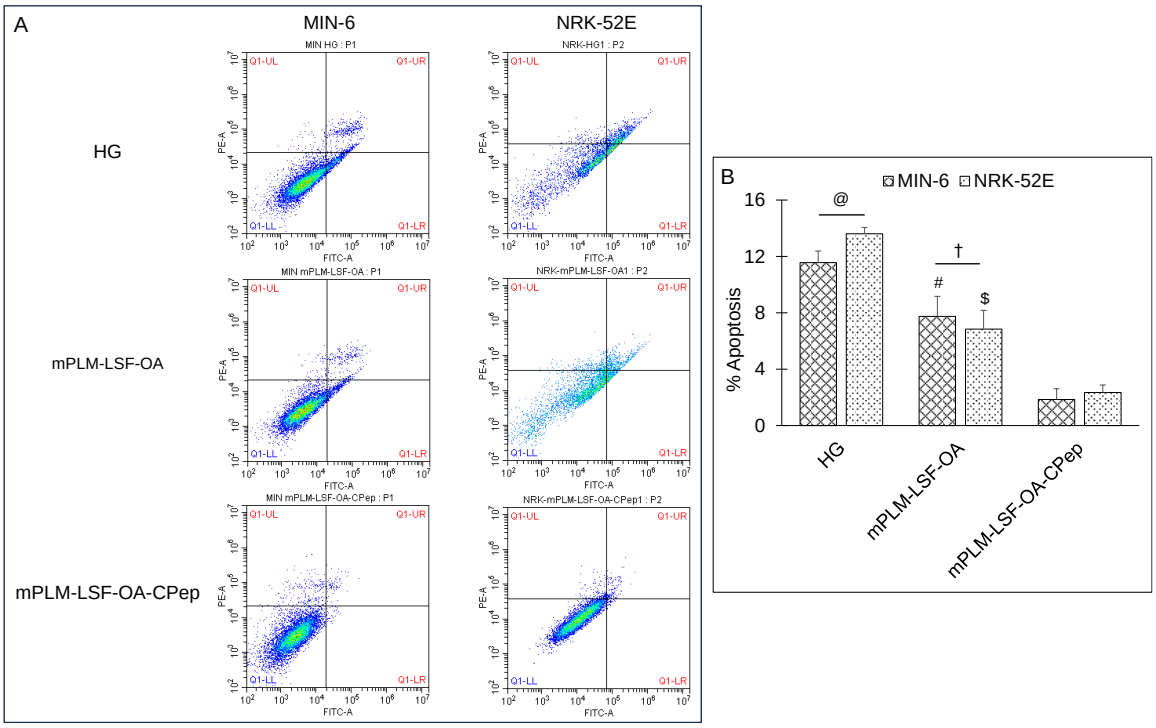


**Figure 5.7** Annexin V/PI staining of MIN-6 and NRK-52E cells after treatment with mPLM-LSF-OA and mPLM-LSF-OA-CPep for 48h analysed by flow cytometry. A) Dot plot and, B) % apoptosis. $^{@}$HG *vs* mPLM-LSF-OA-CPep ($^{@}p<0.0001$), $^{\#}$mPLM-LSF-OA *vs* HG ($^{\#}p<0.05$), $^{\$}$mPLM-LSF-OA *vs* HG ($^{\$}p<0.0005$) and, $^{\dagger}$mPLM-LSF-OA *vs* mPLM-LSF-OA-CPep ($^{\dagger}p<0.005$). All data are represented as mean (n=3) ± SD.

### 5.4.8 *In-vivo* pharmacokinetic study

Non-compartmental analysis of the time vs plasma concentration of LSF and CPep exhibited improvement in the PK parameters when these were administered in the form of mPLM-LSF-OA and mPLM-LSF-OA-CPep (**Figure 5.8 A)**. As indicated in **Table 5.1 A**, mPLM-LSF-OA exhibited 15.42 and 2.60 fold increase in $t_{½}$ in comparison to the free LSF and LSF-OA. Additionally, the MRT of LSF (in mPLM-LSF-OA) increased to 22.157 ± 1.12 h from 0.818±0.06 h as shown by free LSF. With increasing MRT, Cl of LSF in mPLM-LSF-OA decreased by 13 fold than LSF-OA. Additionally, LSF in co-delivery system (mPLM-LSF-OA-CPep) demonstrated 2- and 1.4- fold further higher $t_{1/2}$ and $V_d$ in comparison to the mPLM-LSF-OA formulation.

Also, **Table 5.1 B** confirmed the improvement in PK parameters for CPep in mPLM-LSF-OA-CPep when compared to the free CPep and CPep nano-complexes (NPX). In comparison to the free CPep, NPX proved beneficial with 6.45 fold elevated $t_{1/2}$ and 12.09 fold decreased Cl. mPLM-LSF-OA-CPep demonstrated significant improvement in PK parameters, with 1.55 and 1.94 fold enhanced $t_{1/2}$ and $V_d$ in comparison to NPX. Hence, it is evident that mPLM-LSF-

OA-CPep was able to improve the PK profile of both the therapeutic molecules, LSF and CPep together.

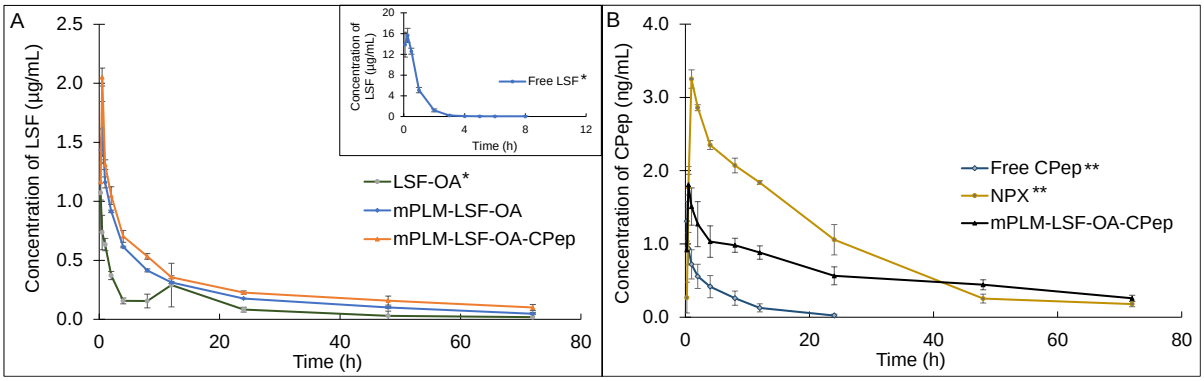


**Figure 5.8** Plasma-concentration time profile of A) LSF at 15 mg/kg (~30 mg/kg of LSF-OA) dose and B) CPep at 1µg/kg dose after i.v. administration in Wistar rats. Each point represents mean (n=3) ± SEM.
The data were referred from Chapter 3* and Chapter 4**. Here it has been given for the sake of comparison and clarity.

**Table 5.1**
Pharmacokinetic parameters of (A) LSF and, (B) CPep administered in Wistar rat.

**Table 5.1 A**

| Parameters | Free LSF* | LSF-OA micelles* | mPLM-LSF-OA | mPLM-LSF-OA-CPep |
|---|---|---|---|---|
| $t_{½}$ (h) | 0.75 ± 0.03 | 4.44 ± 0.47 | 11.59 ± 0.17 | 23.23 ± 0.92 |
| $AUC_{0-\infty}$ (h*ng/mL) | 1.47 ± 5.91 | 6.63 ± 12.71 | 16.14 ± 0.35 | 23.17 ± 2.78 |
| MRT (h) | 0.82 ± 0.06 | 7.91 ± 0.93 | 22.17 ± 1.12 | 30.16 ± 2.80 |
| $V_d$ (mL/kg) | 961.55 ± 79.16 | 14974.42 ± 1588.02 | 3108.29 ± 92.30 | 4370.71 ± 232.91 |
| Cl (mL/h/kg) | 1020.90 ±39.46 | 2415.30 ± 407.29 | 185.89 ± 14.21 | 130.68 ± 14.87 |

Free LSF, LSF-OA micelles, mPLM-LSF-OA and mPLM-LSF-OA-CPep (~15 mg/kg LSF; i.v.) were administered to rats and PK parameters analyzed by non-compartmental method; mean (n=3) ±SEM.
*This data were referred from Chapter 3. [9] Here it has been given for the sake of comparison and clarity.

| **Table 5.1 B** Parameters | Free CPep** | NPX** | mPLM-LSF-OA-CPep |
|---|---|---|---|
| $t_{½}$ (h) | 3.47 ± 0.65 | 21.95 ± 2.63 | 34.06 ± 2.15 |
| $AUC_{0-\infty}$ (h*ng/mL) | 8.145 ± 2.65 | 68.09 ± 5.53 | 57.68 ± 1.88 |
| MRT (h) | 6.17 ± 0.76 | 25.90 ± 2.99 | 26.49 ± 0.59 |
| $V_d$ (mL/kg) | 793.05 ± 283.66 | 462.31 ± 17.37 | 899.97 ± 57.88 |
| Cl (mL/h/kg) | 178.98 ± 86.33 | 14.87 ± 1.17 | 18.33 ± 0.64 |

Free CPep, NPX and mPLM-LSF-OA-CPep (~1 µg/kg CPep; i.v.) were administered to rats and PK parameters analyzed by non-compartmental method; mean (n=3) ±SEM.
**The data were referred from Chapter 4. Here it has been given for the sake of comparison and clarity.

$t_{½}$: half-life, $AUC_{0-\infty}$: area under the curve from time 0 to last measurable concentration, MRT: mean residence time, $V_d$: volume of distribution, Cl: clearance, CPep: C-peptide, NPX: CPep nano-complexes.

### 5.4.9 *In-vivo* efficacy study

The animals underwent weekly monitoring of FGL and body weight, and were sacrificed after 8 weeks. After maintenance of diabetes for one month, the animals were treated with the prepared nanoparticles. At the end of the study, the FGL of mPLM-LSF-OA and mPLM-LSF-OA-CPep treated animals were measured and it was found to be 447.75±29.15 and 331±33.33 mg/dL, respectively, which is 18.29 % and 39.6 % lower than the FGL observed in the DC animals (548.75±18.03 mg/dL; **Figure 5.9 A**). In general, body weight tends to decrease during diabetes. After 8 weeks of the study, the body weight of the DC animals was found 31.39 % lower than that of the NC animals. However, nanoparticle treatment contributed to a partial recovery in body weight with 12.79 % and 17.44 % increased body weight in mPLM-LSF-OA and mPLM-LSF-OA-CPep treated animals respectively in comparison to the DN animals **(Figure 5.9 B)**.

#### 5.4.9.1 IL-6 and TNF-α cytokine estimation

IL-6 and TNF-α signalling pathways play a crucial role in mediating the inflammatory responses that are pivotal to the progression of DN. The signalling pathways of TNF-α and IL-6 are linked to an augmented deposition of ECM within the kidneys, resulting in renal damage mediated by cytotoxic effects. In DC animals, the levels of IL-6 and TNF-α were found to be markedly elevated (3.4 and 9.51 ng/mL) after 8 weeks of disease progression. However, these levels were significantly reduced to 1.26 and 4.63 ng/mL following treatment with mPLM-LSF-OA-CPep for 4 weeks **(Figure 5.9 C)**. This reduction clearly suggests a potential delay in the progression of DN.

#### 5.4.9.2 Insulin level estimation

In diabetic patients, the activation of ROS and inflammatory cytokines contributes to the depletion of pancreatic β cells. This depletion results in reduced insulin levels, ultimately leading to elevated blood glucose levels. Treatment with mPLM-LSF-OA and mPLM-LSF-OA-CPep nanoparticles significantly increased insulin concentration by 4.9 and 6.8 fold as compared to DC animals **(Figure 5.9 D)**. This effect was attributed to the protection of residual pancreatic β cells from pro-inflammatory cytokines and contributes towards control of the blood glucose level.

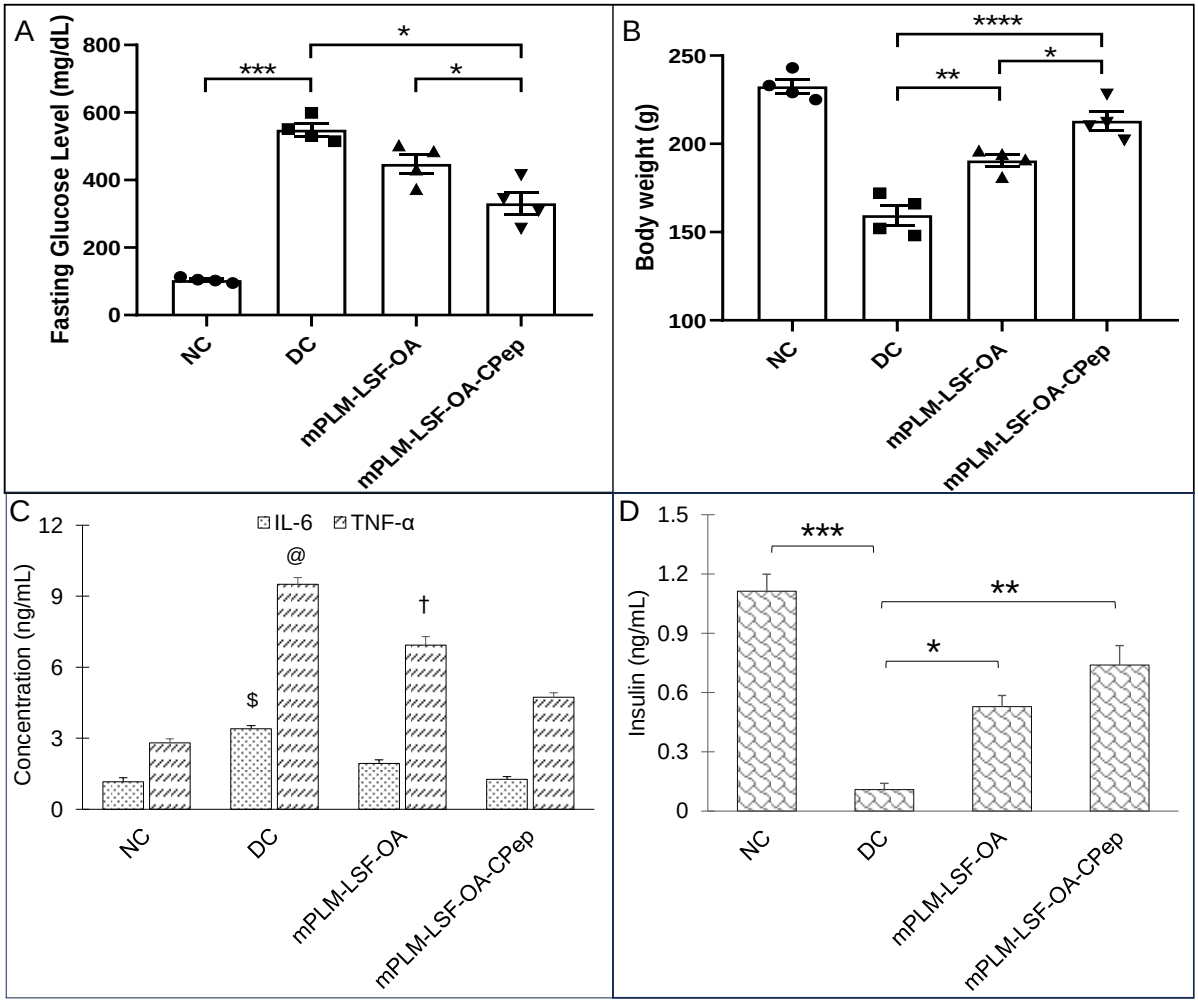


**Figure 5.9** *In-vivo* efficacy study in STZ-induced DN animal model, parameters recorded after 8 weeks. A) Terminal fasting blood glucose level and, B) animal body weight. *p<0.05; **p<0.005; ***p<0.0005; ****p<0.0001. C) Inflammatory cytokines, IL-6 and TNF-α levels in plasma. $DC *vs* mPLM-LSF-OA and mPLM-LSF-OA-CPep ($p<0.005), @DC *vs* mPLM-LSF-OA-CPep (@p<0.0001) and, †mPLM-LSF-OA *vs* DC and mPLM-LSF-OA-CPep (†p<0.005) and, D) Plasma insulin level. *p<0.05; **p<0.005; ***p<0.0005. All data are represented as mean (n=4) ± SEM.

### 5.4.9.3 *In-vivo* histology study

#### 5.4.9.3.1 Effect of kidney

The assessment of renal environmental changes due to DN was carried out by histopathological examination of kidney sections using H&E and PAS staining. In **Figure 5.10 A**, the H&E staining of the kidney shows the glomerulus (G), distal tubule (DT), and proximal convoluted tubule (PCT) in the NC group without any pathological changes. In contrast, the DC reveals severe glomerulosclerosis, shrinkage, and depletion of the glomerulus along with tubular injury. However, the mPLM-LSF-OA and mPLM-LSF-OA-CPep treated groups exhibit well defined glomerular structures and improved nephron conditions. Similarly, after PAS staining, the treatment groups demonstrated reduced hypertrophy and Bowman's capsule expansion with

less basement membrane (BM) space **(Figure 5.10 B)**. DN is characterized by podocytes (P) and mesangial cell (MC) proliferation, along with renal tubular epithelial degeneration. Therefore, the treatment group showed reduced intracellular glycogen accumulation, diminished infiltration of inflammatory cells (seen as blue nucleus in **Figure 5.10 B**), mild mesangial expansion, lesser deposition of mesangial matrix, and almost normal relative glomerular basement membrane thickness, indicating an improved condition of the kidney.

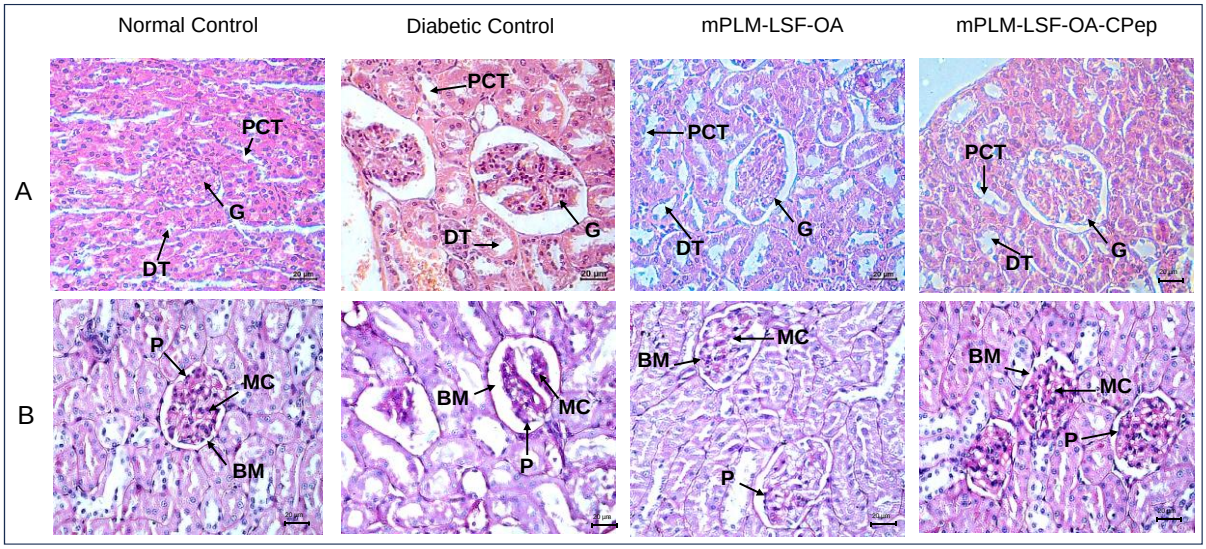


**Figure 5.10** Histopathological examination of kidney sections of different groups after 8 weeks of diabetes induction: A) H&E and, B) PAS staining. Magnification 400X and scale bar 20 µm.
G, Glomerulus; PCT, proximal convoluted tubule; DT, distal tubule; P, podocytes; MC, mesangial cells; BS, basement membrane.

### 5.4.9.3.2 Effect on pancreas

Following a 4-week treatment period for diabetic animals, the animals were euthanized, and pancreatic Islet of Langerhans (IL) morphology was evaluated through H&E staining. In comparison to NC animals, the rat pancreas of DC animals exhibited a significant reduction in the number of β cells (seen as blue coloured cells in **Figure 5.11 A**) accompanied with a damaged structure. The depletion of β cells serves as an evidence of diabetes induction and progression in animals. However, when compared to DC animals, the groups treated with mPLM-LSF-OA and mPLM-LSF-OA-CPep showed a much better-preserved islet structure **(Figure 5.11 A)**.

### 4.9.3.2.1 Immunohistochemical analysis

To corroborate the findings regarding insulin secretion and pancreatic histology indicating the proliferation of pancreatic cells, the presence of intact islet structures after treatment with mPLM-LSF-OA and mPLM-LSF-OA-CPep nanoparticles justifies the existence of beta cells,

subsequently leading to an increase in insulin concentration in the plasma as seen in **Figure 5.9 D**. The proliferation marker Ki-67 was employed to stain the pancreatic tissue sections, revealing more prominent staining of proliferative cells in pancreatic islets in the mPLM-LSF-OA-CPep group compared to the mPLM-LSF-OA treated group **(Figure 5.11 B)**.

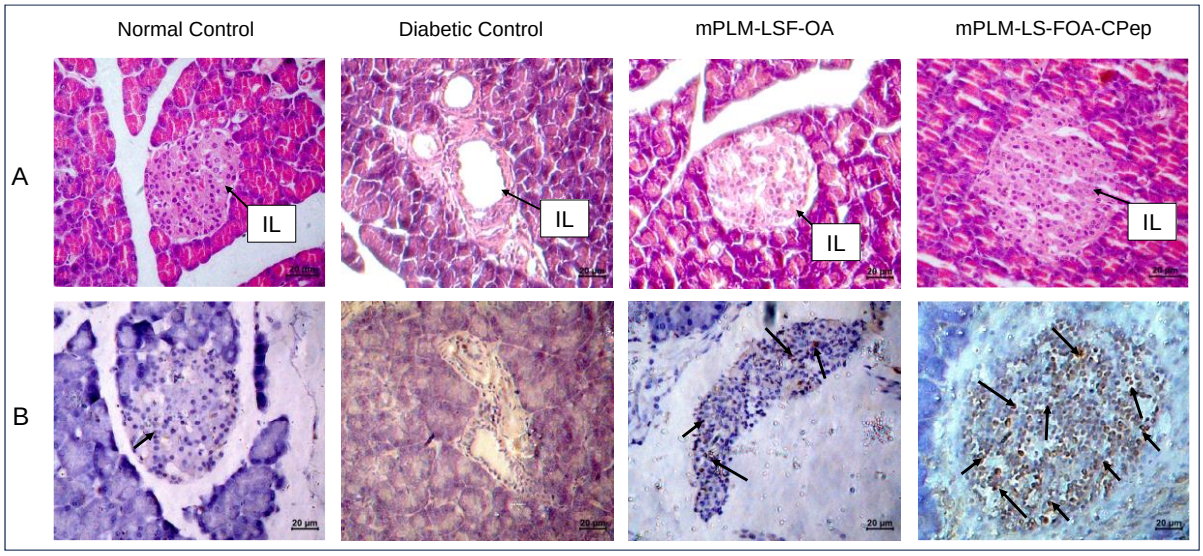


**Figure 5.11** Histological analysis of pancreatic sections of different groups after 4 weeks of treatment. A) H&E staining and, B) immunohistochemical analysis of pancreatic tissue for Ki-67 expression in β cells of islets of langerhans. Magnification 400X and scale bar 20µm.
IL: Islets of Langerhans

## 5. Discussion

The pathophysiology of DN is correlated to the predisposition of DM, a metabolic disorder with prominent indication of chronic hyperglycemia that can advance to the micro- and macrovascular complications in kidney. [22] The molecular mechanism of DN involves activation of different biological pathways, including polyol, PKC, and AGE mediated crosstalk with overproduction of ROS, dysregulated growth factors (GFs), and abnormalities in the non-coding RNAs. [23] Generally, the therapeutic limitations of monotherapy are aggravated by pathological complexity, severity and progression of DM, which necessitate the requirement of delivering a combination of the therapeutic molecules with multifaceted actions. [24] Recently, a microfluidic based liposomal formulation was reported for the co-delivery of anti-diabetic hydrophilic and lipophilic molecules, i.e, metformin and glipizide, which improved the loading efficiency of both molecules and provided 2 fold faster release than the formulation with single molecules. [25] Another niosomal formulation for glipizide and metformin hydrochloride is reported wherein, thin film hydration approach was adopted to encapsulate the hydrophobic metformin while the hydrophilic glipizide was loaded by simple

incubation with metformin loaded nanoparticles. The structural integrity of niosomes was ascertained by incorporation of cholesterol in the formulation. [26] These studies exemplify that the co-delivery strategies are becoming a major area of focus for the treatment of DM and enable "multiple compound – multiple target approach" to achieve reduced dose, better dosage regimen, desirable patient compliance along with possible additive or synergistic outcome. [24]

LSF-LA polymeric micelles formulated using film hyderation method have already been reported by our group to exhibit improved $t_{1/2}$ (2.79 fold) in comparison to the LSF-LA self-assembled micelles. [24, 27] Recently, tannic acid- iron complex-based surface modified PLGA nanoparticles were reported to deliver M2 peptide (YEQDPWGVKWWY) for selective targeting of the tumor associated M2 macrophages. The surface modified PLGA NP complexed the peptide by simple incubation for 3h in bicine buffer (pH 7.4). [28] In the present study, single emulsion method was utilized to develop LSF-OA encapsulated polymeric nanoparticles (mPLM-LSF-OA with 78.89 % EE) with a surface potential of +18.3 ± 2.28 mV; using the cationic mPEG-b-P(CB-{g-DMDP}-co-LA polymer. These nanoparticles were further explored to develop a co-delivery system, mPLM-LSF-OA-CPep wherein, the mPLM-LSF-OA was complexed with CPep by electrostatic interaction resulting in the combination formulation with a particle size 208.6 ± 7.4 nm, surface potential +5.2 ± 2.37 mV and 82.75% CPep complexation capacity **(Figure 5.3 A and B)**. The cationic charges present over the lipid or polymeric nanocarriers may damage the cells causing cell shrinkage, reduced mitosis, endosomal disruption and vacuolization of cytoplasm. This toxicity is generally due to the unbalanced cationic charge on their structures wherein, the groups imparting cationic charge like- quaternary ammonium amphiphiles are more toxic than their tertiary amine counterparts. Also, its also reported that linking PEG on polyethyleneimine (PEI) polymers reduces toxicity without affecting gene delivery efficiency [29, 30] Herein, we utilized PEGylated PEC polymer conjugated with small molecular weight cationic chain, which reduces cellular toxicity as also evident in the hemocompatibility study. There was a ~2 fold reduction observed in hemolysis by mPLM-LSF-OA-Cep (1.68 %) as compared to mPLM-LSF-OA (3.64 %) which might be attributed to the higher surface positive charge of mPLM-LSF-OA which was however, within acceptable limits according to American Society for Testing and Materials (ASTM F756-17) **(Figure 5.4 B).** [31] This also provides an evidence of complexation of CPep to the surface of mPLM-LSF-OA. [32, 33] Next, the cytoprotective effect of mPLM-LSF-OA and mPLM-LSF-OA-CPep in metabolic stress induced MIN-6 and NRK-52E cells was confirmed by MTT assay. HG induced metabolic stress in MIN-6 and NRK-52E is well reported as a cell based

model for pancreatic β-cell dysfunction, hyperglycemia, and induced renotoxicity. [34, 35] In this case, dextrose (100 mM) induced 34.92±2.13% and 38.17±0.89% cytotoxicity in MIN-6 and NRK-52E cells, which clearly indicated the development of hyperglycemic conditions in cells. Additionally, high glucose induced oxidative stress was confirmed by reduction in GSH level and suppression of eNOS expression, which may further induce cytotoxicity by activating the apoptotic marker proteins like caspases and suppressing anti-apoptotic protein, BCL-2. [36-38] The GSH level was compromised by 2.2 fold in MIN-6 and 1.9 fold in NRK-52E. Interestingly, mPLM-LSF-OA-CPep increased the GSH level by 2.06 and 1.80 fold, and mPLM-LSF-OA elevated the level by 1.62 and ~1.27 fold in metabolic stress induced MIN-6 and NRK-52E cells respectively **(Figure 5.6 A)**. This clearly indicated the efficiency of the combination formulation over the mPLM-LSF-OA. While examining the effect of high glucose on eNOS mediated nitric oxide (NO) production, the changes are measured in terms of the level of its oxidized product nitrite ($NO_2^-$) by Griess reaction. In one of the studies, high glucose was able to elevate the eNOS expression by 2 fold in endothelial cells which enhanced the $NO_2^-$ release by 40% along with ~300 fold increased release of superoxide. Together, NO and $O_2^-$ resulted in generation of a potent oxidant, peroxynitrile ($ONOO^-$) which may contribute towards the endothelial dysfunction in human aortic endothelial cells. [39] As per our study, HG treated MIN-6 and NRK-52E cells exhibited ~9.7 and ~8.6 fold increment in $NO_2^-$ production in comparison to the media control group which was found in agreement with the literature reports. mPLM-LSF-OA and mPLM-LSF-OA-CPep further demonstrated their efficiency by reducing the $NO_2^-$ by 1.6 and 2.3 fold in MIN-6 cells, whereas 1.72 and 3.5 fold in NRK-52E respectively. This observation could be correlated to the observed increase in GSH level and interestingly, mPLM-LSF-OA-CPep was found more potent in reducing the oxidative stress in the cells as compared to mPLM-LSF-OA in the HG exposed cells. The oxidative and nitrosative stress leads to apoptosis and necrosis in various cells, also it triggers the reduction of GSH in HG induced endothelial cells leading to DNA damage.[37, 40] The induction and restoration of GSH level protected kidney and insulinoma cells from apoptosis wherein, the nanoparticles demonstrated significantly higher anti-apoptotic effect as evident by the higher percentage of living cells 92.53 % and 94.82 %, respectively **(Figure 5.7)**. Advanced drug delivery has opened pathways to sustain/ target/ dose regimen/ and stabilize the therapeutic molecules, and therefore, CPep was PEGylated with 40 kDa PEG, covalently bound at its N-terminus and screened for neuropathy treatment. The conjugation increased $t_{1/2}$ of CPep to 6-7 days without any adverse effect and marked improvement in VPT after 52 weeks of clinical trials. [15, 41] The beneficial effect of the co-delivery nano system was also prominently seen

in the PK profile of LSF and CPep when administered as mPLM-LSF-OA-CPep. While mPLM-LSF-OA increased the $t_{1/2}$ of LSF by ~ 2.6 fold more than the LSF-OA self-assembled micelles, whereas mPLM-LSF-OA-CPep enhanced LSF $t_{1/2}$ to ~5.23 and 2 fold higher compared to LSF-OA micelles and mPLM-LSF-OA. [9] Also mPLM-LSF-OA-CPep enhanced the $t_{1/2}$ of CPep by ~1.55 fold than the NPX **(Table 5.1)**. This clearly highlighted improved potential of the co-delivery system in comparison to the monotherapy formulations. The synchronized improvement in the PK profile of a combination of active molecules through nanoformulation is well reported in case of silica nanoformulation of CDK4/6 inhibitor, palbociclib and an autophagy inhibitor, hydroxychloroquine in the treatment of pancreatic cancer as well. [42]

Apart from synthesizing novel molecule LSF, Nadler et al. also explored the small molecule in combination with exendin-4 which was delivered via Alzet osmotic mini-pump, providing duo effect of supressing autoimmune cytokines and enhancing the proliferation of β-cells to reverse T1DM in mouse model. It was found that the combination successfully revesed hyperglycemia within a week of beginning the treatment and maintained glucose for more than 3 months, attributed to the recovered insulin secretion and restore back other hormonal levels. Although LSF alone stabilised FGL in some mice; Exendin-4 alone could not improve hyperglycemia and therefore, the combination played a pivotel role in treatment of T1DM. [10, 43, 44] Previously, our group reported the therapeutic efficacy of LSF-OA as an anti-diabetic, anti-inflammatory and anti-oxidant molecule in T1DM. [9] CPep also brings along anti-oxidant, anti-apoptotic, anti-inflammatory and reno-protectivity activity in treatment of diabetes and its complications. [12] Herein, the efficacy of the co-delivery formulation was confirmed in the STZ induced DN animal model. The observed reduction in the FGL level and ~6.7 fold elevated insulin level in comparison to the DN group indicated the efficacy of the co-delivery nanosystem. The observed anti-diabetic effect with enhanced insulin level is attributed to the pancreatic β-cell protection and ability of LSF to induce proliferation of pancreatic cells as reported in the literature. [6, 45] As indicated in **Figure 5.9 B and C,** mPLM-LSF-OA-CPep treated animals demonstrated ~ 2.69 and 2.05 fold reduction in proinflammatory cytokines (IL-6 and TNF-α) while mPLM-LSF-OA exhibited ~ 1.76 and 1.37 fold reduction in the aforementioned cytokine levels in comparison to DN control group. This clearly indicated the superior anti-inflammatory activity of the combination nano-formulation in comparison to the mPLM-LSF-OA, attributed to the presence of an anti-inflammatory and renoprotective molecule CPep along with LSF-OA. [46] Also, H&E and PAS staining of kidney sections

demonstrated reduced intracellular glycogen accumulation, diminished infiltration of inflammatory cells, mild mesangial expansion, lesser deposition of mesangial matrix, and almost normal relative glomerular basement membrane thickness upon treatment with the combination formulation for 4 weeks. Ki-67 staining of pancreas, a marker of proliferation, in different groups also indicated cellular proliferation in mPLM-LSF-OA-CPep treated animals far better than the other groups **(Figure 5.11 B)**. [47] These studies demonstrate and bring forth the potential of mPLM-LSF-OA-CPep to provide an effective delivery system for the small molecule drug, LSF and peptide, CPep along with harnessing their synergistic effect in the treatment of the DN which was evidently higher in comparison to their monotherapy formulations, i.e, mPLM-LSF-OA and NPX.

## 5.6 Conclusion

Here, we investigated a co-delivery strategy to harness the potential benefits of LSF and CPep in treating DN. It is noteworthy to mention here that the combined therapy involving CPep and the anti-inflammatory small molecule drug, LSF has not been explored till date, neither in terms of its effectiveness in treating DN nor for development of a formulation. Hence, this study highlighted the potential synergistic effects and enhanced therapeutic efficacy of this combination approach for the treatment of DN.

## 5.7 Bibliography

[1] K. Ogurtsova, L. Guariguata, N.C. Barengo, P.L.-D. Ruiz, J.W. Sacre, S. Karuranga, H. Sun, E.J. Boyko, D.J. Magliano, IDF diabetes Atlas: Global estimates of undiagnosed diabetes in adults for 2021, Diabetes research and clinical practice 183 (2022) 109118.

[2] A.D. Association, Diagnosis and classification of diabetes mellitus, Diabetes care 37(Supplement_1) (2014) S81-S90.

[3] L. Chen, D.J. Magliano, P.Z. Zimmet, The worldwide epidemiology of type 2 diabetes mellitus—present and future perspectives, Nature reviews endocrinology 8(4) (2012) 228-236.

[4] B. Lin, Y.-Y. Ma, J.-W. Wang, Nano-technological approaches for targeting kidney diseases with focus on diabetic nephropathy: recent progress, and future perspectives, Frontiers in Bioengineering and Biotechnology 10 (2022) 870049.

[5] Z. Yang, M. Chen, J.L. Nadler, Lisofylline: a potential lead for the treatment of diabetes, Biochemical pharmacology 69(1) (2005) 1-5.

[6] J.S. Striffler, J.L. Nadler, Lisofylline, a novel anti-inflammatory agent, enhances glucose-stimulated insulin secretion in vivo and in vitro: studies in prediabetic and normal rats, Metabolism 53(3) (2004) 290-296.

[7] K.S. Italiya, S. Mazumdar, S. Sharma, D. Chitkara, R.I. Mahato, A. Mittal, Self-assembling lisofylline-fatty acid conjugate for effective treatment of diabetes mellitus, Nanomedicine: Nanotechnology, Biology and Medicine 15(1) (2019) 175-187.

[8] J.A. Lillibridge, T.F. Kalhorn, J.T. Slattery, Metabolism of lisofylline and pentoxifylline in human liver microsomes and cytosol, Drug metabolism and disposition 24(11) (1996) 1174-1179.

[9] A.K. Singh, K.S. Italiya, S. Narisepalli, D. Chitkara, A. Mittal, Role of chain length and degree of unsaturation of fatty acids in the physicochemical and pharmacological behavior of drug–fatty acid conjugates in diabetes, Journal of Medicinal Chemistry 64(19) (2021) 14217-14229.

[10] Z. Yang, M. Chen, J.D. Carter, C.S. Nunemaker, J.C. Garmey, S.D. Kimble, J.L. Nadler, Combined treatment with lisofylline and exendin-4 reverses autoimmune diabetes, Biochemical and Biophysical Research Communications 344(3) (2006) 1017-1022.

[11] J.A. Shaw, P. Shetty, K.D. Burns, D. Fergusson, G.A. Knoll, C-peptide as a therapy for kidney disease: A systematic review and meta-analysis, PLoS One 10(5) (2015) e0127439.

[12] J. Chen, Y. Huang, C. Liu, J. Chi, Y. Wang, L. Xu, The role of C-peptide in diabetes and its complications: an updated review, Frontiers in Endocrinology 14 (2023).

[13] N. Zashikhina, V. Sharoyko, M. Antipchik, I. Tarasenko, Y. Anufrikov, A. Lavrentieva, T. Tennikova, E. Korzhikova-Vlakh, Novel formulations of C-peptide with long-acting therapeutic potential for treatment of diabetic complications, Pharmaceutics 11(1) (2019) 27.

[14] S.H. Jung, J.Y. Lee, S.H. Lee, M.H. Kwon, E.T. Han, W.S. Park, S.H. Hong, Y.M. Kim, K.S. Ha, Preventive Effects of Thermosensitive Biopolymer-Conjugated C-Peptide against High Glucose-Induced Endothelial Cell Dysfunction, Macromolecular Bioscience 19(9) (2019) 1900129.

[15] J. Wahren, H. Foyt, M. Daniels, J.C. Arezzo, Long-acting C-peptide and neuropathy in type 1 diabetes: a 12-month clinical trial, Diabetes care 39(4) (2016) 596-602.

[16] A.-J. Lee, Y.-J. Lee, H.-Y. Jeon, M. Kim, E.-T. Han, W.S. Park, S.-H. Hong, Y.-M. Kim, K.-S. Ha, Application of elastin-like biopolymer-conjugated C-peptide hydrogel for systemic long-term delivery against diabetic aortic dysfunction, Acta Biomaterialia 118 (2020) 32-43.

[17] K.S. Italiya, S. Mazumdar, S. Sharma, D. Chitkara, R.I. Mahato, A. Mittal, Self-assembling lisofylline-fatty acid conjugate for effective treatment of diabetes mellitus, Nanomedicine 15(1) (2019) 175-187.

[18] S. Sharma, S. Mazumdar, K.S. Italiya, T. Date, R.I. Mahato, A. Mittal, D. Chitkara, Cholesterol and morpholine grafted cationic amphiphilic copolymers for miRNA-34a delivery, Molecular pharmaceutics 15(6) (2018) 2391-2402.

[19] K.S. Italiya, M. Basak, S. Mazumdar, D.K. Sahel, R. Shrivastava, D. Chitkara, A. Mittal, Scalable self-assembling micellar system for enhanced oral bioavailability and efficacy of lisofylline for treatment of type-I diabetes, Molecular Pharmaceutics 16(12) (2019) 4954-4967.

[20] O. Boscolo, S. Flor, L. Salvo, C. Dobrecky, C. Höcht, V. Tripodi, M. Moretton, S. Lucangioli, Formulation and Characterization of Ursodeoxycholic Acid Nanosuspension Based on Bottom-Up Technology and Box–Behnken Design Optimization, Pharmaceutics 15(8) (2023) 2037.

[21] A. Mittal, D. Chitkara, S.W. Behrman, R.I. Mahato, Efficacy of gemcitabine conjugated and miRNA-205 complexed micelles for treatment of advanced pancreatic cancer, Biomaterials 35(25) (2014) 7077-7087.

[22] N.M. Selby, M.W. Taal, An updated overview of diabetic nephropathy: Diagnosis, prognosis, treatment goals and latest guidelines, Diabetes, Obesity and Metabolism 22 (2020) 3-15.

[23] S. Paul, A. Ali, R. Katare, Molecular complexities underlying the vascular complications of diabetes mellitus–A comprehensive review, Journal of Diabetes and its Complications 34(8) (2020) 107613.

[24] Q. Gao, J. Feng, W. Liu, C. Wen, Y. Wu, Q. Liao, L. Zou, X. Sui, T. Xie, J. Zhang, Opportunities and challenges for co-delivery nanomedicines based on combination of phytochemicals with chemotherapeutic drugs in cancer treatment, Advanced Drug Delivery Reviews (2022) 114445.

[25] S. Joshi, M.T. Hussain, C.B. Roces, G. Anderluzzi, E. Kastner, S. Salmaso, D.J. Kirby, Y. Perrie, Microfluidics based manufacture of liposomes simultaneously entrapping hydrophilic and lipophilic drugs, International journal of pharmaceutics 514(1) (2016) 160-168.

[26] N. Samed, V. Sharma, A. Sundaramurthy, Hydrogen bonded niosomes for encapsulation and release of hydrophilic and hydrophobic anti-diabetic drugs: an efficient system for oral anti-diabetic formulation, Applied Surface Science 449 (2018) 567-573.

[27] K.S. Italiya, A.K. Singh, D. Chitkara, A. Mittal, Nanoparticulate tablet dosage form of lisofylline-linoleic acid conjugate for type 1 diabetes: in situ single-pass intestinal perfusion (SPIP) studies and pharmacokinetics in rat, AAPS PharmSciTech 22 (2021) 1-12.

[28] L. Pang, Y. Pei, G. Uzunalli, H. Hyun, L.T. Lyle, Y. Yeo, Surface modification of polymeric nanoparticles with M2pep peptide for drug delivery to tumor-associated macrophages, Pharmaceutical research 36 (2019) 1-12.

[29] H. Lv, S. Zhang, B. Wang, S. Cui, J. Yan, Toxicity of cationic lipids and cationic polymers in gene delivery, Journal of controlled release 114(1) (2006) 100-109.

[30] A.M. Weiss, M.A. Lopez, B.W. Rawe, S. Manna, Q. Chen, E.J. Mulder, S.J. Rowan, A.P. Esser-Kahn, Understanding How Cationic Polymers' Properties Inform Toxic or Immunogenic Responses via Parametric Analysis, Macromolecules 56(18) (2023) 7286-7299.

[31] F. ASTM, F756-08, Standard Practice for Assessment of Hemolytic Properties of Materials," ASTM International, West Conshohocken, PA, ASTM Book of Standards (2013).

[32] R.F. Pagels, R.K. Prud'Homme, Polymeric nanoparticles and microparticles for the delivery of peptides, biologics, and soluble therapeutics, Journal of Controlled Release 219 (2015) 519-535.

[33] C. Wang, S. Feng, J. Qie, X. Wei, H. Yan, K. Liu, Polyion complexes of a cationic antimicrobial peptide as a potential systemically administered antibiotic, International Journal of Pharmaceutics 554 (2019) 284-291.

[34] L. Lv, X. Wang, J. Shen, Y. Cao, Q. Zhang, MiR-574-3p inhibits glucose toxicity-induced pancreatic β-cell dysfunction by suppressing PRMT1, Diabetology & Metabolic Syndrome 14(1) (2022) 1-11.

[35] M.F. Khan, A. Mathur, V.K. Pandey, P. Kakkar, Naringenin alleviates hyperglycemia-induced renal toxicity by regulating activating transcription factor 4–C/EBP homologous protein mediated apoptosis, Journal of Cell Communication and Signaling (2021) 1-21.

[36] X. Liu, S. Han, Y. Yang, J. Kang, J. Wu, Glucose-induced glutathione reduction in mitochondria is involved in the first phase of pancreatic β-cell insulin secretion, Biochemical and Biophysical Research Communications 464(3) (2015) 730-736.

[37] D.A. Allen, M.M. Yaqoob, S.M. Harwood, Mechanisms of high glucose-induced apoptosis and its relationship to diabetic complications, The Journal of nutritional biochemistry 16(12) (2005) 705-713.

[38] I.P. Salt, V.A. Morrow, F.M. Brandie, J.M. Connell, J.R. Petrie, High glucose inhibits insulin-stimulated nitric oxide production without reducing endothelial nitric-oxide synthase Ser1177 phosphorylation in human aortic endothelial cells, Journal of Biological Chemistry 278(21) (2003) 18791-18797.

[39] F. Cosentino, K. Hishikawa, Z.S. Katusic, T.F. Lüscher, High glucose increases nitric oxide synthase expression and superoxide anion generation in human aortic endothelial cells, Circulation 96(1) (1997) 25-28.

[40] L.A. Powell, S.M. Nally, D. McMaster, M.A. Catherwood, E.R. Trimble, Restoration of glutathione levels in vascular smooth muscle cells exposed to high glucose conditions, Free Radical Biology and Medicine 31(10) (2001) 1149-1155.

[41] H. Foyt, M. Daniels, M. Milad, J. Wahren, Pharmacokinetics, safety, and tolerability of a long-acting C-peptide (CBX129801) in patients with type 1 diabetes, Diabetologia 55(Suppl 1) (2012) S455.

[42] Y. Ji, X. Liu, J. Li, X. Xie, M. Huang, J. Jiang, Y.-P. Liao, T. Donahue, H. Meng, Use of ratiometrically designed nanocarrier targeting CDK4/6 and autophagy pathways for effective pancreatic cancer treatment, Nature Communications 11(1) (2020) 4249.

[43] Z. Yang, M. Chen, L.B. Fialkow, J.D. Ellett, R. Wu, J.L. Nadler, The novel anti-inflammatory compound, lisofylline, prevents diabetes in multiple low-dose streptozotocin-treated mice, Pancreas 26(4) (2003) e99-e104.

[44] G. Xu, D.A. Stoffers, J.F. Habener, S. Bonner-Weir, Exendin-4 stimulates both beta-cell replication and neogenesis, resulting in increased beta-cell mass and improved glucose tolerance in diabetic rats, Diabetes 48(12) (1999) 2270-2276.

[45] M. Chen, Z. Yang, R. Wu, J.L. Nadler, Lisofylline, a novel antiinflammatory agent, protects pancreatic β-cells from proinflammatory cytokine damage by promoting mitochondrial metabolism, Endocrinology 143(6) (2002) 2341-2348.
[46] J. Wahren, Å. Kallas, A.A. Sima, The clinical potential of C-peptide replacement in type 1 diabetes, Diabetes 61(4) (2012) 761-772.
[47] J.-K. Yi, Z.-Y. Ryoo, J.-J. Ha, D.-Y. Oh, M.-O. Kim, S.-H. Kim, Beneficial effects of 6-shogaol on hyperglycemia, islet morphology and apoptosis in some tissues of streptozotocin-induced diabetic mice, Diabetology & metabolic syndrome 11(1) (2019) 1-13.

XXXXXXXXXXXXXXXXX

# CHAPTER 6

# Conclusion and Future Prospects

## 6.1 Conclusion

The previous research work carried out in our lab on drug-fatty acid conjugation approach for LSF reported the desired amphiphilicity of the system which resulted in self-assembly of LSF-LA into micelles with considerably low CMC value. This formulation has been proven to be therapeutically effective in STZ-induced T1D model wherein, it increased MRT of LSF in the body and reduced LSF-PTX interconversion by ~50 %.

In contrast, the main aim in the present thesis work was to emphasize on the designing of a co-loaded delivery system for the LSF-FA prodrug and renoprotective CPep and evaluate its scope in STZ-induced DN treatment. The major objectives of the thesis work are as follows:

(1) Synthesis, characterization and evaluation of different prodrugs of LSF-fatty acid.
(2) Synthesis, characterization and evaluation of polymeric CPep nano-complexes
(3) Development and evaluation of polymeric nano-formulation of LSF-OA prodrug and CPep combination.

Among all the LSF-FA prodrugs, LSF-OA was selected based upon the observed *in-vitro* release profile (only 9.74 ± 2.3% cumulative release in 72h), acceptable BSA binding constant ($6.32 \times 10^4$) with suitable aggregation number ($N_{agg}$= 61). *In-vivo* pharmacokinetic study indicated ~6 fold higher $t_{1/2}$ and ~11 fold enhanced MRT when compared to free LSF and efficient control of glucose level with decreased mortality compared to other prodrugs in STZ-induced T1D animals. Interestingly, LSF-OA prodrug also demonstrated significant reduction in T cells (CD4+ and CD8+) entry into the islets by IHC analysis which is an indication of its anti-inflammatory action. Reduction in plasma ASAT and ALAT level along with the uric acid is also indicative of its possible application in diabetes induced kidney dysfunction.

Reportedly, the hypothesis behind designing polymeric cationic nanocomplex of CPep (NPX) was proved beneficial, with 87.50 % complexation efficiency of CPep with controlled release upto 180 h wherein, only ~40 % release was observed within seven days. This clearly indicated a longer residence time of CPep under the physiological condition. NPX administration in Wistar rats (i.v.) revealed the steady plasma concentration of CPep, maintained till 72 h (above the normal CPep concentration) and demonstrated $t_{1/2}$ of ~22 h. The anti-inflammatory effect of NPX reduced the predominantly elevated proinflammatory cytokine, IL-6 in plasma to 3 fold lesser than the DC group along with 2.3 fold reduction in the expression of TGF-β. Improved kidney histology was another indication of the efficacy of NPX in DN.

After confirming the efficiency of LSF-OA and NPX individually, the efficacy of their combination therapy was explored. The two were utilized together to develop a co-loaded

formulation mPLM-LSF-OA-CPep wherein, the LSF-OA was entrapped in the polymeric cationic nanoparticles (mPLM-LSF-OA) and then complexed with the CPep (mPLM-LSF-OA-CPep). mPLM-LSF-OA was found to be anti-oxidative and proliferative in *in-vitro* metabolic stress-induced MIN-6 and NRK-52E cells. While mPLM-LSF-OA was able to increase the GSH level by 1.62 and 1.27 fold, mPLM-LSF-OA-CPep elevated the level by 2.06 &1.8 fold respectively.

In *in-vivo* efficacy study, the mPLM-LSF-OA-CPep treated animals exhibited ~2.69 and ~2.05 fold reduced pro-inflammatory cytokines (IL-6 and TNF-α) level in comparison to STZ-induced DN control animals. Finally, the efficiency of the co-loaded formulation was confirmed by ~6.8 fold improved insulin level, and higher number of Ki-67 stained cells in the pancreatic islets indicating cell proliferation. Along with this, H&E and PAS staining revealed reduced intracellular glycogen accumulation, diminished infiltration of inflammatory cells, mild mesangial expansion, lesser deposition of mesangial matrix, and almost normal relative glomerular basement membrane thickness with the combination formulation treated group. These observations indicated the potential of LSF-OA and CPep combination and their formulation for the treatment of DN.

## 6.2 Future Scope

a. The co-loaded formulation can be utilized to deliver LSF-FA conjugate with oligonucleotides to target the specific mRNA, translating the proteins responsible for DN pathology.
b. The modification of the polymeric backbone with the other kidney-targeting moiety can improve the efficiency of the formulation strategy.
c. Several glucose-responsive proteins, for e.g., glucose-binding proteins (GBPs), glucose oxidase (GOx), and phenylboronic acids (PBAs) could be conjugated with the co-load system to get the targeted delivery strategy.
d. LSF prodrugs can be explored in combination with other potent antioxidant molecules like polyphenols to explore their efficacy in DM and DM-linked complications.
e. The LSF prodrugs and CPep formulations should be explored in the T2D model, pancreatic islet regeneration and Podocyte biology, to confirm the exact mechanism of action of them in DN.
f. Considering the anti-oxidative effect imparted by the LSF-OA and CPep, their application in other immune diseases should be explored, which would lead to the repurposing of the formulation.
g. The present combination can also be explored in other diabetes link complications-retinopathy, neuropathy, etc.

# Appendix

## A.1. List of Publications

### A.1.1 From Thesis

#### A.1.1.1 Patent

Indian Patent- Anupama Mittal, **Arihant Kumar Singh**, Shubham A Salunkhe, Deepak Chitkara, Formulation of peptide nano-complexes for delivery of peptide and method of preparation (Filed on 7th July 2023, 202311047523).

#### A.1.1.2 Journal Articles

(1) **Arihant Kumar Singh**, Kishan Italiya, Saibhargav Narisepalli, Deepak Chitkara, Anupama Mittal, Role of chain length and degree of unsaturation of fatty acids on physicochemical and pharmacological behaviour of drug-fatty acid conjugates in diabetes, *Journal of Medicinal Chemistry* (2021) 64, 14217-29.

(2) **Arihant Kumar Singh**, Shubham A. Salunkhe, Deepak Chitkara, Anupama Mittal, Potent anti-inflammatory and anti-apoptotic activities of electrostatically complexed C-peptide nanospheres ameliorate diabetic nephropathy, (2024). (*Under review)*

(3) **Arihant Kumar Singh**, Kommera Sai Pradyuth, Deepak Chitkara, Anupama Mittal, Restoring Pathophysiology of Pancreas and Kidney by Treatment with a Polymeric Nano-Formulation of C-Peptide and Lisofylline Combination in Diabetic Nephropathy, (2024). (*Under review)*

### A.1.2 Allied Work

#### A.1.2.1 Patents

1. Indian Patent- Deepak Chitkara, Sudeep S. Pukale, **Arihant K. Singh**, Anupama Mittal, Saurabh Sharma, A lipid-polymer hybrid nanoparticles (387187, Granted on- 24th Jan 2022).
2. International PCT Application- Deepak Chitkara, Sudeep S. Pukale, **Arihant K. Singh**, Anupama Mittal, Saurabh Sharma, A lipid-polymer hybrid nanoparticles (Filed on 2nd Feb 2020, PCT/IB2020/050819)

#### A.1.2.2 Journal Articles

(1) Kommera Sai Pradyuth, Shubham A. Salunkhe, **Arihant K. Singh**, Deepak Chitkara, Anupama Mittal, Belinostat loaded lipid-polymer hybrid nanoparticulate delivery system for Breast Cancer: Improved Pharmacokinetics and Biodistribution in tumor model, *Journal of Material Chemistry B* (2023) 11, 10859-72.

(2) Samrat Mazumdar, Saibhargav Narisepalli, **Arihant K. Singh**, Deepak Chitkara, Anupama Mittal, Enhanced anti-tumor efficacy and tumor accumulation of Tamoxifen through cRGD functionalized cholesterol based lipopolymeric nanoparticles for targeted breast cancer therapy, *Journal of Drug Delivery Science and Technology* (2023) 90, 1-16.

(3) Kishan S. Italiya, **Arihant K. Singh**, Deepak Chitkara, Anupama Mittal, Nanoparticulate tablet dosage form of lisofylline-linoleic acid conjugate for type 1 diabetes: in situ single-pass intestinal perfusion (SPIP) studies and pharmacokinetics in rat, *AAPS PharmSciTech* (2021) 22, 1-12.

(4) Sudeep Pukale, Saurabh Sharma, Manu Dalela, **Arihant K. Singh**, Sujata Mohanty, Anupama Mittal, Deepak Chitkara, Multi-component clobetasol-loaded monolithic lipid-polymer hybrid nanoparticles ameliorate imiquimod-induced psoriasis-like skin inflammation in Swiss albino mice, *Acta Biomaterialia* (2020) 115, 393-409.

(5) Tania Nandi, Sai Pradyuth, **Arihant K. Singh**, Deepak Chitkara, Anupama Mittal, Therapeutic agents for targeting desmoplasia: Current status and emerging trends, *Drug Discovery Today* (2020) 25, 2046-55.

### A.1.2 Achievements and conferences

#### A.1.2.1 Achievements

1. Acceptance of abstract in **8$^{th}$ Nano Today Conference** in April 2023 at San Diego, CA, USA, and **ICMR travel grant awardee** for attending the same. (*Not availed*)
2. **Sun Pharma Science Scholar Award 2021**- Issued by Sun Pharma Science Foundation, New Delhi with a hundred thousand price money, travel grant and a citation in the field of Pharmaceutical Sciences in Jan 2022.
3. **Young Researcher Award 2021**- Issued by Society of young biomedical scientists, India at 3$^{rd}$ National Biomedical Research Competition (NBRCOM) 2021 in pharmaceutical science's oral presentation category with 3$^{rd}$ rank and ten thousand price money.

#### A.1.2.2 Conferences

1. Oral presentation at 4$^{th}$ World Drug Discovery & Development Congress 2023 at IISc, Bangalore on 29$^{th}$ Oct 2023.
2. Presented posters at 21$^{st}$ International Symposium by Controlled Release Society Local Indian Chapter's on Feb 2023 at NMIMS, Mumbai.
3. Presented posters at 20th International Symposium by Controlled Release Society Local Indian Chapter on Feb 2022 (Virtual).
4. Oral presentation at 3$^{rd}$ National Biomedical Research Competition (NBRCOM) 2021 (Virtual) organized by Society of young biomedical scientists, India.
5. Presented poster at the Society of Biological Engineering's 6th Bioengineering & Translational Medicine Conference 2021, organized by AIChE and sponsored by Wiley on 18-20 October 2021.

## A.2 Biographies

### A.2.1 Biography of Prof. Anupama Mittal (Supervisor)

**BIOGRAPHICAL SKETCH**

ANUPAMA MITTAL, Ph.D.
Associate Professor, Department of Pharmacy,
Birla Institute of Technology and Science (BITS), Pilani, Vidya Vihar Campus, 333031
Rajasthan, INDIA

**Professional Experience**

| Positions held | Duration | Institute |
|---|---|---|
| Associate Professor | June 2021-till date | BITS-Pilani, Pilani, Rajasthan |
| Assistant professor | 2014-May 2021 | BITS-Pilani, Pilani, Rajasthan |
| Visiting Research Scholar | Oct 2012- May 2013 | University of Tennessee Health Science Center (UTHSC), Memphis, TN, USA |
| Post-Doctoral Research Associate | May 2013- June 2014 | University of Nebraska Medical Center (UNMC), Omaha, NE, USA |

**Education**

| Degree | Institute | Field | Year |
|---|---|---|---|
| B.Pharmacy | Delhi Institute of Pharmaceutical Sciences & Research, Delhi University | Pharmacy | 2001-2005 |
| M. S.(Pharm) | National Institute of Pharmaceutical Sciences and Research (NIPER), SAS Nagar, Punjab. | Pharmaceutics | 2005-2007 |
| Ph.D. | NIPER, S.A.S. Nagar | Pharmaceutical Sciences | 2007-2012 |

**Personal Statement**

Prof. Anupama Mittal currently working as an Associate Professor in Department of Pharmacy, BITS, Pilani, Pilani campus is an established researcher and scientist in the field of Nanomedicine. She has been involved actively in teaching (on campus as well as industry professionals from various pharmaceutical industries) and independent research since nearly last 10 years. Her research interests and expertise primarily focus upon generating nanotechnology based solutions for diseases like cancer and diabetes. Her lab has been engaged in research activities in the areas of polymer/fatty acid drug conjugates for effective treatment of cancer & diabetes, stem cells and exosomes as biogenic carriers of miRNA & proteins in cancer, nanoparticles & polymeric micelles for site-specific drug delivery, and growth factor and peptide based therapeutics for wound healing and diabetes. She has published more than 60 research and review articles in peer-reviewed international journals and edited 01 book (CRC press), and filed 10 Indian/PCT patent applications among which 04 have been successfully granted. She has been the recipient of prestigious Young Scientist Award-2015 (SERB-DST) and Ranbaxy Science Scholar Award-2011 (Ranbaxy Science Foundation) in Pharmaceutical Sciences. She has also received several awards for best papers presented at National/International conferences. Her lab is generously funded by several extramural research grants from SERB-DST, DST-Rajasthan, DST-Nanomission, ICMR and DBT. She has guided 2 PhD students, several M. Pharm and B. Pharm students and is currently supervising 07 Ph.D. students. She also serves as one of the founding directors of start-up company, Nanobrid Innovations Pvt. Ltd. aimed towards the translation of nanotechnology based products.

## A.2.2 Biography of Prof. Deepak Chitkara (Co-Supervisor)

**BIOGRAPHICAL SKETCH**

DEEPAK CHITKARA, Ph.D.
Associate Professor, Department of Pharmacy,
Birla Institute of Technology and Science (BITS), Pilani, Vidya Vihar Campus, 333031
Rajasthan, INDIA

**Professional Experience**

| Positions held | Duration | Institute |
|---|---|---|
| Associate Professor | June 2021-till date | BITS-Pilani, Pilani, Rajasthan |
| Assistant professor | June 2014-May 2021 | BITS-Pilani, Pilani, Rajasthan |
| Visiting Research Scholar | Oct 2012- May 2013 | University of Tennessee Health Science Center (UTHSC), Memphis, TN, USA |
| Post-Doctoral Research Associate | May 2013- June 2014 | University of Nebraska Medical Center (UNMC), Omaha, NE, USA |

**Education**

| Degree | Institute | Field | Year |
|---|---|---|---|
| B.Pharmacy | University Institute of Pharmaceutical Sciences (UIPS), Panjab University | Pharmacy | 2000-2004 |
| M. S.(Pharm) | National Institute of Pharmaceutical Sciences and Research (NIPER), SAS Nagar, Punjab. | Pharmaceutics | 2004-2006 |
| Ph.D. | NIPER, S.A.S. Nagar | Pharmaceutical Sciences | 2007-2014 |

### Personal Statement

Prof. Deepak Chitkara is an Associate Professor at the Department of Pharmacy, Birla Institute of Technology and Science (BITS)-Pilani, Vidya Vihar Campus, India. Prof. Chitkara has obtained an M.S. (Pharm.) in Pharmaceutics and a Ph.D. in Pharmaceutical Sciences from the National Institute of Pharmaceutical Education and Research (NIPER), SAS Nagar. He was an exchange research scholar at the University of Tennessee Health Science Center, Memphis, TN, for one year. After that, he did his post-doctoral training at the University of Nebraska Medical Center, Omaha, Nebraska, USA. He has published over 60 peer-reviewed publications, edited one book, and is editing two special issues for reputed journals. Further, he has filed 8 Indian patents, one international PCT patent application and 5 Indian patent applications have been granted. His lab is well-funded by various government agencies, including DBT, DST, and ICMR, and Pharmaceutical Industries.

Prof. Chitkara is also the founding director of a faculty-led nanotechnology-based start-up (Nanobrid Innovations Private Limited) incubated at Pilani Innovations and Entrepreneurship Development Society at BITS-Pilani to further take up the commercialization activities. The Company has commercialized a skin care anti-ageing range (Nanobrid Inskin) wherein four products have been launched through their own e-commerce platform (www.inskin.in) as well as other e-commerce platforms, including Amazon and Flipkart.

### A.2.3 Biography of Mr. Arihant Kumar Singh

Mr. Arihant Kumar Singh completed his Bachelor of Pharmacy (B. Pharm) from Gujarat Technological University (Gujarat) in the year 2015 and his Masters of Pharmacy (M. Pharm) in Pharmaceutics from Savitribai Phule Pune University (Maharashtra) in 2017. In February 2015, he was awarded the i-Scale (Innovative Students' Co-Creation Awards for Leadership and Excellence) award 2015 by GTU University for his initiative as a founder of 'Pharma Innovators', a student-driven program for health awareness.

He joined the Department of Pharmacy at BITS Pilani, Pilani campus, in Aug 2018 to pursue a Ph.D. in Pharmaceutical Science. Initially, he joined BITS Pilani as a junior research fellow (JRF) at DST Rajasthan, followed by DST Nanomission under the guidance of Prof. Anupama Mittal. Finally, from 2021 onwards he has been working on his doctoral research project as an institute's senior research fellow. His areas of interest include biomaterials, polymer science, nanoformulation development, peptide delivery, pharmacokinetic studies, *in-vitro* cell culture studies and *in-vivo* studies (diabetes, cancer and psoriasis).

He has published 7 peer-reviewed articles in renowned international journals and filed 5 patents, from which 2 granted, 1 in examination, 1 filed and 1 PCT application (US, EU, JP). He has participated in state, national and international conferences and has also been awarded multiple times for best poster and best model competition. In 2021, Mr Arihant was awarded the Young Researcher Award 2021 by the Society of Young Biomedical Scientists, followed by the Sun Pharma Science Scholar Award 2021 by Sun Pharma Science Foundation, New Delhi, for his Ph.D. thesis work.